UCLouvain Institute of Mechanics, Materials and Civil Engineering (iMMC)
Thermodynamics and Fluid Mechanics (TFL)

Potential of wind and solar resources and macroeconomic implications of the energy transition

---

Elise Dupont

June 2021

Thèse présentée en vue de l'obtention du grade de docteur en sciences de l'ingénieur

Composition du jury:

Pr. Hervé Jeanmart (UCLouvain, Supervisor)
Pr. Thomas Pardoen (UCLouvain, President)
Pr. Emmanuel De Jaeger (UCLouvain, Secretary)
Pr. Jean-François Fagnart (Université Saint-Louis)
Dr. Iñigo Capellán-Pérez (Universidad de Valladolid)

2021 – Elise Dupont

À Oli, Léo et A.

Bien sûr, toutes ces fourchettes de chiffres se discutent, et d'aucuns ne manqueront pas de le faire, mais le principe général l'est moins. L'idée à saisir est que nous sommes face à un mur thermodynamique qui s'approche de plus en plus vite. Aujourd'hui, chaque unité d'énergie est extraite à un coût environnemental, économique et énergétique toujours plus élevé.

Pablo Servigne et Raphaël Stevens - Comment tout peut s'effondrer

Keep fighting for your children now, keep fighting for your land.

Xavier Rudd - Spirit Bird

Remerciements

Au moment de finir cette thèse, je réalise la chance que j'ai eue d'avoir pu consacrer ces (presque) six dernières années à un projet de recherche aussi inspirant et plus que jamais au cœur de l'actualité. Le parcours de chercheur est certes assez solitaire, mais l'inspiration est impossible sans échange.

Pour cela, je dois avant tout remercier mon promoteur, Hervé Jeanmart, pour m'avoir directement accordé sa confiance lorsque je questionnais mon orientation professionnelle, et pour s'être lancé avec moi dans cette aventure. J'ai réellement apprécié sa façon de m'accompagner, avec toujours le mot juste pour me redonner confiance lorsque c'était nécessaire. Au cours de nos nombreuses discussions, j'ai été impressionnée par sa capacité à débloquer en quelques minutes une situation qui me semblait si compliquée, et à me pousser sans cesse à me dépasser.

Je dois également beaucoup à Marc Germain, qui a accepté le défi de développer avec moi un modèle macroéconomique malgré ma quasi-absence de formation en économie. Grâce à sa persévérance, nous sommes parvenus à réconcilier deux approches parfois radicalement opposées, celle de l'énergéticien et celle de l'économiste. Nos échanges réguliers, en particulier ces deux dernières années, en plus d'être très productifs, ont été un réel plaisir.

Je n'aurais pas pu présenter un modèle énergétique aussi abouti sans ma collaboration avec Rembrandt Koppelaar. Avec son expérience et son expertise, il m'a guidé tant au niveau du modèle que de la rédaction.

Finalement, je voudrais remercier les membres de mon jury, Thomas Pardoen, Emmanuel De Jaeger, Jean-François Fagnart et Iñigo Capellán-Pérez, pour le temps consacré à l'évaluation et à l'appréciation de ce travail. Leurs conseils et nos réflexions communes m'ont permis d'améliorer la qualité de ce texte.

Je voudrais également remercier mes collègues pour nos échanges et discussions, et tous les chouettes moments passés ensemble, notamment lors de nos séjours de mise au vert: Max et Gauthier (les BOSS), Véro, Laetitia, et, en leur temps, Benjamin et Nicolas. Cela semble déjà loin mais merci aussi à Maud et Philippe pour nos sorties de course à pied, et, à tous ceux qui se reconnaîtront, pour avoir osé me défier au kicker. Merci aux Jeunes Furieux pour la dynamique que vous instaurez, à mes collègues assistants pour les trop longues heures passées sur Teams. Merci aux "nouveaux" de l'équipe TFL/Energy pour leur intérêt pour mes recherches, et à Pierre de reprendre le flambeau. À tous les autres, j'ai hâte qu'on puisse enfin se retrouver ou se rencontrer à la Cafet. Le contexte actuel nous a malheureusement privé d'une bonne partie de ce qui faisait jusqu'ici notre quotidien si agréable au sein du pôle TFL, et aura permis à chacun de prendre pleinement conscience de l'importance des échanges informels et spontanés entre collègues, des barbecues et des verres improvisés.

J'ai la chance de pouvoir compter sur une famille, une belle-famille et des amis fidèles, qui me soutiennent par leur présence au quotidien. Merci à mes Beautiful Friends pour notre complicité, aux ingénieuses pour notre incroyable parcours ensemble, à Anso et JM pour notre projet de vie commun. Merci à mon papa pour m'avoir transmis sa soif de connaissance, à ma maman pour son écoute, à mon frère pour sa recherche continuelle de sens, à ma sœur pour son soutien et sa présence.

Et puis surtout, merci à Oli d'être si fier de moi, de toujours trouver les mots pour me faire avancer et de rendre notre vie si belle. A notre merveilleux Léo et à sa petite sœur pour qui je veux plus que jamais me battre pour un monde plus juste, plus équitable, et plus durable.

Pour finir, merci à tous ceux qui, de près ou de loin, m'ont, par leur intérêt et nos échanges, fait remettre en question mes certitudes et donné la motivation d'aller toujours plus loin.

Contents

List of publications **xi**

Abstract **1**

1 Introduction **3**
1.1 Context and objectives 3
1.1.1 The paradox: infinite growth in a finite world 5
1.1.2 Energy transition pathways 7
1.1.3 Consideration of physical limits 10
1.1.4 Economic impacts of the energy transition 11
1.2 Thesis questions and objectives 11
1.3 Outline of this thesis 14

2 State of the art: EROI and energy-economy models **15**
2.1 Net energy analysis and EROI 15
2.1.1 Definition and boundaries 19
2.1.2 EROI and quality of life 24
2.1.3 EROI dynamics 28
2.2 Energy-economy models 32
2.2.1 Biophysical approach 33
2.2.2 Economic growth models 37

3 Global available wind energy under physical and EROI constraints **41**
3.1 Limits on wind potential via top-down approaches 43
3.2 Methodology 45
3.2.1 Geographic suitability factor 47
3.2.2 Wind energy outputs 48

3.2.3 Life cycle energy inputs 56
3.2.4 Installed capacity optimisation 64
3.2.5 Kinetic energy available 65
3.2.6 Net energy results calculation 66
3.3 Results 66
3.3.1 Wind farm design 66
3.3.2 Global optimisation results 69
3.3.3 Regional optimisation results 75
3.4 Discussion 82
3.4.1 Comparison with previous bottom-up studies 82
3.4.2 Limitations and perspective 83
3.5 Conclusions and policy implications 84

4 Global available solar energy under physical and EROI constraints 87
4.1 Methodology 88
4.1.1 Geographic constraints 91
4.1.2 Solar resource constraints 93
4.1.3 Solar technology constraints 95
4.1.4 Solar energy inputs 101
4.1.5 Establishing efficiency and CSP collector aperture area relation per grid cell 107
4.1.6 Energy potential and EROI values 109
4.1.7 Global EROI constraints 112
4.2 Results 112
4.2.1 Technology comparison at 1 GW scale 112
4.2.2 Global large scale ground systems energy potential . . 113
4.2.3 Global solar PV rooftop energy potential 116
4.2.4 Resulting spatial distribution of the solar resources . . . 119
4.2.5 Results split by regions 122
4.3 Discussion 124
4.3.1 Limitations of the study design 125
4.3.2 Actual capacity factors of CSP power plants 127
4.4 Conclusion 130

5 Combined wind and solar potential Point-use EROI and application at the European level 133
5.1 Preliminaries . . . 134
5.1.1 EROI definitions . . . 134
5.1.2 Energy efficiency improvements . . . 136
5.1.3 Solar technologies considered . . . 137
5.2 World potentials . . . 137
5.2.1 Evolution of the EROI with the cumulated potential . . . 137
5.2.2 Spatial distribution of the resources . . . 142
5.2.3 Impacts of energy efficiency improvements . . . 144
5.3 EU-28 potentials . . . 146
5.3.1 Evolution of the EROI with the cumulated potential . . . 146
5.3.2 Spatial distribution of the resources . . . 150
5.3.3 Impacts of energy efficiency improvements . . . 154
5.3.4 Discussion . . . 156
5.4 Conclusion . . . 157

6 Feasibility and economic impacts of the energy transition 159
6.1 The macroeconomic model . . . 160
6.1.1 Mathematical Formulation . . . 161
6.1.2 The reference calibration . . . 170
6.1.3 Sensitivity analysis . . . 181
6.2 Articulation with the energy model . . . 184
6.2.1 Outputs of the energy model . . . 185
6.2.2 Allowable space and transition curve . . . 190
6.3 Simulations of the energy transition . . . 195
6.3.1 Exogeneous parameters . . . 195
6.3.2 Exercise 1 - s and η given . . . 196
6.3.3 Exercise 2 - η and g_K fixed . . . 206
6.3.4 Discussion . . . 215
6.4 Conclusion . . . 217

7 Conclusion and perspectives 221
7.1 Conclusion . . . 221
7.2 Perspectives . . . 226
7.2.1 Energy model . . . 226
7.2.2 Economic model . . . 229

Nomenclature **231**

References **235**

A Estimated rooftop area by country **259**

B Mathematical developments for the macroeconomic model **265**

B.1 Relationship between the NDP and the technical parameters . 265

B.2 Link between v, g and g_K 267

B.3 Historical evolution of v, x_f and v_f 267

B.4 Site selection criteria 269

B.5 Interval for p 269

B.6 Calculation of the allowable spaces 270

B.6.1 Exercise 1 - k interval 271

B.6.2 Exercise 1 - Capital growth rate 272

B.6.3 Exercise 2 - k interval 273

B.6.4 Exercise 2 - Savings rate 275

B.7 Future evolution of Y_e and q_f 276

List of publications

Chapter 3 is based on the following peer-reviewed journal publication:

Dupont, E., Koppelaar, R. & Jeanmart, H. (2018). *Global available wind energy with physical and energy return on investment constraints.* Applied Energy, 209, 332-338, http://dx.doi.org/10.1016/j.apenergy.2017.09.085

Chapter 4 is based on the following peer-reviewed journal publication:

Dupont, E., Koppelaar, R. & Jeanmart, H. (2020). *Global available solar energy under physical and energy return on investment constraints.* Applied Energy, 257, 113968, https://doi.org/10.1016/j.apenergy.2019.113968

Chapter 6 is based on the following peer-reviewed journal publications:

Dupont, E., Germain M., & Jeanmart, H. (2021). *Estimate of the societal Energy Return on Investment (EROI).* Biophysical Economics and Sustainability, 2021, 6:2, https://doi.org/10.1007/s41247-021-00084-9

Dupont, E., Germain M., & Jeanmart, H. (2021). *Feasibility and economic impacts of the energy transition.* Sustainability, 2021, 13, 5345, https://doi.org/10.3390/su13105345

Related Publications:

Dupont, E., Jeanmart, H., Possoz, L., Fagnart, J.-F. & Germain, M. (2017). *Transition énergétique et (dé)croissance économique.* Regards Economiques, Numéro 135, Novembre 2017.

Dupont, E. & Jeanmart, H. (2019). *Global potential of wind and solar energy with physical and energy return on investment (EROI) constraints; application at the European level (EU 28 countries).*
Proceedings of ECOS 2019 - The 32nd International Conference on Efficiency, Cost, Optimisation, Simulation and Environmental Impact of Energy Systems.

Dupont, E. (2019). *Poursuivre la croissance dans un monde 100% renouvelable ? Limites physiques à la transition énergétique.* L'ENA hors les Murs, Mai 2019, Numéro 490, Dossier: Energie et environnement.

Abstract

In recent years, a controversy has developed as to whether, within a few decades, renewable energies could meet all the world energy needs, without jeopardising economic growth. From the many articles that have been published, no consensus can be found regarding the answer to this question. To shed a new light on this debate, a new methodology has been developed in this thesis to estimate global wind and solar potentials and the associated Energy Return On Investment (EROI), as these two resources are expected to be the main energy sources of the future energy system. Additionally, the obtained results have been coupled with a macroeconomic model to assess the feasibility and the economic impacts of the energy transition.

The estimation of the potentials includes onshore and offshore wind, solar photovoltaic and concentrated solar power plants. Based on a spatial discretisation of the world, the model calculates, per site and for each of the technologies used on the site: the production potential, the direct and indirect energy inputs required per unit of energy produced and, by relating the two previous quantities, the site EROI.

The model shows that, although having a twice higher global potential, solar technologies present lower EROIs than wind technologies. The global worldwide potentials obtained lie in the lower ranges of the estimations found in the literature, while for the European countries, the total potential is equivalent to the current final energy consumption of this region. This maximum potential can only be achieved if all of the theoretically available areas are covered with wind farms and solar fields, including areas with low energy profitability, especially for solar power plants. This theoretical potential then varies significantly depending on the minimum EROI threshold that is considered sustainable. It

would imply that the actually achievable potential will partly depend on the maximum price, in terms of direct and indirect energy uses, at which we can afford to produce our energy in the future.

In order to take into account the interactions between the energy system and the rest of the economy, a macroeconomic model has been developed. When results of the energy model are coupled with this macroeconomic model, simulations show that in a *business-as-usual* context, a complete energy transition on a global scale is unachievable before the end of the century. The reason lies in the increasing capital needs of the energy sector as the share of renewable energies progresses, which slows, if not stops, economic growth and the energy transition itself. Provided that (i) future energy demand remains similar to its current level, (ii) a sufficient rate of capital growth is sustained (above its historical level), and (iii) substantial progress is made in terms of energy efficiency, a complete transition could be achieved by 2070. However, this strategy requires a significant increase in the savings rate with a negative impact on public and private consumption, which would end up stagnating at the end of the transition.
The EROI decreases during the energy transition, but not significantly, suggesting that it would be the increase in the capital intensity of the energy sector that is mainly responsible for the slowdown in economic activity.

Pour sortir de la schizophrénie dont nous sommes tous atteints, il faut rompre avec certains modes de pensée. Remettre en question notre imaginaire.

Philippe Squarzoni - Saison Brune

1 Introduction

1.1 Context and objectives

Economic growth and energy consumption have always been closely linked. Indeed, the industrial revolution was made possible thanks to abundant and easily accessible coal, and, since the beginning of the twentieth century, the use of gas, oil and electricity have significantly improved the living standards of the privileged populations with access to them [1, 2]. It is this easy access to energy, and the associated productivity gains, which have enabled industrial societies to devote their factors of production to new economic activities, giving them great potential for expansion, and ensuring their growth [3]. But it is partly because of this easy access that economic models have long underestimated or even ignored the role of energy in economic production [4].

As one can see from the graph in Fig. 1.1, global energy consumption and gross domestic product (GDP) have been evolving together for decades. GDP growth (3.3% average annual growth since 1965) is, however, slightly higher

than that of primary energy production (2.5% average annual growth since 1965), thanks to technological progress which has made it possible to reduce the amount of energy needed to produce one unit of GDP (i.e. the energy intensity of the GDP, whose evolution is shown in Fig. 1.2). The latter figure reminds us that the search for ever greater efficiency is not new. There have been constant improvements in energy efficiency, sometimes accentuated by difficult economic circumstances (oil shocks, economic crises, etc.). However, as we progress and approach physical limits, further efficiency gains become increasingly small and difficult to achieve.

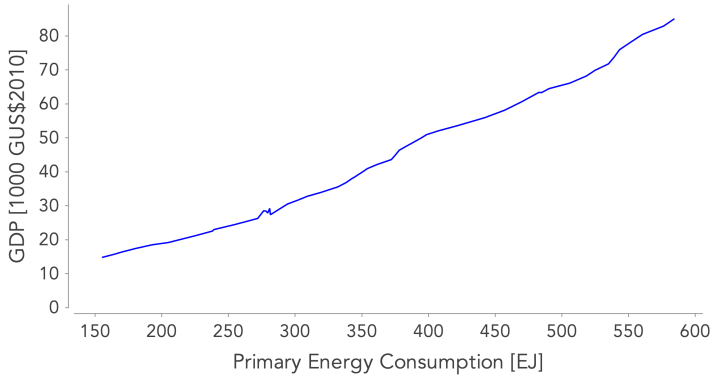


Figure 1.1 *– Evolution of primary energy consumption versus world GDP for the time period 1965-2019 (Sources: BP and World Bank).*

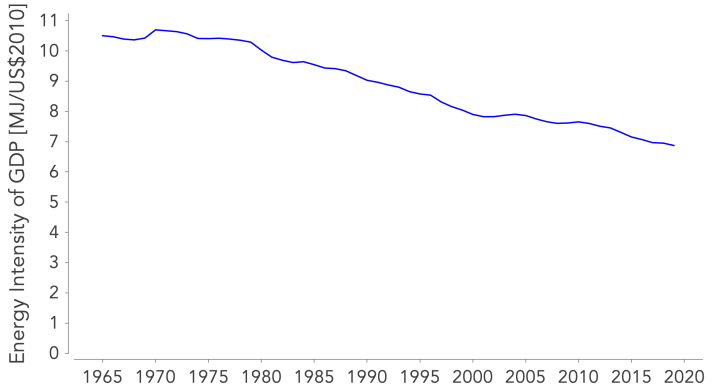


Figure 1.2 *– Temporal evolution of the primary energy intensity of the GDP (i.e. the ratio between primary energy supply and GDP) (Sources: BP and World Bank).*

1.1.1 The paradox: infinite growth in a finite world

From the engineer's point of view, it seems quite obvious that there is a very close coupling between economic activity and energy consumption. Indeed, by definition, economic activity consists in bringing added value through the production of goods and services, i.e. in transforming production factors (raw materials, intermediate products, labour, energy, etc.) into new products. All these transformation processes require a certain amount of energy, which technical progress nevertheless tends to progressively reduce (Fig. 1.2).

A second observation, which is also quite obvious, is that the resources on earth, and therefore the available factors of production, are limited. The amount of energy that humans are capable of mobilising is no exception, although the quantities available may seem limitless.
On the one hand, the amount of non-renewable energy is limited by definition. For all non-renewable resources (for fossil fuels, but also for other essential factors of production such as metals and other mineral resources), the production peak is defined as the moment when the extraction of this resource at the global level reaches its maximum rate. After this peak, the rate of extraction declines irreversibly due to the gradual depletion of the available resources, or to the diversion of the production to other, more affordable, sources. According to the International Energy Agency (IEA), conventional oil reached its peak in 2006 [5]. However, world production continues to grow, thanks in particular to the exploitation of shale oil in the United States. The use of new techniques has so far made it possible to push back the peak, but at the cost of increasingly energy-intensive and polluting exploitation techniques. Some recent estimates place the global peak oil in the next 10 years [6–8].
As for renewable energies, they are less limited in terms of stock, but more in terms of recoverable flows, i.e. the quantity that can be extracted per unit of time [9, 10]. The question of the feasibility or not of the energy transition therefore depends on the potential of the main renewable energy sources, and therefore on their capacity to ensure the same level of supply as we know today.

Combine these two observations (coupling between energy consumption and economy activities, and limited resources) and you arrive at a paradox: that of the search for economic growth, necessary for industrial societies to prosper, in a world of finite resources. This paradox is not new, but it is still struggling to

be heard. The alarm bell sounded in the early 1970s by the Meadows Group's "Limits to Growth" report [11], was taken very little seriously. They projected, however, that society would collapse before 2100 if no radical changes were made to reduce our dependence on economic growth, particularly because of population growth [12].

50 years later, while most of the world's resources continue to be unsustainably exploited, the situation seems to have hardly changed. Primary energy needs continue to grow inexorably, with an energy system still relying mainly on non-renewable resources, and the distribution of wealth is still as unequal as ever. Indeed, while the GDP doubled between 1990 and 2015, almost half of the people in the world are still living below the poverty line[1], and although inequalities between some countries have indeed decreased, over this period an increase in inequalities has been observed within more than two thirds of the countries of the world [13].
Moreover, climate change, whose main culprit is none other than the fossil fuel-based energy system[2], strikes in an equivalent uneven manner. Over the past 25 years, the richest 10% have emitted more than half of the cumulative CO_2 emissions, while the poorest 50% emitted only 7% of the total emissions [13, 14].

Nothing has changed in the figures, but in recent years there has nevertheless been a collective awareness of these issues. Exacerbated by the increasingly visible consequences of pollution and the successive Intergovernmental Panel on Climate Change (IPCC) reports predicting irreversible damage in the event of inaction, the question of the transition to a "sustainable" energy system has become a central issue in the political debate. The need to act as quickly as possible is no longer questioned by the scientific world, although the pathways envisaged to achieve this are sometimes radically different.

[1] The population living below the extreme poverty line has however decreased from 30 to 10%.

[2] According to ourworldindata.org, about 75% of global CO_2 emissions can be attributed to electricity, heat and transport production, compared to 18% for agriculture, forestry and land use.

1.1.2 Energy transition pathways

At present, the share of so-called modern renewable energies[3] in the world's energy production is relatively low. According to the IEA, in 2018 and at the global level, the share of renewable energies in primary energy production amounted to 13.8%, of which 9.3% came from biomass (mainly used to produce heat in developing countries), 2.5% from hydroelectricity and only 2% from other renewable sources (mainly wind and solar). Since 1990 this share has increased from 0.4 to 2%, while the energy supply has grown by 63%. Renewable energies are therefore still far from replacing fossil fuels, whose share in the total has remained constant at around 80% for the last three decades (Table 1.1). At a time when political strategies for the coming decades are to be decided, it is essential to question their real potential.

	1990	*2000*	*2010*	*2018*
Coal	25.3	23.1	28.4	26.9
Oil	36.9	36.6	32.1	31.5
Natural gas	19	20.6	21.3	22.8
Total fossil	**81.2**	**80.3**	**81.8**	**81.2**
Hydro	2.1	2.2	2.3	2.5
Wind, solar, etc.	0.4	0.6	0.9	2
Biofuels and waste	10.3	10.1	9.4	9.3
Total renewables	**12.8**	**13**	**12.6**	**13.8**
Nuclear	6	6.7	5.6	5
TPES growth rate % 1990	-	14.4	46.5	62.9

Table 1.1 *– Fuel shares in world total primary energy supply (TPES), from IEA statistics. The last row shows the growth rate of total TPES compared to the level of 1990.*

The dominant position is that the transition to a 100% renewable energy system, while maintaining economic growth, is entirely feasible from a technical and economic point of view. This position, which is based on the theory of green growth, is shared by many scientists [15–22], and is massively relayed by the media and the political class. According to their estimates, renewable energies potential far exceeds current needs, so it would be sufficient to put in

[3]Mainly wind and solar power, but also hydraulic power, whose installed capacity should however no longer increase significantly.

place the appropriate policies and make the necessary investments in renewable energies and in improving energy efficiency. Among the scenarios considered, two trends can be distinguished, depending on whether or not continued economic growth would be accompanied by an increase in energy consumption. Some believe in an absolute decoupling, i.e. an increase in economic growth accompanied by a decrease in energy consumption, through energy efficiency and a "dematerialisation" of the economy. This idea of absolute decoupling unfortunately seems to be a utopia, as indicated in the conclusions of a recent report of the European Environmental Bureau [23] :

"... not only is there no empirical evidence supporting the existence of a decoupling of economic growth from environmental pressures on anywhere near the scale needed to deal with environmental breakdown, but also, and perhaps more importantly, such decoupling appears unlikely to happen in the future."

Historically, no improvement in energy efficiency has ever been accompanied by a decrease in energy consumption, mainly due to the so-called *rebound effect*[4] inherent to the capitalist system. At most, a relative decoupling has been observed in developed countries (i.e. a slower growth of energy consumption compared to the growth of the economy), but this can be explained as much by a delocalisation of energy-intensive activities to less developed countries as by a real decrease in energy intensity. This has been the case in Europe in recent years: although figures suggest an absolute decoupling of economic growth and greenhouse gas emissions, the primary cause is in fact the outsourcing of a significant proportion of its emissions, mainly to China, India and Brazil. If, instead of accounting for the emissions emitted within the territory of a country (called *production-based emissions*), we account for those linked to the consumption of goods and services (*consumption-based emissions*), we note that greenhouse gas emissions have in fact slightly increased in all European countries [24]. The latter study shows for example that in the major economies of Western Europe, net imported emissions account for 20 to 50% of consumption-related emissions.

Since an absolute decoupling seems unrealistic in the light of the trends observed to date, renewable energies should be able to fully replace fossil fuels

[4] A classic example is provided by car engines. Technical progress has led to significant savings in fuel and pollutant emissions for the same use. These savings have, however, been largely offset by an increase in the number of kilometres travelled, as well as by the use of heavier vehicles (because they are more powerful and better equipped), and therefore more energy consuming.

on the one hand, and on the other hand, they should continue to ensure the increase in energy consumption linked to economic and demographic growth.

The key to coherent climate policies therefore lies in the most accurate possible estimate of the real development potential of renewable energies. Based on the dominant discourse, the perceived message is that there is no limit to their development. Researchers are divided on the subject, as shown by the disparity in global wind potential estimates found in the literature (Fig. 1.3). On the one hand, there are several orders of magnitude between the lowest and highest estimates, and on the other hand these estimates do not seem to converge over time, quite the contrary. If we really have resources far beyond our needs, there seems indeed to be no technical barrier to energy transition. Unfortunately, the most "optimistic" estimates of the potential actually available seem to overlook a number of physical and technological limitations [25–28].

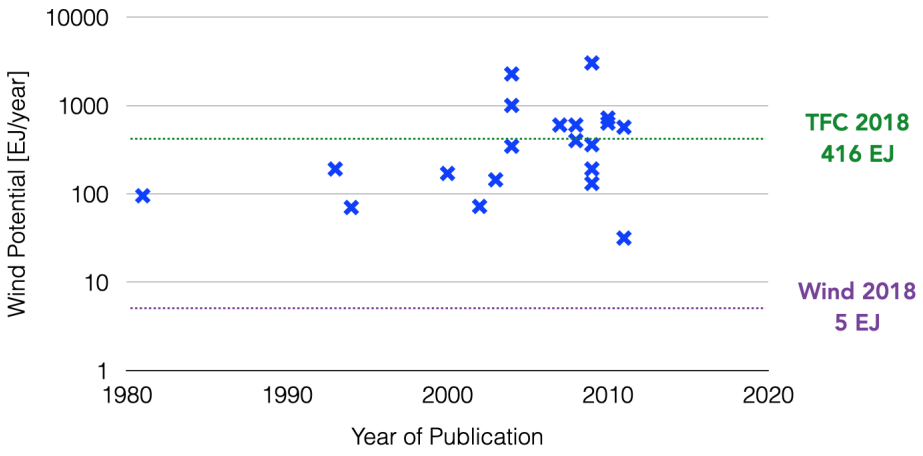


Figure 1.3 *– Global wind electricity production potential estimates from the literature, data from Dupont et al. [29], compared with today's total final consumption (TFC).*

1.1.3 Consideration of physical limits

Besides the dominant discourse promising green growth, voices are being raised to challenge this blind faith in human ingenuity, and these studies promising the energy transition without profoundly questioning our living standards. They points to the limits, severely constraining the amount of renewable energy that can be harnessed globally. Over the last ten years, models have been developed which, although based on sometimes very different methodologies and hypotheses, share common conclusions: the energy transition could be accompanied by an exacerbation of the capital needs of the economy, resulting, under certain conditions, in an extended phase of economic decline. 50 years later, despite all the technological advances, and although the causes of the collapse are different, the conclusions of the Meadows report are still very much valid.

Models following this trend all attempt to take into account the physical limits in terms of *availability*, i.e. how much renewable energy is actually exploitable, and *accessibility*, i.e. at what cost this energy can be made available for human activity.
To study availability, the most conventional method is based on so-called *top-down* analyses. Starting from the total amount of incident solar radiation, models, known as global circulation models, make it possible to estimate the fraction that reaches the earth's surface (a significant part of it being dissipated in the intermediate layers of the atmosphere). Methods that add up local potentials without taking into account the maximum rate of energy actually generated at the global level can lead to inconsistencies. The most telling example is wind energy: while it is well known that the production in very large wind farms is strongly constrained by the interactions between successive rows due to the wake effect, few studies take into account the limits of the power that can actually be extracted at the global level.
In order to study accessibility, *bottom-up* methods are usually applied, where local constraints are taken into account in order to estimate the places on earth that are really accessible for the implementation of renewable power plants. In addition, life cycle analyses, or other methods for estimating the costs associated with the different technologies, make it possible to estimate the financial and/or energy profitability of these sites. An indicator that is increasingly used to study the energy efficiency of any energy transformation process, and on which this thesis is based, is the EROI, which is defined in detail in Chap-

ter 2.

It is imperative to combine these two aspects (availability and accessibility), which is the subject of the first part of this thesis.

1.1.4 Economic impacts of the energy transition

It is not simply a question of taking into account these physical limitations constraining the deployment of renewable energies, it is also a question of understanding the impacts that a change in the energy system would have on our economic model. Without taking into account the strong link between economic activity and energy consumption, it is impossible to predict how the economy can react and adapt to a radical change in the way energy is produced, and to a potential decrease in energy return rates. Models presenting 100% renewable scenarios within a few decades also promise that this energy transition will create many jobs (a net gain of almost 25 million jobs in [18], 35 million by 2050 in [30]). Behind this, however, lies a much less promising reality, since it implies that in the future we will need to mobilise more labour, and also more capital, to meet our energy needs. This can only result in a decrease in the activity of other economic sectors, less "vital" but just as essential to ensure the continuity (or even the improvement for certain populations) of our living standards.

The second part of this thesis therefore aims to study and quantify these impacts, by combining an energy model with an economic model.

1.2 Thesis questions and objectives

In summary, although there is general agreement that we should urgently move away from fossil fuels and accelerate the transition to a renewable and sustainable energy system, there is no consensus on the possible and desirable pathways to achieve this. Given the challenges the world is facing, it is essential to accurately estimate the real potential of renewable energies, mainly wind and solar, as their installed capacity is expected to increase exponentially over the coming decades. It is also imperative to reconcile the world of energy specialists with that of economists, in order to truly understand the implications of a transition towards a decentralised and capital-intensive energy system on the functioning of our economy.

This thesis aims to answer the two following scientific questions:

- What would be a realistic limit to the global potential of wind and solar energy, and what would be the associated EROI?
- Given the link between energy availability and economic growth, and based on the answer to the previous question, (i) is the energy transition feasible, and if so, at what pace, and (ii) what would be the economic impacts of this transition?

To answer the first question, a new methodology is proposed to estimate, as accurately as possible, an upper bound for the global potential of wind and solar energy and the associated EROIs.

To answer the second question, a stylized macroeconomic model with two sectors (energy and economy) is presented. The results of the methodology developed for wind and solar potentials are used to assess the evolution of a number of technical parameters of the economy as a function of the penetration rate of renewable energies. By considering different scenarios, the economic model can then assess if the transition to a 100% renewable energy system is feasible within the current century.

The models and results presented in this thesis are based on the following assumptions:

- The analysis focuses on wind and solar energies, which are considered as the two main sources of energy for the future (see in particular [31] for a detailed justification, this position also being that of the IEA and of the U.S. Energy Information Administration (EIA) [32, 33]). Apart from biomass, other renewable energy sources are not expected to play a significant role in the energy transition. Indeed, either their potential for future development is limited (hydropower), or their technical potential is relatively low (wave and tidal energies), or their development does not seem as promising as expected (geothermal energy). Finally, nuclear power is deliberately omitted from the discussion. Indeed, its use is highly controversial, and as a result it is excluded from the energy transition policies of many countries. Moreover, its share in global primary energy production is relatively small, and moreover it is declining (see Table 1.1).

- Biomass is the third renewable energy source that will play an important role in the future, but the choice was made to focus only on solar and wind power and to add an economic dimension to the thesis. Indeed, although biomass is currently the leading source of renewable energy worldwide, it is mainly for domestic use by the most underprivileged populations. In addition to presenting a very wide variety of deposits and conversion technologies, its intensive development as an energy source is highly controversial as it competes with other essential uses (mainly food supply, but also biodiversity conservation, CO_2 capture, etc.). This aspect of the research is discussed at the end of the thesis in the perspectives (Chapter 7).

- The study of wind and solar potentials is limited to production directly at the site gate, meaning that the management of the intermittency of these energy sources has not been taken into account. However, studies show that from 25 to 30% of renewable electricity in the energy mix, the quantity of energy curtailed[5] increases significantly [34]. Storage needs also increase significantly with the energy transition, which increases the capital needed by the energy sector and decreases the final energy produced (given the efficiencies associated with storing and restoring electricity) [35, 36]. For this reason, in the following work we will always speak of an upper envelope for the calculated potential. Taking the intermittency into account is beyond the scope of this work, since it would have been necessary to add a temporal discretisation to the spatial one and to incorporate a complete portfolio of the options available to manage it (grid management, storage, overcapacity, etc.).

[5]The curtailment concerns the decision to voluntarily stop, despite the presence of wind or sun, the production of a wind or solar unit for various reasons (grid overload, nuisances...).

1.3 Outline of this thesis

This thesis is structured as follows. Chapter 2 presents key concepts used in this work. First the concepts of EROI and net energy analysis are developed in detail, then the chapter ends with a literature review on existing energy-economy models. Chapter 3 presents the methodology developed in order to assess an upper limit for wind potential at a global scale. The main result is a decreasing curve of the exploitable potential as a function of the EROI. Regional results are also explored and discussed. In Chapter 4 the methodology is adapted to global solar potential, considering different types of solar photovoltaic (PV) and concentrated solar power (CSP) technologies. The next chapter combines the results of Chapters 3 and 4 in order to obtain a better visibility of the total potential that can be achieved. The results are also presented at the European level. Chapter 6 first presents the macroeconomic model developed in order to evaluate the direct and indirect energy inputs to the energy sector, hence the societal EROI. Then, with the outputs from the energy model, a dynamic model is developed in order to study the possible trajectories of the energy transition. The feasibility and duration of the transition is assessed on the basis of different assumptions and scenarios. Finally, Chapter 7 summaries the main findings of this thesis and ends up with a set of possible future developments, both at the level of the energy model and at the level of the macroeconomic model.

Quiconque pense fait penser.

Voltaire

2

State of the art: EROI and energy-economy models

2.1 Net energy analysis and EROI

In order to assess realistic upper limits for wind and solar potentials, and the possible impacts of the energy transition on the economy, it was decided to look at this issue with a particuler point of view: the one of *net energy analysis*.

The main idea is simple: it takes energy to produce energy, whether it is renewable or not. As presented in the introductory chapter, the question remains as to whether or not renewable energy can provide the current and future needs of our growing society. To contribute to this debate, we believe that the best way to measure the sustainability of an energy system is to study in detail its own energy needs and, thus, the energy surplus it is capable of providing.

To introduce the concepts used in this work, we make a simple analogy

with a farmer. If a person producing food is just able to produce his own food needs, he will spend his life producing food without any other development perspective. If, on the other hand, he is able to produce more than his own self-consumption, then the possibility of merchandising his production opens up, and with the income generated this farmer will be able to improve his living conditions by purchasing goods and services, other than his basic needs for food. Some may think about recreational and consumer goods, but for many of the world's land workers this surplus means being able to satisfy much more basic needs: housing, education and health care for their families.
If, after satisfying these so-called *basic needs*, there is still a surplus (obtained either by increasing the quantity produced, or by improving the quality of its production, by switching to organic farming for example), then there is the possibility of satisfying what are know as *secondary needs*. These needs are not essential for human survival, but are nevertheless indispensable for its psychological and social development. Satisfying these needs improves the quality of life of those with access to them.

From this example, admittedly simplistic, emerges the idea that an individual's quality of life would be directly linked to the surplus that he is capable of generating, compared to his own self-consumption. This comparison can be extended to the level of a society as a whole, and to the analogy between a society, which would be described as underdeveloped, where all the workforce is used for the production of elementary goods and services, and a more developed society, where only part of the workforce works in elementary goods production, while another part can devote itself to activities that generate a surplus of comfort for its population.

What if the same were true for the amount of energy that a society is able to produce thanks to its energy system? It was indeed emphasised in the introductory chapter that energy is an essential factor of economic production, and that economic development has been made possible thanks to access to abundant and easily accessible sources of energy. As energy and food productions have ceased to be the main occupation, societies have been able to diversify and to improve the living standards of their citizens, by providing access to what was qualified earlier as secondary needs.

It therefore seems relevant to study and quantify this ease of access, through

the study of a particular indicator: the energy return rate. This involves evaluating, for a specific conversion process of primary energy (i.e. as available in the nature and therefore not directly usable) into final energy, or for an entire sector, on the one hand the total amount of energy that can be generated, and on the other hand all the energy that has had to be invested, directly or indirectly (i.e. in the form of goods such as infrastructure, services, etc.), during the lifetime of the system under study. The ratio between the final energy produced and the sum of the inputs converted into energy flows gives an idea of the energy return rate of the system in question, which is called the EROI (Energy Return on Investment) (sometimes known as the ERoEI (Energy Returned on Energy Invested)).

$$\text{EROI} = \frac{\text{Final energy produced}}{\text{Direct and indirect energy inputs}} \tag{2.1}$$

In Fig. 2.1, this concept is schematised in a simplified way.

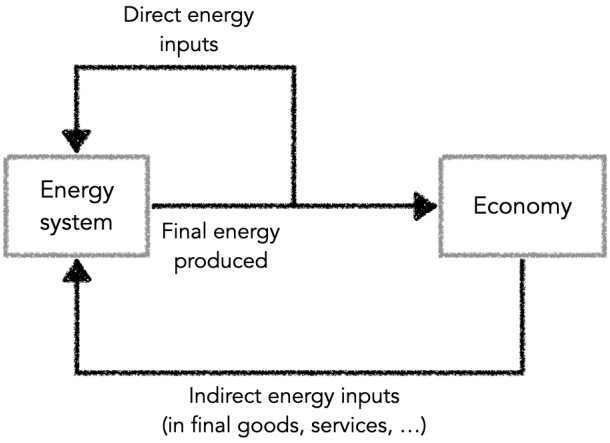


Figure 2.1 *– Simple representation of the EROI. The "direct" inputs represent the energy in final form that is directly re-injected into the energy system, and the "indirect" inputs represent the energy that has been needed by the economy to produce the goods and services necessary for the proper functioning of the energy system.*

While the estimation of the total amount of energy produced is generally not very controversial (variants exist, however, see below), it is much more difficult to estimate the energy invested and to set limits on what should and

should not be included in the calculation of the denominator of the EROI. In the case of fossil fuels, most of the energy invested is the energy in direct form that is continuously used to extract and transform these fuels. In the case of renewables, such as wind and solar, most of the energy investment is made before electricity generation begins, for the manufacture of the equipment (and thus the extraction and processing of the raw materials), and its installation on site.
The final energy produced before subtraction of possible self-consumption of energy is sometimes referred to as the *gross* energy produced while the difference between this gross energy and the energy that had to be invested is called the *net* energy produced. The latter is the energy that will feed the economy to meet basic needs in priority. The surplus, if any, can then be used for consumption or investment activities. The difference between gross and net energy represents the self-consumption of the energy sector (in direct **and** indirect form), and is not available to fuel the other economic activities.

$$\begin{aligned} \text{Net final energy} &= \text{Final energy produced - (direct + indirect energy inputs)} \\ &= \text{Final energy produced x (1 - 1 / EROI)} \end{aligned}$$

After the emergence in the 1970s of the concepts of net energy and EROI, interest in this type of analysis rapidly declined. At that time, fossil fuels, because easily accessible, had high EROIs. Only when their energy profitability started to decline did the issue of energy costs reappeared, especially for oil. Indeed, as easily accessible oil reserves began to be depleted, oil-extraction became more energy-intensive, which had a negative impact on its profitability, rekindling interest in studying its energy profitability.

In the followings, various concepts are presented. First, in Section 2.1.1, the concept of EROI is defined in detail, and the boundaries will be clarified (i.e. what is included or not in the calculation). Indeed, there is a rather detailed scientific literature on the subject. There are different levels of EROI according to the boundaries and temporality chosen, each of these definitions being relevant in a particular context.

Once these concepts are well defined, we focus in Section 2.1.2 on the idea that there is a link between a society's EROI and its level of development, and thus the quality of life it can offer to its individuals. It is the idea behind

the surplus that was necessary for the farmer to start satisfying his secondary needs. Several scientists have looked into this theory, and discussed the fact that there would be a critical threshold for the EROI at the societal level, below which the quality of life could be affected.

Therefore, since there would be a critical threshold for the EROI, it would be important to ensure, in order to maintain current living standards, that the EROI of our energy system does not decrease (too much) over time. Theories have been developed to model the evolution of the EROI with resource exploitation, which are presented in Section 2.1.3. It is shown that the EROI of all energy sources is expected to decline due to the gradual depletion of the available resources and the increasing need for infrastructure. Based on these models, it would appear that the EROI of the energy system is expected to decline over time.

Finally, the limitations of such an aggregate indicator as the EROI are presented. The study of the EROI alone is not sufficient to characterise the real potential of an energy source, nor its ability or not to substitute for historical fuels.

2.1.1 Definition and boundaries

A priori the EROI definition (Eq. 2.1) is quite simple and has many advantages. In theory, the EROI should allow for easy comparison of different energy sources and their respective extraction and transformation technologies. However, without a clear methodology that is shared by all, it is difficult to compare the figures obtained. These debates are the subject of numerous publications [37–42]. The conclusion is that all the definitions are relevant, but that it is necessary to be very transparent about the assumptions made when estimating a particular EROI. Different authors have examined detailed methodologies to standardise these concepts [37, 43, 44], and have proposed new terminologies for the different EROI definitions. In the end, it can however be seen that the generic term EROI is the most widely used in practice. We propose to summarise these different definitions here, and we will eventually explain the EROI definition chosen for the rest of this work.

Discrepancies between estimates concern the following levels: the boundaries chosen for the calculation of the numerator and of the denominator, the temporality of the calculations (over the lifetime or over one year), and whether

or not to include a correction factor related to the quality of the energy produced. The distinctions presented here are mainly based on the methodological work of Murphy et al. [37].

The numerator For fossil fuels, there are large differences in the figures when considering the energy produced at the site exit and the energy available to the end user (at the petrol pump for example). Three levels are therefore distinguished by Murphy et al. [37]: extraction (*mine-mouth*), transformation (*refinery gate*), and distribution (*point-of-use*). These levels are represented in Fig. 2.2.
According to Brockway et al. [40], the EROI of fossil fuels for electricity generation in 2011 is estimated to decrease from ∼30 to 6 between the mine-mouth and the end user.

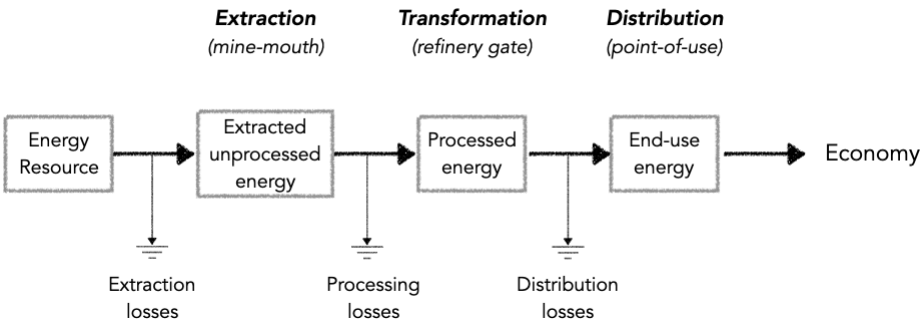


Figure 2.2 *– 3 different levels for the numerator of the EROI, adapted from [37]. This distinction is particularly adapted for fossil fuels.*

In the case of renewable energies, these different levels tend to overlap. The distinction between the site production and the end user is the consideration of power line losses and storage requirements. However, few studies take the latter into account because they do not appear at the level of a given site, but only when the share of renewables in the energy system exceeds a certain threshold (25-30% according to [34, 35]), which is far from being reached today. To date, only the MEDEAS model proposes a methodology which allows these needs to be dynamically taken into account at the global level [36].

The denominator On the one hand, inputs increase sharply depending on the definition of the numerator, on the other hand one can also be very exhaustive in the range of categories that are included in the energy needs accounting. 5 levels are distinguished by [37]:

1. Internal energy consumption: the final energy produced and directly self-consumed within a production site.
2. External energy consumption: the final energy produced or transformed outside a site and consumed by that site for its operation.
3. Materials consumption: the grey energy contained in the infrastructure of a given site (from the energy required to extract raw materials to the energy used to install the infrastructure on site).
4. Auxiliary services consumption: the final energy consumed by services (goods transport, maintenance, cleaning, etc.).
5. Labour consumption: the energy needed to "make a living" for the workers.

Externalities or environmental costs can also be added [45]. These externalities can be negative (soil erosion, pollution, loss of habitat, etc.), as well as positive (creation of jobs, etc.). In practice, given the complexity of transforming these externalities into energy flows, these impacts are usually included in other indicators and not in the EROI calculation.

The inclusion of the energy produced and directly self-consumed on a production site (i.e. corresponding to level 1) is the subject of a methodological discussion. Brandt and Dale [43] introduce the appellation *external*, which consists in considering only the self-consumption of direct energy *external* to the sector or process under study. They define 4 energy return ratios (ERRs), each giving specific information about the system under study: the GER (gross energy ratio), the NER (net energy ratio), the GEER (gross external energy ratio) and the NEER (net external energy ratio). The differences lie in whether the numerator takes into account the total final energy produced (i.e. the gross energy), or only the net final energy produced, and whether or not the numerator and denominator include *internal* energy consumption, i.e. the energy directly self-consumed within a production site.

Let E_{prod} be the (gross) amount of energy produced, $E_{dir,internal}$ the internal direct energy inputs, $E_{dir,external}$ the external direct energy inputs, and E_{ind} all the indirect energy inputs. Then the net amount of energy produced would be $E_{prod,net} = E_{prod} - (E_{dir,internal} + E_{dir,external} + E_{ind})$, and we have the following ratios:

$$\begin{aligned} \text{GER} &= \frac{E_{prod}}{E_{dir,internal} + E_{dir,external} + E_{ind}} \\ \text{GEER} &= \frac{E_{prod}}{E_{dir,external} + E_{ind}} \\ \text{NER} &= \frac{E_{prod,net}}{E_{dir,internal} + E_{dir,external} + E_{ind}} \\ \text{NEER} &= \frac{E_{prod,net}}{E_{dir,external} + E_{ind}} \end{aligned}$$

Temporality In general when calculating the EROI of a specific site or technology, calculation of the energy produced and invested is carried out over the lifetime of the installation, through life cycle analyses for example. If, on the other hand, we look at the scale of a sector or a geographical area, composed of a large number of installations at different stages of life, it becomes difficult to estimate the energy invested and produced over the lifetime of all the installations. Annual energy production and consumption data are then used to approximate the EROI of the sector. Various authors advise that the calculated EROI should be called a Power Return On Investment (PROI) because it corresponds to an estimate for a specific year [38, 44, 46, 47]. The PROI and EROI converge only in a stationary state. During the growth phase of the energy system, important energy flows can be observed for the construction of new infrastructures (this will be particularly the case during the growth phase of renewable energies), the PROI (calculated with annual flows) will then probably be lower than the life-cycle EROI of the system under study. The vast majority of estimates made at a more aggregated level than that of a particular facility use annual data and are therefore PROIs.

Primary energy conversion factor (PEF) A final controversial issue is whether or not to include a factor to account for the difference in quality between energy carriers. The justification for applying a correction factor is to consider that a joule of electricity or heat as not the same economic utility as a joule of coal, for example. Indeed, electricity production is currently

mainly based on the combustion of fossil fuels, given the associated yields, it takes between 2 and 3 joules of fuel to produce 1 joule of electricity. It is generally advisable to transform the electricity inputs into their *primary energy equivalent*, in order to take into account the energy that has actually been invested to produce these services. To estimate this conversion factor accurately, the electricity mix of the geographical area under study is used as a basis. At the global level, Kis et al. [48] find a conversion factor of electricity to primary energy of 2.24 for 2015 at the global level, based on IEA data for the energy mix, and on the average conversion efficiencies of the electricity generation technologies. According to this principle, any electricity input from the grid should be multiplied by the PEF.

EROI definition for this thesis First, we will study the standard EROI of two specific energy sources (wind in Chapter 3 and solar in Chapter 4), and we will end up looking at both standard and point-of-use EROIs at the societal level (Chapter 6). In line with the above considerations, the EROI of wind and solar are calculated over *the lifetime of the installations*, while the societal EROI, which is in fact a PROI, is calculated for *a reference year*.

Standard EROI In Chapters 3 and 4, the EROIs calculated correspond to the definition of the EROI standard (EROI_{st}) or primary, as defined by de Castro and Capellán-Pérez in [42]. Following the most widely used methodology, it was chosen to consider the gross final energy produced, i.e. electricity, in the numerator and to stop at the site exit. The distribution of electricity is therefore not taken into account: neither line losses in the network, nor the eventual storage needs (which do not appear at the level of a given site), nor the adaptations to be foreseen at the level of the electrical grid.

In the denominator, all direct final energy supplies are considered, and indirect supplies included in infrastructure and services (levels 1 to 4 of the denominator). Level 1 (internal energy consumption) is included here at both the numerator and denominator, but will be discussed in the following chapters. Finally, in line with the discussion above, a PEF is applied to any electricity supply (from outside a production site).

$$\text{EROI}_{std} = \frac{\text{Final energy produced by the plant or energy source}}{\text{Direct + Indirect (in capital and services) final energy inputs to produce the energy}} \tag{2.2}$$

Point-of-use EROI In Chapters 5 and 6, the distribution of electricity is included and discussed. Only direct energy inputs for the distribution are considered, so the point-of-use EROI calculated correspond to the final EROI defined by de Castro and Capellán-Pérez [42], and to the EROI at final stage in the contribution of Brockway et al. [40].

$$\text{EROI}_{pou} = \frac{\text{Final energy delivered}}{\text{Direct + Indirect (in capital and services) final energy inputs to deliver the energy}} \tag{2.3}$$

The inclusion or not of the internal direct energy consumption lead to different EROIs, that are discussed.

Societal EROI The estimate of the societal EROI is part of the macroeconomic model presented in Chapter 6. Energy and economic data, as well as indicators estimated from input-output tables, are used to estimate the direct and indirect energy inputs of the whole energy sector, for a reference year.

To be consistent with available IEA data about the energy consumption of the energy sector, internal energy consumption within a production site (level 1) is excluded from both the numerator and the denominator of the societal EROI calculated.

2.1.2 EROI and quality of life

The example of the farmer presented at the beginning of this chapter gave us the intuition that there would be a link between the energy surplus that a society is capable of producing, and the quality of life of its individuals. This intuition is schematised in Fig. 2.3, with a very simplified representation of the energy sector. Starting from a certain amount of primary energy that a society is capable of harvesting, and given the conversion techniques at its disposal, a certain amount of final energy is produced. Of this amount of energy produced, a fraction is reinvested in primary energy extraction and conversion techniques, either directly or indirectly. The remaining, i.e. the net energy, is then available to other sectors of the economy. The society will satisfy in priority the basic needs of its individuals, and if a surplus remains, it can be used to support consumption and growth-generating activities. If the EROI decreases, the net energy available decreases, and since the basic needs of the population are fixed, consumption and growth are impacted. One can then imagine that below a given threshold, the amount of net energy available de-

creases so much that there would be no more consumption and growth, and (perhaps) just enough left to meet basic needs.

The estimation of a lower bound below which a prosperous way of life would not be sustainable remains highly speculative. Overall, it can be seen that estimates of the minimum societal EROI vary significantly from one contribution to another. This may be the result of differences in (i) the methodology, (ii) the boundaries used for the EROI calculation, and (iii) the objective that this lower bound is supposed to reflect. As a result, the estimates are hardly comparable.

Hall et al. [49] estimate that the main fuels would need to offer an EROI around 5 to maintain "all that we call civilization", but this figure is the result of an educated guess, not a calculation. Using an econometric equation linking growth rates, energy expenditures, capital formation and population for the United States, Court and Fizaine [50] estimate the minimum EROI necessary to maintain economic growth at 11. A recent study by Court [51] shows that the minimum sustainable societal EROI at the global level has declined from just over 20 in 1900 to stabilize at around 6 since the 1970s. This is the result of significant improvements in the efficiency of primary to final energy conversion and in final energy use, which have however slowed down in recent decades. Brandt [52] uses an input/output model of a fictive 4-sectors economy whose intersectoral technical coefficients are estimated from US data and expressed in orders of magnitude (i.e. in powers of 10). This model leads to a minimum societal EROI of around 5. Below this threshold, the needs, especially in terms of capital, of the energy sector become too heavy for the economy to bear.

Some studies have shown the correlation between GDP and energy consumption [4], but few research has been conducted on the impacts of energy quality, energy quantity, and EROI levels on economic growth and prosperity, except the work of Lambert et al. [53]. They proposed a methodology for estimating the EROI at a country level. The national societal EROI is calculated as the amount of energy that the country can produce or import with a unit of energy invested in its economy. More precisely, (i) the numerator is the amount of energy produced or imported with one dollar of GDP, and (ii) the denominator is the amount of energy needed by the country to produce that dollar. The denominator corresponds to the energy intensity of the country,

i.e. the ratio between energy consumption and GDP. Linking the estimated societal EROI and the Human Development Index (HDI) for a large sample of countries, Lambert et al. have shown that (i) societal EROI and HDI are positively correlated[1] and (ii) with few exceptions, countries with a high level of development (HDI above 0.75) are characterised by a societal EROI above 20.

Clearly there is a lack of understanding of the potential impacts of a decreasing EROI accompanied by a shift in energy quality, due to a lack of data on the one hand but also to a lack of research on the other hand. Given the potential impacts of a decreasing EROI on our living standards, it is important to quantify future EROI scenarios on the one hand, while working on this minimum EROI threshold on the other hand.

[1] The relationship is, however, non-linear (in the sense that the HDI increases less and less rapidly with societal EROI) and is characterized by a saturation effect.

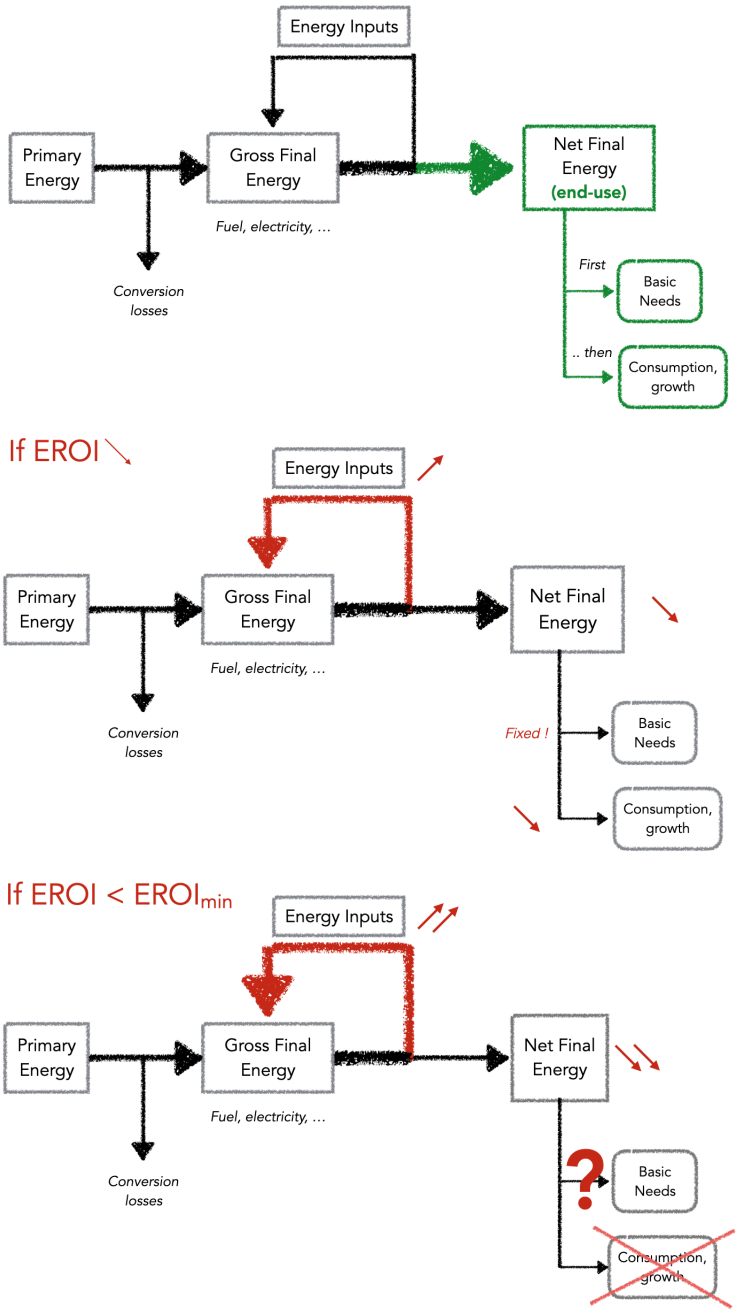


Figure 2.3 *– Simple diagram to illustrate the possible implications of a decrease in the societal EROI on consumption and growth activities, given a fixed amount of gross final energy produced.*

2.1.3 EROI dynamics

Several studies have shown that the EROI of fossil fuels (mainly oil and gas) decreases over time [40, 53–57]. Conventional reserves are depleting and it is therefore necessary to turn to fields that are more difficult to exploit. This observation is also confirmed for most non-renewable raw materials (see [58] for metals): the richest and most easily accessible deposits are exploited first, so that the complexity of extraction and transformation processes can only increase with the exploitation of the resources. Although technical progress can improve the efficiency of the infrastructure used, it is not sufficient to counteract the depletion effect.

On the other hand, studies have also estimated that most renewable energies have significantly lower EROIs than the EROIs historically achieved by fossil fuels (e.g. [49], the results of which are shown in Fig. 2.4, but also [59, 60]). On the basis of these figures, modern renewables would indeed present much lower EROIs, and sometimes even below the critical thresholds estimated in the previous paragraph (as it seems to be the case for solar photovoltaic and biodiesel).

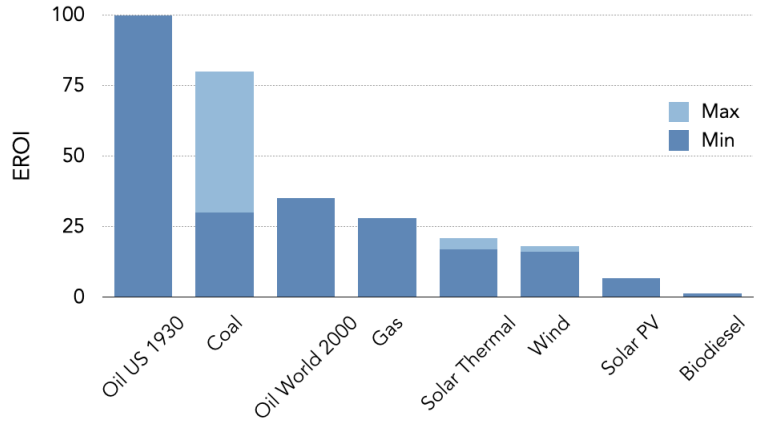


Figure 2.4 *– Estimations of the EROI of different technologies, from the study of Hall et al. [49].*

However, more recent studies have revised EROI estimates for fossil fuels downwards, in particular by considering end use rather than extraction only. For electricity generating technologies, Kis et al. obtain the estimates shown in Fig. 2.5. According to those, wind power would have an average EROI comparable to coal-fired power plants.

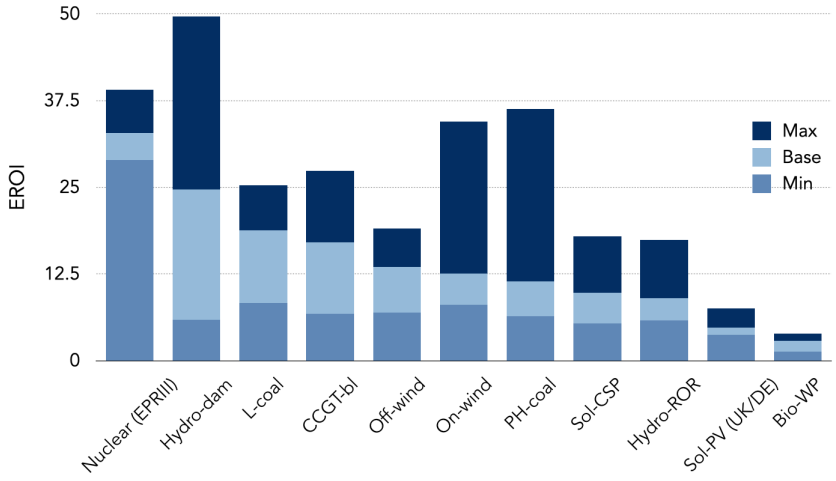


Figure 2.5 *– GEER estimates, data from Kis et al. study [48]. Legend: L-coal: lignite coal plant, CCGT-bl: combined cycle gas turbine baseload, PH-coal: pulverized hard coal , Hydro-ROR: run-of-river hydroelectricity, Sol-CSP: concentrated solar power - parabolic through, Sol-PV : polysilicon solar-PV, Bio-WP : biomass wood pellets.*

Brockway et al. [40] also argue that EROI estimates of fossil fuels must necessarily be made at the end use level in order to allow for an objective comparison with renewables, which produce electricity. According to their methodology, for electricity generation, the EROI of fossil fuels would decrease from ∼30 at the extraction level (defined as the *EROI at primary energy stage*), to about 6 at the end user level (*EROI at final energy stage*) (with a temporal decrease from 6.8 for 1995 to 6.1 for 2015). As a result, the EROIs of fossil fuels would not be so far away from those of renewable energies which are supposed to replace them.[2]

[2]For other uses such as transport or high-temperature industrial processes, the conclusions are of course different.

Based on the results presented, we see that the comparison between the current EROIs of fossil fuels and those of renewable alternatives is subject to debate, but that EROIs of fossil fuels decrease well over time, due to resource depletion. Just as the EROIs of fossil fuels are impacted by the quality of the exploited deposits, the EROIs of renewables will be impacted by the quality of the exploited sites. Assuming that the most profitable sites, i.e. relatively accessible, close to consumers and with good resources, are exploited first, the efficiency of renewable power plants will necessarily be impacted by their expansion.
In fact, two contradictory effects can be expected: on the one hand, technological progress will make it possible to further reduce the amount of energy needed to produce them and to increase the amount of energy produced. On the other hand, EROIs will be impacted by the need to exploit less favourable sites. However, technological progress is constrained by physical laws, the limits of which are close to being reached in many areas, driven in particular by globalisation coupled with constant pressure on companies' profitability. According to the work of scientists working in this field, the decline in the quality of the resource would eventually outweigh the technological progress, leading to a decline in the energy efficiency of renewable energies when the world's installed capacity increases significantly [31, 58, 61, 62].

The idea of modelling the evolution of the EROI of energies according to their exploited potential was developed by Dale [60], an idea he used to model the future evolution of energy supply in his GEMBA model [63, 64]. This idea is represented in Fig. 2.6, where it is shown that the EROI of a given resource would tend to increase initially due to technological progress, but this latter being limited, the negative impact of the decrease in quality of the sites ultimately prevails and the EROI ends up decreasing with the cumulative production. This model applies both to renewable energies (the cumulative production is then the annual production), and to non-renewable energies (the cumulative production then represents the total quantity produced since the beginning of the exploitation of the resource considered). The combination of these curves with an estimate of the minimum EROI threshold would thus make it possible to give an estimate of the exploitable potential of a given resource. Dale used point estimates of the EROI and of the technical potential of the

main energy sources to reconstruct these curves. By integrating them into a system dynamics model, he showed that the decrease in the EROI of all energy sources, and thus of the energy system as a whole, leads in the long run to a decrease in the amount of energy produced at the global level due to feedback effects. De facto, economic activity would also decrease.

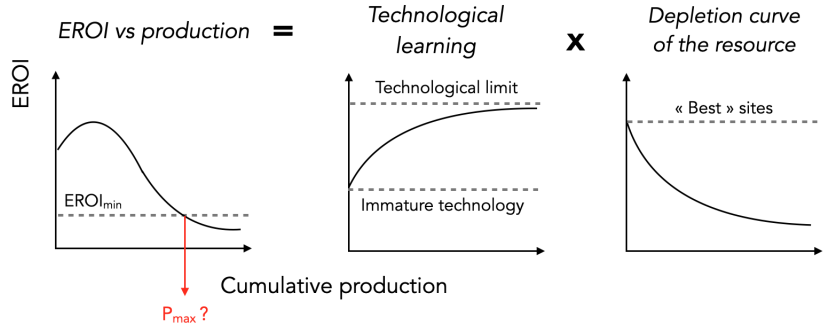


Figure 2.6 *– Dynamic function for the EROI, adapted from [60]. The EROI is the product of the technological learning (an increasing curve) and a depletion cruve representing the decreasing quality of the sites.*

Since then, other studies have exploited the declining energy efficiency of different energy sources, and all conclude that energy production is declining as the capital needs of the energy sector become too important for the economy to sustain, and its output (and thus the GDP) eventually declines. These models, which link energy consumption and economic activity, are described in Section 2.2.

EROI limitations Having a dimensionless indicator is an advantage but also presents its limitations. The main ones that we point out, and which we wish to address with this work, are that (i) this indicator does not give any information on the total potential of the resource in question (one could therefore have a technology with a very favourable EROI but whose total potential is negligible at the global level), and (ii) it does not provide any information on the distribution of the needs of the energy system between those in the form of final energy and those in the form of capital and services. However, one of the conclusions of the simulations carried out with Dale's GEMBA model was

that it is the changing needs of the energy sector that causes a slowdown and then a decrease in economic growth.[3]

2.2 Energy-economy models

Back in 1927, Tyron already wrote [65]:

"Anything as important in industrial life as power deserves more attention than it has yet received from economists."

The close link between energy and the economy is certainly not a new observation, for many years scientists have been studying this correlation and its implications [66–69]. These authors advocate for a better consideration of energy by neo-classical economists, who still represent the dominant point-of-view. According to the former, policy decisions affecting millions of people and endangering our ecosystems are based on economic models that do not take sufficient account of, or even ignore, the fundamental laws of nature.

The most widely used models to study the energy transition and its impacts on climate change are integrated assessment models (IAMs). These models belong to the dominant literature presented in the introduction and most of them seem to show that the energy transition would only be constrained by the available monetary investments. This type of models is notably the basis for the recommendations made by the IPCC.

However, many limitations of IAMs have been pointed out in the literature [36, 70]. Among these limitations: the availability of fossil and renewable resources is largely overestimated, the investments and the materials needed for the energy transition, as well as the needs for managing the intermittency of renewable resources, are often ignored. These models fail to capture the feedback principles that apply to different sectors of the economy, considering instead a unidirectional link between economic growth and energy consumption (GDP growth leads to an increase in energy production, but constraints on energy supply do not limit GDP growth). According to the literature, system dynamics models would allow a more correct representation of these interactions, in particular the fact that the limited availability of certain resources can lead to an economic decline.

[3] Dale estimates that for non-renewable energies, energy inputs in the form of capital account for 10% of the denominator of the EROI, compared to 90% for renewable energies, which are much more capital intensive.

2.2.1 Biophysical approach

To address these limitations, models, following the principles of *biophysical economics*, have been developed in order to highlight the feedback mechanisms that arise due to constraints on the availability of natural resources.

One of the first biophysical models, taking into account the interactions between population, industrial growth, food production and the limits of natural resources, is the World3 model, the first version of which was published in 1972 [11]. The simulations carried out show that the shortage of raw materials and the excessive increase in pollution, caused by the industrial system and population growth, will sooner or later lead to a lasting global crisis.

Since then, and increasingly over the last 10 years, other models have been presented, with the aim of assessing the feasibility of the energy transition and its compatibility with continued economic growth. While it was the scarcity of raw materials and rising pollution that caused global decline in the World3 model, more recent models have highlighted that the energy transition could result in an exacerbation of the capital needs of the energy sector, with a possible crowding out effect on the rest of the economy in terms of investment allocation. This effect would have a negative impact on economic growth, and if sufficiently strong, the energy transition could be accompanied by a prolonged phase of (suffered) economic decline.

In the following we present in detail two biophysical models which, to date, are the only ones that combine the concepts of net energy and EROI with an aggregated model following the principles of biophysical economics. They aim at assessing the impacts of a change in the energy system (via the energy transition) on the societal EROI and on the economic growth. These models are the GEMBA (*Global Energy Modeling with a Biophysical Approach*) and MEDEAS (*Modeling Energy System Development under Environmental and Socioeconomic constraints*) models.

GEMBA

GEMBA was developed as part of Michael Dale's PhD thesis in 2010 [71], based on the principles of net energy analysis and biophysical economics, and modelled with the software *Vensim*. As mentioned in Section 2.1.3, one of the major contributions of this model is the modelling of the evolution of the EROI as a function of total cumulated production for the main energy sources. The

results then show that the transition to renewable energies would be induced by the decreasing efficiency of fossil fuels. The evolution of energy supply is shown in Fig. 2.7. After peaking around 2060, energy production begins to decline, even though the technical potentials of the different energy sources have not been reached. This is because the rising energy costs of energy production eventually slow down the production of goods in the main economy through the crowding out effect, leading to its decline and thus to a decrease in energy demand.

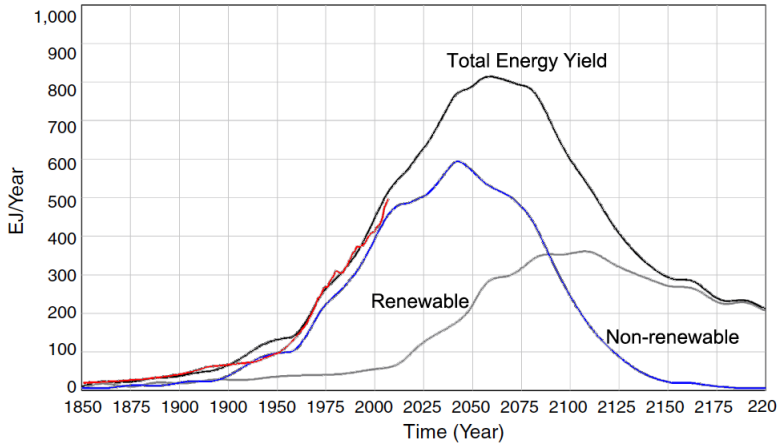


Figure 2.7 *– Results from the GEMBA model [64]. The red line corresponds to historic data, the other lines correspond to the GEMBA model outputs: total (black), non-renewable (blue) and renewable (grey) energy productions.*

However, this model presents certain limitations. First, in modelling the availability of renewable resources, the model of the evolution of the EROI as a function of cumulative production uses point estimates of EROI and total potential to reconstruct the left curve of Fig. 2.6. A more detailed modelling of energy availability could be based on a bottom-up approach, applied to each technology [27, 28, 72–75].

The capital factor (i.e. the ratio between indirect and total energy inputs) could also be modelled in a more detailed way, instead of being fixed at a constant value (10% for non-renewable energies, and 90% for renewable energies).

Finally, in the modelling of the economy, we can highlight the absence of final consumption in the model (i.e. no distinction is made between consumption and investment), as well as the fact that the technical parameters, such as

the energy intensity of the economy, do not evolve over time.

MEDEAS

MEDEAS [36] is also a model of system dynamics, which has been developed with the aim of facilitating the political decisions of the coming decades concerning the energy transition. This model aims to take into account the biophysical, economic, social and technological constraints. It is the most comprehensive model to date, made up of 9 main modules (economy, energy demand, energy availability, energy infrastructures and EROI, minerals, land-use, water, climate/emissions, and social and environmental impact indicators), whose interactions are modelled in a very detailed manner. The modules concerning the economy and the energy system are the most detailed, and they are also those that are of particular interest to us in the context of our research questions.

The economic module is of the input-output type, demand-led and sectorally disaggregated (35 different industries are represented). The World Input-Output Database (WIOD [76]) is used to estimate the intermediate consumptions of these different sectors, as well as their energy intensity. Final demand is calculated as the sum of private and public consumption and capital investment, and the production needed to satisfy this demand is estimated using the technical coefficients of the different sectors. The required production is then confronted with the available resources, in particular energy, and, if there are limitations in terms of supply, the demand may not be fully met.

The model represents 25 different energy sources and technologies. The availability of non-renewables is modelled through a review of the literature on depletion curves for each fuel. For renewables, the model is based on estimates of their potential at the global level, and also takes into account the infrastructure needed to manage their intermittency (storage, grid development, overcapacity and flexible demand management). The model allows us to dynamically calculate the evolution of the EROI of the different technologies, and at the level of the energy system.

The results obtained confirm the conclusions of previous models: the continuation of current trends will lead to significant biophysical shortages and other impacts that will most likely lead to regional retrenchment and conflicts, and ultimately to a lasting global crisis. The results presented in their 2020 paper [36] are based on a reference *business-as-usual* simulation, and 4 scenar-

ios: the baseline scenario takes into account the limits in terms of availability of the different energy sources and the impacts of climate change-related damage. Then 2 scenarios remove one of these 2 constraints, and the last one is the scenario without any constraint. Only this last scenario does not lead to a decrease in energy supply (see Fig. 2.8), and permits a constant increase in GDP of 2% per year until the end of the simulation (2100). In the other three cases, if one or both of the two constraints are activated, energy supply and GDP begin to decline from the middle of the century, eventually reaching levels below those needed to meet the basic needs of the current socio-economic system, as shown by the evolution of the system's EROI in Fig. 2.9.

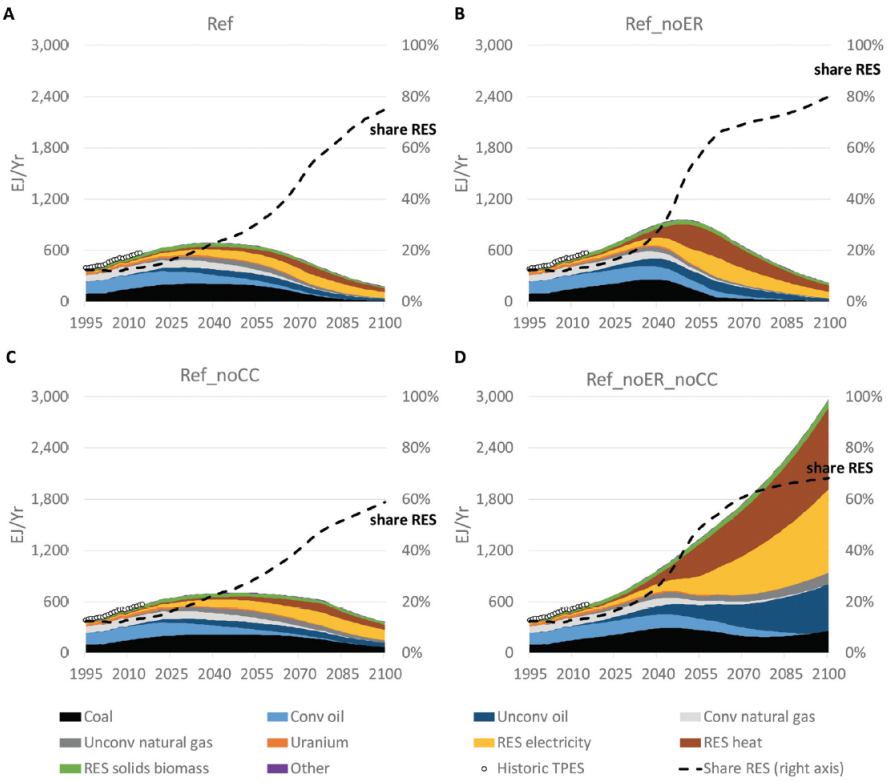


Figure 2.8 *– MEDEAS results from [36]: TPES mix and share of renewables, for the 4 scenarios. (A)Ref is the reference scenario, (B) Ref_noER is the scenario without energy availibitlity constraints, (C) Ref_noCC is the scenario without climate change damage, and (D) Ref_noER_noCC has none of the precited constraints.*

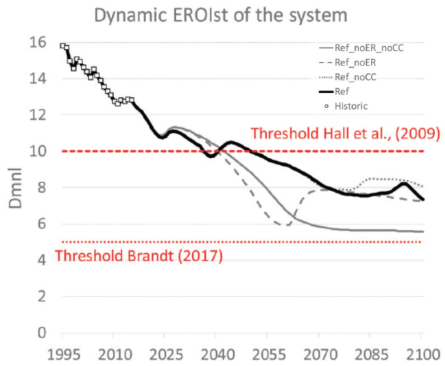


Figure 2.9 *– MEDEAS results from [36]: Dynamic EROI of the system, and representation of system EROI thresholds to sustain high levels of development in current industrical societies.*

The only limitation that can be noted on the basis of the study of the "energy availability" module is the modelling of the evolution of wind and solar productions with the installed capacity. A constant capacity factor is taken for these 2 technologies, without taking into account the location effect, i.e. the fact that the capacity factor is decreasing when the installed capacity increases. However, the methodology developed in this thesis to assess wind and solar potentials will be introduced in a new version of the model, in order to take into account the evolution of these capacity factors with the cumulated production at the global and regional levels.

The team of de Castro, Cappelan-Pérez et al., at the origin of this model, are the authors of an abundant literature highlighting the physical limits of wind and solar energies, and the associated energy costs [42, 56, 77–81].

2.2.2 Economic growth models

A recet paper from Rye and Jackson [82] presents a detailed review of energy-economy models that incoporate the EROI metric. In early models, the EROI was not explicitly modelled, but the associated dynamics were incorporated by modelling the depletion of non-renewable resources and the transition to more infrastructure-intensive resources. Some neo-classical economic growth models have addressed the issue of the energy transition, but very few explicitly model the concepts related to the EROI, apart from the contributions of Fagnart and Germain [83–85] and Court et al. [86]. These models belong to the economic

theory of growth, they assume market equilibrium and explicitly model the behaviour of economic agents. Finally, the model EENGM (*Energy Extended Neoclassical Growth Model*) of Režný and Bureš [87] has the particularity of combining a growth model with a system dynamics model.[4]

The model of Court et al. shows that the energy transition can only take place in a smooth way if the efficiency of primary-to-useful exergy conversion increases considerably (a minimum increase of about 200% within 2 centuries). They also model the impact of a carbon tax, which would allow for a smoother transition in a wider range of scenarios. Their work has the particularity of proposing a model for the evolution of the capital intensity of non-renewable and renewable energies in order to capture: (i) the negative impact of resource depletion, (ii) the positive impact of technological progress, and (iii) the fact that non-renewable energy was initially extracted at lower costs than those associated with renewable energy. However, the parameters modelling resource scarcity are taken constant and equal for the two sub-sectors, and no justification for this choice can be found in their paper. They also estimate that the rate of self-consumption of both types of energy is 1%, *due to the lack of available data*. The data available in the literature, however, seem to suggest that non-renewable energies consume a much greater amount of final energy in direct form than renewable energies.

Fagnart and Germain developed an endogenous growth model with two sectors (energy and final good) in order to measure the impacts of the decrease of the EROI of the energy system. They show that the EROI is inversely related to the share of final production that should be devoted to the energy sector. A decreasing EROI therefore leads to increasing needs of the energy sector, to the detriment of consumption and investment. If the EROI becomes too low, this crowding out effect can therefore result in a decrease in final production. According to their results, the energy transition would be accompanied by important economic changes, especially in the allocation of capital between the two sectors and in the distribution of the total production of the economy between consumption and investment. They show that a decline in economic activity is possible before the end of the energy transition, and that, to support the growing capital needs of the energy system, the savings rate of the economy

[4]This paper also presents the interest of reviewing a series of energy-economic models.

could exceed 40%. Such savings rates have so far only been observed in totally war-oriented economies. This increase in the savings rate is also observed with the EENGM model [87].

In all these contributions, the energy and capital requirements of the renewable and non-renewable subsectors are modelled with a very simplified approach, and the estimated global energy production potential is not based on detailed studies of the actual availability of the different types of energy. Because of this modelling, which is sometimes far from reality, the results obtained can be questioned. The aim of this thesis is to propose an extension to Fagnart and Germain's model, with a sophisticated modelling of the renewable subsector.

Nothing lasts forever but the earth and sky,
And all your money won't another minute buy.

Kansas - Dust in the wind

3

Global available wind energy under physical and EROI constraints

---

This chapter is an updated version of the following publication:
Dupont, E., Koppelaar, R. & Jeanmart, H. (2018). *Global available wind energy with physical and energy return on investment constraints.* Applied Energy, 209, 332-338, http://dx.doi.org/10.1016/j.apenergy.2017.09.085.

Wind power achieves a prominent share in the power generation mix in many techno-economic future energy studies of countries and regions [88–90]. Without an upper-bound based on geographic potential however, overestimates can occur resulting in unrealistic transition scenarios. A major challenge to impose realistic potentials in planning scenarios is the large discrepancy between studies on the global and regional wind energy potential (Table 3.1). The difference in wind potential estimates results in a wide range of possibilities for the future role of renewables.

Study	Estimated Potential [EJ/year]	Constraints		Installed Capacity Density [MW/km^2]
		Wind regime	Land use	
World				
Archer and Jacobson, 2005 [25]	2,256	$\bar{v}_{80m} \geq 6.9$ m/s	No	9
Lu et al., 2009 [26]	3,024	$C_f \geq 20\%$	Yes	Onshore: 9 Offshore: 5.85
Miller et al., 2011[91]	570-2,150	Top-down	No	-
DeCastro et al., 2011[77]	32	Top-down	Yes	-
GEA, 2012 [92]	250-1,200	$\bar{v}_{80m} \geq 6.9$ m/s	Yes	-
Eurek et al., 2017 [28]	2,720	$C_f \geq 18\%$	Yes	5
World, onshore only				
Hoogwijk, 2005 [72]	346	$\bar{v}_{80m} \geq 6.9$ m/s	Yes	4
Moriarty and Honnery, 2009 [93]	229	$\bar{v}_{70m} \geq 6$ m/s	Yes	2
Bosch et al., 2017 [27]	2,112	$C_f \geq 15\%$	Yes	6.52
Europe				
EEA, 2009 [94]	153	$\bar{v}_{10m} \geq 4$ m/s	Yes	Onshore: 10 Offshore: 6.4

Table 3.1 *– Global wind power potential estimates. Regarding bottom-up approaches, the limiting constraint vary between studies: either a minimum capacity factor (C_f) is fixed, or a minimum average wind speed at a given height ($\bar{v}_{80m}$ being the average wind speed at 80 meters above the ground).*

In this chapter a novel methodology is described and implemented that to our knowledge is the first to combine physical, geographic, and economic constraints, derived from setting a minimum EROI as a limiter to the harvestable wind resource. Thereby we gain a more precise value for the maximum offshore and onshore wind potential at a global and country level. These can be utilised to create more realistic future energy systems scenario studies to underpin policy decisions and investment need assessments.

In Section 3.1 key considerations to be taken into account in the analysis of wind energy potential are discussed, based on top-down approaches found in the literature. They are followed by the methodology employed in this study in Section 3.2, results are presented in Section 3.3 and discussed in Section 3.4. Finally, the chapter ends with a set of conclusions and the implications for

energy strategy policies in Section 3.5.

3.1 Limits on wind potential via top-down approaches

The amount of wind energy that is available at a global scale is constrained by physical factors including incoming solar radiation, heat gradient, geography, and electricity transport distance. A considerable number of studies estimate the technical potential of wind energy via a bottom-up approach neglecting energy conservation laws that are in effect at a global scale [25–28, 72, 94]. Global potential is in these studies calculated from the sum of local potentials, based on the implicit assumption that the extraction of a large amount of wind power has no impact on global wind generation. However, wind power potential is not only limited by our ability to build and install more a more wind turbines, but also by the power generated by the sun. Therefore a global estimate of maximum kinetic energy extraction rates is needed, and should be taken into account as a physical constraint to the sum of local potentials.

In order to reach a significant contribution to the energy mix, wind farms will on average have to be composed of an substantial number of turbines. In very large wind farms, the horizontal flux of kinetic energy is captured by the first rows of turbines and can therefore be neglected. The power that can be captured is thus primarily limited by the vertical downward transport of kinetic energy [95].

On top of this limitation, global wind speeds will be reduced if a significant amount of wind power is extracted. A reduction in global wind speeds as a consequence of large scale wind turbine placement will potentially further reduce the energy produced by wind farms and likely have an impact on local and regional meteorology [96]. At present it is hard to picture that we could reach a level of wind energy production that could alter the global climate, but this is because wind energy extracted today still represents a small fraction of total wind energy available globally.

Literature estimates

In past decades several methods have been proposed to quantify limits on available energy from wind power generation.

Generation of kinetic energy It has been shown that the conversion process of incident solar radiation into kinetic energy is currently maximal at a rate of 2%, corresponding to an available power flux of 900 TW globally [97–101], with about a third dissipated within the surface boundary layer [102]. This gross estimation yields 292 TW kinetic energy dissipated in the atmospheric boundary layer. This value is consistent with results from other approaches: Jacobson and Archer [103] found 253 TW for the saturation wind potential at 100 m and Miller and Kleidon [104] found a dissipation rate of 270 TW via global circulation model (GCM) simulations.

Maximum extraction rates Miller et al. [91, 105] studied maximum extraction rates for wind turbine technology, and by combining different approaches they found a 18-68 TW range for the wind energy potential, which equates to 567 to 2144 EJ/year. de Castro et al. [79] studied the global wind energy potential with a top down approach based on the portion of kinetic energy that can be converted, with limitations of height, geography, wind turbines, economically viable areas, wind speeds, and conversion efficiency. The results yielded 1 TW as the global wind potential, which equates to 32 EJ/year. In comparison, total wind electricity production in 2016 was 3.5 EJ. Prior to the publication of these studies, all the bottom-up approaches overestimated the global potential, while most have since revised their estimates downwards. In 1979, Gustavson [99] estimated that the global limit for wind power extraction was 130 TW, assuming that up to 10 % of the near-surface dissipation of kinetic energy could be extracted.

Limits on power production density Some studies use general circulation models or mesoscale models with wind turbine parametrization in order to predict climatic impacts of very large wind farms [91, 103, 106–108]. The analyses also have highlighted that by increasing the installed capacity density of wind farms the power produced saturates at capacity densities smaller than most current wind farms. Studies showed that for wind farms larger than 100 km^2 in windy regions (like the US Midwest and Western Europe) power production saturates at about 1 W_e/m^2 [107, 109]. This value was also found by Best in 1978 [110]. Miller [104] compared global circulation model simulations with estimates of vertical kinetic energy fluxes and found maximum electricity generation rates of 0.32 and 0.37 W_e/m^2 on land and 0.59 and 0.29 W_e/m^2 over oceans, with global wind speed reductions of 42 % and 44 %. Their results

seem to confirm that few land areas are able to generate more than 1 W_e/m^2, and that large scale deployment would reduce the production of each turbine.

The results cited above, which take into account physical limits to energy availability, predict that it will be more difficult than anticipated for wind energy to contribute significantly to the world's energy needs.

The insights demonstrate that it is fundamental to combine a bottom-up with a top-down approach, so as to obtain a better estimate of the global wind energy potential. As a start we create and implement a novel bottom-up approach in this study, as outlined in Sections 3.2.1 to 3.2.4, which allows for an estimate of the energy generated in every geographic location, taking into account local constraints. We include in the analysis an assessment of energy inputs to ascertain how much energy output is available, net of inputs. The evaluation is subsequently adjusted with a constraint on the total available kinetic energy based on a simplified energy distribution model described in Section 3.2.5.

3.2 Methodology

To derive a more precise estimate of the global wind energy potential, the availability of wind energy is modelled on a net energy basis with a grid cell approach. The methodology is shown in Fig. 3.1 and includes the following steps:

- **Bottom-up approach**
    1. First a **suitability factor** is associated to each cell, as discussed in Section 3.2.1, in order to take into account geographical and technical constraints.
    2. The theoretical **energy output** in each cell is evaluated as outlined in Section 3.2.2:
        - The **capacity factor** of a wind turbine is estimated, by combining wind speed distribution and turbine specifications (Section 3.2.2).
        - **The array placement efficiency** is then added (Section 3.2.2)

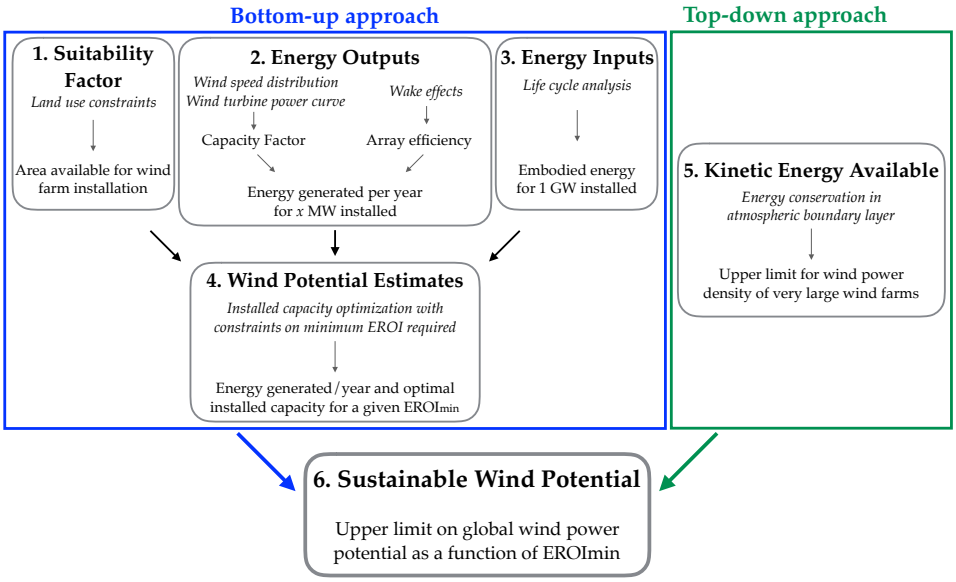


Figure 3.1 *– Methodology used in this study to estimate the evolution of the standard EROI of wind energy with cumulated annual production.*

in order to include wake effects of multiple turbines in geographic proximity.

3. Based on a detailed life-cycle inventory the **energy inputs** for a typical wind farm are evaluated in Section 3.2.3 (onshore, bottom-fixed offshore and floating offshore). The influence of distance to coast and water depth on energy inputs is incorporated.

4. An optimisation procedure for the **installed capacity** is presented in Section 3.2.4, with the objective to find the maximum electricity generated on a net energy basis, using as a constraint a desired minimum EROI value.

- **Top-down approach**

5. A study of the **kinetic energy available** in the atmospheric boundary layer is made in Section 3.2.5. Energy conservation at a planetary scale is used as a constraint on the results from the bottom-up

approach.

- **Results**

  6. **The sustainable wind power potential** is calculated by adding constraints of step 5 to the optimisation procedure of step 4 (Section 3.2.6). An upper limit to global wind power potential as a function of a minimum cut-off EROI is obtained.

The grid size of the model is 0.75° x 0.75° (4,000 km^2 on average), which corresponds to the smallest resolution available for wind speed data at hub height (71 and 124 m) in the ERA-Interim dataset [111]. As for land use types, the model resolution is 0.01° x 0.01° (each 0.75° x 0.75° cell is further divided into 5,625 subcells).

As explained in Section 2.1.1, the EROI calculated in this chapter and in the next one correspond to the boundaries of the standard EROI (Eq. 2.2). The limitations linked to this choice are discussed in Section 3.4.2.

3.2.1 Geographic suitability factor

Since many areas are not suitable for wind farm installation, realistic assumptions should be taken regarding geographical constraints. Following the approach used in several bottom-up studies [27, 28, 72, 112], a suitability factor is associated to each grid cell, defined as the cell fraction suitable for wind farm installation.

Onshore suitability factor

For onshore areas, the suitability factor depends on land cover. Values used in this study are given in Table 3.2, which are coherent with those in precited studies. Land cover of each grid cell was retrieved from the GlobCover 2009 dataset, created by the European Space Agency (ESA) and the Université catholique de Louvain (UCLouvain) which classifies global land cover in 22 classes, at a 10 arc-second resolution [113]. Because of the spatial area of the cells in our model ($\sim$ 4,000 km^2) it would be too coarse to associate a single land cover to an entire cell. Therefore, each 0.75° x 0.75° grid cell was divided into a subgrid of 0.01° x 0.01° subcells. By retrieving the land cover associated with the center of each subcell in the GlobCover dataset, the repartition of a cell's area into the 22 different land covers was estimated.

Bioreserves from the world database on protected areas (WDPA) [114] are excluded, as well as relatively remote and unpopulated areas (Antarctica, Greenland and small remote islands). Countries for each grid cell are retrieved from the Flanders Marine Institute database [115].

Offshore suitability factor

Offshore areas are restricted to exclusive economic zones, i.e. sea zone up to 200 nautical miles from the coast (retrieved from the Flanders Marine Institute database [115]). Offshore wind energy potential and cost is dependent on water depth and distance to shore. Water depth will have an impact on the type of foundations since at greater depths pile based substructures are not possible. Current commercial substructures are limited to water depths of about 40 meters. In a report for the European Environment Agency (EEA) [94], the authors restricted offshore areas to sea depths below 50 meters. However, experimental floating substructures are in advanced stages of development and are expected to be adaptable for a wide range of water depths. Based on a National Renewable Energy Laboratory (NREL) report [116], water depths up to 1000 m are allowed in the model.

Once the depth of offshore areas are set they are split according to the distance to the nearest coast. Assumptions and the resulting proportions of available area are summarised in Table 3.2. These values are based on the considerations found in [94, 116] to take into account other uses of the sea area. For example, up to 5 nautical miles from the coast (about 10 km), wind turbines can be seen by the human eye and therefore their construction up to this distance is assumed to be limited to 10% of the area.

The combination of these constraints (protected areas, land-use, elevation, water depth, distance to shore) results in a calculated suitability factor for each grid cell, shown on a map in Fig. 3.2.

3.2.2 Wind energy outputs

Capacity factor

The annual production of a wind turbine is obtained through an estimation of its capacity factor. The capacity factor is the ratio between the energy produced by a wind turbine over a period of time and the energy it would have produced if operating continuously at its nominal power rating during the same

	Land Cover	Land use factor [%]	Area [10^6 km^2]
Onshore	Sparse vegetation, grassland, barren areas	90	42.46
	Forests	10	36.65
	Croplands	70	7.31
	Shrubland	50	8.5
	Mosaic vegetation - croplands	60	17.29
	Mosaic grassland - forest or shrubland	50	8.94
	Urban Areas	0	0.28
	Excluded areas, i.e. Antarctica, Greenland, remote, protected	0	20.49
	Total		**149.46**
	Suitable		**58.07**
Offshore, exclusive economic zones	Distance to shore < 5 nmi	10	5.47
	Distance to shore 5 - 20 nmi	33	16.36
	Distance to shore > 20 nmi	67	127.28
	Water depth > 1000 m	0	109.72
	Protected Area	0	4.19
	Total		**149.11**
	Suitable		**15.35**

Table 3.2 *– Repartition of the available areas into land use categories, and for each category the land use factor, consistent with values from [27, 28, 72, 93].*

period, or equivalently it is the ratio of the mean power produced to its rated power. In most studies a linear relationship between capacity factor and mean wind speed at hub height is used. Here, instead of using mean wind speed we take into account wind speed distribution in order to obtain a more precise calculation [117].

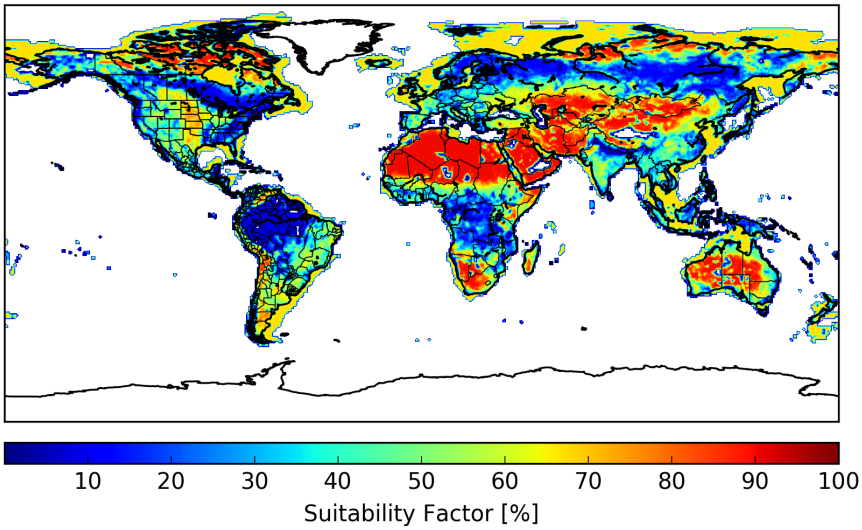


Figure 3.2 *– Map of the suitability factor, i.e. the proportion of each cell that is considered as suitable for wind farm installation in the model.*

The capacity factor is calculated as follows:

$$C_f = \frac{\bar{P}}{P_r} = \frac{1}{P_r} \int_0^\infty P(v) f(v) dv \tag{3.1}$$

With :

- v : the wind speed
- $\bar{P}$: average power produced by the wind turbine
- P_r : rated power of the wind turbine
- $P(v)$: power curve of the wind turbine
- $f(v)$: wind speed distribution

Wind speed distribution ERA-Interim dataset, a global atmospheric reanalysis [111], was used in order to estimate means and standard deviations of wind speed at a geographical grid cell level (Fig. 3.3). In order to have a wind profile as close as possible from the wind profile at hub height, estimates of wind speed at 71 meters and 125 meters were used. The arithmetic mean was used to estimate wind speeds at 100 meters.

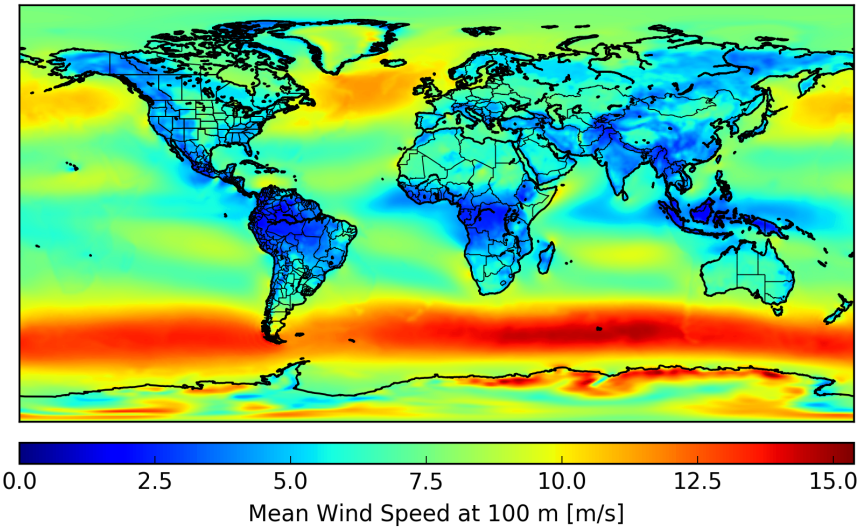


Figure 3.3 *– Mean wind speed estimates at 100 m, calculated based on data obtained from ERA-Interim reanalysis [111], every 6 hours from 01-01-2007 to 31-12-2016, at a* $0.75° \times 0.75°$ *precision.*

Wind speed data are well fitted with a Weibull distribution with probability function f:

$$f(v) = \frac{k}{c}\left(\frac{v}{c}\right)^{k-1} \exp\left[-\left(\frac{v}{c}\right)^{k}\right] \tag{3.2}$$

Shape parameter k and scale parameter c are estimated from mean wind speed $\bar{u}$ with standard deviation σ using the empirical method of Justus [118] :

$$k = \left(\frac{\sigma}{\bar{u}}\right)^{-1.086}$$

$$c = \frac{\bar{u}}{\Gamma(1+1/k)}$$

Wind turbine power curve The power output of a wind turbine is modelled as follows (Fig. 3.4):

$$P(v) = P_r \begin{cases} 0 & v < v_c, \\ \frac{v^3 - v_c^3}{v_r^3 - v_c^3} & v_c \leq v \leq v_r, \\ 1 & v_r \leq v \leq v_f, \\ 0 & v \geq v_f. \end{cases} \tag{3.3}$$

With v_c, v_r and v_f being respectively the cut-in, rated and cut-out wind speeds.

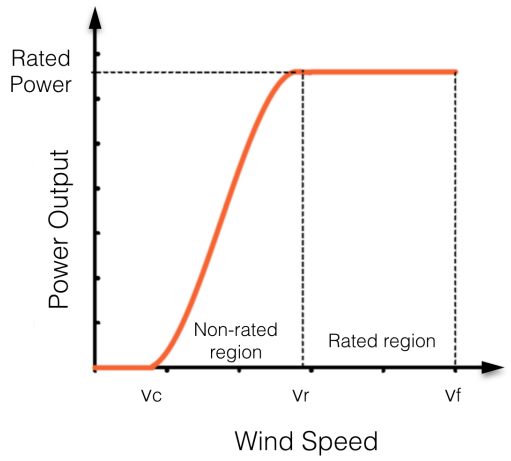


Figure 3.4 *– Typical wind turbine power curve : the turbine begins to operate at the cut-in speed v_c, then the power output increases with wind speed following a cubic curve until wind speed reaches the rated speed, where the turbine begins to operate at its rated power. The rotor is stopped when the wind speed exceeds the cut-out speed, in order to prevent damages. Typical values ranges are v_c =3-4m/s, v_r =11-17 m/s and v_f =25 m/s.*

With expressions (3.2) and (3.3), integral (3.1) is resolved in order to derive an expression for the capacity factor as a function of the local weibull parameters c and k, and the wind turbine design parameters v_c, v_r and v_f. This expression is independent from the rated power.

$$C_f = -e^{-\left(\frac{v_f}{c}\right)^k} + \frac{3c^3\Gamma\left(\frac{3}{k}\right)}{k(v_r^3 - v_c^3)}\left(\gamma\left(\left(\frac{v_r}{c}\right)^k, \frac{3}{k}\right) - \gamma\left(\left(\frac{v_c}{c}\right)^k, \frac{3}{k}\right)\right) \tag{3.4}$$

With Γ and γ being respectively the gamma and incomplete gamma functions.

$$\Gamma(x) = \int_0^\infty t^{x-1}e^{-t}dt$$

$$\gamma(u,x) = \frac{1}{\Gamma(x)}\int_0^u t^{x-1}e^{-t}dt$$

Wind turbine specifications The cut-in speed v_c is usually around 3-4 m/s, because at lower wind speeds there is insufficient torque exerted on the blades to make them rotate. The cut-out speed v_f is usually 25 m/s in order

to avoid damage, and the rated speed v_r has a range of 11-17 m/s, depending on local wind conditions.

The power that is extracted from the wind by a turbine is given by:

$$P = C_p \frac{1}{2} \rho A v^3$$

With ρ the air density, A the rotor swept area, and C_p the performance coefficient. The maximum theoretical value of the performance coefficient is 59.26 % according to Betz law. With technological progress aerodynamic and mechanical losses are reduced. Modern large wind turbines achieve peak values for C_p in the range of 45 to 50 %. The relationship between rated power, rotor diameter (RD), and rated wind speed for modern turbines can therefore be better expressed as:

$$P_r = C_{p,max} \frac{1}{2} \rho \frac{\pi R D^2}{4} v_r^3 \tag{3.5}$$

For low wind speed sites, a lower rated wind speed allows for a greater capacity factor. Therefore, compared to wind turbines for high wind speed sites either the rated power is lower for the same rotor diameter, or the rotor diameter is larger for the same rated power.

Array placement efficiency

The theoretical capacity factor calculated in Section 3.2.2 is valid for an isolated wind turbine or small wind farms. However turbines are placed increasingly into large wind farms with hundreds of turbines. When a wind turbine extracts energy from the wind, there is a wake downstream with reduced wind speed. Because wind power is proportional to the cube of wind speed, in order to reduce power losses there should be enough space between wind turbines to allow for wind speed recovery via horizontal or vertical replenishment of kinetic energy. In large turbine arrays horizontal transport of kinetic energy can be neglected and the amount of energy that can be extracted is limited by the vertical replenishment of kinetic energy.

Various studies show that these interferences increase quite rapidly if the wind turbines are less than 10 rotor diameters (RD) apart [95]. Turbine wake interference has been widely studied, but data is so far limited on the effect for very large turbine arrays. In order to take this effect into account, a global average array efficiency inclusive of wake effects was calculated and applied to each wind farm output, based on the ratio between the output of a turbine in

the wind farm to the output of the same turbine alone without any interference. It has been shown that the critical parameter constraining array efficiency is a spacing parameter λ that is the ratio of the rotor swept area to the land surface area occupied by a wind turbine in the wind farm ([119–122] and Fig. 3.5).

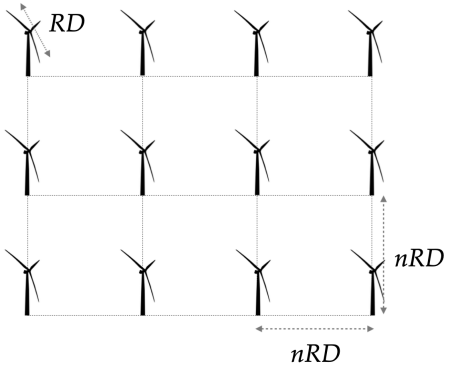


Figure 3.5 *– Wind farm configuration : we assume wind turbines are regularly placed in arrays, the spacing is expressed as a multiple n of the rotor diameter RD. With such a configuration, the spacing parameter λ is a fonction of n^2 only ($\lambda = \frac{\pi RD^2/4}{(nRD)^2} = \frac{\pi}{4n^2}$).*

We use array efficiencies for different λ and array sizes from [99], as per Table 3.3, that we fitted to a negative exponential of type $ae^{-b\lambda}$, via non linear regression with a least squares approach (Fig. 3.6). These results are coherent with recent numerical studies which show that optimal turbine spacing in large wind farms may be considerably higher ($\sim$ 15 RD) than the 7 to 10 RD used in current configurations [95].

In most studies on global wind power, the use of constant array efficiencies plausibly leads to an overestimation of the power produced. For example in [94] the array efficiency used is 90 % for offshore locations and 92.5 % for onshore locations. The assumptions on installed capacity densities in this study (10 MW/km^2 onshore and 8 MW/ 1.25 km^2 offshore) and rotor diameters (80 m onshore and 120 m offshore) correspond to turbine spacings of 5.6 RD onshore and 9.3 RD offshore. Spacing at these RD's in large wind farms, however, does not allow for array efficiencies as high as 90%, according to [99]. In [27, 28, 72], the authors also assume a constant array efficiency of 90 % with a turbine spacing of 5 to 7 RD, which is not consistent with the values for large arrays from Table 3.3.

The array effect shows that for a given area, there is a trade-off between

very dense wind farms where wind turbines have low yields, and sparse wind farms where the output of each turbine is maximised. In practice other factors may favor the choice of dense wind farms: for example the fact to minimise land permits or internal cabling.

		$\lambda = \frac{A_{rotor}}{A_{turbine}} = \frac{\pi}{4n^2}$			
		0.03 (5RD)	**0.01** (9RD)	**0.003** (16RD)	**0.001** (28RD)
Array Size	**5 x 5**	85	94	98	99
	10 x 10	70	86	96	98
	50 x 50	29	62	87	95
	Infinite	10	38	73	89

Table 3.3 *– Array efficiency estimates [%], for different array sizes and spacing parameters λ, from [99].*

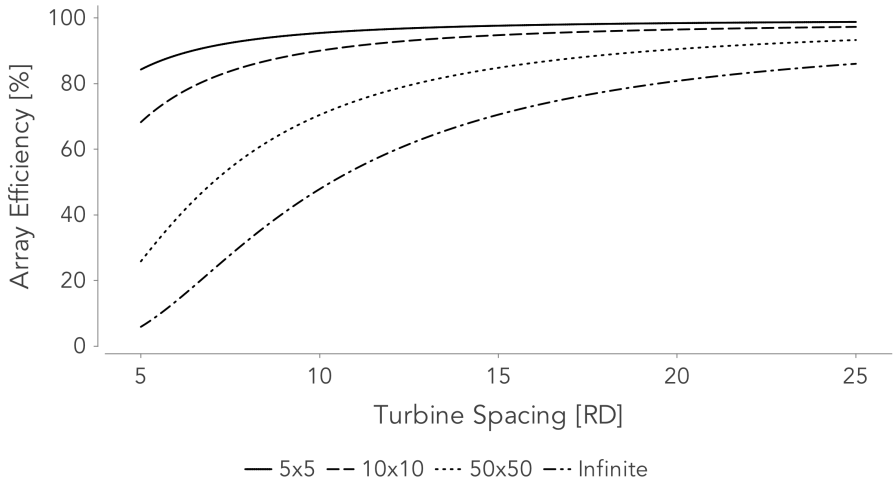


Figure 3.6 *– Array efficiency as a function of turbine spacing, for different array sizes, data from [99] fitted to a negative exponential :* $\eta \sim ae^{-b\lambda}$.

Availability factor and transmission losses

Transmission losses are not taken into account in the model as we only consider the electricity production at the site exit. The cabling required to connect offshore wind farms to the nearest coastline is included in the calculation of

energy inputs, but related losses in terms of electricity production have not been included in the calculation of outputs. The onshore cabling required to connect the site to the existing grid has not been included in the model, as we could not find a database listing the distance from any geographical location to the nearest electrical connection.

An availability factor, also referred to as production loss factor, is taken into account at 97% for onshore areas, and 95 % for offshore areas, in order to take into account the loss of capturing the wind when it blows due to sudden and periodic maintenance of turbines. These values are a conservative estimate based on recent industry reported values estimated by monitoring tens of thousands of onshore and hundreds of offshore turbines [123, 124].

3.2.3 Life cycle energy inputs

Several existing studies calculate the EROI or a cumulative energy demand (CED) figure for wind power using life cycle approaches [125–128]. Results for net energy assessment studies can yield a wide range due to different boundary assumptions, age of manufacturing input data, and key technology assumptions [129]. Previously studied life-cycle stages for wind power include: the manufacturing of components, transport, installation, operation and maintenance, grid connection, and decommissioning. We expand upon these results by taking a complete cradle-to-grave boundary approach for onshore and offshore wind (fixed monopile and floating ballast), encompassing nine stages from raw materials to final decommissioning, inclusive of embodied energy from raw materials extraction and processing. Data values are presented for 1 GW of onshore and offshore wind power capacity in this section. All electricity values, except for operational parasitic load, were converted into primary grid inputs so as to obtain a primary energy equivalent EROI value [130]. The electricity to primary fuel conversion was carried out with a multiplying factor of 2.24 calculated from the 2015 global electricity mix [131].

In the next two subsections first a fixed value for the energy embodied in a typical wind farm of 1 GW is estimated, for onshore, offshore fixed monopile and offshore floating. Then the increase in energy inputs with distance to coast (for all types of wind farms) and water depth (for fixed monopiles) are taken into account.

Life cycle data for 1 GW of wind power

The main components of a wind farm are wind tower generators, internal cables and a transformer station, plus external transmission cables for offshore wind to connect to the onshore grid. A wind tower generator is composed of a tower, nacelle, rotor, and foundation, which are individually built and then combined on-site. The nine life-cycle stages included in this study are i) raw materials extraction and conversion to an intermediary material (such as aluminium or steel slabs or rolls), ii) transport to the factory, iii) manufacturing of the wind generator and other components, iv) transport to the installation site, v) installation, vi) operation, vii) maintenance, viii) decommissioning, and ix) decommissioning transport. Tables 3.5, 3.6, and 3.7 summarize the components and energy inputs associated with each stage in the life cycle for onshore and offshore wind power. Energy intensities used for materials extraction and transport calculations are given in Table 3.8.

The example case yields a total life cycle primary energy input for a 1 GW onshore, fixed offshore (15 m depth), and floating offshore wind farm of 20.2, 25.9, and 30.5 PJ, respectively. If for the onshore wind farm a lifetime of 25 years and a capacity factor of 22% is assumed this results in 179.5 PJ of electricity output and a life cycle EROI of 8.9. If for the fixed and floating offshore wind farm the same lifetime is assumed with a capacity factor of 39% this results in 309.6 PJ electricity output and a life cycle EROI of 12, and 10.4, respectively.

Energy inputs for wind energy are dominated by extraction and processing of minerals (about 25-30% of inputs), the manufacturing of the wind turbine and grid infrastructure (about 35-40% of inputs), and the operational parasitic load (about 7-8% for 10 MW offshore and 30% for 3 MW onshore turbine parks). For offshore wind, installation (about 7-15% of inputs) and maintenance costs (about 8-10% of inputs) are significant, varying with distance. The most critical variable factor for offshore is the foundation (typically steel monopiles), which increases in weight with water depth and turbine size, raising raw material and installation energy costs, although this is compensated for by higher offshore load factors. Offshore grid connection costs are also substantial at 0.5 PJ in embodied and installation energy for every 100 km of 132 kV cable.

Influence of distance to coast

Final transport distance for installation and maintenance was variably incorporated for both onshore and offshore wind farms. The mean distance to the nearest coast for each 0.75° grid cell for wind generator installation was taken from NASA's Ocean Biology Processing Group dataset [132]. The distance was multiplied by the fuel intensity values in Table 3.8. An additional fixed distance for installation of 600 km for truck and 10,000 km for ship transport was incorporated from factory to port [133]. Raw materials extraction plus processing and ship transport distances were incorporated using a static value as per Table 3.7. The nearest coast distance factor was also applied to the transmission cables from substation to shore for offshore wind, based on values in [134, 135]. Data in Table 3.5 present the embodied energy per km of offshore cable for a 1 GW offshore wind farm. These inputs are then multiplied by the distance to the nearest coast in the model.

Influence of water depth

The impact of water depth on offshore wind was incorporated using a scale factor given in Table 3.4 based on the values in [136, 137]. The factor was applied to monopile steel and ballast concrete requirements per wind generator. Mean water depth of every grid cell was taken from 1 arc-minute global relief model of Earth's surface of NOAA [138]. Scaling was limited to water depth up to 40 meters, with nearly all fixed foundation projects built up to this depth [139]. At greater depths floating substructures will be employed in the future, potentially up to a kilometer of water depth. Several prototypes are in operation, and 200 MW of demonstration projects are underway in Scotland and France [140]. The closest to operation is the Statoil funded HyWind project, based on a ballast design, for which specific steel and concrete values are available [141]. On the basis of this project for water depths greater than 40 meters concrete and steel values of 375,000 and 275,000 tonnes for 1000 MW of wind were taken into consideration, replacing the monopile offshore foundation values in Tables 3.5, 3.6, and 3.7. All other calculations at depths greater than 40 meters were similar to non-floating offshore wind.

Depth [m]	Multiplying Factor
0-15	1
15-20	1.08
20-25	1.34
25-30	1.57
30-35	1.95
35-40	2.19

Table 3.4 *– Multiplying factor for variability in offshore foundation material inputs, based on [136, 137]*

	Material	Weight [t]		Electricity [GJ]		Diesel [GJ]	
		Onshore	Offshore	On.	Off.	On.	Off.
Tower	Steel	52,920	27,500	123,282	64,064	1,184,350	615,450
	Coating	420	331	18,783	14,791	9,074	7,146
Nacelle	Steel	19,993	46,502	46,576	108,331	447,451	1,040,718
	Copper	1,250	1,754	95,358	125,726	14,634	19,294
	Aluminum	770	484	96,113	19,294	17,764	60,373
	Coating	17	7	810	323	361	144
Hub and blades	Steel	6,643	13,562	15,476	31,595	148,678	303,525
	Fibre Glass	4,013	7,217	143,838	258,639	64,213	115,464
	Epoxy Resin	2,810	5,054	251,776	452,847	112,400	202,164
	Coating	21	38	1,035	1,861	462	831
Foundation	Concrete	380,000	7,813	502,208	16,173	786,600	10,326
	Steel	12,000	155,375	27,955	361,962	268,560	3,477,293
Park cabling (183 km)	Steel	0	1502	0	3,604	0	33,633
	Copper	266	846	20,419	64,974	2,925	9,306
	Aluminium	1358	0	181,420	0	31,349	0
	Other	1471	1463	70,648	70,242	29,437	29,267
Substation	Steel	337	337	808	808	7,540	7,540
	Copper	88	88	6,758	6,758	968	968
	Other	214.5	214.5	10,296	10,296	4,290	4,290
Cables to shore (/km)	Steel	-	25.3	-	61	-	567
	Copper	-	19.8	-	1,517	-	217
	Other	-	34.1	-	1,637	-	682

Table 3.5 *– Embodied energy in materials for 1 GW turbine generators, substation and cables. Raw data onshore: materials [126], substation and cables [142, 143]. Raw data offshore: materials [126, 144, 145], substation and cables [143, 146].*

		Onshore	Offshore
Manufacturing Primary Energy [GJ]	Wind turbine	7,869,000	8,523,000
	Park cabling (183 km)	52,128	66,030
	Substation	16,632	16,632
	Cables to shore (1 km)	583	1,282
Installation Primary Energy [GJ]	Wind turbine	129,660	1,709,830
	Park cabling (168 km)	13,159	33,338
	Substation	10,603	34,991
	Cabling to shore (1 km)	-	4,681
Operation Electricity [GJ/GJ]		0.035	0.007
Maintenance Diesel [GJ/GW/year]		1,656	65,587
Decommissioning Primary Energy [GJ]		6,450	1,283,000

Table 3.6 *– Manufacturing, installation, operation, maintenance and decommissioning energy inputs for 1 GW of wind. Raw data onshore: installation and decommissioning [147], operation and maintenance [142, 148]. Raw data offshore: installation and decommissioning [134, 135, 146], operation and maintenance [144, 146]*

	Material	Mode	Weight [t]		Distance [km]		Diesel [GJ]	
			Onshore	Offshore	On.	Off.	On.	Off.
Raw materials	Cement	Truck	380,000	7,813	20	20	9,500	195
	Steel	Truck	91,557	242,939	150	150	17,167	45,551
	Copper	Truck	1,330	1,754	430	430	715	943
	Aluminium	Truck	770	484	60	60	58	36
	Other	Truck	7,282	12,647	20	20	182	316
	Copper	Ship	1,330	1,754	4,200	4,200	161	212
	Aluminium	Ship	455	484	3,000	3,000	39	42
	Other	Ship	7,282	12,647	4,000	4,000	839	1,457
Factory to site	Cement	Truck	380,000	7,813	250	250	118,750	2,442
	Steel	Truck	91,557	242,939	600	600	57,223	182,204
	Copper	Truck	1,330	1,754	600	600	416	1,316
	Aluminium	Truck	770	484	600	600	667	363
	Other	Truck	7,282	12,647	600	600	5,462	9,485
	Steel	Ship	91,557	242,939	10,000	10,000	26,368	69,966
	Copper	Ship	1,330	1,754	10,000	10,000	383	505
	Aluminium	Ship	770	484	10,000	10,000	222	139
	Other	Ship	7,282	12,647	10,000	10,000	2,097	3,642
Decommissioning	All	Truck	480,939	265,637	350	350	210,411	116,216
	All	Ship	96,188	53,127	5,000	5,000	138,510	76,503

Table 3.7 *– Transport energy inputs for 1 GW of wind. Raw data onshore: manufacturing [142, 148], installation and decommissioning [147], O&M [142, 148]. Raw data offshore: manufacturing [144], installation and decommissioning [134, 135, 146], O&M [144, 146]*

Material	**Electricity** [**GJ/t**]	**Fuel** [**GJ/t**]	**Source**
Cement	0.6	3.0	[149, 150]
Steel	1.0	22.4	[151–153]
Aluminium	55.7	23.1	[154, 155]
Copper	32.0	11.0	[156]
Epoxy resin	80		[157, 158]
Glass Fibre	32		[157]
Coatings	43		[157]

Transport	**Fuel** [**MJ/tkm**]	**Source**
Truck	1.25	[159–161]
Ship	0.29	[162]

Table 3.8 *– Energy intensity values w/o primary conversion.*

3.2.4 Installed capacity optimisation

By combining results from the previous sections, the energy outputs and associated EROI for a given installed capacity in each grid cell can be estimated. Previous studies on global wind power potentials take the assumption of a constant installed capacity density, varying in general from 2 to 10 MW/km^2, with a constant array efficiency independent from turbine spacing and array size. But given wake effects within a wind farm (Section 3.2.2), there is an optimal installed capacity in order to maximise energy output. In this study we propose a new approach with a varying installed capacity density per cell, in order to maximise the net energy produced over a wind farm's lifetime in every grid cell.

Given Eq. (3.5), and with the farm configuration as in Fig. 3.5, the installed capacity density is expressed as a function of the rated wind speed v_r and the spacing parameter n:

$$CD(v_r, n) = \frac{P_r}{(nRD)^2} = \frac{C_p 1/2 \rho \pi / 4 v_r^3}{n^2} \text{ [MW/km}^2\text{]} \tag{3.6}$$

For example, a 2 MW turbine with a rated speed of 11 m/s has a rotor diameter of 80 m, and occupies 0.31 km^2 with n=7, while a 10 MW turbine with the same rated speed has a rotor diameter of 176 m and therefore occupies the same land area as five 2 MW wind turbines. Knowing that the capacity factor depends on v_r only and that the array efficiency depends on n only, not only the installed capacity but also the energy produced per unit of area does not vary with turbine size, with the hypothesis described in Section 3.2.2.

Under the considerations above, an optimisation problem can be solved for each cell: find for each cell i the optimal installed capacity, i.e. the optimal rated speed $v_{r,i}$ [m/s] and spacing parameter n_i, in order to maximise net energy produced.

$$\text{Max(Net Energy Produced)} = \text{Max(Energy Produced - Energy Inputs)} \tag{3.7}$$

With:

$$\text{Energy Produced}_i = C_{f,i}\ \eta_i\ \text{MW}_i\ \text{Life Time} \tag{3.8}$$

- $MW_i = CD(v_{r,i}, n_i) *$ Suitable Area$_i$: the installed capacity in cell i, i.e. the installed capacity density from Eq. (3.6) over the suitable area of cell i.

- $C_{f,i} = C_f(v_{r,i})$: the capacity factor of cell i for the rated wind speed $v_{r,i}$, as calculated in Section 3.2.2.
- $\eta_i = \eta(n_i)$: the array efficiency for the spacing parameter n_i over the suitable area of cell i, as calculated in Section 3.2.2.

The energy inputs for a wind farm of size MW_i on cell i, are calculated inclusive of water depth variability as per Section 3.2.3.

The solution must be such that the EROI in cell i is greater than a given threshold:

$$\text{EROI}_i \geq \text{EROI}_{min} \tag{3.9}$$

EROI_i is calculated as the net energy produced:

$$\text{EROI}_i = \frac{\text{Energy Produced}}{\text{Energy Inputs}} = \frac{C_{f,i}\ \eta_i\ \text{MW}_i\ \text{Life Time}}{\text{Energy Inputs}(\text{MW}_i)}$$

In some cells it may not be possible to reach EROI_{min} because the wind speeds are too low.

The reason for including a minimum EROI is that, at a particular threshold, the scaling of the energy sector to cover its own energy needs becomes potentially too large. Indirect energy required to build, install, and operate the turbines becomes too large for extraction to be feasible from an economic point of view of maintaining growth and living standards. When summing mean power produced, or annual energy production in each cell, an upper limit on the global wind power potential as a function of EROI_{min} is obtained.

3.2.5 Kinetic energy available

The approach presented in Section 3.2 so far neglects energy conservation laws. Implicitly an assumption was made that extracting a large amount of wind power has no impact on global wind generation and therefore does not alter the total production potential. The array effect, that takes into account local wind speed reduction, is considered independent from total capacity, therefore large-scale atmospheric processes that constrain global winds are neglected.

Based on literature results presented in Section 3.1, we propose a simplified approach to take into account the limited rate of kinetic energy available. We start from the estimate of 292 TW of the kinetic energy dissipated in the atmospheric boundary layer over the globe [102]. Since turbulent dissipation is linked to the wind speed squared, we make the assumption that this power

is distributed over each cell proportionally to the mean wind speed squared :

$$\text{Kinetic Energy Generation Rate}_i \sim \frac{\bar{v}_i^2 A_i}{\sum_{j \in world} \bar{v}_j^2 A_j} 292 \text{ TW} \tag{3.10}$$

In order to take into account the estimated kinetic energy generation rates, the following constraint is added to the maximisation problem described in 3.2.4 :

$$\text{Power Produced}_i \leq \text{Kinetic Energy Generation Rate}_i \tag{3.11}$$

3.2.6 Net energy results calculation

In each cell the rated speed and spacing parameter are computed, by maximising the function of two variables from Eq. (3.7) with constraints defined in Eqs. (3.9) and (3.11). The optimisation procedure is repeated for different level of EROI_{min}, and the global potential is then calculated by summing the gross or net energy theoretically produced per year with those optimal parameters. For a given EROI_{min}, a function for the evolution of the EROI with annual production is obtained by classifying the sites by decreasing EROI and then by drawing the evolution of the EROI with cumulated annual production.

3.3 Results

3.3.1 Wind farm design

Capacity factors

Capacity factors calculated with Eq. (3.4) with a constant rated wind speed of 11 m/s are shown in Fig. 3.7. Results are compared with capacity factors of existing onshore wind farms in Table 3.9. The comparison shows that the calculated capacity factors for low wind speeds (class III) are higher than the IEA values from 2013-2014 for most countries. These results are mainly dependent on the rated wind speed, as a higher rated wind speed would yield lower capacity factors.

Optimisation variables ($v_{r,i}$ and n_i)

As explained in Section 3.2.4, the net energy that can theoretically be produced in each cell is maximised by optimising the wind turbine design, via the rated wind speed v_r, and the wind farm configuration, via a spacing parameter n,

Country	2014 data from EIA			C_f for this study	
	Installed Capacity [GW]	**Production [TWh/y]**	C_f	**Class IV** $\bar{v} \geq 6m/s$	**Class Ill** $\bar{v} \geq 7.5m/s$
Brazil	5.96	12.21	23.4	21.5	-
Canada	9.69	22.54	26.5	27.1	33.7
China	115	156.08	15.5	24.1	33.1
Denmark	4.89	13.08	30.5	40.1	40.1
France	9.07	17.25	21.7	26.4	35.2
Germany	39.19	57.36	16.7	26.1	34.7
India	22.47	37.16	18.9	20.6	-
Italy	8.68	15.18	20	25.9	31.7
Poland	3.84	7.68	22.9	26.2	35.5
Portugal	4.86	12.11	28.5	25.5	-
Spain	22.98	52	25.8	27	36.1
Sweden	5.1	11.23	25.2	26.5	36.2
Turkey	3.63	8.52	26.8	26.7	35.2
UK	12.99	32.02	28.1	35.8	36.9
USA	64.23	181.66	32.3	26.5	34.8

Table 3.9 *– Capacity factors of existing onshore wind farms by country (data retrieved from the IEA statistics [163]) compared to the theoretical onshore capacity factors calculated in this study (Eq. (3.4)) for different wind classes, with a constant array placement efficiency of 90 % and availability factor of 97 %. Results are based on wind speed distribution at 100 m, and for wind turbine design parameters v_c = 3 m/s, v_r = 11 m/s and v_f = 25 m/s. Usually wind farms are put on sites of class III and lower in order to be cost effective.*

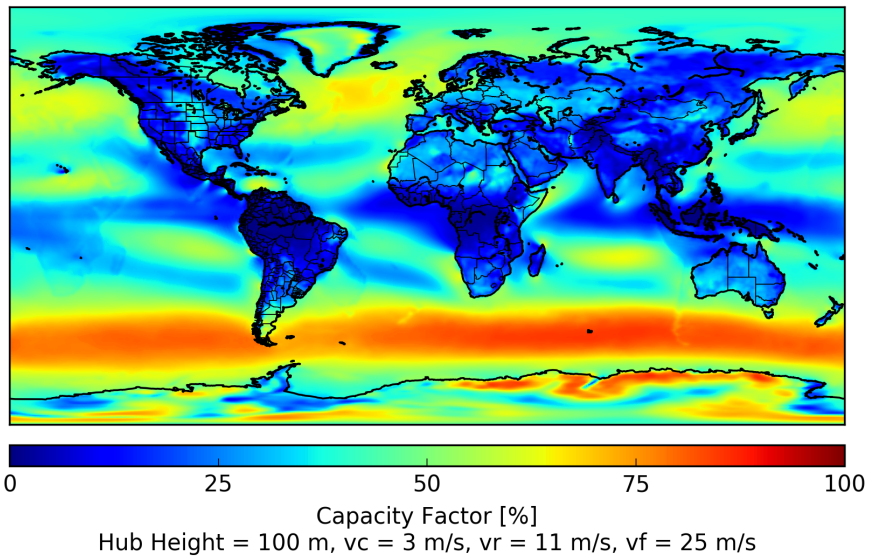


Figure 3.7 *– Map of capacity factor estimates.*

representing the spacing between two wind turbines in the wind farm in units of rotor diameter (RD). The optimal values directly give the optimal installed capacity densities, and, with results from the methodology in Section 3.2.2, the energy produced is computed. In order to remain within realistic turbine designs, the rated wind speed was allowed to vary from 10 to 16 m/s and the spacing parameter from 1 to 20 RD. The found results for the optimal value range was found to be between 10 and 13.65 m/s for the optimal rated speed, and from 6.8 to 20 RD for the optimal spacing parameter, corresponding to installed capacity densities varying from 0.6 to 9.26 MW/km^2.

The minimum value for the optimal spacing parameter increases with EROI_{min}, to values that are greater than current configurations but more consistent with results from wake aerodynamic studies (i.e. a spacing between each turbine varying between 12 to 20 RD) [95, 121, 122].

Kinetic energy generation rates

The global rate of kinetic energy available on suitable areas is assessed with Eq. (3.10). If restrictions are set to allow only onshore areas and offshore areas with water depths below 1 km, the 292 TW global total is reduced to 68 TW. In combination with the suitability factors defined in Section 3.2.1, the resulting

available energy potential is 15.85 TW over suitable onshore areas and 8.35 TW over suitable offshore areas.

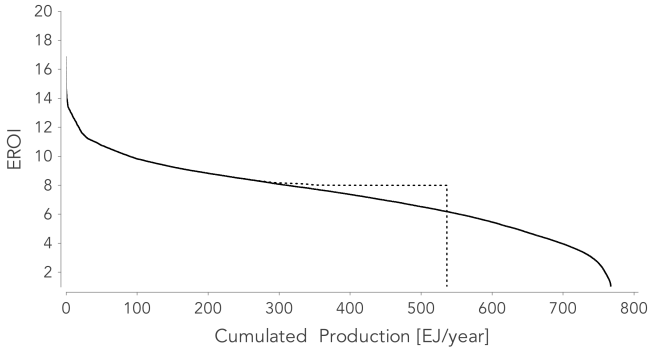
3.3.2 Global optimisation results

Evolution of the cumulative available wind energy flux based on EROI values

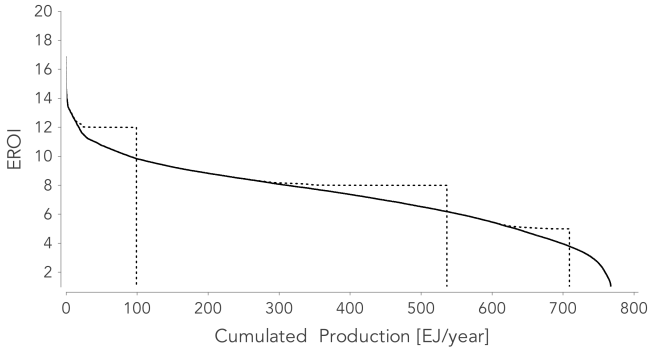
The results for the available energy that can be extracted from wind power is shown in this section, based on a curve, as described in Section 3.2.6, with the total production potential from the optimisation on the x-axis, relative to the EROI value on the y-axis. The shape of this curve gives a good idea of the repartition of the resources, i.e. if the initial slope is very steep, high EROI resources are limited. If in contrast there is a plateau at high EROI values it means that many places on earth are suitable to produce electricity from wind with only low energy input requirements relative to energy output.

In Fig. 3.8a the results with no constraint on EROI_{min} is shown. The initial slope is quite steep, indicating that only a small part of the available wind energy flux is available with high EROI values. The potential for EROI greater than 10 equates 89 EJ/year out of a total global value of 767 EJ/year.

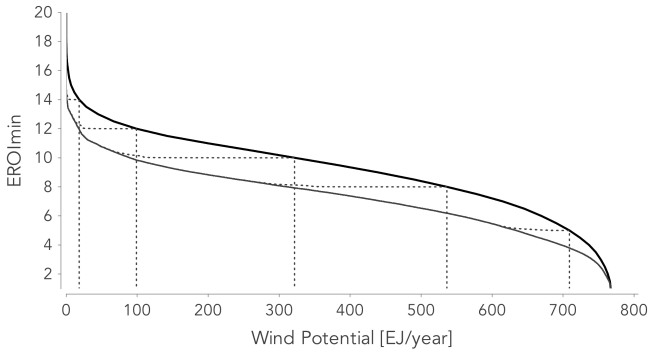
In the same graph (Fig. 3.8a), the resulting function when EROI_{min} is fixed at 8 (dotted line) is shown. The curve for EROI_{min}=8 follows the unconstrained curve until an EROI of 8, where there is a plateau until the potential drops to zero, because all sites where no wind park configuration allows for an EROI above 8 are excluded. The total potential available wind energy flux at this EROI amounts to 536 EJ per year globally, compared to 312 EJ in the unconstrained case. Surprisingly, the constraint on EROI_{min} allows to reach a significantly higher potential for the same level of EROI. This is because the EROI_{min} constraint forces less dense farms on certain cells in order to increase the energy outputs per MW installed, and reach the EROI_{min} imposed. In the following graph (Fig. 3.8b) the curves for EROI_{min} of 5 and 12 are added. Because optimal parameters depend on the EROI_{min} required, the evolution of the EROI with annual production will be slightly different for each value of EROI_{min}. The total global potential available wind energy flux at an EROI_{min} of 5 and 12 are 709 EJ/year and 99 EJ/year, respectively.



(a) EROI function with no constraint on EROI_{min} (plain line), and for EROI_{min}=8 (dotted line).



(b) EROI function with no constraint on EROI_{min} (plain line), and for EROI_{min} of 5, 8 and 12 (dotted lines).



(c) Enveloppe of the wind potential as a function of EROI_{min}.

Figure 3.8 *– Construction of the enveloppe for the wind potential, i.e. the maximum potential achievable for a given* $EROI_{min}$*.*

Enveloppe of the wind potential

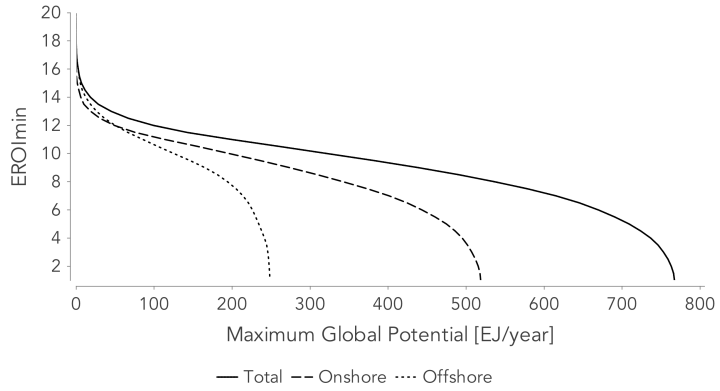
The results for the various evaluated $EROI_{min}$ levels as described above can be combined to generate an enveloppe curve of the total available wind energy flux, as shown in Fig. 3.8c. The curve can be used to read the potential available wind energy flux for every $EROI_{min}$ value from 1 to 20. The results using this enveloppe curve including variation by $EROI_{min}$ are given in Table 3.10. For example, for an $EROI_{min}$ of 5 an upper limit of 709 EJ per year is found, but it is reduced to 7 EJ/year for an $EROI_{min}$ of 15. As a comparison, global primary energy consumption was about 550 EJ in 2015 [131], and is expected to be in the range of 700-830 EJ by 2040 [164, 165].

	$EROI_{min}$	**2**	**5**	**8**	**10**	**12**	**15**
Total	Gross energy [EJ/year]	763	709	536	322	99	6.9
	Net energy [EJ/year]	645	612	475	291	91	6.4
	Installed capacity [TW]	143	114	66	31	7	0.4
	Area [10^6 km^2]	70	60	45	29	8	0.4
Onshore	Gross Energy [EJ/year]	516	475	342	196	49	1.5
	Installed Capacity [TW]	115	90	49	22	4	0.1
Offshore	Gross Energy [EJ/year]	247	234	194	125	50	5.4
	Installed Capacity [TW]	28	24	17	10	3	0.3

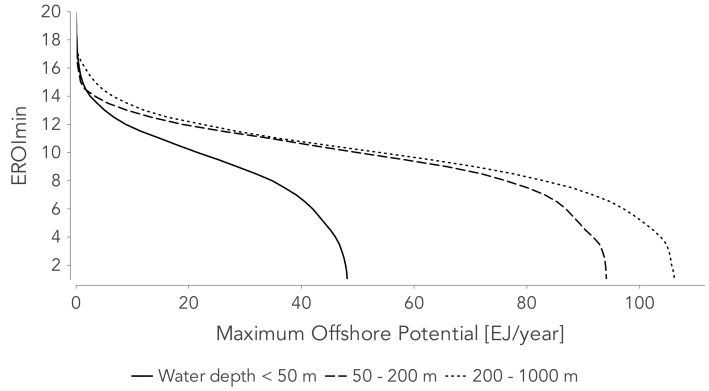
Table 3.10 *– Upper limit of the global wind potential for different values of $EROI_{min}$, expressed in gross annual production and net annual production (i.e. gross annual production - energy inputs). The potential is further divided in onshore and offshore potential.*

Onshore - offshore repartition

In Fig. 3.9a, the available energy flux is further divided into onshore and offshore areas. Onshore potential is higher for low EROI values, with a total flux of 519 EJ/year available compared to 248 EJ/year for offshore areas. When $EROI_{min}$ exceeds 12, the offshore potential exceeds onshore potential. As shown in Fig. 3.9b, where the offshore potential is further divided by water depth, a significant part of the potential is in deep water ($>$ 50 m depth). The total available energy flux for water depth between 50 meters and 1000 meters water depth is 200 EJ/year versus 48 EJ/year for depths lower than 50 meters.



(a) Onshore - offshore repartition.



(b) Offshore repartition by water depth.

Figure 3.9 *– Repartition of the global potential between onshore and offshore areas (Fig. 3.9a), and of the offshore potential divided by water depth (Fig. 3.9b).*

Spatial distribution of the resources

Results are shown on a world map for two values of EROI_{min} to visualize the evolution of the spatial distribution of the resources. In Fig. 3.10a optimal installed capacity densities are shown for $\text{EROI}_{min} = 5$, with a resulting mean installed capacity density of 1.98 MW/km^2. In Fig. 3.10b optimal installed capacity densities are shown for $\text{EROI}_{min} = 12$ with a mean installed capacity density of 1.05 MW/km^2.

The same analysis was conducted for power densities based on the mean power produced per unit area. The mean value increases with EROI_{min}. At a low EROI_{min} of 5 the mean is 0.37 W_e/m^2 (0.3 over land and 0.54 over sea),

and it increases to a mean of 0.57 W_e/m^2 for $EROI_{min} = 15$. These results are coherent with results of global circulation models from [104].

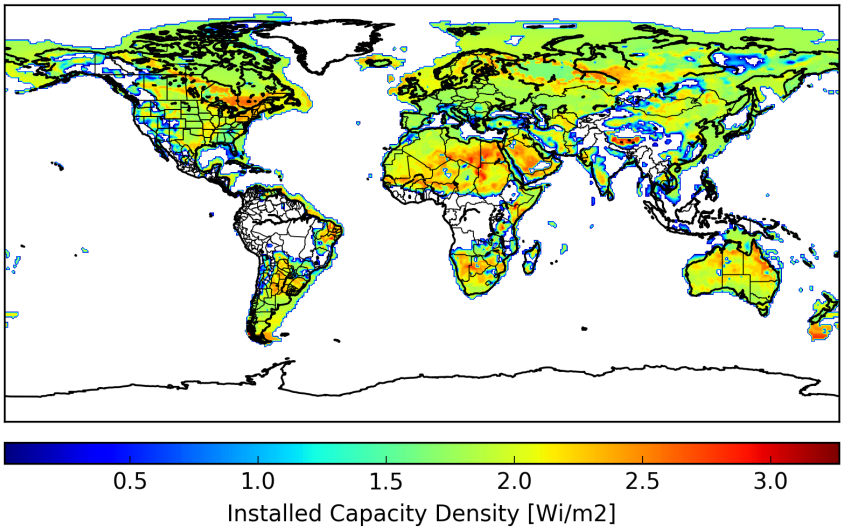
For an EROI threshold of 12, we see in Fig. 3.10b that the locations that remain profitable are mainly offshore, mostly in cold climate areas. Icing is common in most of the areas concerned (Northern Europe, America and Asia), particularly at hub height. The presence of ice on wind turbine blades considerably reduces the power generated by the turbine, as it deterioates their aerodynamic performance. The mechanical properties of steel, concrete, polymers are altered as the temperature decreases, and low temperature can also damage electrical components. Low temperatures therefore require adaptations to all components of a wind turbine, as well as special heating systems (see for example the IEA Wind publication [166]). The additionnal direct and indirect energy consumption for these additional devices, that would decrease the EROI, have not been taken into account in this study.

Limit on kinetic energy available

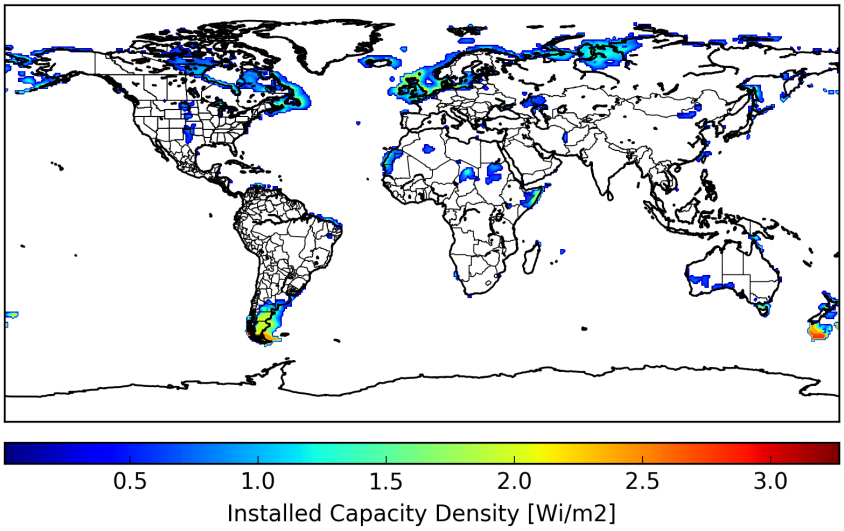
A sensitivity analysis was run to illustrate the impact of the constraint from Eq. (3.11). The results are compared with 3 other scenarios in Fig. 3.11: first by applying a factor 1.5 to the estimate from Eq. (3.10), then with a constant upper limit of 1 W_e/m^2, and third with no upper limit on the wind power density. The difference between the curves when $EROI_{min}$ decreases is substantial, with a total available global wind energy flux of 1988 EJ/year for the unconstrained case. However for $EROI_{min} \geq 10$ all scenarios yield similar potentials. Indeed, for high EROI values the optimal installed capacity densities are relatively low in order to maximise the output of each turbine. With sufficiently sparse wind farms, the power densities are not exceeding the upper limit from Eq. (3.10), and the 4 scenarios are converging for high EROI values.

Installed capacity densities

The enveloppe for the wind potential is also compared with the results of the model using fixed installed capacity densities in Fig. 3.12. This emphasizes the benefit of the optimisation at cell level, since the global potential remains constant but the curve shifts to lower EROI values when installed capacity density increases from 2 to 9 MW/km^2. Beyond 2 MW/km^2, the array effect becomes increasingly significant, as explained in Section 3.2.2. Therefore, adding more



(a) EROI$_{min}$=5.



(b) EROI$_{min}$=12.

Figure 3.10 *– Repartition of the optimal installed capacity densities (i.e. the wind power capacity installed by unit of area) for different EROI$_{min}$, results are in $W_{installed}$ / m^2.*

turbines does not allow to produce more electricity per unit of area.

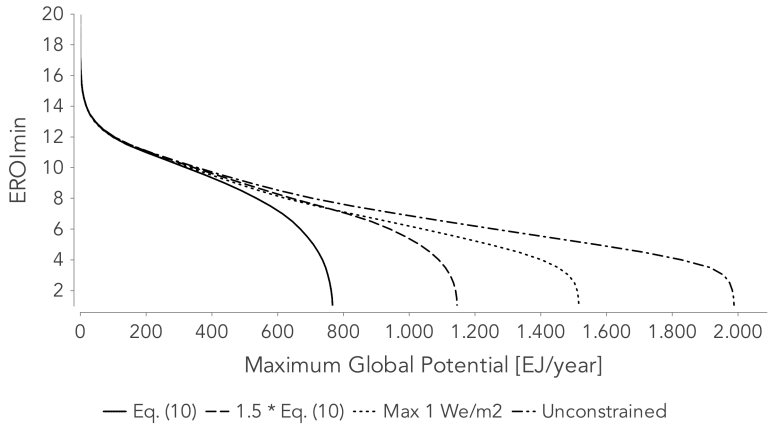


Figure 3.11 *– Impact of the constraint Eq. (3.11): the global gross potential [EJ/year] for different $EROI_{min}$ was optimised for 4 scenarios : first with the kinetic energy estimated from Eq. (3.10), then by applying a factor 1.5 to Eq. (3.10), third with a constant upper limit of 1 W_e / m^2, and finally without upper limit on the wind power density.*

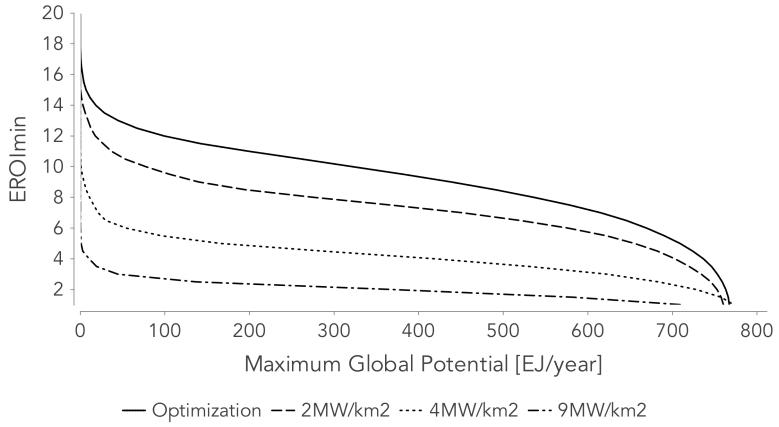


Figure 3.12 *– Enveloppe of the wind potential for different installed capacity densities. The optimisation results (at cell level) are compared with results with fixed installed capacity densities.*

3.3.3 Regional optimisation results

Results can also be computed for a specific area, so as to find a realistic constraint on the available wind resource per region or country that can be applied in energy modelling and to inform policy design. The first approach, as shown here first for the whole world and then for the European Union (EU-28) coun-

tries, is to assess the regional potential for a given cut-off EROI_{min}. Then we do the same exercise with a minimum capacity factor requirement, for comparison purposes (Section 3.3.3).

Regional potentials

The about 100 EJ/year of high EROI resources (EROI $\geq$ 12) are distributed as follows (Table 3.11 and Fig. 3.10b):

- 20% in North America, mainly the North and East coasts of Canada (75 % of the potential), evenly distributed among onshore and offshore areas.
- 16% in Patagonia (southern Chile and Argentina), evenly distributed among onshore and offshore areas.
- 15.5% in Europe, especially in the UK (40 % of the potential), Ireland, Norway, and Iceland, and mainly offshore (77 % of the potential).
- 14% in Oceania, mainly in the Tasman sea around New Zealand (80% of the potential).
- 14% in Africa (Morocco, Western Sahara, Mauritania, Sudan, Chad, East-Ethiopia, and Somalia), onshore.
- 13% along the Russian coast line, mainly onshore (70 % of the potential).

Among the remaining 6% the highest shares are in Kazakhstan, Brazil, China, Venezuela, and Japan.

EU-28 countries

Results for the EU-28 countries are shown in Fig. 3.13a, divided into onshore and offshore potential. The upper limit for the available wind energy flux in the EU-28 territories ranges from 34 EJ for EROI $\geq$ 5, to 0.4 EJ for EROI $\geq$ 15. Final energy consumption within the EU-28 countries in 2014 was 1 061.7 million tonnes of oil equivalent (Mtoe) [167], equivalent to 44.5 EJ, while wind energy production was accounting for 2 % of that consumption.

The spatial repartition of these resources is shown in Figs. 3.14a and 3.14b, where the optimal installed capacity densities are shown for 2 levels of EROI_{min}. The potential for countries with high EROI resources is detailed in Table 3.12. The offshore potential represents 58 % of the potential with

Region/Country	Potential [EJ/year] EROI ≥ 12		
	Total	**Onshore**	**Offshore**
North America	19.75	10.25	9.49
Canada	*15.07*	*7.93*	*7.15*
Argentina and Chile	15.92	8.65	7.27
Europe	15.53	3.35	12.18
United Kingdom	*5.65*	*1.63*	*4.02*
Norway	*2.24*	*0.09*	*2.16*
Ireland	*2.11*	*0.32*	*1.78*
Iceland	*1.44*	*0.1*	*1.34*
Oceania	14.32	1.8	12.53
New Zealand	*11.63*	*0.3*	*11.33*
Australia	*2.6*	*1.5*	*1.11*
Africa	14.28	13.07	1.21
Somalia	*3.77*	*3.53*	*0.23*
Sudan	*2.65*	*2.65*	*0*
Western Sahara	*2.14*	*1.63*	*0.5*
Chad	*2.12*	*2.12*	*0*
Russia	13.07	9.12	3.95
Kazakhstan	0.84	0.84	0
Brazil	0.82	0.38	0.44
China	0.77	0.71	0.05
Venezuela	0.22	0.07	0.16
Japan	0.19	0.05	0.14
Rest of the World	3.3	0.58	2.72
Total	**99**	**49**	**50**

Table 3.11 *– World regions/countries with high EROI resources (EROI ≥ 12), classified by decreasing potential.*

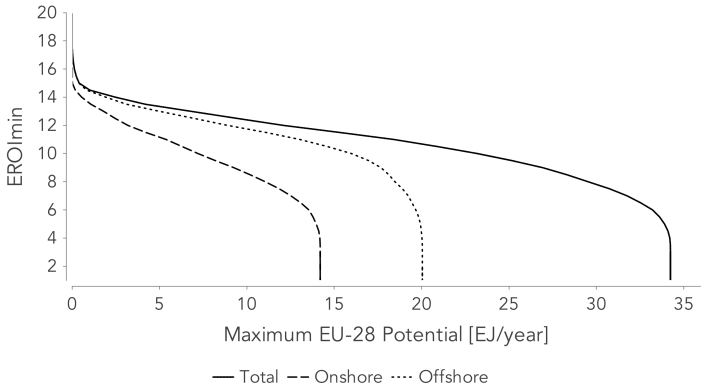
EROI ≥ 5, and 75 % of the potential with EROI ≥ 12. As already mentioned below, about a half of the EU-28 potential with EROI ≥ 12 is located in the UK.

These results are compared with results from the EEA study [94]. In their analysis, the installed capacity densities used were 10 MW/km^2 for onshore areas, and 6.4 MW/km^2 for offshore areas. By applying land-use constraints

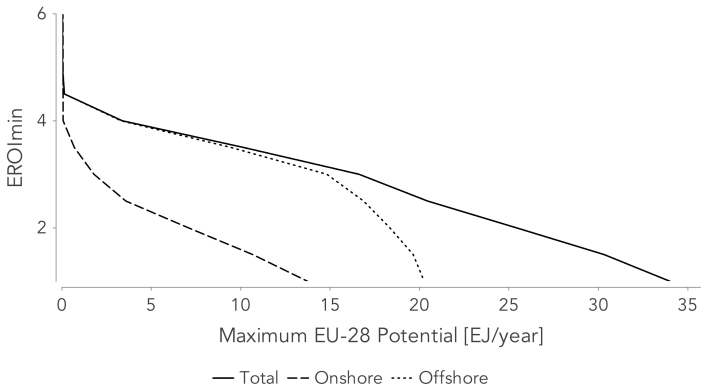
and wind regime constaints, the authors estimated an economically competitive potential for 2030 of 97 EJ/year over onshore areas and 12.25 EJ/year over offshore areas (restricted to water depths below 50 m). The results based on these capacity density parameters were reproduced here as shown in Fig. 3.13b. The high installed capacity densities as applied by EEA yield very low EROIs. Indeed in Fig. 3.13b there is no potential with EROI ≥ 5. For EROI ≥ 2 the global potential is of 25 EJ/year, only one fourth of their estimated economically competitive potential of 109 EJ/year.

Country	**Potential [PJ/year] EROI $\geq$ 5**			**Potential [PJ/year] EROI $\geq$ 12**		
	Total	**Onshore**	**Offshore**	**Total**	**On.**	**Off.**
UK	8,999	2,090	6,909	5,653	1,628	4,025
Ireland	3,530	466	3,064	2,107	324	1,783
Denmark	1,411	259	1,151	906	234	672
France	3,499	2,257	1,242	669	322	347
Netherlands	949	117	831	660	69	592
Germany	1,640	1,191	449	507	212	295
Sweden	1,684	844	840	423	94	330
Poland	1,411	1,219	192	255	120	135
Latvia	598	215	383	204	50	154
Estonia	382	89	293	168	19	149
Spain	2,406	1,604	801	136	27	109
Finland	1,127	415	712	84	7	77
Belgium	195	185	10	65	58	8
Lithuania	345	254	90	23	-	23
Greece	664	111	553	21	-	21
Portugal	185	97	88	5	-	5
Italy	1508	577	931	3	3	-
Rest of EU-28	2,598	1,781	816	-	-	-
Total	33,131	13,771	19,355	11,889	3,167	8,725

Table 3.12 *– EU-28 countries with high EROI resources, classified by decreasing EROI $\geq$ 12 potential.*

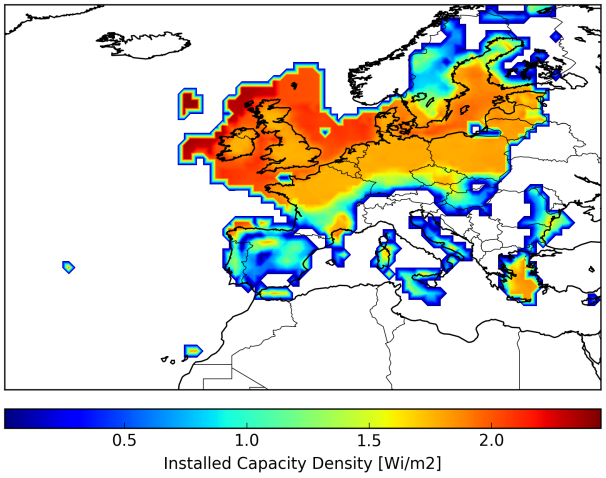


(a) EU-28's potential with the optimal installed capacity densities.

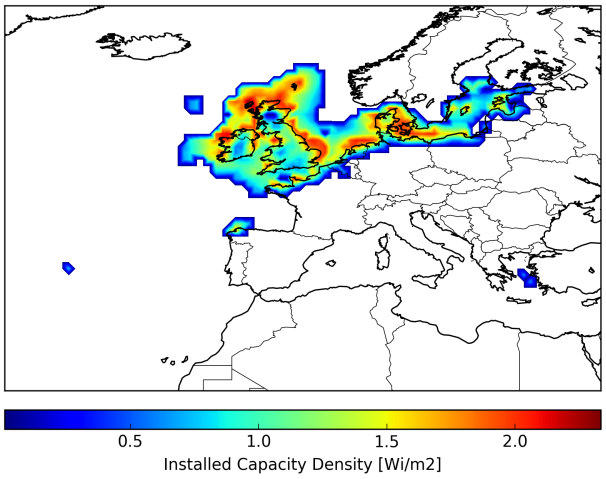


(b) EU-28's potential with installed capacity densities from the EEA study [94].

Figure 3.13 *– Enveloppe of the EU-28's wind potential as a function of* $EROI_{min}$*, with the optimal installed capacity densities (Fig. 3.13a) and with the fixed installed capacity densities from the EEA report (Fig. 3.13b).*



(a) EROI$_{min}$=8.



(b) EROI$_{min}$=12.

Figure 3.14 *– Repartition of the optimal installed capacity densities in EU-28 countries (i.e. the wind power capacity installed by unit of area) for different EROI$_{min}$, in $W_{installed}$ / m^2.*

Regional potentials with minimum capacity factor requirement

The second approach to calculate regional potentials is taken from and compared with the study of Bosch et al. [27] for onshore wind for comparative purposes. Bosch et al. took into account only areas with a wind capacity factor $> 15\%$ in computing the onshore wind potential. In all regions we find a five times lower onshore potential, and in India, Russia and South Asia a ten times lower potential, as shown in Table 3.13. Key differences include an assumed fixed installed capacity density of 6.52 MW/km^2 and 90% wind farm efficiency in [27] which lead to significantly inflated potentials relative to our study where the mean installed capacity density is in that case 2 MW/km^2 and the corresponding wind farm efficiency is around 82 %.

Region	Suitable Area [km^2]		Technical potential $C_f \geq 15$ % [TWh/y]	
	This Study	Bosch, 2017	This Study	Bosch, 2017
Canada	2,896,431	2,820,408	9,971	37,760
China	2,336,744	2,004,487	6,225	25,555
European Union	1,163,162	1,231,712	3,656	14,828
India	160,914	161,933	353	3,037
Latin America	2,164,392	2,076,996	7,503	29,546
Middle East	3,300,730	3,850,136	8,812	51,006
Oceania	4,340,244	4,318,259	13,641	55,597
Rest of Africa	10,824,219	9,581,313	34,322	142,590
Russia	4,567,391	9,536,004	14,251	126,492
South Asia (except India)	252,750	223,469	684	5,653
South East Asia	109,687	964,280	263	13,864
East Asia (except China)	793,041		2,178	
USA	2,276,426	1,557,990	7,248	17,061
Total	**38,863,592**	**41,747,248**	**120,858**	**586,750**

Table 3.13 *– Regional potentials for onshore areas with capacity factor $\geq$ 15 %, compared with the study for Bosch et al. [27]*

The onshore potentials found in this study based on this approach are lower than the required outputs of onshore wind in several recent 100% renewable energy scenarios. For example, Gulagi et al. [168] require 467-616 TWh of

onshore wind output per year to reach 100% renewable electricity in India. And the analysis of Jacobson et al. [18] utilises 3,028 TWh of onshore wind to reach 100% renewable energy including heat and transport in India. For China Jacobson et al. require 8,271 TWh/year versus a maximum potential of 6,195 TWh/year in our study when limiting to $> 15\%$ capacity factor areas.

3.4 Discussion

The three novel contributions of this work are the inclusion of an upper limit for the wind power density (Eq. (3.11)), the optimisation of installed capacity densities, and the evaluation of total available wind energy flux relative to the EROI of wind turbine based power generation. The model does not take into account the distance to electricity consumers, and therefore a significant portion of the available energy flux is plausibly located in remote areas.

3.4.1 Comparison with previous bottom-up studies

Because we use a similar approach to bottom-up studies reported in Table 3.1, results should be in similar order of magnitude. In these studies the available areas are restricted to areas with mean wind speed greater than class III ($v_{10m} \geq 4$ m/s, equivalent to $v_{70m} \geq 6$ m/s), based on the hypothesis that this wind speed limit corresponds to economically viable sites. In Table 3.14 results for onshore areas with mean wind speed greater than class III are given, with optimal parameters and installed capacity densities from [25, 72, 93].

We conclude that only the lower estimates of studies using capacity densities of 4 MW/km^2 or lower ([72] and [93]) are consistent with our approach for the available maximum wind energy flux. For studies with installed capacity densities above 4 MW/km^2, the literature results are an order of magnitude higher than our results. The reason is the overestimation of array efficiency in these literature studies according to our analysis (Section 3.2.2). The optimisation of capacity densities for wind farms and regions is thus of key importance to ensure higher EROI extraction of the available wind resources.

The comparison with the key 100% renewable energy scenario studies of Jacobson [18] for 139 regions and detailed regional studies such as the one of Gulagi et al. [168] showed that for specific countries such as India and China the required scenario potential is higher than the realistic upper bound for onshore wind potential. Further country by country study is required to analyse what

$\mathbf{EROI}_{min}$	Optimal Parameters	2 MW/km^2	4 MW/km^2	9 MW/km^2
2	735	321	515	667
5	689	321	515	377
8	355	287	226	10
10	203	78	35	0
12	52	12	3	0
15	2	0	0	0

Table 3.14 *– Onshore global potential [EJ/year], restricted to areas with mean wind speed at 70 m $\geq$ 6 m/s and without the constraint on the limited rate of kinetic energy (Eq. (3.11)). Results with the optimal parameters are compared with constant installed capacity densities used in the literature (Table 3.1). Results found here are closed to results from [72, 93] and the lower estimates of [92], but only up to $EROI_{min} \geq 8$. For higher EROIs, the potential is significantly reduced.*

are realistic upper bounds inclusive of wind-regime and land constraints, for application in renewable energy scenario studies and to inform policy design.

3.4.2 Limitations and perspective

Static vs dynamic approach

The model assumes a set of static conditions, which correspond to the current energy mix and technologies available. However, as discussed by de Castro and Capellán-Pérez in [42], such a potential assessment should be done dynamically or at least include a sensitivity analysis in order to assess the impact of the expected future evolution of some of the model parameters. These impacts are difficult to quantify a priori as some parameters will positively affect the overall potential and the associated EROI, while others will have a negative impact. On the one hand technological progress will increase the energy produced and decrease the energy embodied in the building of the infrastructure for a given installed capacity, i.e. it will incresae the numerator and decrease the denominator of the EROI. On the other hand, because of the decline in the ore content of some deposits, the energy required for the extraction and refining of certain metals will increase with the energy transition. The increasing need for intermittency management will also seriously affect the EROI.

A sensitivity analysis concerning the future evolution of the parameters that have a significant impact on the EROI would allow to refine the results

obtained.

Standard vs point-of-use EROI

Limiting oneself at the standard EROI may result in erroneous conclusions about the profitability of certain sites. In particular, it can be seen at Fig. 3.10b that the sites that are theoretically the most profitable in terms of standard EROI are offshore sites that are potentially not easily accessible and with extreme weather conditions. To get a better view of the sites which are really profitable, both in terms of energy production and in terms of accessibility, it is necessary to look at the point-of-use EROI (Eq. 2.3). Indeed the standard EROI does not include the electricity losses in the distribution network, which affect both the numerator and the denominator of the point-of-use EROI, and the costs for the maintenance and possibly the extension of the distribution network, which affect the denominator. To take into account the distribution of electricity to the end user, it would be necessary to be able to estimate, for each cell in the model, the distance to the existing grid in order to add the cost of the additional cabling needed to connect them. So far we have not found such a database in the literature. It would be reasonable to expect a significant drop in EROI, and a change in the ranking of the sites in terms of profitability.

In Chapter 5, a simple approach is proposed to get a first idea of the impact of electricity distribution, but it does not yet incorporate the indirect energy costs related to the grid, which should be the subject of a more detailed study.

3.5 Conclusions and policy implications

The study provided a new method including land constraints, wind regimes, kinetic energy limits, and EROI constraints, to analyse the global available wind energy potential. Constraints impacts were evaluated at three levels: i) only bottom-up constraints including land use, capacity factors, and array efficiency, ii) an added minimum Energy Return on Investment value ($EROI_{min}$), iii) inclusion of a top-down limitation on the kinetic energy available in the atmospheric boundary layer. The global wind energy potential at these three levels of constraints is a follows:

- Only bottom-up constraints, a global available annual wind energy flux of 1988 EJ/year, of which 1226 EJ/year from onshore and 762 EJ/year from offshore wind.

- Bottom-up + EROI_{min} constraints, a global available wind energy flux at an EROI_{min} constraint of 5, 8, 10 and 12 yielded a global wind energy flux of 1568, 707, 356 , and 104 EJ/year. The underlying values broken down into onshore wind are 1011, 437, 215, and 52 EJ/year and for offshore wind are 556, 271, 141, and 52 EJ/year, respectively.

- Bottom-up + Top-down + EROI_{min} constraints, a global wind available energy flux inclusive of an EROI_{min} constraint of 5, 8, 10, and 12 was found as 709, 536, 322 , and 99 EJ/year, respectively. The result is composed of an onshore wind potential of 475, 342, 196, and 49 EJ/year and an offshore wind potential of 234, 194, 125, and 50 EJ/year, respectively.

The results can be further split into regional potentials as shown in Table 3.11, and in Table 3.12 for the EU-28 territories. Total EU-28 potential net of energy inputs for bottom-up + top-down constraints are 30, 26, 21, and 11 EJ/year at an EROI_{min} of 5, 8, 10 and 12, respectively.

Similarly, constraints can be set to capacity factor minimum which at >15% shows for onshore wind an upper potential of 435 EJ/year, and a value of 36, 22, 1, 51, and 26 EJ/year for Canada, China, India, Russia, and the USA, respectively.

Four key implications for energy policy and wind energy investment can be drawn. First, the study confirms that scenarios assuming wind can reach a multi-digit share of global energy production are realistic. If only the best onshore and offshore wind sites with an EROI_{min} of 12 are fully occupied 99 EJ/year would be captured, based on optimally designed 4 TW and 3 TW of onshore and offshore wind capacity, or around 20% of current global energy use. This would require installing 8 times current onshore and 214 times offshore capacity relative to 2016 onshore and offshore wind capacity of 0.485 and 0.014 TW. Second, the study finds that floating offshore wind is an essential policy priority to unlock the total potential, given the offshore potential of < 50 m is half the potential of 50 to 200 m depth waters. Third, power and turbine density design of large wind parks tailored to local winds is key, so as to gain the maximum energy output at lowest cost. If not taken into account it can result in local overbuilding of capacity, lowering of capacity factors, and not capturing a portion of the available energy flux. Optimal turbine spacing varies significantly per site, with a rotor diameter distance between turbines ranging from 7 to 20 (12 to 20 for $\text{EROI}_{min} \geq 10$), equivalent to capacity density of 0.6 to 9.3 MW/km^2 (0.6 to 3.2 MW/km^2 for $\text{EROI}_{min} \geq 10$). The use of dynamic

capacity and power densities for regional wind energy potential is essential, as studies taking fixed densities without taking constraints into account can lead to substantial overestimates. As an example in this study the EU-28 territories potential for onshore wind was established at 12 EJ/year, versus 97 EJ/year in [94] due to more realistic power and capacity density constraints. Four, the use of detailed upper constraints on wind energy at a regional and country level is key in building energy scenarios so as to reach energy policies outcomes that are based on realistic available resource potentials.

Further work to inform policy will be carried out in three respects. First, to carry out more precise analyses of top-down kinetic energy constraints using global circulation models. Second, to specify country by country potentials using the combined constraints methodology inclusive of land use and planning. Finally, to refine the results obtained by including a sensitivity analysis on the model parameters, and by including an assessment of the point-of-use EROI.

A general recommendation for further study is to assess what EROI_{min} factor consists of a suitable cut-off factor from an economic perspective, in context of an electricity system with double-digit wind energy shares, since many countries only have a < 10 EROI wind resource available.

Nothing vast enters the life of mortals without a curse.

Sophocle

4

Global available solar energy under physical and EROI constraints

---

This chapter is an updated version on the following publication:
Dupont, E., Koppelaar, R. & Jeanmart, H. (2020). *Global available solar energy under physical and energy return on investment constraints.* Applied Energy, 257, 113968, https://doi.org/10.1016/j.apenergy.2019.113968

As mentioned in the introduction, solar power, together with wind power, will be an essential source of energy for the future. However, as can be seen in Table 4.1, estimates of the available potential vary considerably from one study to another. In order to reconcile these estimates, this chapter contributes to the literature by providing a novel comprehensive multi-constraint methodology to assess the potentially available renewable solar energy that can be sustainable harvested, and by exploring the global and regional results of this novel methodology.

Study	Technical Potential [EJ/year]		
	Centralised PV	**Rooftop PV**	**CSP**
Hoogwijk M., 2004 [72]	1,300	22	-
de Vries et a., 2007 [73]	14,778		
Trieb et al., 2009 [169]	-	-	10,605
GEA, 2012 [92]	6,000 - 280,000	-	-
de Castro et al., 2013 [79]	60 - 120 (total)		
Deng et al., 2015 [170]	316 - 2,815	210	131 - 1,078
Jacobson et al., 2017 [18]	41,461	47	31,104

Table 4.1 *– Previous studies in the literature and the constraints included to assess the harvestable solar energy potential*

The methodology presented in this chapter is similar to that presented in the previous chapter for wind power, but some points have been adapted to correspond to different solar energy conversion technologies.

This study is the first to carry out a multi-constraint analysis for the solar energy potential that takes into account land use constraints, physical available energy constraints, and constraints by requiring the delivery of a minimum amount of net energy to society, calculated using the EROI indicator. It also is the first study that incorporates the trade-offs between solar photovoltaic and concentrated solar power technologies, instead of analysing technologies in isolation, resulting in a much improved estimation than previously available. The results are usable for creating more realistic scenarios for the deployment of solar technologies for individual geographies and countries by taking into account a more realistic estimate of the solar resource available.

This chapter is structured as follows: the methodology is presented in Section 4.1, followed by the results in Section 4.2. The results are discussed in Section 4.3, and the final section concludes by summarising the results and proposing prospects for the future development of the methodology.

4.1 Methodology

To derive a more precise estimate of the global solar energy potential, as was done in the previous chapter, a grid cell model was developed to divide the globe into cells with a resolution of (i) for land use caracterization: 0.01° x 0.01°, and (ii) for solar irradiation data: 0.75° x 0.75° (cells of 4000 km^2 on

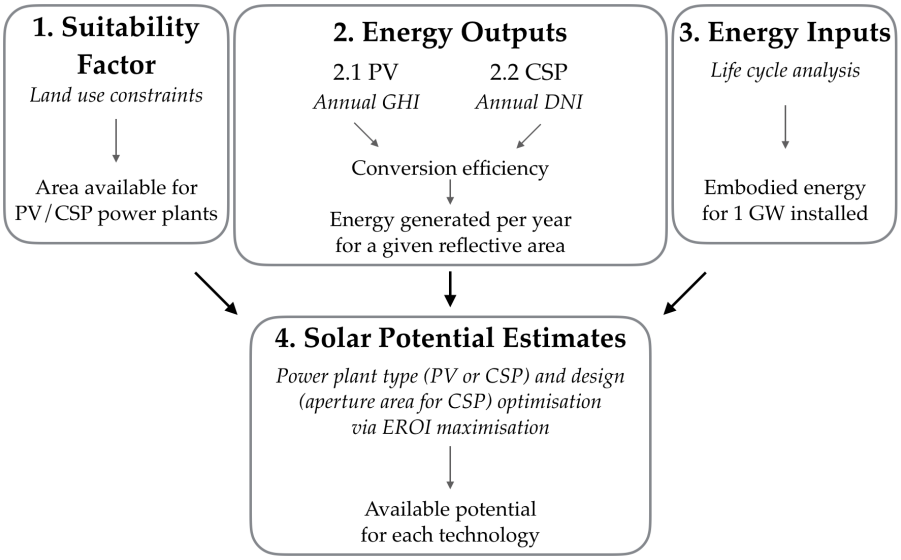


Figure 4.1 *– Diagram of the methodology used to evaluate the global available solar potential.*

average).

The multi-criteria constraints model selects which cell area is available for solar energy generation (geographic constraints), how much solar radiation is incoming in each cell (solar resource constraints), what share of solar energy photons are captured and converted into heat and electrical energy (solar technology constraints), and what share falls under or above a set EROI threshold (net energy constraint). The five technologies that were evaluated include polycrystalline silicon photovoltaic power plant (poly-Si-PV), monocrystalline silicon photovoltaic power plant (mono-Si-PV), parabolic trough power plant with oil as heat transfer fluid (HTF) (PT-oil), parabolic trough power plant with molten salt as heat transfer fluid (HTF) and 12 hours capacity of thermal energy storage (PT-salt-TES), and solar tower power plant with molten salt as HTF and 12 hours capacity of thermal energy storage (ST-salt-TES). For an overview of solar technologies and their physical system descriptions the review paper of Kumar and Kumar [171] can be consulted.

The model uses an optimisation algorithm so as to find the upper limit of energy that can be generated within these sets of constraints for each technology, reflecting the theoretical maximum within a series of realistic constraints.

The grid size of the model was selected to establish a parsimonious model that delivers a sufficiently accurate spatial granularity at a reasonable computational time. Specific aspects and parameters for establishing solar-PV and solar-CSP technology theoretical potentials are elaborated upon in Sections 4.1.1 to 4.1.7, based on seven modelling steps (Fig. 4.1) as outlined:

1. A **suitability factor** for solar energy is associated to each cell, discussed in Section 4.1.1, in order to take into account geographical constraints.

2. The availability of **solar energy** in each cell are assessed, as described in Section 4.1.2, to establish solar resource constraints.

3. The **conversion efficiency** of available solar energy flux into electricity is assessed, as well as the ground cover area of the complete systems, as described in Section 4.1.3, to take into account solar technology constraints.

4. The **energy inputs** for each type of solar plants are evaluated as described in Section 4.1.4.

5. The **scaling of CSP plants** collectors to fit with maximum power production was established relative to the power block rating and storage capacity, as described in Section 4.1.5.

6. Based on the findings from Sections 4.1.1 to 4.1.5 **the energy and EROI** values of each solar technology and grid cell was subsequently calculated, as described in Section 4.1.6

7. A EROI threshold limit was then applied to derive **EROI dependent estimates of the energy potential** at a global scale, as per Section 4.1.7, resulting in an integration of geographical, solar resource, solar technology, and net energy constraints.

In general the selection of parameter values has been carried out based on criteria for consistency by using where available global standards, studies that have a consistent coverage of a majority of countries and geographies, and review studies that use a meta-analytical method. Each section outlines specific parameter values and how they were estimated or obtained from previous studies. Whilst as much as possible country or geography specific values were evaluated or calculated, in certain cases averages were still utilised that

were deemed representative enough to cover different geographies based on the literature.

4.1.1 Geographic constraints

Since a majority of land mass is not suitable for solar power deployment, realistic assumptions should be taken regarding the available area to account for geographical constraints. To incorporate this for various technology types, solar technologies are divided in the multi-constraint model in large-scale applications, i.e. power plants of several megawatts; and smaller kilowatt size rooftop solar PV panel systems. Geographic criteria for both differ since these two kinds of applications do not compete for the same land area. For large scale megawatt plants, a suitability factor is associated to each grid cell, defined as the cell's fraction suitable for a CSP and a PV solar power plant installation.

Centralised power plants

The suitability factor was determined usng a three step process. First, the types of land use suitable for large scale megawatt plant deployment are selected, using similar assumptions as in chapter 3 adapted to solar power constraints. Land cover of each grid cell was retrieved from the GlobCover 2009 dataset, created by the European Space Agency (ESA) and the University catholique de Louvain (UCL) which classifies global land cover in 22 classes, at a 10 arc-second resolution [113]. Bioreserves from the world database on protected areas (WDPA) [114] are excluded, as well as urban areas and isolated and unpopulated areas (Antarctica, Greenland and small remote islands). To assing countries to each grid cell the dataset from the Flanders Marine Institute [115] was utilised.

The second step was to take an approximation of the share of available land for those land use types where large solar power plants could be deployed. The share was set at between 5% to 10% of global area depending on the land use type for land with suitable land use and slopes (see Table 4.2) [72]. Large scale solar power plants are difficult to combine with other land uses, beyond a few exceptions such as sheep grazing, therefore the suitability factor should be significantly lower [172]. Note that these parameter values are rough approximations and are unlikely to be representative across geographies for different

land uses. More precise GIS based estimations have been developed, but have not yet been deployed to create country by country assessments.

The final step was to apply exclusion criteria based on terrain slope [173]. CSP plants are not suitable for areas with an average slope greater than 2% [169], while PV plants may be placed in areas with slopes up to 30 % ($\sim 16.7°$) [170]. The global terrain slope and aspect database from the International Institute for Applied Systems Analysis (IIASA) was used, which provide 8 classes of terrain slope gradients [174]. A total of 38% of land area (47 millions km^2) has an average slope below or equal to 2 %, and 87.5% of the total land area (107 millions km^2) has an average slope above or equal to 30%.

The total geographic constraints that result in area per land use type suitable for solar-PV and CSP deployment is outlined in Table 4.2. The suitability factors depicted in Fig. 4.2 combine, in each cell, the land use factor, the slope constraints and country and protected areas exclusions.

Rooftop area

For kilowatt scale rooftop applications, a separate methodology was used based on estimates of available rooftop area in m^2 for each country in the world. To our knowldge, the only available globally applicable dataset of rooftop area for residential and commercial buildings covering 139 countries has been developed by Jacobson et al. [18], which is adopted for this study. Their estimates are calculated rooftop area based on floor area per capita adjusted for the number floors per building, the population, a rooftop slope adjustment, and a building overhang adjustment. Calculated floor area per capita was then estimated using a regression equation validated with EIA data for the US and the Entranze floor area database for EU countries [175]. After rooftop area is calculated, the proportion suitable for solar-PV can then be defined based on a usability factor, so as to take into account orientation and shading restrictions. Three methods with varying complexity have been created to estimate the usability factor, which were reviewed by the NREL [176] covering 35 studies, that cover estimates for a subset of geographies such as individual cities or countries. The resulting average usability factors used here, based on the NREL's meta-review, is 65% for commercial rooftops and 25% for residential rooftops for solar-PV [176]. The values are not extensively analysed and further research would

Land Cover	**Land use factor** [%]	**Area** [10^6 **km**^{2}]
Sparse vegetation, grassland, barren areas	10	37
Forests	0	32.4
Croplands	10	7.6
Shrubland	10	8.5
Mosaic vegetation - croplands	5	17.9
Mosaic grassland - forest or shrubland	5	6.9
Urban Areas	0	0.32
Water bodies	0	11.9
Total		**122.5**
Protected Areas	0	17.8
Slope $> 2\%$	0 (CSP)	69.6
Slope $> 30\%$	0 (PV & CSP)	9.4
Suitable for solar-PV plants		**5.4**
Suitable for CSP plants		**2.7**

Table 4.2 *– Repartition of the available areas into land use categories with a land use factor and slope evaluation.*

be needed to assess the suitability of these factors, and ideally to generate a country by country specific listing of rooftop usability factors.

The list of the estimated available residential, and commercial/industrial rooftop areas per country used in this study is showed in Appendix A.

4.1.2 Solar resource constraints

To calculate solar power output, a general formula was employed to establish physical constraints and solar technology constraints, so as to establish average power output per unit of area:

$$P_c = A_c \cdot I_c \cdot \eta \cdot \mathrm{GCR} \quad [W/m^2] \tag{4.1}$$

With :

- P: power output of the solar technology system for a grid cell c in watts.

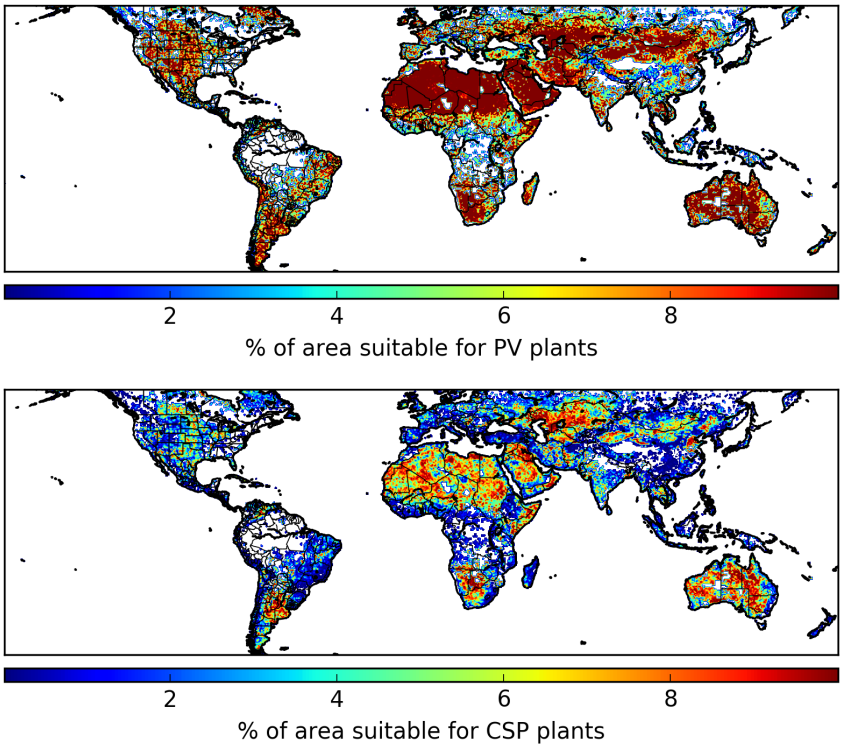


Figure 4.2 *– Proportion of the area suitable for centralised solar power plants (from 0 to 10 % of a cell's area).*

- A: applicable ground area for a cell in the grid model derived from Section 4.1.1.
- I: the yearly averaged irradiation $[W/m^2]$ in GHI for PV and DNI for CSP for a cell in the grid model.
- η: the conversion efficiency as the ratio of the electricity output to the solar irradiance of the CSP and PV technology systems.
- ground cover ratio (GCR), the ratio of the surface occupied by the PV cells or solar collectors to the total ground area occupied by the solar power plant.

To obtain data for parameter I, data for global horizontal irradiation (GHI) and direct normal irradiation (DNI) was used as input in the multi-constraints model. Global Solar Atlas data was used, which contains values with a resolution of 30 arcsec (approximately 1 km) [177]. To estimate yearly averages up to

20 years of data were captured with daily GHI and DNI totals (Fig. 4.3). Global Solar Atlas is a global standard funded by the World Bank developed under the ESMAP initiative on renewable energy resource mapping [178]. Outputs of the Global Solar Atlas have been validated using measurement data with over 200 high quality ground measurements in all continents.

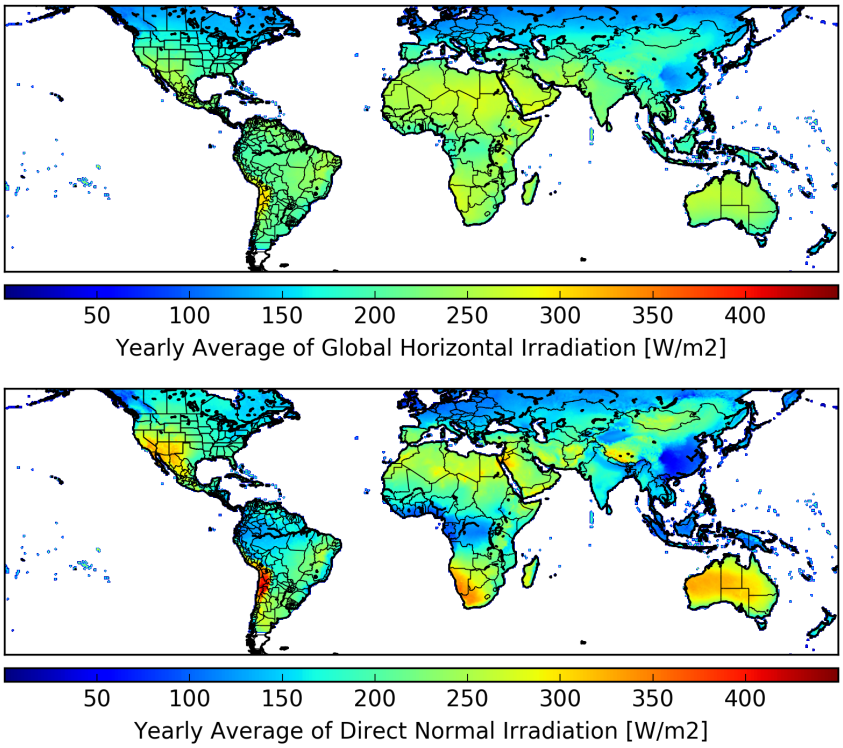


Figure 4.3 *– Longterm yearly average of GHI and of DNI, data obtained from the Global Solar Atlas, owned by the World Bank Group and provided by Solargis.*

4.1.3 Solar technology constraints

Solar photovoltaic conversion

The full cycle conversion efficiency η for solar-PV in Eq. (4.1) is calculated for each grid cell using the estimated electricity produced by a solar system, relative to the incoming solar radiation per grid cell. The electricy produced

after n years of operation for a solar-PV system is calculated as :

$$E_n = \sum_{i=0}^{n-1} \eta_{STC} \cdot p_r \cdot H_{\text{yearly}} \cdot (1-\alpha)^i$$
$$= \eta_{STC} \cdot p_r \cdot H_{\text{yearly}} \frac{1-(1-\alpha)^n}{\alpha} \tag{4.2}$$

With H_{yearly} the average annual cumulated irradiation (kWh/m^2/year), α the degradation rate, η_{STC} the efficiency of solar modules measured under standard test conditions (STC), and p_r the ratio of the actual performance of the system to its performance under STC. The duration of operation was taken at 25 years based on solar-PV module warranties or performance guarantees. The efficiency of solar modules is measured by manufacturers under STC and defined as the nominal power of a photovoltaic panel expressed in watt-peak, W$_p$. STC are an irradiance of 1 kW/m^2 with a cell temperature of 25°and a solar irradiation angle of 45 degrees. These conditions correspond to a spectrum similar to sunlight hitting the earth's surface at latitude 35°N during the summer period [179].

The estimated efficiency of solar modules deployed in 2018 has been estimated at 17.7% based on a global PV project database taking into account the impacts of fixed tilt and tracking on efficiency [180]. The value is aligned with an estimated average efficiency of 19% for polysilicon cells sold by producers found in the International Technology Roadmap for Photovoltaic (ITRPV) for 2018, taking into account lower efficiencies for modules versus individual cells [181]. ITRPV estimates are based on survey data from 55 solar supply chain companies from China, Germany, Spain and the United States [181]. Based on these values for this study a 17% efficient solar value was taken for the poly-Si-PV technology to reflect current technologies. An efficiency of 17 % corresponds to 170 W$_p$/m^2, whereby 1 kW$_p$ would occupy 5.9 m^2.

In case of mono-Si-PV technology a higher cell efficiency was taken to reflect upcoming cell technology with significantly improved efficiency, including passivated emitter and rear cell (PERC) designs and heterojunction cells [182]. The reason for incorporating such values is to adequately take into account likely improvements to have a better estimate for the conversion constraint for solar-PV technologies. The average efficiency of mono-silicon cells sold in

2018 was estimated at 21.5% based on industry surveys carried out by industry body ITRPV, with PERC designs incorporated in 35% of mono-silicon cells, and heterojunction designs in <1% of sold cells [181]. Industry expectations include heterojunction solar cells of n-type to gain a market share of 15% by 2029 with an average cell efficiency of 25%, and PERC cells to gain a market share of 70% with average cell efficiency on the market of 23.5% and 24% for p-type and n-type mono-Si [181]. The industry expectations are aligned with 24.7% and 25.1% efficient HJS mono-silicon cells that have been developed by Panasonic and Kaneka respectively, at pilot scale [182]. Based on these evaluations a module efficiency of 24% was utilised for mono-Si-PV technologies as a reasonable estimate for conversion efficiencies that will be reached around 2030.

The real-life output of a solar-PV plant is further influenced by optical, array and system losses, independent from the location and the panel orientation. Recommendations for the performance ratio (PR) has been established in the global methodology guidelines on life cycle assessment of photovoltaic electricity developed by the IEA. Based on a literature review a default PR value of 75% was recommended for rooftop and 80% for ground-mounted utility installations [183]. The recommendations are corroborated based on an evaluation of 30,000 solar-PV systems with data from 2006 and 2014 located in France, UK, Belgium and Spain [184]. The analysis applied a weibull distribution with individual systems ranging from 60% to 90% at extremes when looking at data from a large sample of solar-PV plants, with a mean and median around 80%. Typical perfromance ratios were established as the mode of the distribution at 81% for the UK, 80% for Belgium, 78% for France, and 81% for Spain. The data for Spain covered mostly large-scale PV plants versus rooftop systems for the other countries. An analysis of the PR of 7000 solar-PV systems in the UK using data from 2002 and 2013 established a typical PR of 83% as the mode of the data distribution across all systems [185]. An analysis for Germany evaluated the PR for 100 rooftop solar-PV systems and found a median PR of 84% [186].

Meta-reviews of many systems in other climate geographies were not found in the literature, yet individual system analyses are available. The PR of four large megawatt scale solar power plants in Thailand were evaluated obtaining PR's between 75% and 80% when regularly cleaned, dropping by up to 5% if

dust is not cleared on a timely basis [187]. The performance of three kilowatt scale solar-PV systems in Peru was evaluated finding PR ratio's at 84%, 82% and 74.5% respectively [188]. An 11 kilowatt-peak scale solar-PV plant in Iran was evaluated finding a PR of 80.8% for mono-Si-PV and 83% for poly-Si-PV [189]. The PR for a solar-PV system of 8 kiloWattpeak in Nanjing, China was evaluated at 75% to 85% for mono-Si pV and poly-Si PV varying per month of the year [190]. PR analyses for India established values of 72% for a 20 MW solar-PV plant [191], 74% for a 190 kiloWatt peak plant [192], 82.7% for a 186 kiloWatt peak plant [193], 77% for a 5 kiloWatt peak rooftop system [194], and a 77% PR rating for a 25 MW plant [195]. A PR for a 3.2 kW solar-PV system in South Africa was established at 84% [196].The performance of a mall kilowatt scale rooftop system in Ghana was studied finding a PR of 68% for mono-Silicon and 76% for poly-Silicon technologies [197]. Based on the evaluation of the studies above the PR recommended by the IEA was found to be similar to those established from more recent meta-studies and individual systems in various geographies and climate zones. The use of average PR ratio for different geographies is thereby a reasonable assumption, and the recommended PR by the IEA of 80% was applied in this study.

The degradation rate is included to take into account performance decline over time caused by smaller or larger failures of technology components [198]. An extensive literature review of 2000 studies with published degradation rates since the 1960s covered values from all continents, with most data points from the US, Europe, Japan and Australia [199]. Their median degradation rate for mono-Si modules was established at 0.47% for installations before 2000 and 0.36% for installations after 2000, and for poly-Si modules at 0.61% for installations before 2000 and 0.64% for installations after 2000. Based on this evaluation a value of 0.5 % per year was utilised in this study for the solar PV conversion calculation.

The full cycle conversion efficiency η was based on these parameters established at 13% over 25 years for a cell efficiency of 17%, a performance ratio of 80%, and a degradation rate of 0.5 %, the average efficiency of the system over 25 years would be 13 % (18.6 % for a 24 % efficiency panel).

Concentrated solar power conversion

The conversion efficiency η for CSP plant was established as the product of the efficiencies of the solar field, of the receiver technology, and of the power block:

$$\eta_s = \eta_{\text{field}} \cdot \eta_{\text{receiver}} \cdot \eta_{\text{power block}} \tag{4.3}$$

The efficiency of the solar field is defined as the ratio of the incoming solar radiation that is transferred as heat to the heat transfer fluid. It includes optical and geometrical losses including cosine effect, row-to-row shading, and soiling. The receiver efficiency mainly includes thermal losses, for example due to loop piping for parabolic through CSP. In total the thermal efficiency of the solar field has been evaluated around 35-40% [200]. The power block efficiency depends on the temperatures of the steam cycle and is established at ∼40%, depending on the temperatures reached.

The full cycle solar-to-electric efficiency is currently 15% for parabolic through technologies, and 20% for power tower technology [201]. Efficiency increases with the level of irradiance with measurements of 12 % at 1800 kWh/m^2/year and up to 16 % at 4000 kWh/m^2/year in [202].

Unlike PV plants, where the efficiency does not vary with the size of the installation, the design of CSP plants must be optimised due to the fixed size of the power block. The main parameter to optimise is the total aperture area (total reflective surface), i.e. the optimal number of concentrators (mirros/heliostats) for a given rated power and storage capacity. First, the area needed to produce the power block rated power at a design point (in general 950 W/m^2 of direct solar irradiance at solar noon on the summer solstice) is estimated, and then a multiplication factor, the solar multiple (SM), is applied to the calculated area in order to take into account lower irradiation levels and storage needs. Typical values for the SM range from 1.3-1.4 (plants without storage) to 2.7 for 12 hours of storage [203].

$$\text{Aperture Area } [m^2] = \text{SM} \frac{P_r[W]}{\eta_{\text{design}} \cdot \text{DNI}_{\text{design}}[W/m^2]} \tag{4.4}$$

Therefore, for a given rated power of the power block, the solar multiple is the parameter that must be adapted to the annual average DNI and latitude of a location. According to Eq. (4.4), the reference area (corresponding to a SM of

1) for a power block of 1 MW and an design efficiency of 22 % would be 4,785 m^2.

Increasing the aperture area above the reference area allows to increase annual production (hence changing the capacity factor), but it also decreases the solar-to-electric conversion efficiency of the plant. Given the fixed power block rating power, oversizing the aperture area increases the risk of curtailment during hours with high direct solar radiation. In addition, increasing the aperture area also increases energy dissipation (thermal losses due to longer pipes for parabolic trough, and optical losses with increasing distance to the receiver for power tower).

In order to model the evolution of the efficiency with the aperture area and location, simulations were run with the NREL the System Advisor Model [204] (SAM) [205]. For a representative number of locations and solar multiples, the annual energy prodution of CSP plants was estimated and the annual solar-to-electric efficiency was calculated. The simulation results are presented in Section 4.1.5.

Solar technology ground cover ratio

The GCR parameter in Eq. (4.1) covers the total spatial requirement of large scale solar-PV and concentrated solar power plants relative to the area of the solar panels and concentrating mirrors. According to [202] the GCR is 20% for PV plants and 13.5% for CSP plants. As a result solar PV power plant including all infrastructure covering access roads and space for logistics occupies 5 times the area of the PV panel alones. And 7.5 times the area of the concentrating mirrors is used for a CSP plant. The values are similar to the results of an analysis of existing, under construction and proposed utility-scale facilities in the United States conducted by the NREL [206]. The evaluation of land-use requirements of 32 utility-scale PV plants and 22 CSP plants yielded an average GCR of 19.5% for solar PV and 15.5% for CSP. In the multi-constraints model the values established by the International Renewable Energy Agency (IRENA) [202] are utilised. Finally, for rooftop applications, a spacing factor is already included in the usability factor described in Section 4.1.1.

In practice, the optimal ground cover ratio decreases with latitude, as a greater distance between successive panels is required to reduce losses due to shading. According to Martin-Chivelet[207], the ground cover ratio would de-

crease as a quadractic function of the latitude. This influence has not been taken into account in this study.

4.1.4 Solar energy inputs

Many existing studies calculate the EROI using life-cycle approaches for solar-PV modules, and only a few have studied the EROI of CSP. Meta-analyses for solar-PV have been published by Bhandarie et al. [208], Koppelaar [129] and Palmer and Floyd [209], and for CSP by Burkhardt et al. [210]. Study results vary due to different boundary and technology assumptions and age of manufacturing input data. Existing results are advanced by taking a complete cradle-to-grave boundary approach, encompassing nine stages from raw materials to final decommissioning, similar to [48], including i) raw materials extraction and conversion to an intermediary material (such as aluminium rolls), ii) transport to the factory, iii) manufacturing of the energy technology and other components, iv) transport to the installation site, v) installation, vi) operation, vii) maintenance, viii) decommissioning, and ix) decommissioning transport. Values include both operational and embodied energy from raw materials extraction and processing.

Data values are presented for 1 GW of 17% efficient poly-Si-PV, 24% efficient mono-Si-PV, PT-oil, POT-salt-TES, and ST-salt-TES. The reference of 1 GW was arbitrarily chosen, and does not reflect the current or expected size of the facilities. All electricity values, except for operational parasitic load, were converted into primary grid inputs, to obtain a fuel energy equivalent EROI value, also referred to as primary energy equivalent [39]. The electricity to fuel conversion was carried out by multiplication with a factor of 2.42, indicating that, globally, 2.42 GJ of fuel is required at present to produce 1 GJ of electricity. The value was obtained by weighting the electrical to primary efficiency of each power source based on their share of produced power in 2018 from global electricity mix data derived from [211] and primary to electrical efficiencies for each power source data per source derived from [212], as described in Table 4.3. The used values are representative for solar systems integrated in a fuel based energy system. In contrast a fully 100% future renewable scenario study would assume a 1.0 multiplication factor.

Power source	Share of produced power (2018)[%]	Electrical efficiency to primary (fuel) efficiency [GJ/GJ]
Coal	37.95	2.94
Oil	3.02	3.13
Natural Gas	23.23	2.70
Nuclear	10.15	3.03
Hydro-power	15.75	1
Bio-energy	2.35	3.85
Wind Power	4.77	1
Solar Power	2.20	1
Other Renewables	0.58	1
Total	**100**	**2.42**

Table 4.3 *– Estimation of global primary to final conversion factor. Source of data: [211], [212], this study.*

Solar-PV life cycle data

The main components of a solar-PV plant are solar modules, inverters, internal cables and a transformer station. A solar module is composed of solar cells, a film for protection typically made of EVA or Tedlar, glass, an aluminium frame and electronics. Six stages can be distinguished in the production of solar modules, i) extraction of quartz, ii) processing into metallurgical silicon, iii) upgrading to solar grade silicon, iv) manufacturing of wafers from silicon ingots, v) transformation of wafers into solar cells, vi) assembly of solar modules from all components. In addition to these manufacturing stages other phases in the life cycle are included. Table 4.4 summarizes the energy inputs associated with each stage in the life cycle. The calculation are based on the material needed, the estimated transport distances for each stage, and the energy intensities for materials extraction and transport calculations.

Data is presented firstly for poly-Si-PV based on a 17% efficient solar module as a lower limit solar-PV efficiency technology, and secondly presented for mono-Si-PV based on 24% efficient modules as a reasonable upper limit solar-PV scenario at efficiencies expected by the industry in 2030s, as discussed in detail in Section 4.1.3. The 24% efficient technologies include input data for

hetero-junction mono-silicon manufacturing with ultra-thin amorphous layers (HJS) [213]. Materials data and manufacturing energy inputs data for metallurgical silicon to silicon modules manufacturing was obtained from recent studies covering Chinese factories for state-of-the-art mono-Si technology [214] and poly-Si technology [215]. Materials and manufacturing data for the additional HJS cell processes, namely amorphous layer deposition PEVCD (plasma enhanced chemical vapor deposition) process and transparent conductive oxide (TCO) sputtering, was taken from [216]. For a detailed methodological description the reader is referred to [217]. To cover installation materials for ground-mounted solar, the most common mounting infrastructure for solar-PV panels was taken, using galvanized steel based on pile driving, as opposed to concrete ballast systems. All other life cycle energy values were calculated using the parameters in a recent comprehensive study by one of the authors where further details can be found [48].

Energy inputs for solar-PV systems are dominated by extraction and processing of minerals (about 60% of inputs), the manufacturing of the solar modules (about 30% of inputs), maintenance (about 7% of inputs), and operational parasitic load (1% of outputs). About 35% of fixed energy input is electricity converted into primary energy based on the earlier 2.42 GJ:GJ factor. The implication is that if the supply chain were to be based on a fully renewable system where such conversions are not occuring, the fixed energy inputs would be reduced by 20%. Fixed inputs being defined as inputs from raw material to decommissioning that are capital related (e.g. as opposed to operational inputs).

CSP life cycle data

Parabolic trough systems are composed of curved solar mirrors usually made out of tempered glass, a HTF pipe system with receiver pipes, and a power plant system. Solar power tower systems are composed of a central tower with a receiver, a field of heliostat flat solar mirrors that focus on the receiver, and a power plant system. Data is presented for three systems, including PT-oil, PT-Salt-TES, and a ST-Salt-TES, as outlined in Tables 4.5 and 4.6 for each stage of the life cycle.

The basic PT-oil without storage is based on an oil HTF system. It represents the until recently commonly installed technology and is based on NREL

data for the SAM [218], adjusted to exclude thermal storage. Based on the work of [219] a solar multiple (SM) of 1.3 was taken for capacity of the parabolic throughs, indicating that the field is slightly oversized relative to the power block.

The ST-Salt-TES also utilises NREL SAM data, which is based on the Ivanpah 377 MW plant in California, USA. The heliostat data is derived from BrightSource Energy's LH-2.2 heliostat [218]. Storage is based on a tank system with a molten salt mixture including sodium nitrate and potassium nitrate. The system was scaled based on the work of [219] with a SM of 2.7 to account for 12 hours of thermal energy storage, indicating that the field is substantially oversized relative to the power block. A 35% thermal to electric storage efficiency was assumed [220].

The PT-Salt-TES represents a next-generation technology. A state of the art trough design is taken based on thin 1 mm steel sheets coated with a reflecting polymer film [221]. The storage system is based on polymer encapsulated phase change salts, which increases thermal conductivity and thus increases energy density and reduces salt storage needs [222], with materials and embodied energy costs taken from [223]. Energy for the manufacturing of heat transfer fluids was obtained from [224]. All other components are assumed similar to that outlined in [218]. Similar to the ST-Salt-TES a SM of 2.7 and a 35% thermal storage to electricity efficiency is assumed [219].

Energy input data in Table 4.5 are presented for the materials needed for the default aperture area for an installation of 1 GW: 6,22 km^2 for PT-oil and 12,9 km^2 for PT-Salt-TES and ST-Salt-TES (corresponding to a solar mutiple of 1.3 without storage and 2.7 for 12 hours of thermal storage capacity). This distinction allows to easily scale up or down the energy inputs for the mirror field, given the optimal aperture area calculated for each location and technology.

The energy inputs for CSP are dominated by extraction and processing of minerals (50% of inputs for installations without storage, up to 70 % with storage), power plant manufacturing (30% of inputs without storage (mainly due to the oil HTF), and 10% with storage), the maintenance (12-15% of inputs), and the operational parasitic load (7% of the outputs).

		poly-Si-PV		mono-Si-PV	
		[GJ/GW]	**Share** [%]	**[GJ/GW]**	**Share** [%]
Processes	Raw material	12,211,500	65	8,880,750	55
	Manufacturing	4,394,480	23	5,596,460	35
	Construction	71,650	0.4	61,280	0.4
	Maintenance	1,322,800	7	1,131,300	7
	Decommissioning	71,650	0.4	61,280	0.4
Transport	Raw material	33,930	0.2	24,660	0.2
	Construction	303,480	2	218,450	1
	Decommissioning	315,520	2	226,150	1
Total [GJ/GW]		**18,725,010**	**100**	**16,200,320**	**100**
Operation[GJ/GJ]		0.0097			

Table 4.4 *– Summary of life cycle energy inputs for solar-PV technologies. Sources : [48, 214, 215]*

About 15% of fixed energy input is electricity that is converted into primary energy based on the earlier 2.42 GJ:1GJ factor. It means that in a fully renewable scenario (i.e. with a PEF equal to 1), fixed energy inputs would be reduced by 10%.

		PT-oil		PT-Salt-TES	
		[GJ/GW]	**Share** [%]	**[GJ/GW]**	**Share** [%]
Processes	Raw material	10,775,620	50	30,350,790	70
	Manufacturing	6,735,420	31	4,412,440	10
	Construction	106,000	0.5	220,160	1
	Maintenance	2,673,540	12	5,511,600	13
	Decommissioning	114,400	1	237,600	1 1
Transport	Raw material	63,650	0.3	116,630	0.3
	Construction	517,960	2	1,494,040	3
	Decommissioning	630,320	3	1,156,100	3
Total [GJ/GW]		**21,616,910**	**100**	**43,499,360**	**100**
Operation[GJ/GJ]		0.073			

Table 4.5 *– Summary of life cycle energy inputs for CSP technologies. Sources of data including [218] for PT-oil, PT-Salt-TES, and [223], [218] for ST-Salt-TES.*

		ST-Salt-TES	
		[GJ/GW]	**Share** [%]
Processes	Raw material	24,891,800	67
	Manufacturing	3,642,820	10
	Construction	220,160	1
	Maintenance	5,511,600	15
	Decommissioning	237,600	1
Transport	Raw material	108,510	0.3
	Construction	1,222,840	3
	Decommissioning	1,049,220	3
Total [GJ/GW]		**36,884,540**	**100**
Operation[GJ/GJ]		0.073	

Table 4.6 *– Summary of life cycle energy inputs for CSP technologies (cont.). Sources of data including [218] for PT-oil, PT-Salt-TES, and [223], [218] for ST-Salt-TES.*

4.1.5 Establishing efficiency and CSP collector aperture area relation per grid cell

To provide for an upper theoretical limit for CSP technologies within constraints, the optimal ratio between solar collector field size (aperture area) and the power block and storage system needed to be established. To this end a relationship was established for the evolution of the solar-to-electric conversion efficiency with the average DNI of the location and the solar mutiple of the plant. The end result is an understanding of the solar multiple for each cell that results in the optimal conversion from solar energy to electricity.

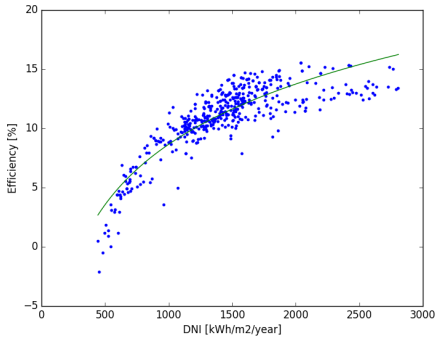
In order to do so, first 400 representative locations over the world were selected in SAM [205], and, for each, the annual output of a power plant was simulated for a set of solar multiples, around the values usually applied in existing power plants, which are based on economic evaluations (1.3 without storage and 2.7 with 12 hours of thermal energy storage). The dependence of latitude on CSP efficiency was neglected in our study, as in [169], as no empirical relationship for the evolution of efficiency with latitudes has been established to present.

For each simulation, SAM estimates the annual production of the plant based on hourly resolved irradiance data. The solar-to-electric efficiency is calculated afterwards, based on the average DNI of the location and the aperture area (size of the collector field):

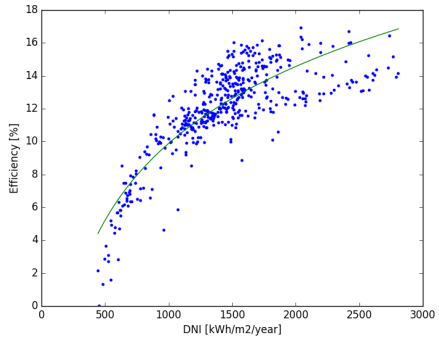
$$\eta_{\text{solar}\to\text{elec}} = \frac{\text{Annual Production } [kWh/year]}{\text{Aperture Area } [m^2] \cdot \text{DNI } [kWh/m^2/year]} \tag{4.5}$$

To find a regression function for the dependence on DNI and the solar multiple, first the evolution of the efficiency with DNI was studied for a fixed value of the solar multiple. The simulation points exhibit a logarithmic dependence of type $\eta = a \ln \text{DNI} - b$, as one can observe in Fig. 4.4. The parameters a and b were estimated with a least squares linear regression (R^2 between 0.5 and 0.75).

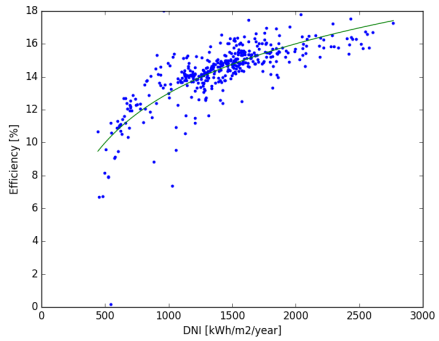
Second, the evolution of the parameters (a and b) with the solar multiple was then studied. The range of the solar multiple was simulated from 0.9 to 2 without storage, and from 2.5 to 4 for 12 hours of storage (with a step of 0.1). These ranges were selected in order to remain within realistic design configurations compared currently established CSP plants. The parameters exhibit a perfect linear dependence ($R^2 > 0.99$), i.e. a et b are interpolated



(a) PT-oil, SM = 1.3



(b) PT-salt-TES, SM = 2.7



(c) ST-salt-TES, SM = 2.7

Figure 4.4 *– Evolution of the efficiency with annual DNI, for PT-oil with a solar multiple of 1.3, and PT-salt-TES and ST-salt-TES with a solar multiple of 2.7, interpolated with the logarithmic function* $\eta = 7.349 \ln DNI - 42.12$*,* $\eta = 6.747 \ln DNI - 36.72$*, and* $\eta = 4.339 \ln DNI - 16.97$*.*

as linear functions of the solar multiple. The function for the evolution of the efficiency that we proposed in this study is therefore of the following form:

$$\eta(\mathrm{DNI}, \mathrm{SM}) = (a_1\ \mathrm{SM} + a_2)\ \ln(\mathrm{DNI}) + (b_1\ \mathrm{SM} + b_2) \tag{4.6}$$

With the parameters a_1, a_2, b_1 and b_2 estimated for each technology with a large set of simulations (Table 4.7).

	a_1	a_2	b_1	b_2
PT-oil	-3.38	11.55	23.85	-72.26
PT-Salt-TES	-1.578	11.17	10.65	-66.33
ST-Salt-TES	-1.62	8.742	11.01	-46.86

Table 4.7 *– Parameters for Eq. (6.21) for each technology, with DNI expressed in* $kWh/m^2/year$.

The efficiency is maximised for low values of the solar multiple such that the configurations allow to convert almost all incoming solar radiation into electricity. From an economic point a view they are not optimal as the power block and storage system are underused, yet from an energetic point of view, the optimal SM maximises the energy output.

4.1.6 Energy potential and EROI values

A value for the global solar potential and EROI values in each geographical cell was calculated for the five technologies presented in Section 4.1.4. The electricity production potential for each cell and for each country is evaluated as the gross electricity produced, calculated based on Eq. (4.1) using the life time of the facility, and excluding on-site operational electricty inputs. The calculated potential therefore corresponds to the amount of electricty that actually leaves a production site.

$$\text{Electricity Production Potential} = \text{Gross Energy Produced} \tag{4.7}$$

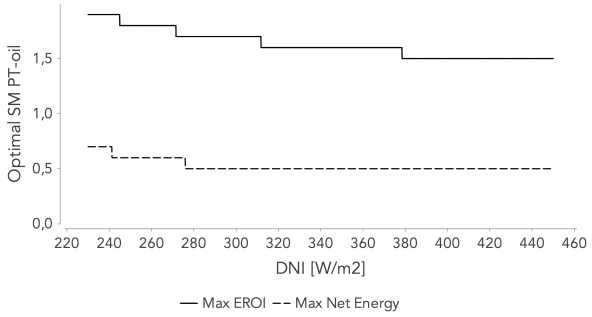
$$- \text{Operational Electricity inputs} \tag{4.8}$$

The EROI is then calculated as the ratio of gross energy produced to energy inputs, i.e. in cell/country i:

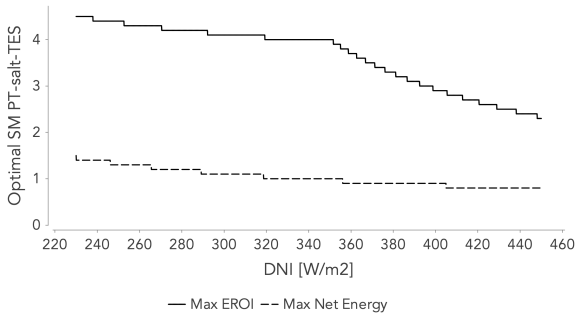
$$\begin{aligned} \text{EROI} &= \frac{\text{Gross Energy Produced}}{\text{Energy Inputs}} \\ &= \frac{\text{Suitable Area}_i \cdot I_i \cdot \eta(I_i, \text{SM}_i) \cdot \text{GCR} \cdot \text{Life Time}}{\text{Energy Inputs(Rated Power, Aperture Area)}} \end{aligned} \tag{4.9}$$

With the suitable area as a geographic constraint evaluated in Section 4.1.1, I_i the physical constraint of GHI/DNI of the location depending on the technology as evaluated in Section 4.1.2, η the solar-to-electric efficiency (depending on the irradiance and solar multiple for CSP applications), and GCR the ground cover ratio as technology constraints which were described in Section 4.1.3.

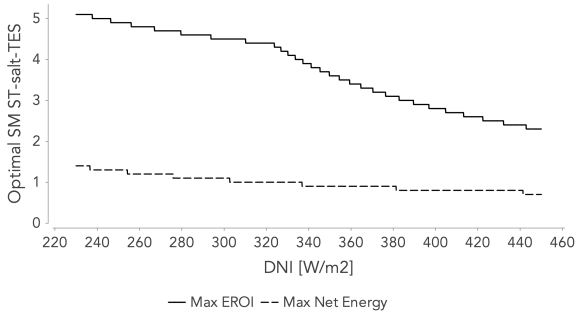
In case of CSP power plants the efficiency parametrisation from SAM simulations, as described in Section 4.1.5 was combined with the detailed life cycle inputs data from Section 4.1.4 in a dynamic manner. The energy inputs were divided in a fixed part linked to the power block and thermal storage, and a variable part linked to the mirror field, so as to obtain cell specific energy inputs fitting with optimised solar multiples. The EROI of each CSP power technology was subsequently calculated for each DNI and solar multiple per cell by selecting the solar multiple that maximises the EROI. The optimal solar multiple as a function of the DNI is shown in Fig. 4.5 for the 3 CSP technologies, as well as the solar multiple that maximises the net energy produced per unit of area. The solar multiple was set to a maximum for ST-Salt-TES in order to remain within realistic designs, such as due to growing atmospheric attenuation losses when allowing the distance between the heliostats and receiver to grow without bounds. The maximum was set to 4 for installations with 12 hours storage corresponding to the change in slope in Fig. 4.5. The slope change is observed because at higher solar multiple there is considerable curtailment where energy captured by the heliostat exceeds the power block and storage capacity.



(a) PT-oil



(b) PT-salt-TES



(c) ST-salt-TES

Figure 4.5 *– SM maximising the EROI or the electricty production potential of the installation as a function of the annual DNI.*

4.1.7 Global EROI constraints

The resulting outputs from Eq. (4.8) for electricity production potential and Eq. (4.9) for EROI were combined to establish a function depicting the evolution of the EROI with the electricity production potential, similar to the methodology in [60]. The function classifies geographies or countries by decreasing EROI and then draws the evolution of EROI with the cumulative energy potential. The total energy production potential is plotted on the x-axis against the associated EROI on the y-axis. The shape of the curve provides insights in the repartition of the resources. If, for example, the initial decrease is steep it implies that high EROI resources for solar power limited on earth. On the opposite, if there is a large plateau at high EROI, it implicates that many geographies are suitable for extracting energy from solar radiation at low energy input requirements compared to energy ouputs generated. In addition, the function allows for selecting a net energy constraint by allowing partioning of the cumulative energy resource at an EROI cut-off threshold for what energy resource is extracted. Cut-offs were selected based on the shape of the function at EROI values equal or greater than 5, 7.5 and 9, to establish the variation in energy solar resource. The procedure was carried out for each of the individual technologies. In addition, to obtain a globally integrated picture based on a selection of solar technologies which are optimal for each location, one of the five technologies was selected based on which provided the highest EROI value in that cell.

4.2 Results

4.2.1 Technology comparison at 1 GW scale

Before evaluating global grid cell multi-constrained results, a summary of results for each of the five solar technology systems at 1 GW scale is first presented. To create a fair comparison the results are presented when operating under the same irradiance conditions corresponding to Sevilla, Spain at a yearly averaged GHI of 207 W/m^2, and a yearly averaged DNI of 237 W/m^2. In Table 4.8 solar-PV and CSP technology system results can be found for area occupied, solar-to-electric efficiency, capacity factor, life time energy outputs and inputs, and EROI. Among PV technologies, mono Si-PV based on the specifications has a higher EROI and energy production density due to its

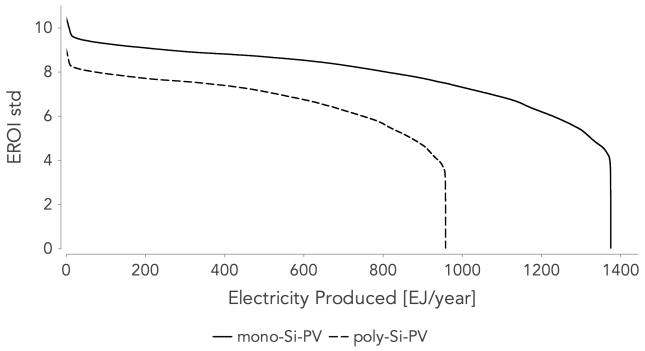
	poly-Si	mono-Si	PT-oil		PT-salt-TES		ST-salt-TES	
SM	-	-	1.3	1.9	2.7	4	2.7	4
Area [km^2]	29	21	47	68	97	144	102	150
C_f [%]	16	16.2	19.2	25.6	45.2	59	50.6	66.8
$\eta_{\text{solar}\rightarrow\text{elec}}$ [%]	13	18.6	13	11.9	14.8	13	15.8	14
Outputs [PJ]	125.8	127.9	181.6	242.1	427.8	557.7	478.5	631.5
Fixed Inputs [PJ]	18.7	16.2	21.6	27.7	43.5	51.6	36.9	42.6
Variable inputs [J/J]	0.01		0.073					
EROI$_{std}$	6.3	7.3	5.2	5.3	5.7	6	6.7	7.1

Table 4.8 *– Life cycle inputs, outputs and EROI of 1 GW installed for the 5 technologies, with irradiance conditions corresponding to Sevilla, Spain (a yearly averaged GHI of 207 W/m^2, and a yearly averaged DNI of 237 W/m^2).*

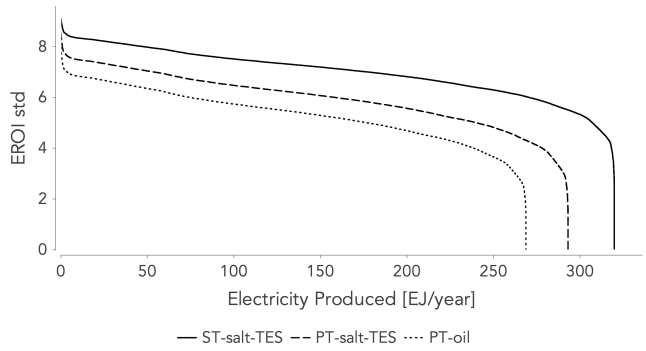
greater efficiency, despite higher energy inputs. In case of CSP technologies, the high energy cost of synthetic oil HTF negatively impacts the EROI of PT-oil compared to PT-Salt-TES [224]. ST-Salt-TES exhibits the best conversion efficiency at similar energy inputs needs PT-Salt-TES. The high capacity factor provided by CSP plants with storage gives these technologies additional benefits for electricity systems, despite their lower EROI. However, the capacity factor was not included as a driving variable in the multi-constraints optimisation model to select the best technology for each location.

4.2.2 Global large scale ground systems energy potential

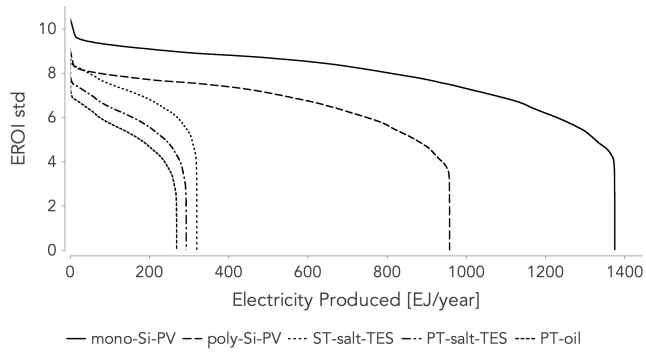
The result for the available energy that can be extracted from solar power is presented in this section, based on the mapping of EROI to cumulative energy, as described in Section 4.1.7. The resulting function is shown for each individual technology in Fig. 4.6. The total global potentials (after deduction of on-site operational energy inputs) for each individual technology was evaluated at 958, 1374, 269, 293 and 320 EJ/year for poly-Si-PV, mono-Si-PV, PT-oil, PT-Salt-TES, and ST-Salt-TES, respectively. In comparison, world final energy consumption in 2016 was estimated at 96 Mtoe($\sim$400 EJ). The potential for CSP is significantly lower than for solar PV from an individual perspective because of slope restrictions and higher ground cover ratios. The curves show that the best geographic sites for these technologies have an EROI$_{std}$ at 9.1, 10.5, 8.2, 8.6 and 9.1 for poly-Si-PV, mono-Si-PV, PT-oil, PT-Salt-TES, and ST-Salt-TES, respectively.



(a) Global potential for the different PV technologies



(b) Global potential for the different CSP technologies



(c) Global potential for all solar technologies

Figure 4.6 *– Global solar potential for the different technologies considered in this study.*

The global potential was also calculated by choosing, for each cell, the

technology with the highest EROI, see Fig. 4.7. The total global potential with the best technology in each cell was evaluated at 1274 EJ/year and is dominated by the selection of mono-Si-PV technologies. It is lower than the global potential of mono-Si-PV if selected alone without other technologies, because CSP provides for a better EROI in cells with very high DNI levels, yet has a lower production per unit of area due to a larger ground cover ratio.

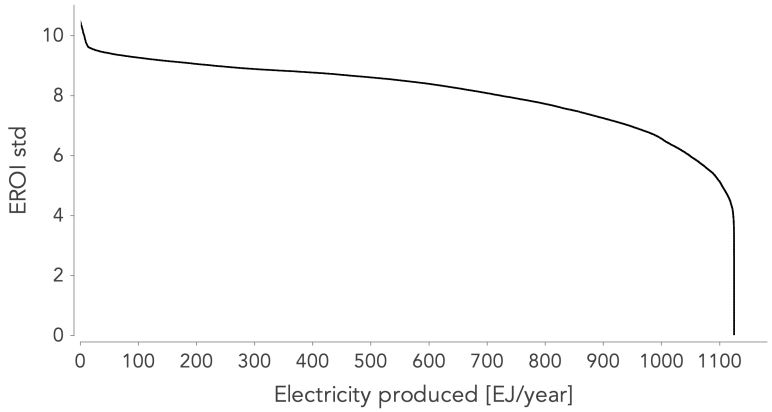


Figure 4.7 *– Global solar potential as a decreasing function of the EROI, obtained by selecting the technology with the highest EROI in each cell.*

Impacts of EROI constraints on the energy potential

The evaluation found that of the total energy potential 98% or 1248 EJ/year can be obtained at EROI greater than 5, 75% or 952 EJ/year at an EROI greater than 7.5, and 20% or 253 EJ/year at an EROI greater than 9 4.10. The results indicate that large areas of land are available with a good solar resource quality. In contrast, a similar grid cell method for the global wind energy potential [225] resulted in a far steeper decline in EROI. A key difference is that there are large areas with the highest resource, such as high solar radiation areas like deserts, which are in general not suitable for human activities, i.e. thereby suitable for large solar power plants.

As discussed in Section 2.1.2, the threshold represents a minimum EROI that needs to be maintained for societies economic balance to continue, without requiring to shift capital from non-energy sectors to energy sector. The minimum EROI that a sustainable society must have is difficult to estimate and an

on-going research effort [49]. Here EROI thresholds were chosen as outlined in Section 4.1.7 based on changes in the steepness of the curves, to explore points at which the energy potential changes significantly when the minimum EROI requirement increases.

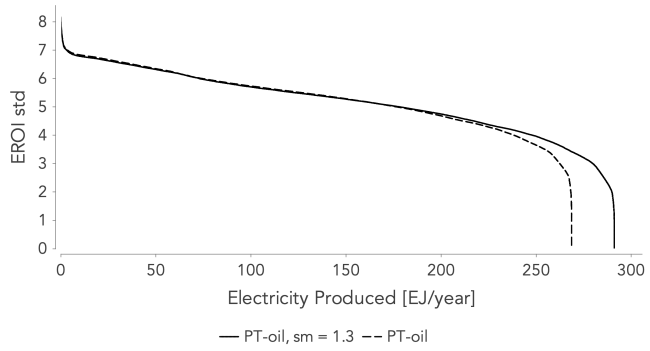
Impact of the CSP solar multiple design optimisation

In Fig. 4.8 the impact of the design optimisation is presented. For each type of CSP technology the global energy potential as a function of EROI was drawn. Both with a standard solar multiple and an optimal SM value as described in Table 4.8. In case of CSP technologies without storage there is almost no difference as the model will select similar solar multiples in both the standard and optimal case. For model runs with 12 hours of storage capacity the curve with the optimal solar multiples delivers marginally higher EROIs, yet at a cost of 30 EJ of lower global energy potential due to the greater land occupation as a consequence of the higher solar multiple.

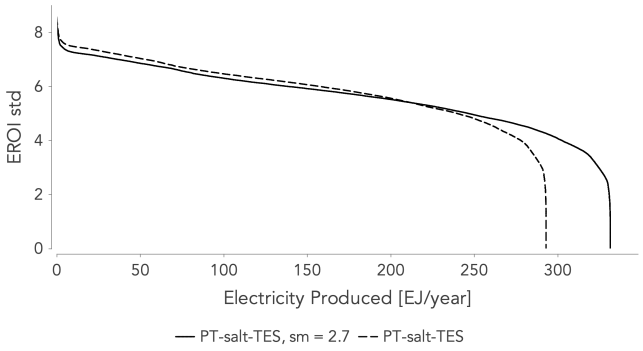
4.2.3 Global solar PV rooftop energy potential

The results provide for a global energy potential is split into residential and commercial rooftops, respectively. The values are 33 and 33.7 EJ/year for 24% efficient mono-Si-PV, and 23 and 23.5 EJ/year for 17% efficient poly-Si-PV. Results are presented as a function of the decreasing EROI in Fig. 4.9. Despite high variations in usability factors, as defined in Section 4.1.1, the total suitable residential and commercial rooftop areas are similar. Compared to the ground mounted power plant potential, the rooftop solar potential is less than 5% of the global potential for both PV technologies (46.5 EJ/year compared to 958 EJ/year for poly-Si-PV, and 66.7 EJ/year compared to 1374 EJ/year for mono-Si-PV). Based on these results theoretically rooftop solar could provide for 7.5% of the current world's energy needs, indicating that both rooftop and ground mounted solar power systems are required in a renewable energy transition.

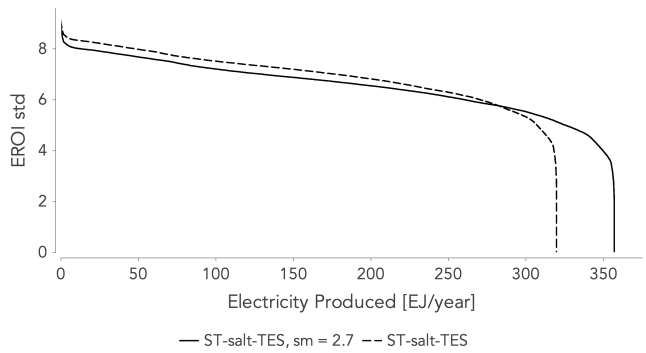
The combined value in this study for mono-Si-PV is 45% of the joint 102.5 EJ/year potential for residential buildings and 46.7 EJ/year for commercial buildings, as estimated by [18], despite using similar 24% efficiency solar modules. The results in this study are significantly lower due to more conservative usability factors (see Section 4.1.1) and conversion efficiencies.



(a) PT-oil

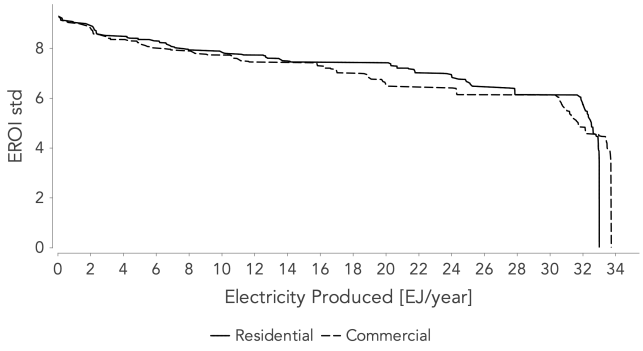


(b) PT-salt-TES

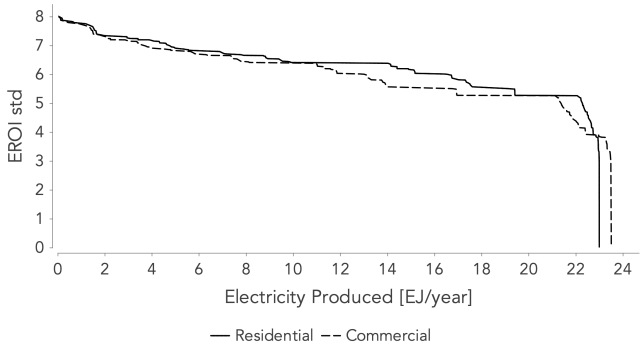


(c) ST-salt-TES

Figure 4.8 *– Global potential for each CSP technology, with the usual solar multiple (1.3 without storage and 2.7 with a storage capacity of 12 hours) and with the solar multiple optimised by the model.*



(a) mono-Si-PV



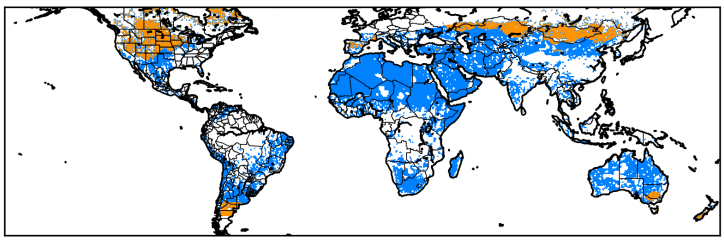
(b) poly-Si-PV

Figure 4.9 *– Residential and commercial rooftop PV potentials.*

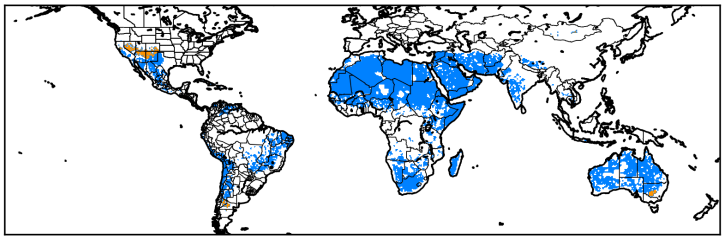
4.2.4 Resulting spatial distribution of the solar resources

In order to analyse areas with the highest potential and the areas that would need to be covered with power plants, the simulation results are presented on a geographic map of the world in Fig.s 4.10. The results are presented for three cases using the selected thresholds at an EROI of 5 (98% of the global potential), 7.5 (75% of the global potential) and 9 (20% of the global potential) as defined in Section 4.1.7. The technology selected by the model in each cell (i.e. the one maximising the EROI) is represented: areas in blue for PV and areas in orange for CSP. The comparison shows that a large part of the potential is realised at low EROIs. When the minimum EROI requirement is increased to 7.5 the energy potential is reduced drastically in Europe, China, South-East Asia, Japan, North America, and Russia. At a minimum EROI requirement of 9 only Chile, countries in the eastern Sahel region, Namibia, Somalia, Saudi-Arabia, Oman and Yemen, and Western Australia still possess significant solar energy potential.

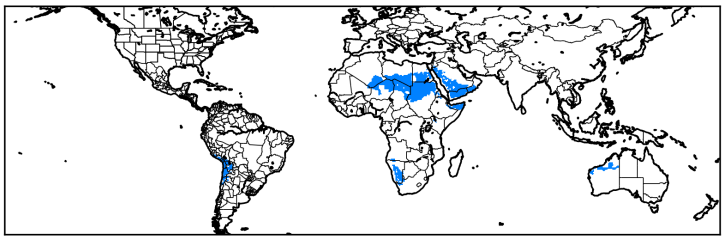
Most of the time, mono-Si solar PV performs better than CSP, except in very high solar radiation regions including the USA, south of Chile and Argentina, Australia, western China, Kazakhstan and Mongolia 4.10. When the EROI threshold increases, the fraction of the potential viable with CSP significantly decreases, until eventually there is no CSP left at an EROI threshold of 9. In Fig. 4.11, the results were computed with poly-Si-PV as the unique PV technology. The results differ significantly, since for poly-Si-PV the EROIs of CSP and PV are similar. In contrast to the previous results, CSP is now preferred to solar-PV in Chile, the American Southwest, South Africa, and Australia. In the last map, showing the available solar potential at an EROI ≥ 8 (15% of the global potential), almost no PV is viable.



(a) EROI $\geq$ 5, 98% of the global potential

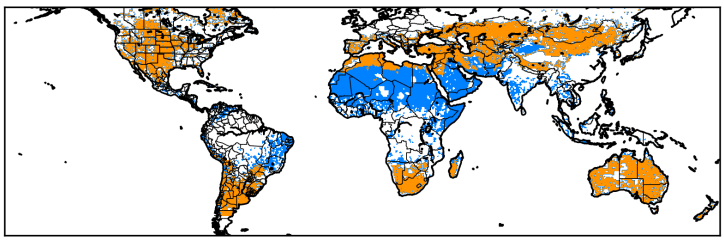


(b) EROI $\geq$ 7.5, 75% of the potential

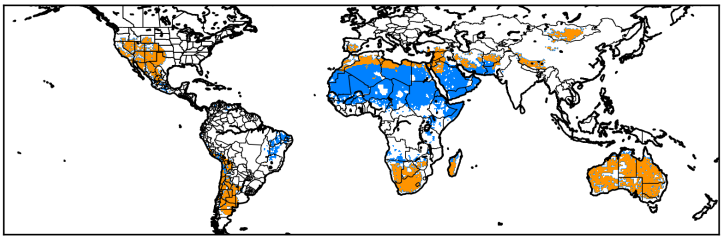


(c) EROI $\geq$ 9, 20% of the potential

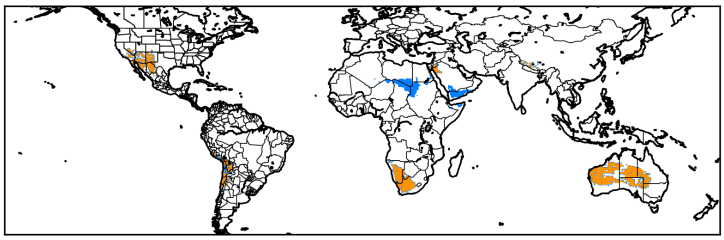
Figure 4.10 *– Spatial distribution of the potential, with mono-Si-PV as PV technology. The areas in blue are the areas where mono-Si-PV performs better than CSP, and orange the opposite. The areas with a solar potential are presented for increasing values of the minimum EROI required, from top to bottom.*



(a) EROI $\geq$ 5, 97% of the global potential



(b) EROI $\geq$ 7, 70% of the global potential



(c) EROI $\geq$ 8, 15% of the global potential

Figure 4.11 *– Spatial distribution of the potential, with poly-Si-PV as unique PV technology. The areas in blue are the areas where poly-Si-PV performs better than CSP, and orange the opposite. The areas with a solar potential are presented for increasing values of the minimum EROI required.*

4.2.5 Results split by regions

This global potential is further split by continent in Fig. 4.12 and Table 4.9. The potential of the African continent drives the global curve with 37-38% of the global solar energy potential, followed by Asia at 25% to 31% of the potential solar energy potential. A comparison of the EROI dependent energy curves between continents shows an almost horizontal curve for the African continent and an almost vertical curve for the European continent, emphasising the uneven quality distribution of the solar power resources on earth.

In Table 4.10, it can be seen that when the EROI threshold is set to 9, the share of the potential of the African continent increases to 65 % (mainly from the Sahara as per Fig. 4.10), followed by a share of 19% from the Asian continent.

	EJ/year			**Repartition [%]**		
	Total	PV	CSP	Total	PV	CSP
Africa	502	502	121	39	37	38
Asia	373	423	80	29	31	25
Oceania	145	146	59	11	11	18
SouthAmerica	132	137	25	10	10	8
NorthAmerica	84	125	27	7	9	8
Europe	31	33	5	2	2	2
Total	**1274**	**1374**	**320**	100	100	100

Table 4.9 *– Global potential split by continent without an EROI threshold, all values in EJ/year.*

	Total (PV only)	%
Africa	164	65
Asia	47	19
Oceania	24	9
SouthAmerica	17	7
NorthAmerica	1	0
Europe	0	0
Total	**253**	**100**

Table 4.10 *– Global potential at EROI $\geq$ 9, split by continent, all values in EJ/year. The table contains solar-PV values only since the CSP resource potentials viable at this EROI threshold are negligible.*

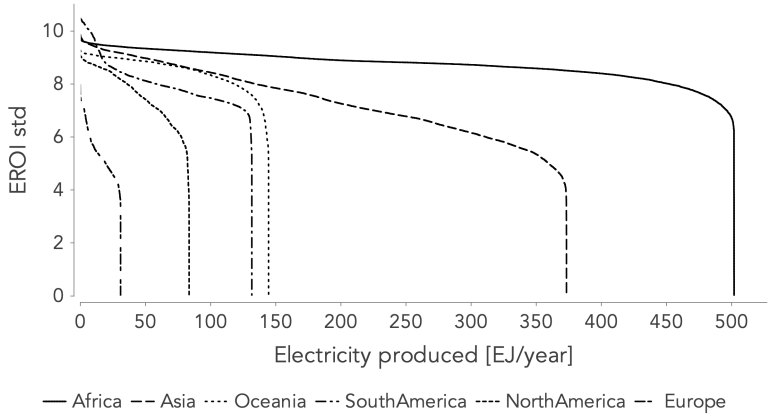


Figure 4.12 *– Global solar potential split by continent.*

EU-28 countries

Individual results for the EU-28 countries are shown in Fig. 4.13. The potentials for each individual technology evaluated in isolation as if solely deployed was established at 17, 24, 2, 3 and 3 EJ/year for poly-Si-PV, mono-Si-PV, PT-oil, PT-Salt-TES, and ST-Salt-TES, respectively. As presented in Table 4.9, the potential of the European continent represents only 2% of the global potential. In addition, the EROI of the resource are lower and decreasing faster, indicating substantial limitations to the expansion of solar power to provide a significant part of European energy needs.

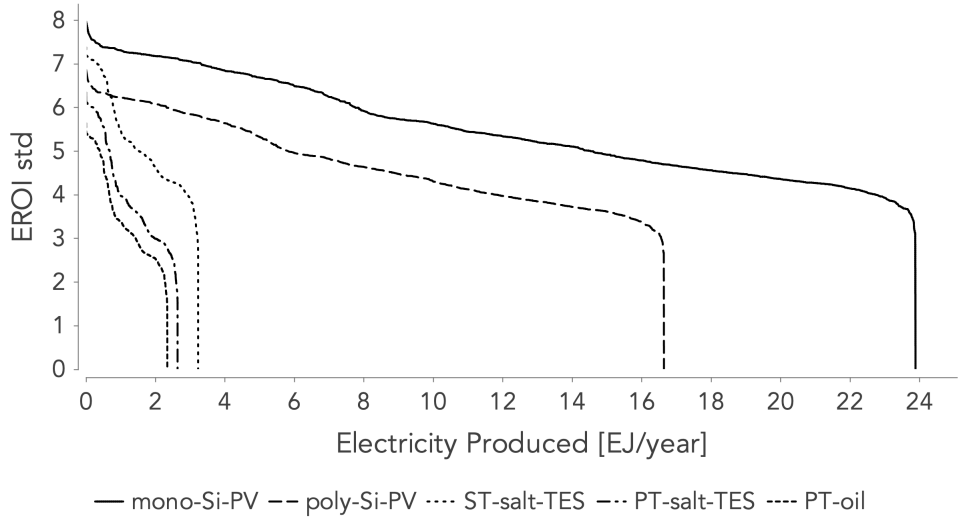


Figure 4.13 *– EU-28 countries potential.*

4.3 Discussion

The results obtained here can be compared with results from previous studies (Table 4.1). The global potential obtained is similar to the results from Hoogwijk [72] of 1300 EJ/year, when no restriction is applied on the minimum EROI required, and significantly lower than all the other estimates, except the results for the top-down approach by De Castro et al. [79]. The results demonstrate that it is important to take into account energy input requirements when assessing the available potential of a renewable resource.

4.3.1 Limitations of the study design

The study provides estimates for different geographies and countries, yet in certain cases it is potentially biased due to the use of average non-country specific factors. This is especially the case for rooftop solar-PV estimations, where average values were used to estimate the proportion of rooftop area that is applicable to solar-PV systems, as derived from the literature. Further studies that provide better granularity for such averages, like country by country studies of typical building typologies to derive suitability of solar-PV systems would be helpful to reduce the uncertainty of this assumption.

Working with EROI as the only decision variable for the choice of a type of technology (i.e. PV or CSP) and the optimal design of a power plant (i.e. the selection of the solar multiple for CSP power plants) has shown some limitations. Regarding the type of technology, the model is currently not able to take into account the capacity factor in its selection. While the need for storage remains small under the current global share of renewable energy, it will increase significantly as renewable energies grow in the mix, negatively impacting the EROI [35]. As such, comparing solar-PV power plants with CSP power plants with 12 hours of thermal energy storage (TES) can result in an apples with pears comparison. Further analysis is needed to understand the effect of introducing significant battery storage for solar-PV on the global energy potential with EROI constraints, such as the effect of batteries on the EROI value of solar-PV power plants. To implement this a temporally solved simulation is required that takes into account hourly dynamics.

The research is also limited in its application to existing commercial solar technologies, whilst new cell types could provide promising low energy costing high efficiency routes to extract more of the global solar resource. In particular perovskite cells and dye-sensitized solar cells would have been interesting technologies to assess in how they would in theory change the global solar energy potential. Available data to adequately assess these technologies is still limited however, with no manufacturing scale energy input data being available for adequate assessment.

Regarding the design of CSP power plants, the EROI maximisation will always select larger aperture areas than current systems until the marginal cost

of an additional mirror is higher than surplus production generated. The reason is the absence of costs associated to land use in the model. An additionnal constraint that specifies the area occupied by power plants within the model as a dynamic factor instead of a static one should be developed to overcome this limitation.

Then, in terms of the overall methodology, the limitations pointed out in the previous chapter (Section 3.4.2) regarding the concept of a static approach looking at standard EROI only are also applicable here.

Static vs dynamic approach

The use of a static approach can be questioned as it does not take into account the uncertainties around the values of certain parameters as well as the annual evolution of the energy system within an energy transition context. Follow-up research would be needed to integrate a dynamic approach to take into account the many potential dynamic factors, as for example: the evolution of technological efficiencies, material intensities, the energy embodied in materials extraction, the decrease of primary energy inputs due to the electrification of the energy system, an evolution in land cover ratios, etc. All these dynamic factors are subject to uncertainties and would affect both the numerator and the denominator of the EROI. A detailed sensitivity analysis would make it possible to estimate the potential impact of these different factors on the potentials obtained.

Standard vs point-of-use EROI

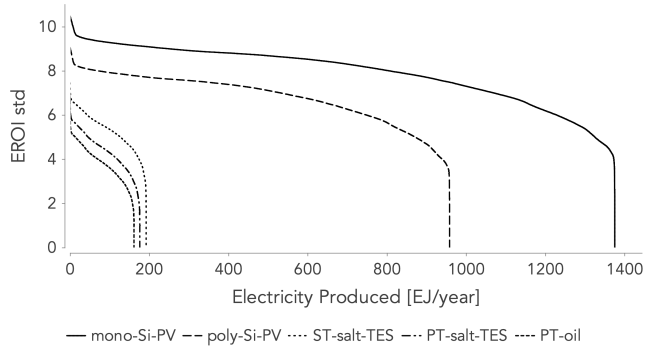
As discussed in Section 3.4.2, the standard EROI estimated here does not take into account the distribution of the electricity produced to the end-users. However, it can be seen in Fig. 4.10c that the most profitable sites in terms of standard EROI are situated in remote and sparsely populated areas. Including including electricity distribution is likely to change the ranking of the sites and significantly reduce their EROI and the production potential. For example, Palmer et al. [226] found that ignoring grid constraints can lead to overestimates of the potential area of solar farms of 61% to 97% in the UK.

4.3.2 Actual capacity factors of CSP power plants

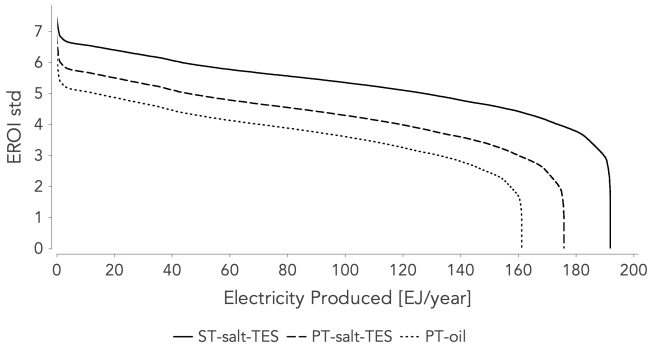
In theory, CSP technologies with storage could allow for reaching capacity factors close to 100%, yet only one system in practice has attained a 75% capacity factor and more typical storage coupled systems have a capacity factor below 50% at present [227]. CSP technologies are potentially more suitable for baseload generation than solar-PV power plants without storage, whose capacity factors do not exceed 24%. A recent study from de Castro et al. [81] however questions these theoretical capacity factors of CSP plants. By analysing production data of CSP plants currently in operation, they found that the actual performances are significantly lower than initially expected. Capacity factors of real plants currently in operation are estimated to be in the range of 15-30%, while manufacturers expect a range of 20-50% and the academic literature generally uses a range of 25-75%. In the light of these results, CSP would only play a limited role in the energy transition.

According to de Castro et al., to correspond to more realistic operating conditions, a reduction factor of 0.6 should be applied to the theoretical capacity factors of CSP plants. CSP potentials were calculated applying this reduction factor to the theoretical capacity factor, in Fig. 4.14 the corrected potentials are compared with PV potentials, and in Fig. 4.15 the curves corresponding to the theoretical and corrected capacity factors are compared for each CSP technology. The corresponding resultings potentials are then given in Table 4.11. Unsurprisingly, the calculated electricity production potentials and the associated EROIs are significantly reduced. According to Fig. 4.14a we conclude that PV would in that case always be more efficient than CSP.

With this analysis, we reach the same conclusions as de Castro et al, i.e. that the potential contribution of CSP in the future energy mix would probably be very limited.



(a)

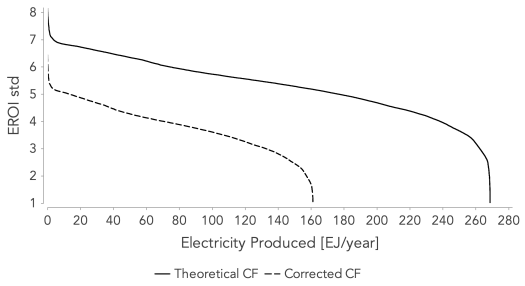


(b)

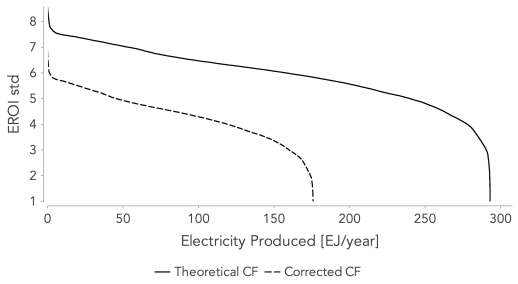
Figure 4.14 *– Comparison of electricity generation potential for the 5 technologies (Fig. 4.14a) and for CSP technologies only (Fig. 4.14b), results obtained with a reduction factor of 0.6 applied to the calculated capacity factors of CSP, as estimated by de Castro et al. [81].*

CF	**EROI**$_{min}$	PT-oil	PT-salt-TES	ST-salt-TES
Theoretical	**1**	269	293	320
	5	177	240	307
	7.5	1	9	102
Corrected	**1**	161	176	192
	5	13	46	127
	7.5	0	0	0

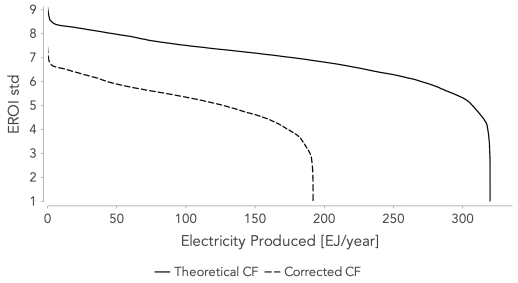
Table 4.11 *– CSP global electricity potential at different EROI thresholds: comparison of the results obtained with the theoretical capacitify factors obtained in this study, and by applying a correction factor of 0.6 as advised by de Castro et al.*



(a) PT-oil



(b) PT-salt-TES



(c) ST-salt-TES

Figure 4.15 *– EROI curves for the 3 CSP technologies: comparison of the results obtained with the theoretical and with the corrected capacity factors.*

4.4 Conclusion

The study provides a novel metholodogy to integrate land, physical solar resource, solar technology constraints, and net energy constraints, so as to estimate the global solar energy potential. It is also the first to provide an integrated estimate for both solar photovoltaic and concentrated solar power in the analysis, including currently commercialised and state of the art technologies. And a new parametrisation has been outlined for concentrated solar power plants. The final results are a series of solar energy potential curves, with the cumulative global available solar potential on the x-axis and the corresponding energy return on energy investment level plotted on the y-axis.

The global electricty production potential, after deduction of on-site operational electricity inputs, was established as follows:

- Solar-PV:
  - Monocrystalline silicon photovoltaic power plant with 24% efficiency: 1374, 1325, 956, and 253 exajoules per year, at EROI thresholds of 1, 5, 7.5, and 9, respectively.
  - Polycrystalline silicon photovoltaic power plant with 17% efficiency: 958, 872, 343, and 1 exajoules per year, at EROI thresholds of 1, 5, 7.5 and 9, respectively.
- Concentrated Solar Power:
  - Parabolic trough power plant with oil heat transfer fluid (HTF): 269, 177, and 1 exajoules per year, at EROI thresholds of 1, 5, and 7.5, respectively.
  - Parabolic trough power plant with molten salt and 12 hours of thermal energy storage capacity: 293, 240, and 9 exajoules per year, at EROI thresholds of 1, 5, and 7.5, respectively.
  - Solar tower power plant with molten salt and 12 hours of thermal energy storage capacity: 320, 307, and 102 exajoules per year, at EROI thresholds of 1, 5, and 7.5, respectively.
- Integrated solar technologies based on selecting the highest energy return on energy investment providing cells:

- Primarily dominated by monocrystalline silicon photovoltaic plants combined with solar tower power plant with molten salt heat transfer fluid: 1274 exajoules per year

Altough many studies conclude that the available solar potential will not be a limiting factor for renewable energy development, this study shows that the energy inputs, i.e. the capital stock and operational requirements of the energy sector that would have to be mobilised, could require a significant shift of efforts from non-energy sectors to the energy sector, which plausibly would have significant economic impacts, especially for low quality solar resource regions such as the European countries. Increasing the land use factors would allow to significantly increase the potentials obtained, but at the cost of aggravating current land competition trends [80, 228]. Finally, taking into account load factors closer to actual observed values highlighted that CSP technologies might not be competitive in the future.

Further work can explore different aspects. First, the impacts of a dynamic approach combined with an estimate of the point-of-use EROIs would improve the relevance of the results and the ranking of the sites in terms of profitability. Then, a combination of the results for wind and solar power potential would be worthwhile, also including additional storage technologies, so as to better evaluate the extent to which they would be complementary from an geographic and energy return on energy investment perspective. As these two sources of energy are seen as the most promising in order to build a sustainable energy system, this kind of work is essential to build forward looking energy scenarios based on realistic available resource potentials per country and geography.
A third route for further research is needed to reduce the ambiguity on what energy return on energy investment cut-off level would be desirable from a societal perspective, to prevent significant implications of the energy system performance falling below the required energy return on energy investment cut-off. Having an understanding of such thresholds would greatly increase the usefulness of the research for sustainable energy systems design. Finally, the research can be expanded by including novel solar technologies once sufficient energy input and technology data is available, such as perovskite cells and dye-sensitized solar cells.

The measure of intelligence is the ability to change.

Albert Einstein

5

Combined wind and solar potential Point-use EROI and application at the European level

In this chapter, the results of the two previous chapters are combined in order to assess the total potential of these two resources, as they are considered as the two main sources of energy for the future. In addition to the standard EROI which has already been studied, we propose here to calculate the amount of electricity that could actually be delivered to end-users and the associated point-of-use EROI, by taking into account electricity losses in the distribution network. A sensitivity analysis is then carried out to assess the potential impacts of energy efficiency improvements in the future. The potential obtained, and the distribution of the associated costs between direct and indirect energy costs, will serve as inputs for the macroeconomic model presented in the next chapter. We also propose an application at the European level, in order to assess if these two sources are indeed capable of providing the current energy

needs of our continent.

5.1 Preliminaries

5.1.1 EROI definitions

Three different EROI boundaries are compared in this chapter: the standard, point-of-use, and point-of-use "external" EROIs. As presented in Section 2.1.1, standard EROI is the ratio between the amount of gross energy produced and the direct and indirect energy inputs needed to produce that energy, and point-of-use EROI is the ratio between the energy delivered and the direct and indirect energy inputs needed to produce and deliver that energy. The difference between point-of-use and point-of-use "external" EROIs lie in the accounting or not, as direct energy inputs, of on-site operational energy, which correspond to the energy produced that is directly self-consumed within a given production site.

Be E_{prod} the (gross) electricity produced, η_{op} the losses related to internal (operational) energy consumption (as a percentage of the gross electricity produced), η_{dist} the distribution losses (as a percentage of the electricity leaving the site), then Table 5.1 gives the value of the numerator and of the direct energy inputs in the denominator of the different EROIs. As the indirect energy inputs related to the electrical grid were not computed in the model, the indirect energy inputs linked to electricity distribution are not included and the total indirect energy inputs are considered to be the same for all 3 EROIs. In practice, taking them into account would result in lower point-of-use EROIs. The point-of-use EROI calculated here therefore corresponds to the EROI final at consumer point-of-use (EROI_{final}) from de Castro et al. [42]. In their contribution, they also define the extended EROI, by including indirect investments for the distribution of electricity.

	Numerator	Denominator, direct energy inputs
EROI_{std}	E_{prod}	$E_{prod}\ \eta_{op}$
EROI_{pou}	$E_{prod}\ (1-\eta_{op})\ (1-\eta_{dist})$	$E_{prod}\ (\eta_{op}+(1-\eta_{op})\ \eta_{dist})$
$\text{EROI}_{pou,external}$	$E_{prod}\ (1-\eta_{op})\ (1-\eta_{dist})$	$E_{prod}\ (1-\eta_{op})\ \eta_{dist}$

Table 5.1 *– Numerator and direct energy inputs associated with the 3 different EROIs calculated.*

Given these definitions we have:

$$\text{EROI}_{std} < \text{EROI}_{pou,external} < \text{EROI}_{pou}$$

Electricity distribution losses According to Table 5.1, going form standard to point-of-use EROIs means including distribution losses in both the numerator (as they reduce the useful output) and the denominateur (as direct energy inputs). According to the MEDEAS documentation [229], worldwide losses related to the distribution of electricty represented approximatively 9.5% of the electricity consumed over the period 1980-2010. Based on the IEA statistics[1], we indeed obtain a mean value of 9.56% for the 10-year period 2009-2018. Over the last 30-year period (1990-2018), the distribution losses were in average slightly higher (10.06%) (see Fig. 5.1).

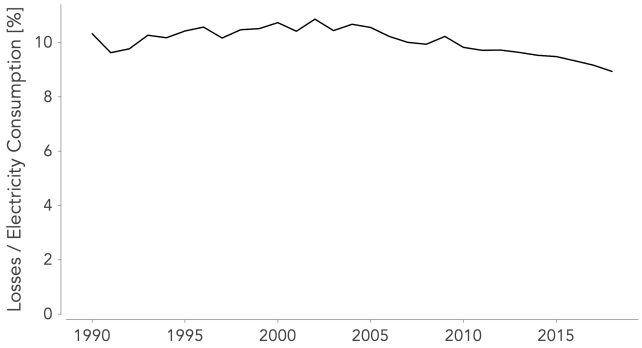


Figure 5.1 *– Ratio between transmission and distribution losses and total final consumption of electricity at the world level, from the IEA statistics.*

[1] `https://www.iea.org/data-and-statistics`

In relation to electricity production, these losses represent 8.7% (= 9.5%/(1+ 9.5%)) of the total generated, i.e. $\eta_{dist} = 8.7\%$ (while η_{op} depends on the technology considered). The difference between the electricity produced and that actually delivered corresponds to losses in the electrical grid, considered as fixed in the calculations. The difference would be greater if we took into account the increase in these losses with the increase in the share of electricity in the energy mix, as is done for example in the MEDEAS model [229]. Based on a NREL study, they developed a relationship between the share of variable renewable energy in the electricity mix and the transmission and distribution losses. According to their estimation, the related losses would increase by 80% when approaching a full intermittent energy mix.

5.1.2 Energy efficiency improvements

All the calculations carried out in Chapters 3 and 4 are static, in the sense that they do not take into account the possible future evolution of certain parameters, for example in terms of technological efficiencies, material intensities, energy embodied in materials, etc. However, energy transition scenarios foresee some improvement in energy efficiency in different areas, so it would be interesting to see the impacts on the EROI curves. For example, published literature finds that material intensity improvements may play a role in enabling a higher EROI in the future [230–232].

According to us, energy efficiency improvements will mainly concern the denominator of the EROI, and only marginally the numerator. Indeed, conservative assumptions were taken regarding the conversion efficiencies of wind and solar energy into electrical energy, which are close to the physical limits. For this reason, we consider in this chapter and in the next one that improvements concern the indirect energy inputs part of the denominator of the EROI only. In this chapter we will do a simple sensitivity analysis to get a first idea of the impacts of a decrease in the energy needs of wind and solar installations, by applying a reduction factor to the indirect energy inputs part of the denominator. The modified EROI curves are presented in Sections 5.2.3 and 5.3.3.

A more in-depth dynamic analysis will be done in the framework of the macroeconomic model (Chapter 6).

5.1.3 Solar technologies considered

The inclusion of CSP technologies in the calculation of total solar potential is currently questioned for various reasons.

- The theoretical efficiency of CSP power plants has been questioned in a recent study by de Castro et al. [81]. By applying a correction factor to the theoretical capacitify factors obtained in Chapter 4, it is found that PV is always more favourable than CSP (see Section 4.3.2).
- Their contribution to the total solar potential decreases rapidly as the EROI increases.
- For a given area, the power density produced is lower than that obtained with PV technologies. Therefore, when maximising the EROI of each site, the total potential obtained is lower than that obtained with PV alone.

For these reasons, which call into question the role of CSP in the energy future, or at least the ability of the model to correctly capture this role, we will only consider PV technologies in this chapter and the next one.

5.2 World potentials

5.2.1 Evolution of the EROI with the cumulated potential

The potential and associated standard and point-of-use EROIs are computed in each grid cell, for onshore and offshore wind, centralised and rooftop PV applications. The results are given for a few EROI thresholds in Tables 5.2 and 5.3, and the resulting curves are presented in Figs. 5.2 and 5.3.

In the tables, results are presented for the 2 PV technologies considered in Chapter 4. The total potential depends on the technological choices that will be made for the large-scale deployment of this technology. If we consider mono-Si-PV panels, with a conversion efficiency of 24%, we obtain a total potential 25% higher than that of poly-Si-PV panels, with a conversion efficiency of 17%, but whose manufacturing processes are also simpler.

On a global scale, we observe a solar potential twice as large as the wind potential, but that difference decreases rapidly as the EROI threshold increases. Above an EROI_{std} of 10, the wind potential is significantly higher.

In Fig. 5.2, we see the significant differences between standard EROIs, calculated at the site exit, and point-of-use EROIs, calculated at the end-user level. While the total potential is reduced by 20%, the maximum EROI is reduced by more than half. However, there is not much difference between EROI_{pou} and $\text{EROI}_{pou,external}$, since internal self-consumption of electricity is relatively low in wind and solar installations (3.5% of the electricity produced for onshore wind, 0.7% for offshore wind, and 1% for PV).

These results highlight once again the importance of clearly stating the boundaries of the calculated EROI. The maximum EROI_{std} at the global level are evaluated at 14 for onshore wind, 22 for offshore wind, 10.4 for mono-Si-PV and 9 for poly-Si-PV, while the maximum EROI_{pou} are estimated in the model at 5.7 for onshore wind, 6.9 for offshore wind, 5 for mono-Si-PV and 4.6 for poly-Si-PV. It explains why there is no potential left at an EROI_{pou} higher than 6 in Table 5.3.

EROI$_{std,min}$	**2**	**4**	**6**	**8**	**10**	**12**
Wind, onshore	516	495	443	342	196	49
Wind, offshore	247	242	226	194	125	50
Wind, total	**763**	**737**	**669**	**536**	**321**	**99**
mono-Si-PV, centralised	1,330	1,327	1,176	762	7	
mono-Si-PV, rooftops	67	66	62	14		
mono-Si-PV, total	**1,397**	**1,393**	**1,238**	**776**	**7**	
Total produced with mono-Si-PV	**2,160**	**2,130**	**1,907**	**1312**	**328**	**99**
% of total potential	*100*	*98*	*88*	*61*	*15*	*5*
poly-Si-PV, centralised	926	905	713	49		
poly-Si-PV, rooftops	46	45	30			
poly-Si-PV, total	**972**	**950**	**743**	**49**		
Total produced with poly-Si-PV	**1,735**	**1,687**	**1,412**	**585**	**321**	**99**
% of total potential	*100*	*97*	*81*	*34*	*18*	*6*

Table 5.2 *– Electricity production potential for increasing EROI$_{std,min}$ thresholds for wind and solar PV technologies, all values in EJ/year.*

EROI$_{pou,min}$	**2**	**4**	**6**
Wind, onshore	440	178	
Wind, offshore	224	201	35
Wind, total	**664**	**379**	**35**
mono-Si-PV, centralised	1,202	896	
mono-Si-PV, rooftops	61	35	
mono-Si-PV, total	**1,263**	**932**	
Total delivered, with mono-Si-PV	**1,927**	**1,311**	**35**
% of total potential	*99*	*67*	*2*
poly-Si-PV, centralised	837	417	
poly-Si-PV, rooftops	42	7	
poly-Si-PV, total	**880**	**424**	
Total delivered, with poly-Si-PV	**1,544**	**803**	**35**
% of total potential	*99*	*51*	*2*

Table 5.3 *– Delivered electricity potential for increasing EROI$_{pou,min}$ thresholds for wind and solar PV technologies, all values in EJ/year.*

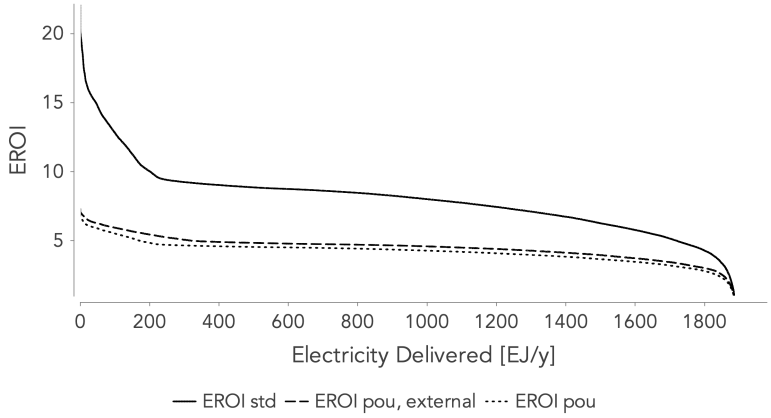


Figure 5.2 *– The 3 EROIs as a function of the total delivered electricity potential (with only centralised mono-Si-PV).*

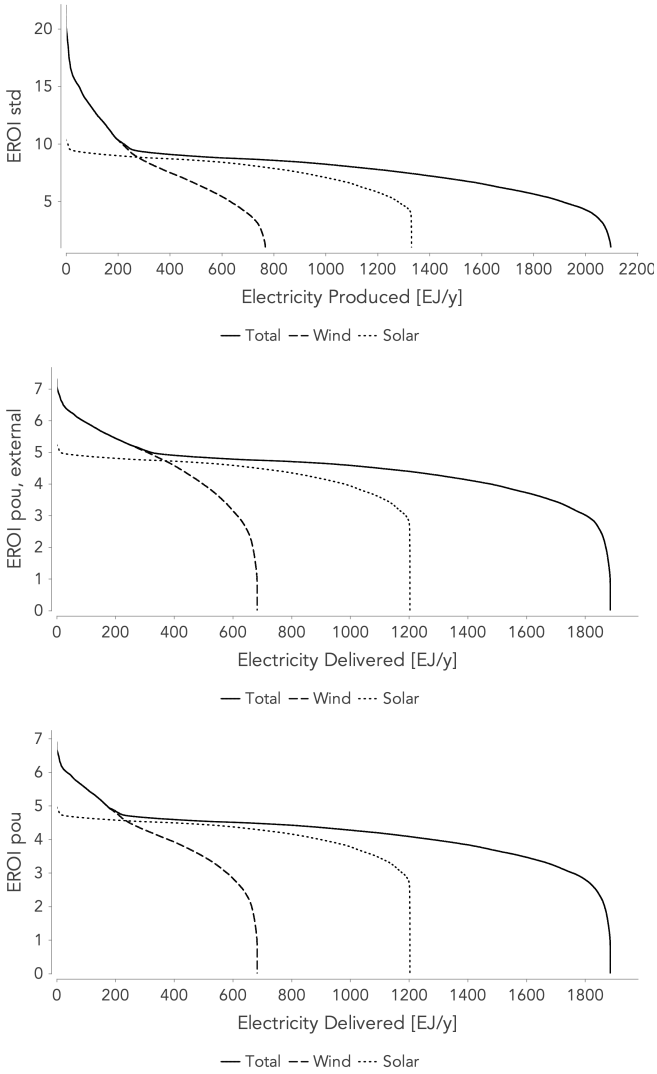
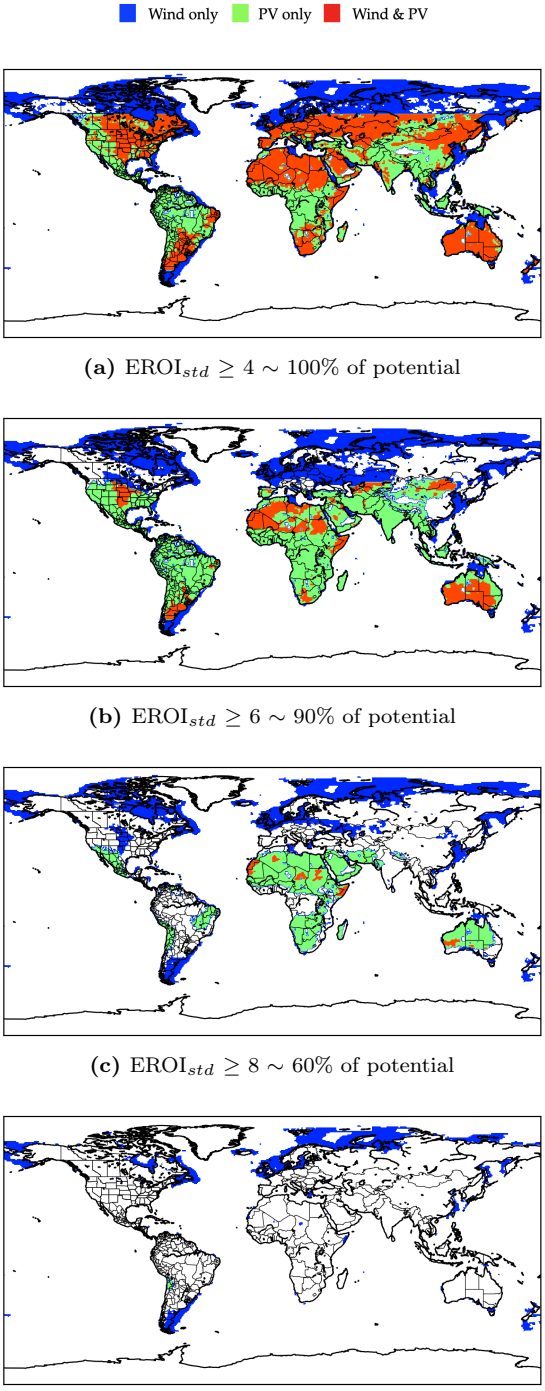


Figure 5.3 *– Combined wind and solar (centralised) annual electricity production potential as a function of the* $EROI_{std}$*, and total electricity delivered as a function of the* $EROI_{pou,external}$ *and* $EROI_{pou}$ *(with mono-Si-PV).*

5.2.2 Spatial distribution of the resources

In Figure 5.4, several maps are presented with the areas where wind and solar are best combined. The results are presented for increasing values of the EROI_{std} thresholds, corresponding respectively to 100, 90, 60 and 15% of the total potential.
The colour code corresponds to different combinations between the 2 types of technology available (wind and solar PV), in order to see the locations where only one of these 2 technologies is profitable, and those where a combination of wind and solar is profitable.

These maps highlight the uneven distribution of wind and solar resources on earth. While wind power is definitely very profitable in the north of the globe, as well as in some coastal regions, the vast majority of the solar resources are located on the African continent. On this continent, wind seems to be less favourable as it progressively disappears when the minimum EROI increases from 4 to 8 (the continent goes from a majority of red, corresponding to a combination of wind and solar, to mainly green, corresponding to solar only). In agreement with the results presented in Table 5.2, when the admissible EROI_{std} threshold increases, solar energy disappears more and more, and for a threshold of 10, only wind fields, mainly offshore, are found on the map. However, in addition to the difficulties of connecting them to the existing electricity grid, the remaining offshore plants are mostly located in very cold weathers. In practice this requires additional devices and more self-energy consumption which would reduce their EROI.



(a) $\text{EROI}_{std} \geq 4 \sim 100\%$ of potential

(b) $\text{EROI}_{std} \geq 6 \sim 90\%$ of potential

(c) $\text{EROI}_{std} \geq 8 \sim 60\%$ of potential

(d) $\text{EROI}_{std} \geq 10 \sim 15\%$ of potential

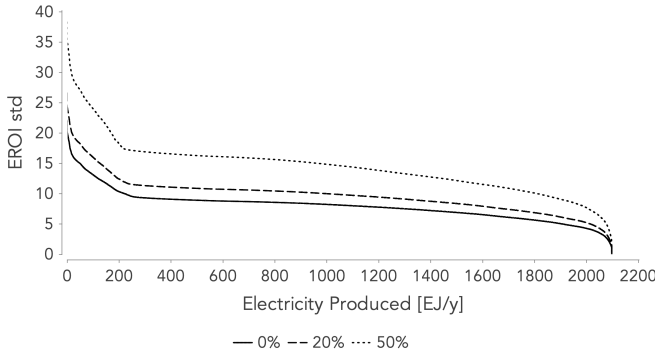
Figure 5.4 *– Geographical representation of the combinations of technologies that are profitable for increasing $EROI_{std}$ thresholds, respectively corresponding to 100, 90, 60 and 15% of the total electriction production potential.*

5.2.3 Impacts of energy efficiency improvements

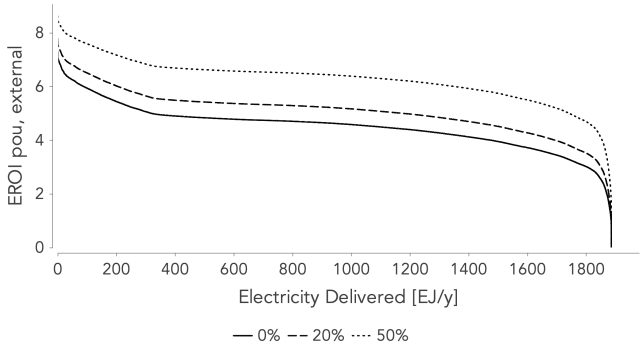
The impacts of a reduction in the indirect energy inputs part of the EROI are shown in Fig. 5.5. As energy efficiency improvements do not affect the numerator of the EROI, the global potential obtained is the same. However we see an increase in the corresponding EROI as the rate of improvement increases. This increase is however more pronounced in terms of standard EROI (Fig. 5.5a), than in terms of point-of-use EROI (Figs. 5.5b and 5.5c). The maximum EROI_{std} starts from 22 with no improvement, reaches 28 for a 20% improvement and 39 for a 50% improvement, the maximum $\text{EROI}_{pou,external}$ equals 7.3, 7.8 and 8.6, while the maximum EROI_{pou} equals 7, 7.3 an 8, respectively.

As expected, the energy efficiency improvements considered allow for an upward shift in the calculated curves, which can be relatively large in the case of considerable energy efficiency improvements. However, the impacts on the point-of-use EROI are limited, even in the case of a 50% reduction in indirect energy requirements.

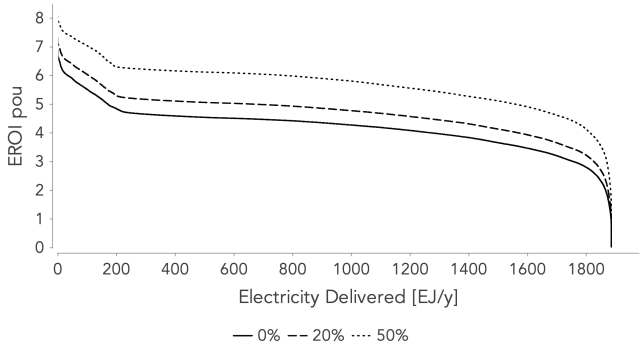
In Chapter 6, we propose scenarios for the temporal evolution of the energy efficiency, as this temporal evolution cannot be captured in the EROI curves as drawn here.



(a) EROI_{std}



(b) $\text{EROI}_{pou,external}$



(c) EROI_{pou}

Figure 5.5 *– Impacts of a reduction of 0, 20 and 50% in the indirect energy inputs part of the EROI.*

5.3 EU-28 potentials

5.3.1 Evolution of the EROI with the cumulated potential

Results limited to the territories of the EU-28 countries[2] are given in Tables 5.4 and 5.5, and in Figs. 5.6 and 5.7. Wind power is undoubtedly better suited for this specific region: it presents significantly higher EROIs and a potential that is 1.5 larger than solar power. This difference increases with the minimum EROI requirement, for example at an $EROI_{std}$ threshold of 6 the wind potential is almost 5 times higher than the solar potential, and there is no solar potential left at an $EROI_{std}$ higher than 8. This is quite obvious given the European climate, but it shows that, contrary to what is possible on a global level, at the European level solar energy will not be predominant.

Comparing with the global curves from the previous sections, the EROIs obtained at the European level are lower and they decrease faster. The maximum $EROI_{std}$ obtained are estimated at: 12.5 for onshore wind, 16.8 for offshore wind, 7.8 for mono-Si-PV and 6.7 for poly-Si-PV, while the maximum $EROI_{pou}$ are estimated at 5.4 for onshore wind, 6.2 for offshore wind, 4.2 for mono-Si-PV and 3.8 for poly-Si-PV. It explains why there is no potential left at an $EROI_{pou}$ higher than 6 in Table 5.3.

These figures are to be compared with the net energy consumption in Europe, in order to assess which proportion could realistically be provided by wind and solar power. According to the European Commission data [233], final energy consumption in the EU-28 was around 1,108 Mtoe in 2016, corresponding to 46.4 EJ. The amount of electricity produced was 3,255 TWh (11,4 EJ), of which 10% (1.1 EJ) came from wind power and 3.5% (0.4 EJ) from solar power. Therefore, in 2016, wind power was providing 2.4% of the final energy consumption, and solar power less than 1%.

These results suggest that it will be difficult to reach the 46.4 EJ of final energy consumption with wind and solar power only, moreover taking into account the fact that storage needs were not included in the study. Indeed this value corresponds to the amount of electricity that could be delivered at $EROI_{pou} \geq 2$ (between 45 and 52 EJ from Table 5.5). At $EROI_{pou} \geq 4$ only half of this potential remains available.

[2]The EU-28 is the abbreviation for the European Union (EU), composed of 28 countries.

EROI$_{std,min}$	**2**	**4**	**6**	**8**	**10**	**12**
Wind, onshore	14.2	14.2	13.5	11	7.2	3.2
Wind, offshore	20.1	20.1	19.7	18.5	16.1	8.9
Wind, total	**34.3**	**34.3**	**33.2**	**29.5**	**23.3**	**12.1**
mono-Si-PV, centralised	20.2	19.1	6.1			
mono-Si-PV, rooftops	2.6	2.3	0.9			
mono-Si-PV, total	**22.8**	**21.4**	**7**			
Total produced with mono-Si-PV	**57.1**	**55.7**	**40.2**	**29.5**	**23.3**	**12.1**
% of total potential	*100*	*98*	*70*	*52*	*41*	*21*
poly-Si-PV, centralised	14.1	9.6	1.7			
poly-Si-PV, rooftops	1.8	1.1				
poly-Si-PV, total	**15.9**	**10.7**	**1.7**			
Total produced with poly-Si-PV	**50.2**	**45**	**34.9**	**29.5**	**23.3**	**12.1**
% of total potential	*100*	*90*	*70*	*59*	*46*	*24*

Table 5.4 *– EU-28: electricity production potential for increasing EROI$_{std,min}$ thresholds for wind and solar PV technologies, all values in EJ/year.*

$\mathbf{EROI}_{pou,min}$	**2**	**4**	**6**
Wind, onshore	12.5	7.2	
Wind, offshore	18.2	17.9	7
Wind, total	**30.7**	**25.1**	**7**
mono-Si-PV, centralised	19.3	1.2	
mono-Si-PV, rooftops	2.4		
mono-Si-PV, total	**20.7**	**1.2**	
Total delivered, with mono-Si-PV	**51.4**	**26.3**	**7**
% of total potential	*100*	*51*	*14*
poly-Si-PV, centralised	12.7		
poly-Si-PV, rooftops	1.6		
poly-Si-PV, total	**14.3**		
Total delivered, with poly-Si-PV	**45**	**25.1**	**7**
% of total potential	*100*	*56*	*16*

Table 5.5 *– EU-28 : delivered electricity potential for increasing $EROI_{pou,min}$ thresholds for wind and solar PV technologies, all values in EJ/year.*

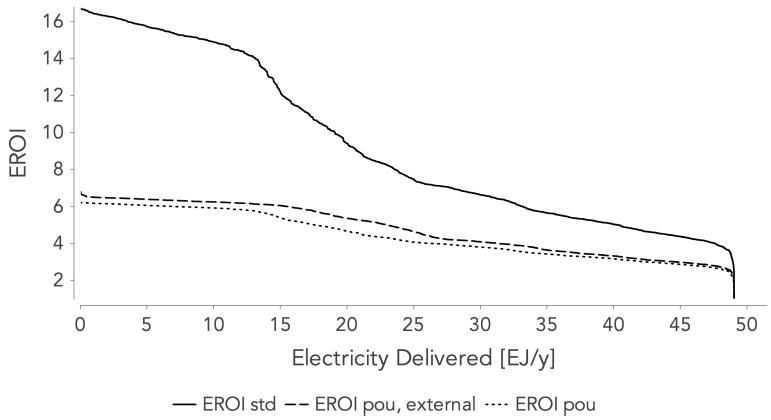


Figure 5.6 *– The 3 EROIs as a function of the EU-28 delivered electricity potential (with only centralised mono-Si-PV).*

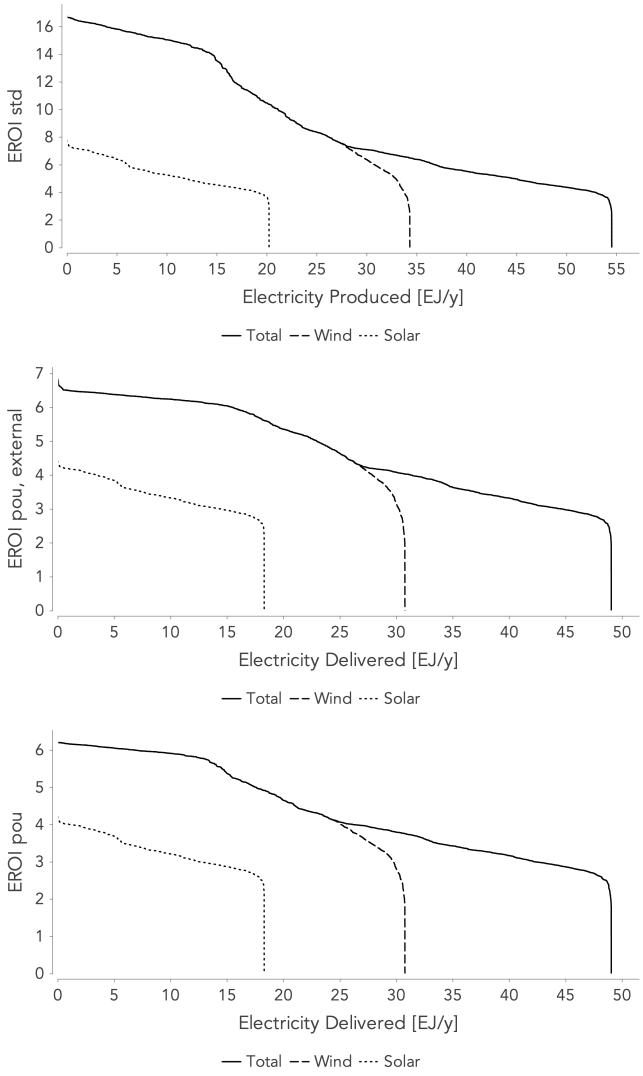


Figure 5.7 *– EU-28 : Combined wind and solar (centralised) annual electricity production potential as a function of the* $EROI_{std}$*, and total electricity delivered as a function of the* $EROI_{pou,external}$ *and* $EROI_{pou}$ *(with mono-Si-PV).*

5.3.2 Spatial distribution of the resources

The results are presented on a map in Figures 5.8 to 5.10.

EROI

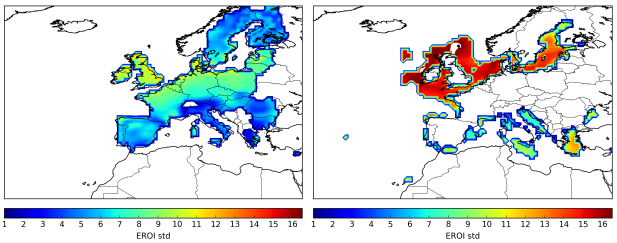
First the standard EROI of each technology is presented in Fig. 5.8, and the point-of-use EROI in Fig. 5.9, regardless of the suitability factor. For wind technology the EROIs increase from South to North, and the most suitable region are around onshore and offshore United Kingdom, and all the northern coast of France, Belgium, the Netherlands, Germany, Denmark, Poland, Lithuania, Latvia and Estonia. For solar technology we observe the opposite trend, the EROIs increase from North to South, the most suitable countries being Portugal, Spain, South of Italy and Greece. As already mentioned the EROIs are significantly lower than for wind.

Combination of wind and solar

In Fig. 5.10, several maps are presented with the areas where wind and solar are best combined. The results are presented for increasing value of the EROI threshold, corresponding respectively 98, 70, 52 and 41% of the total potential. In blue are the areas where only wind is profitable, in red we found a combination of wind and PV, and in green only PV.

Power production density

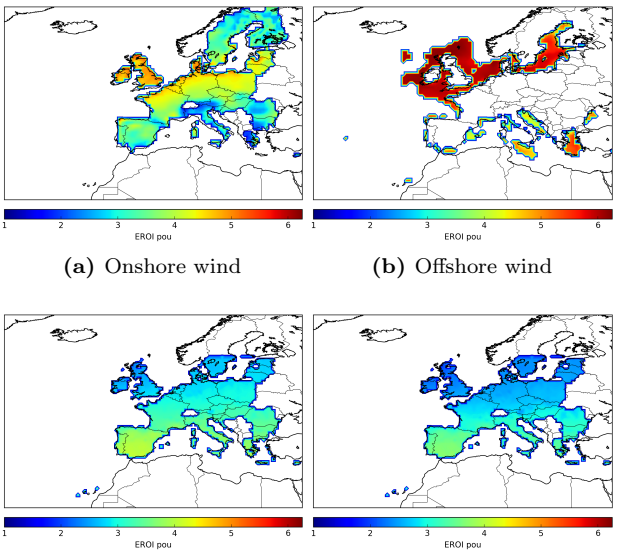
Then, in Fig. 5.11 the power production density is presented, regardless of the EROI. The power production density was calculated as the production potential divided by the suitable area. The maximum values observed amount 0.46 W_e/m^2 for onshore wind, 0.73 W_e/m^2 for offshore wind, 0.52 W_e/m^2 for mono-Si-PV.



(a) Onshore wind **(b)** Offshore wind

(c) mono-Si-PV **(d)** poly-Si-PV

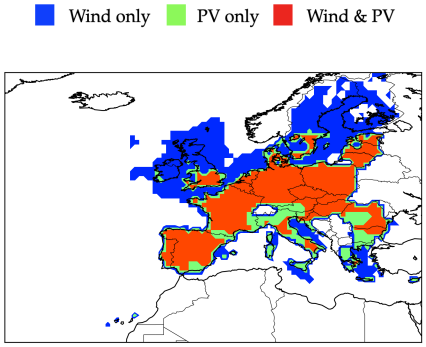
Figure 5.8 *– EU-28 : $EROI_{std}$ of the technologies considered in the study.*



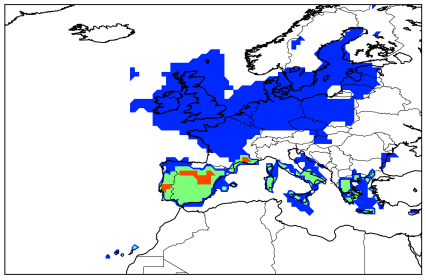
(a) Onshore wind **(b)** Offshore wind

(c) mono-Si-PV **(d)** poly-Si-PV

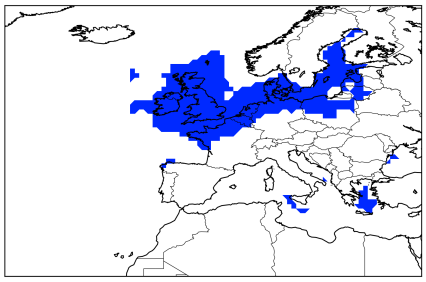
Figure 5.9 *– EU-28 : $EROI_{pou}$ of the technologies considered in the study.*



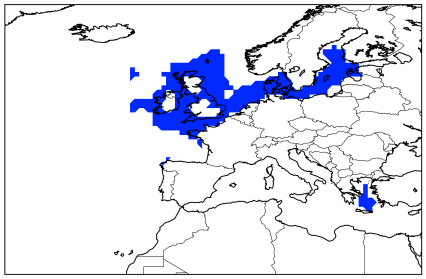
(a) $\text{EROI}_{std} \geq 4 \sim 100\%$ of potential



(b) $\text{EROI}_{std} \geq 6 \sim 70\%$ of potential

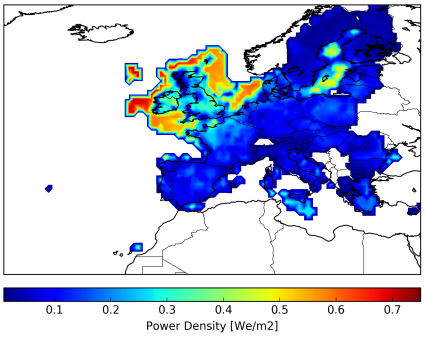


(c) $\text{EROI}_{std} \geq 8 \sim 50\%$ of potential

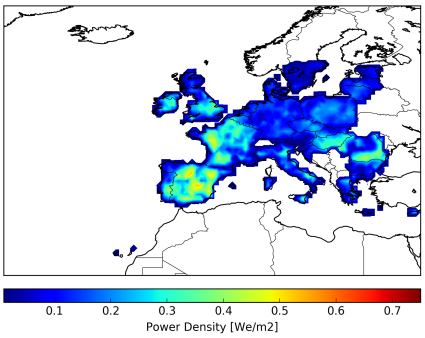


(d) $\text{EROI}_{std} \geq 10 \sim 40\%$ of potential

Figure 5.10 *– Repartition of wind and solar installed capacities: in blue are the areas where only wind is profitable, in red we found a combination of wind and PV, and in green only PV. At EROIs higher than 6 there is no solar potential left.*



(a) Wind

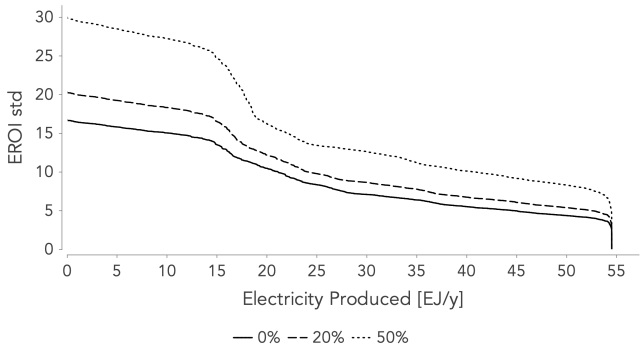


(b) mono-Si-PV

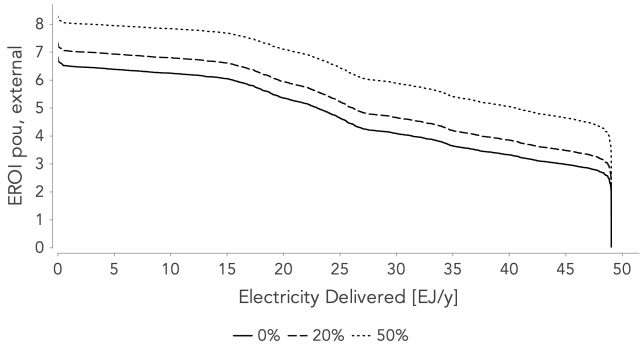
Figure 5.11 *– Power production density [W_e/m^2]: for wind power (both onshore and offshore) and for mono-Si-PV.*

5.3.3 Impacts of energy efficiency improvements

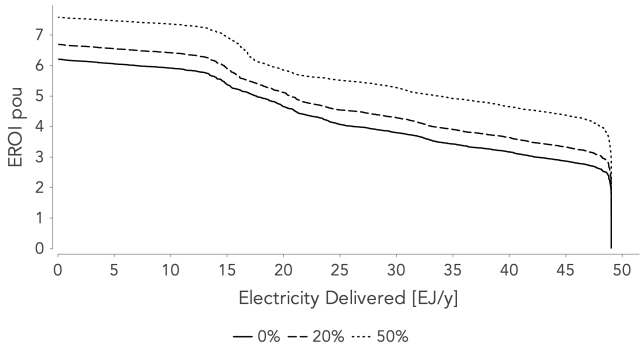
As in Section 5.2.3, the EROI curves are plotted for 3 levels of energy efficiency improvement (in the sense of a reduction in the indirect energy inputs part of the denominator), in Fig.5.12. The maximum EROI_{std} starts from 17 with no improvement, reaches 20 for a 20% improvement and 30 for a 50% improvement, the maximum $\text{EROI}_{pou,external}$ equals 6.8, 7.4 and 8.3, while the maximum EROI_{pou} equals 6.2, 7.7 and 7.6, respectively. As it was already observed at the global level, the impacts on the EROI_{pou} are moderated, compared to the significant ones on the EROI_{std} that is almost multiplied by a factor 2.



(a) EROI_{std}



(b) $\text{EROI}_{pou,external}$



(c) EROI_{pou}

Figure 5.12 *– EU-28 : Impacts of a reduction of 0, 20 and 50% in the indirect energy inputs part of the denominator of the EROI.*

5.3.4 Discussion

In this section we have applied the methodology developed in the two previous chapters of this thesis in order to assess a realistic upper bound for wind and solar power potential at the European level. The maximum realisable potentials were estimated at 14.2 EJ for onshore wind, 20.1 EJ for offshore wind, and 22.8 EJ for solar PV. Wind potential is significantly higher and more profitable (in terms of EROI) than solar power for the EU-28 countries as a whole. When looking at specific countries however, we notice that the Northern part is the most profitable for wind power plant installations, and the Southern part (Spain, Portugal, South of Italy and Greece) is the most profitable for solar power plants.

The calculated potentials are to be compared with the energy consumption in Europe today, in order to see to what extent a fully renewable energy system woud be feasible. According to the European Commission [233], in 2016 final energy consumption in the EU 28 countries amounted 46.4 EJ. This value is close to the upper limit found in our study, with no EROI restriction, and in practice it means covering all the estimated suitable area with wind and solar power plants. This result may contradict the results of previous studies claiming there is no technical nor physical limit for the transition to a fully renewable energy system.

On top of the global studies assessing wind and solar potentials already mentioned in Chapters 3 and 4, there exist more and more studies focusing on this particular region of the world [75, 234–236].
Connolly et al. [236] have studied the possibility of a 100% renewable energy system in Europe by the year 2050. Intermittent electricity production in the form of wind and solar power is the main source of energy production in their *Smart Energy Europe* scenario, complemented by biomass. In this scenario, primary energy supply amounts 16,000 TWh in 2050, from which about 4,000 TWh are provided by biomass. The corresponding aditionnal installed electricity capacity is estimated at approximately 2,750 GW of offshore wind, 900 GW of onshore wind, and 700 GW of solar PV. According to our model, producing 12,000 TWh (i.e. 43.2 EJ) with wind and solar technologies will require to cover all the area with EROI_{std} higher than 6, corresponding to the whole area coloured in Fig. 5.10b. Like our own findings, according to their results offshore wind will have a predominant role at the European level, with more than 60% of the additionnal installed capacity.

Ruiz et al. [75] have developed a database of wind, solar and biomass energy potentials for the EU-28, called ENSPRESO (ENergy System Potentials for Renewable Energy SOurces). Resulting potentials for the reference scenario are 8,400 TWh (30.2 EJ) for onshore wind, 1,300 TWh for offshore wind (4.7 EJ), and 11,000 TWh for solar PV (39.6 EJ). Focusing on onshore wind, Mc Kenna et al. [235] found a technical potential of 14,602 TWh (52.6 EJ) for the EU-28 countries and Hoefnagels et al. [234] found a realisable potential between 1,963 (7.1 EJ) and 6,498 TWh (23.4 EJ). All these estimates are higher than the estimated potentials found in this chapter.

5.4 Conclusion

As wind and solar are the main sources of energy supply in most 100% renewable scenarios, it is important to be able to assess their total potential. The combination of wind and solar potentials does not bring new conclusions compared to the previous chapters, but it allows us to better understand that these two resources do not have the same characteristics. While wind energy has generally higher EROIs, its total potential is about half of the total solar potential. The results show once again that the potential is extremely variable depending on the EROI threshold chosen. The energy future will therefore depend on how much we can afford to pay for our energy production. Since estimates of EROI thresholds found in the literature are usually very speculative, it is important to be able to make these figures speak for themselves by giving them an economic dimension. Only an economic model will make it possible to highlight the possible consequences on economic activity of an energy transition to wind and solar power, accompanied by the decreasing yields that can be observed very clearly with the energy model.

With the spatial distribution of the available potential, we see that the resources are not evenly distributed on earth and that the areas remaining profitable for high EROI thresholds are not necessarily the most accessible ones. This highlights the limitations of this model, which cannot capture these location effects in relation to end-users. When focusing on the EU-28 countries, we noticed that the total unconstrained potential is just equal to our current total final consumption, but the model does not allow to assess how much of this potential will actually be achievable in practice.

Finally, a sensitivity analysis showed that improvements in terms of grey energy (indirect energy inputs) could have a significant impact on the standard EROI, but that the impacts on the point-of-use EROI were relatively small, even in the case of a very significant improvement. The simulations carried out in the macroeconomic model will provide a better understanding of the benefits of incremental energy efficiency improvements.

Anything as important in industrial life as power deserves more attention than it has yet received from economists.

Tryon, 1927

6

Feasibility and economic impacts of the energy transition

This chapter is based on the following publications:

- Dupont, E., Germain M., & Jeanmart, H. (2021). *Estimate of the societal Energy Return on Investment (EROI)*. Biophysical Economics and Sustainability, 2021, 6:2, https://doi.org/10.1007/s41247-021-00084-9.
- Dupont, E., Germain M., & Jeanmart, H. (2021). *Feasibility and economic impacts of the energy transtion*. Sustainability, 2021, 13, 5345, https://doi.org/10.3390/su13105345.

The aim of this chapter is to develop a simple macroeconomic model, accounting for the crowding out effect already highlighted by other models (see Section 2.2), and to couple it with the methodology developed in Chapters 3 and 4, accounting for the location effect (i.e. the declining sites quality). The

macroeconomic model, an input-output type model with two sectors (energy and non-energy), has the advantage of being relatively high-level and to lead to transparent analytical results linking economy growth to the penetration rate of renewable energies. The energy model is able to calculate the maximum potentials of solar and wind energy on a global scale, and the associated costs broken down in terms of direct energy costs, goods and services and capital use.

The articulation of the macroeconomic model with the energy model allows us to answer the following questions: given a future trajectory of the energy demand, hypotheses on the evolution of the technical parameters of the economy and on the behaviour of economic agents in terms of consumption and savings, (i) is a transition to a fully renewable energy system possible and (ii) if so, at what pace? As a corollary, it is possible to determine conditions that ensure that the energy transition is completed over a given period of time.

The structure of this chapter is as follows. Section 6.1 presents the macroeconomic model, its calibration for a reference year, and a sensitivity analysis assessing its robustness to variations in estimated parameters of the model. Section 6.2 presents how it is coupled with the energy model, and formulates the hypotheses regarding the future evolution of some exogenous parameters. The results of the various simulations of the energy transition are presented in Section 6.3, based on assumptions regarding (i) the behaviour of economic agents in terms of consumption and savings and (ii) the potential and pace of technical progress achievable in the coming decades. The end of the section discusses the main assumptions and their impacts on the simulation results. Finally, for the reader without an economic background.

6.1 The macroeconomic model

In this section we propose a simple macroeconomic model with two sectors, an energy sector and a non-energy sector aggregating the rest of the economy. The energy sector produces an energy flow, some of which is delivered directly to final consumption (private and public) and the remainder to the non-energy sector. The non-energy sector produces a general-purpose good used either for final consumption, or for the intermediate consumptions of both sectors, or to renew (and possibly increase) the capital stock available to both sec-

tors. Based on the calibration of the technical parameters (sectoral energy intermediate consumption, capital, and non-energy intermediate consumption intensities, and capital depreciation rates), two indicators are then calculated: (i) the societal EROI (both standard and point-of-use), defined as the ratio between the final energy produced (standard) or delivered (point-of-use) and the (direct and indirect) related consumptions, and (ii) the Net Energy Ratio (NER), which measures the fraction of the final energy produced that is ultimately available for the production of goods by the non-energy sector, i.e. after deduction of the energy needs (direct and indirect) of the two sectors. A sensitivity analysis is then carried out and reveals that the model results are not sensitive to variations in the estimated parameters of the model.

The EROI metric only takes into account the direct (intermediate energy consumption) and indirect (non-energy intermediate consumption and capital consumption) consumptions of the energy sector. Consequently, it does not allow the calculation of the energy actually available for final demand (sum of private and public consumptions and net investment) because it ignores the intermediate and capital consumptions of the rest of the economy. This is why we propose to estimate for the first time a second indicator introduced by Fagnart and Germain [84], called the "Net Energy Ratio" (NER) of the economy.[1] This concept is broader than the EROI, in that it takes into account the energy embodied in the intermediate and capital consumptions of the entire economy. By doing so, it becomes possible to determine the fraction of the energy produced by the energy sector that is "really useful", i.e. that contributes either to consumption (private and public) or to net investment.

6.1.1 Mathematical Formulation

The model (illustrated in Fig. 6.1) is that of a closed economy, with two sectors of activity: (i) the energy sector (ES) which produces energy for the rest of the economy and (ii) the non-energy sector (FS) which produces a general-purpose good used for intermediate and final consumptions and investment. The output of the ES is distributed between energy intermediate consumption (EIC) of the two sectors and deliveries for final consumption, *final* referring to private (household) as well as public (government) consumption. Both sectors

[1] This concept, which measures the share of the total energy produced that is available for final demand, is to be differentiated from the NER as defined by Brandt [43], which is a variant of the EROI which measures the ratio between the net energy produced and the energy invested.

use three factors of production: capital, energy and goods (in the following we will refer to the intermediate consumption of goods produced by the non-energy sector as non-energy intermediate consumption (NEIC)). The capital stock of the economy is shared between the two sectors according to their respective needs.

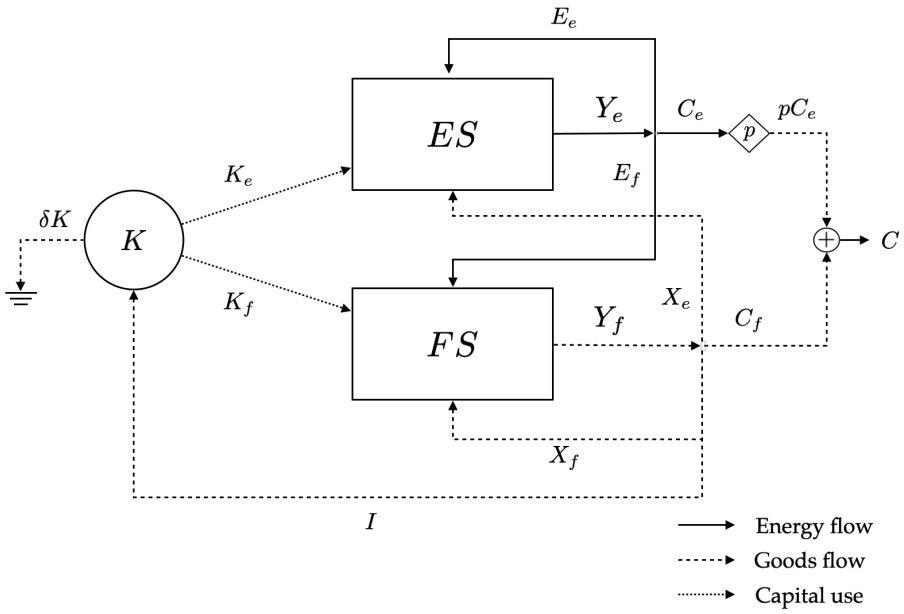


Figure 6.1 *– Diagram of the economy, closed and with two sectors: the ES producing energy, and the FS producing general-purpose goods. Y_i represent the output flows, E_i represent the energy intermediate consumption input flows, X_i the non-energy intermediate consumption input flows (i.e. intermediate consumption of goods), K_i the stocks of capital used by each sector, C_i the final consumptions.*

The energy and non-energy sectors are identified by the indices e and f, respectively. The model is dynamic in the sense that the variables are are discrete functions of time. However, to simplify the notations, time-dependency is omitted in the equations.

Sectoral outputs and factor consumptions are linked by the following relationships:

$$Y_i = \frac{K_i}{v_i} = \frac{E_i}{q_i} = \frac{X_i}{x_i} \tag{6.1}$$

where:

- Y_i, K_i, E_i and X_i refer to the production, capital stock, EIC and NEIC of

sector i, respectively. Energy production and consumption are measured in units of energy (ue); good production, NEIC, and capital stock in units of final good (ug).

- v_i, q_i and x_i refer to the capital, EIC, and NEIC intensities of sector i, respectively, i.e. the quantities of these inputs per unit of output. These intensities are likely to change over time as technologies evolve.

Capital stocks

The total capital stock is shared between the two sectors:

$$K = K_e + K_f \tag{6.2}$$

The share of the capital stock devoted to the ES is defined by μ:

$$\mu = \frac{K_e}{K} \tag{6.3}$$

Capital accumulation is described by:

$$\Delta K = I - \delta K = I_{net} \tag{6.4}$$

where I and I_{net} refer to gross and net investments, respectively.
δ refers to the average depreciation rate of capital ($0 < \delta < 1$). It is the weighted average of the sectoral depreciation rates:

$$\delta = \frac{\delta_e K_e + \delta_f K_f}{K} \tag{6.5}$$

Further the growth rate of a given variable x is defined as $g_x = \frac{\Delta x}{x}$. In particular, the capital growth rate is defined as:

$$g_K = \frac{\Delta K}{K} \tag{6.6}$$

Sectoral outputs, GDP, NDP

The production of the FS is divided into sectoral NEIC, deliveries for final consumption and investment:

$$Y_f = X_e + X_f + C_f + I \tag{6.7}$$

The output of the ES is divided between sectoral EIC and final energy consumption (defined as private and public consumption of energy, similarly as final consumption of good):

$$Y_e = E_e + E_f + C_e \tag{6.8}$$

Total consumption is defined as the sum of final consumptions (of goods and energy):

$$C = C_f + pC_e \tag{6.9}$$

The price of the production good is chosen as the numeraire and is equal to 1. With p being the real price of energy (in ug/ue), the sectoral *gross* added values (AV_i) are calculated as:

$$\begin{aligned} AV_f &= Y_f - X_f - pE_f = (1 - x_f - pq_f)Y_f & (6.10)\\ AV_e &= p(Y_e - E_e) - X_e = (p(1 - q_e) - x_e)\, Y_e & (6.11) \end{aligned}$$

By definition, the GDP is the sum of the sectoral added values, i.e.:

$$GDP = AV_f + AV_e = (1 - x_f - pq_f)Y_f + (p(1 - q_e) - x_e)\, Y_e \tag{6.12}$$

The second equality derives from Eqs. (6.10) and (6.11) and splits the GDP in terms of sectoral deliveries to the final demand. From Eqs. (6.7) to (6.12), one can easily rewrite Eq. (6.12) to express the GDP as the sum of total consumption and investment:

$$GDP = C + I \tag{6.13}$$

The sectoral *net* added values (NV_i) are obtained from the gross sectoral added values by subtracting the sectoral consumptions of capital (understood as the depreciation of capital in the two sectors):

$$NV_i = AV_i - \delta_i K_i = AV_i - \delta_i v_i Y_i, \quad i = e, f$$

Given Eqs. (6.10) and (6.11), one obtains:

$$\begin{aligned} NV_f &= (1 - w_f - pq_f)Y_f & (6.14)\\ NV_e &= (p(1 - q_e) - w_e)\, Y_e & (6.15) \end{aligned}$$

where, by definition:

$$w_i = x_i + \delta_i v_i, i = e, f \tag{6.16}$$

The technical parameters w_i represent the consumption of goods of the two sectors per unit produced, in the form of NEIC and capital consumption.

By definition, the net domestic product (NDP) is the sum of the sectoral net added values. Given the previous equations, one obtains:

$$NDP = NV_f + NV_e = (1 - w_f - pq_f)Y_f + (p(1 - q_e) - w_e)\, Y_e \tag{6.17}$$

From Eqs. (6.4) and (6.13), one also gets:

$$NDP = C + I_{net} \tag{6.18}$$

NDP accounts for the output of the economy which is used for total consumption and economic growth.

The macroeconomic savings rate is defined by:

$$s = \frac{I}{GDP} \tag{6.19}$$

It represents the share of GDP invested in capital production, the remaining going to final consumption. It follows that:

$$C = (1 - s)\, GDP \tag{6.20}$$

The share of private and public consumption devoted to energy expenditures is defined by:

$$\eta = \frac{pC_e}{C} \tag{6.21}$$

Parameters s and η (Eq. (6.21)) concisely describe savings and consumption choices.

The capital intensity of the economy is defined as the ratio between the total capital stock and the GDP:

$$v = \frac{K}{GDP} \tag{6.22}$$

Finally, let α denote the share of the added value of the ES in the GDP:

$$\alpha = \frac{AV_e}{GDP} = \frac{p(Y_e - E_e) - X_e}{GDP} \tag{6.23}$$

The EROI

The calculation of the EROI follows the approach of Fagnart and Germain [84]. Both standard and point-of-use EROIs are calculated, defined by Eqs. (2.2) and (2.3), i.e.:

$$\begin{aligned} \text{EROI}_{std} &= \frac{\text{Energy produced}}{\text{Direct + Indirect energy inputs to produce the energy}} \\ \text{EROI}_{pou} &= \frac{\text{Energy delivered}}{\text{Direct + Indirect energy inputs to deliver the energy}} \end{aligned}$$

In order to produce an amount of energy Y_e, the ES consumes E_e as EIC (i.e. direct energy consumption) (in ue), X_e as NEIC (in ug), and uses a stock of capital K_e (in ug).

Direct energy inputs In order to differentiate between production and distribution of energy, we assume that only the direct energy inputs vary. It means that no distinction is made between production and distribution at the level of the capital and NEIC flows, and that E_e is composed of $E_{e,\text{prod}}$ (direct energy inputs for the production of Y_e) and $E_{e,\text{dist}}$ (direct energy inputs for the distribution of Y_e).

$$E_e = E_{e,\text{dist}} + E_{e,\text{prod}} \tag{6.24}$$

We also define the energy intensity of the ES only accounting for direct energy inputs associated to the production and transformation processes:

$$q_{e,\text{prod}} = \frac{E_{e,\text{prod}}}{Y_e}$$

Indirect energy inputs Since the EROI only accounts for energy flows, it is necessary to estimate the embodied energy included in the indirect energy inputs, i.e. the intermediate consumption flow X_e and capital stock K_e. As annual flows are considered in the model, we have chosen to take into account the capital depreciation in the denominator of the EROI, i.e. to distribute the investment K_e over the life-time of the facilities. The capital flow in the denominator of the EROI is estimated as $\delta_e K_e$, i.e. all the energy that was required to produce, install, maintain and dismantle the fraction of the ES

capital stock consumed during the period under consideration. This estimate is therefore based on the energy content of the share of the investment (at time t) used to replace the capital that has become obsolete (at time t). An alternative approach would have been to estimate the embodied energy in the capital stock based on the energy content of past investments. Since q_f decreases over time, this approach would lead to a higher estimate of the embodied energy contained in the flow measuring capital depreciation.
Note that this approach only concern the calculation of the denominator of the EROI. In the simulations carried out in Section 6.3, the investment in capital is not distributed over the life-time of a facility but is considered as upfront investment (i.e. a given installation of the ES is built before it begins to produce energy).

Let E_{X_e} and $E_{\delta_e K_e}$ (both in ue) be the energy embodied in the flows measuring the NEIC X_e and capital depreciation $\delta_e K_e$. Since (i) the production of the FS is assumed to be homogeneous and (ii) it takes q_f ue to produce one ug, this embodied energy flow can be estimated by:

$$E_{X_e} + E_{\delta_e K_e} = q_f(X_e + \delta_e K_e) = q_f(x_e + \delta_e v_e)Y_e = q_f w_e Y_e \tag{6.25}$$

given Eqs. (6.1) and (6.16). With these assumptions, the EROI_{std} rewrites:

$$\begin{aligned} \text{EROI}_{std} &= \frac{Y_e}{E_{e,\text{prod}} + E_{X_e} + E_{\delta_e K_e}} = \frac{Y_e}{E_{e,\text{prod}} + q_f w_e Y_e} \\ &= \frac{1}{q_{e,\text{prod}} + q_f w_e} \end{aligned} \tag{6.26}$$

given the previous equation and Eq. (6.1).

The energy delivered (i.e. the amount that reaches the FS plus the amount used for final consumption) is defined as the gross energy produced Y_e, minus the direct energy inputs E_e. The EROI_{pou} then becomes:

$$\begin{aligned} \text{EROI}_{pou} &= \frac{Y_e - E_e}{E_e + E_{X_e} + E_{\delta_e K_e}} = \frac{Y_e(1 - q_e)}{E_e + q_f(x_e + \delta_e v_e)Y_e} \\ &= \frac{1 - q_e}{q_e + q_f w_e} \end{aligned} \tag{6.27}$$

Given the fact that annual flows are used, the EROI calculated here at the level of the energy sector corresponds to a PROI as defined by Dale [44].

To be consistent with available IEA data, for the calibration and simulations of the model we chose for the accounting of direct energy inputs the concept of gross external energy ratio (GEER) as defined by Brandt and Dale [43]. The energy produced and directly consumed at a production site is excluded from both the numerator and denominator of the GEER. It means that E_e only contains external energy inputs, i.e. a distinction is made between the energy self-consumed within the energy sector (accounted for) and that self-consumed within a particular production site (not accounted for). For processes with a significant fraction of self-consumed energy, the GEER is significantly greater than the gross energy ratio (GER), where this self-consumed energy is found in both the numerator and the denominator.[2] The GEER is chosen here for the EROI calculation because (i) it is consistent with the IEA definition of the energy industry own use and (ii) it is more relevant for assessing the capacity of a process to generate a surplus of energy available for the economy.
The EROI_{pou} calculated here therefore corresponds to the $\text{EROI}_{pou,external}$ from Chapter 5. However, to simplify the notations, we will refer to it as EROI_{pou}.

Energy leakages in the economy

The output of the economy that can be considered as "useful" is that which serves for total consumption and net investment. It is measured by the NDP, equal to GDP minus capital consumption, or equally to the sum of total consumption and *net* investment (Eq. (6.18)).

Following the approach of Fagnart and Germain [84], $NDP_{max} = \frac{Y_e}{q_f}$ is defined as the theoretical *maximum* useful output, which would be obtained if the totality of the ES output could be devoted to final consumption C or net investment I_{net}. The following relationship between the actual NDP and NDP_{max} is established in Appendix B.1:

$$NDP = \Big((1 - q_e - \zeta)(1 - w_f) - q_f w_e + p\zeta q_f \Big) NDP_{max} \tag{6.28}$$

where $\zeta = C_e/Y_e$ represents the fraction of the output Y_e that directly goes to final consumption, and w_i are defined by Eq. (6.16).

We see that only a fraction of the theoretical quantity NDP_{max} contributes

[2] For example, for global power generation, Kis et al. [48] obtain an estimate of 7.4 for GER and 11.3 for GEER.

to the actual NDP, because there are "leakages" (in the sense of reduced useful output) in the economy.

- The first leakage comes from the intermediate and capital consumption (ICC) of both sectors. The direct needs of the ES correspond to a fraction q_e of its output, while the indirect needs are measured by the technical coefficient w_e. The needs of the FS correspond to a fraction $\frac{w_f}{q_f}$ of the incoming energy flow (i.e. $1 - q_e$). In total the fraction of NDP lost is measured by $L_1 = q_e + q_f w_e + (1 - q_e)w_f$. We find the result of Fagnart and Germain [84]: they define the value $1-L_1$ as the NER of the economy, i.e. the fraction of the energy produced that can be transformed into final output of the FS. This concept is broader than the EROI as it takes into account the losses related to the ICC of *the whole economy*, whereas the EROI only takes into account the losses related to the ICC of the ES.

$$\text{NER} = 1 - L_1 = 1 - (q_e + q_f w_e + (1 - q_e)w_f) \tag{6.29}$$

- The second part is related to C_e, the amount of energy production delivered directly to final consumption that is not available for the FS. The resulting loss of production of goods by the FS equals $\frac{C_e}{q_f}(1 - w_f)$. Since $C_e = \zeta Y_e$, the *fraction* of $\frac{Y_e}{q_f}$ lost via C_e equals $(1 - w_f)\zeta$. However, the loss in the FS production is (partly) offset by pC_e, the value of direct energy deliveries. Measured as a fraction of $\frac{Y_e}{q_f}$, this compensation is worth $pq_f\zeta$. Consequently, the lost fraction of NDP_{max} related to C_e is ultimately measured by $L_2 = (1 - w_f - pq_f)\zeta$.

Given the above, Eq. (6.28) becomes:

$$NDP = (1 - L_1 - L_2)\ NDP_{max}$$

If we look at the case where $w_f = 0$ (no ICC in the FS) and $\zeta = 0$ (no direct private or public energy consumption), then Eq. (6.28) is reduced to:

$$\begin{aligned} NDP &= (1 - q_e - q_f w_e)NDP_{max} \\ &= \left(1 - \frac{1}{\text{EROI}}\right) NDP_{max} \end{aligned}$$

Only in this very special case does the EROI alone determine the useful fraction of NDP_{max}.

The above results are listed in Table 6.1. The first column shows the losses considered (in ascending order) and the second column shows the corresponding NDP values. NDP_{max}, NDP_{EROI} and NDP_{NER} are theoretical values, while the last row shows the actual NDP. The different leakages are measured by the difference between 2 successive NDPs (for example, $NDP - NDP_{\text{NER}}$ measures the loss of NDP due to C_e).

Losses	NDP
Nil	$NDP_{max} = \frac{Y_e}{q_f}$
ICC ES	$NDP_{\text{EROI}} = \left(1 - \frac{1}{\text{EROI}}\right) \frac{Y_e}{q_f}$
ICC ES+FS	$NDP_{\text{NER}} = (1 - L_1) \frac{Y_e}{q_f} = \text{NER} \frac{Y_e}{q_f}$
ICC ES+FS + C_e	$NDP = (1 - L_1 - L_2) \frac{Y_e}{q_f} = (\text{NER} - L_2) \frac{Y_e}{q_f}$

Table 6.1 *– Nature of leakages and corresponding NDP*

6.1.2 The reference calibration

First, we calibrate the model based on global observations for a so-called reference year. Next, a sensitivity analysis is performed on the model parameters that need to be estimated, and whose values are therefore characterised by some uncertainty. It will be shown that the reference calibration is robust to variations in these parameters because the current energy system mainly relies on direct energy inputs.

Observed data

Good flows are expressed in billions of 2010 US dollars (GUS$ 2010), while energy flows are expressed in exajoules (EJ). Time dependency in the units is deliberately omitted as the focus is on a particular year. The reference year is 2018, the latest year for which the IEA provides public data on global energy production and consumption. The model only records final energy flows, in the sense that it does not account for primary energy flows.

Energy data Regarding final energy production and consumptions, IEA statistics[3] provide the following data worldwide:

- TFC (including non-energy uses): 416.1 EJ

[3] `https://www.iea.org/data-and-statistics`

- Energy industry own use (EIOU): 35.1 EJ
- Losses in energy distribution, transmission and transport: 9.3 EJ
- Non-energy uses (NEU): 38.4 EJ
- Households and public consumption: C_e = 144.1 EJ, considering that the direct final energy consumption by households includes all residential energy consumption (88.3 EJ) and 46.1% of the energy dedicated to transport (121 EJ).[4]

Two major assumptions are made here regarding: (i) losses in energy distribution, transmission and transport and, (ii) non-energy uses:

- In Brockway et al. [40], the distribution of the energy produced is assumed to be part of the ES. The losses in energy distribution, transmission and transport from the IEA data are therefore added as direct energy inputs to the ES (corresponding to $E_{e,\text{dist}}$ from Eq. (6.24)). Indeed it would then correspond to an additionnal flow of final energy that need to be produced by the ES to ensure a certain flow of energy delivered to the FS.

  On the other hand, some may argue that these losses should not be considered at all in the model, as they can be assimilated to losses in the transformation processes. Therefore, in order to be as consistent as possible, results for both asumptions will be mentioned, respectively called results with *losses in* Y_e and results with *losses not included*.

- The fraction of non-energy uses in final consumption was 9.2% in 2018 (= NEU / TFC). Similarly to Capellán-Pérez et al. [62], non-energy uses are not accounted for in energy production and are assumed to be produced by the FS As a result, the data provided by the IEA require slight adjustments. Non-energy uses are removed from total energy consumption, and self-consumption of the ES is split between the energy requirements of the ES and the FS (i.e. between E_e and E_f) in proportion to the fraction of non-energy uses in final energy consumption.

With these observed data and the above assumptions, the energy flows of the model are computed, depending on the assumption regarding the acounting or not of losses in distribution, transmission and transport. The resulting

[4] See [237] for the breakdown by mode of transport of the energy dedicated to transport at the global level.

model parameter values as well as the details of the calculation are given in Table 6.2.

	Losses in Y_e	Losses not included
$E_{e,\text{dist}}$ [EJ]	9.3	0
$E_{e,\text{prod}}$ [EJ] (=(1 - NEU/TFC) EIOU)		31.9
E_e [EJ] (=$E_{e,\text{dist}}$ + $E_{e,\text{prod}}$)	41.2	31.9
Y_e [EJ] (=TFC - NEU + E_e)	422.1	412.8
E_f [EJ] (=$Y_e - E_e - C_e$)		236.8
q_e [%]	9.8	7.7
$q_{e,\text{prod}}$ [%]	7.6	7.7

Table 6.2 *– Energy flows calculated from observed energy data, depending of the assumption chosen for losses in distribution, transmisssion and transport.*

Energy data for 2018 indicate that of the amount of energy leaving the ES (i.e. Y_e minus self-consumption E_e = 381 EJ in 2018), 62% were allocated to deliveries to the FS and the remaining 38% were allocated to direct private and public consumption.

Notes on EIOU IEA data Two important observations can be underlined here concerning the EIOU IEA data:

- First, it is good to point out that self-consumption in the sense of the IEA includes all final energy consumption of the ES industries for heating, lighting and the operation of the various types of equipment used for the extraction and transformation of primary energy (mainly fossil fuels) into final energy. However, other consumptions are excluded, e.g. coal burned in power stations at extraction sites, and gas burned during extraction. In these two cases, it is a self-consumption of *primary* energy which is not included in the accounts since it has never left the production sites. This fits well with the GEER concept chosen for the EROI (see Section 6.1.1).

- Second, the EIOU IEA data may suffer some limitations. Indeed there is a high level of aggregation as these data were produced from country data so there might be some inconsistencies among the reported data.

However, despite these limitations, these data are globally relevant and have been used by several other authors [40, 62, 238, 239].

Economic Data The World Bank[5] provides the following data:

- World GDP, excluding taxes and subsidies (i.e. corresponding to the indicator *gross value added at basic prices*): $GDP_{2018} = 73014$ GUS$ 2010 and $GDP_{2017} = 71344$ GUS$ 2010. The growth rate of the economy is therefore given by:

$$g_{2018} = \frac{GDP_{2018} - GDP_{2017}}{GDP_{2017}} = 2.29\%$$

- Savings rate: $s = 25.12\%$.

Estimated parameters

From the model variables defined in Section 6.1.1, several interesting parameters can be calculated, namely (i) the capital stock allocation between the two sectors, (ii) the share of the ES's added value in GDP, (iii) the share of the private and public budget that is devoted to energy expenditures, and (iv) the total intermediate consumptions of the FS. Unlike the savings rate, these parameters are not directly observable. But they can be estimated from the literature and from published economic data. The estimation of these 4 parameters, in addition to the depreciation rate of the capital in both sectors, allows to calibrate the model and therefore to calculate all the variables presented in Section 6.1.1, and in particular the EROI and the NER.

In the following paragraphs, reasonable ranges of values for each of these parameters are proposed. This will allow a sensitivity analysis (around the central value of the interval) to be performed in Section 6.1.3 to assess how sensitive the model calibration is to these variations.

Capital depreciation rate As Eq. (6.4) indicates, capital depreciates exponentially. However, the depreciation rate differs according to the sector (see Eq. (6.5)). The depreciation rate δ_i of sector i can be approximated by:

$$\delta_i \approx \frac{1}{T_i} \tag{6.30}$$

[5] `https://data.worldbank.org` *Gross savings (% of GDP)* (s) and *Gross added value at basic prices (GVA) (constant 2010 US$)*) (GDP).

where T_i is the average lifetime of capital in sector i. Estimating this lifetime is not an easy task, as the capital stock is composed of long-life equipment (e.g. buildings) and very short-life equipment (e.g. computers).

Regarding the FS, the European Central Bank estimates T_f around 20 years [240]. For Canada, T_f is estimated at (i) about 25 years for buildings and (ii) between 11 and 15 years for machinery and equipment [241]. This leads us to choose 20 years as the reference value for T_f, with a range of variation equal to $[15, 25]$ years.

Although some models consider a homogeneous capital stock (for example Dale [64] assumes that $T_e = T_f = 20$ years), it can be argued that the infrastructure of the ES has a longer lifetime. For Canada, the average lifetimes of oil refineries and natural gas processing plants are estimated to be 23 and 25 years respectively. For machinery and equipment related to power generation, values range from 23 to 37 years for the largest components (steam generators, turbines, engines) and 15 years for smaller equipment . This leads us to choose 25 years as the reference value for T_e, with a range of variation equal to $[20, 30]$ years.

Share of the capital stock devoted to the ES: μ, Eq. (6.3) The GEMBA model from Dale [64] is used to estimate μ. The calibration of this model provides, for 2010 and expressed in terms of energy content, 4000 EJ for the industrial sector capital stock and 280 EJ for the energy sector capital stock, which gives $\mu = 6.5\%$. An interval of $[3, 10]\%$ will be tested in the sensitivity analysis.

To estimate the last three parameters necessary for the calibration of the model, we rely among others on the input-output tables published by the Organisation for Economic Cooperation and Development (OECD).[6] These tables give, by sector and by country, and expressed in current US $, intermediate consumption, added value and total output. By aggregating the data by country and sector, worldwide estimates of various indicators are computed, for the year 2015 which is the last year for which these tables are currently available.

Share of the energy sector in GDP: α, Eq. (6.23) Using the input-output tables, an estimate of 6% is found for α for 2015. To do this, the following 3 sectors of activity are associated to the ES: *Mining and extraction of*

[6] `https://stats.oecd.org/Index.aspx?DataSetCode=IOTS`

energy producing products, *Coke and refined petroleum products*, and *Electricity, gas, water supply, sewerage, waste and remediation services*, while the GDP corresponds to the sum of all sectors' added values. Point estimates between 3% and 4% are found for the United States, Japan, and some European countries (Germany, France, Italy, and the United Kingdom). Significantly higher values are found for example for China (6 %), Canada (9 %) or Russia (13.5 %).

Kummel et al. [242] give an estimate of 5 % worldwide, while Ayres et al. [243] give a range between 4 and 8 %. Estimates of Court and Fizaine [50] for the world are also in this range.

Given these estimates, the reference value chosen for α is 6%, with a range of variation equal to $[4, 8]$%. Energy, although essential to any economic activity, only represents a small fraction of the added value of the economy.

The estimate of α gives a lower bound for the energy price p, as the added value of ES is necessarily lower than the product $p(Y_e - E_e)$:

$$p > p_{min} = \frac{AV_e}{Y_e - E_e} = \frac{\alpha GDP}{Y_e - E_e} \tag{6.31}$$

Private and public energy expenditures: η, Eq. (6.21) The input-output tables provide a breakdown of final consumption by economic sector. By identifying the sectors related to the energy sector and removing all taxes and subsidies, an estimate of 3.8% for η is found for the year 2015. However, this value is slightly lower than that of previous years (around 4.2%), so we will use a reference value of 4% for the calibration, with a range of variation equal to $[3, 6]$%. For the United States and China, where energy is comparatively cheaper than in other countries, η is estimated at around 3%. Given the lower bound on the price of energy Eq. (6.31), η must satisfy the following condition:

$$\eta > \eta_{min} = \frac{p_{min} C_e}{C} = \frac{\alpha C_e}{(1-s)E}$$

With the estimate of 6% for α, and the observed values for C_e, E and s, it comes that $\eta_{min} = 3\%$.

Intermediate consumption of the FS The ratio between the intermediate consumption of the FS (in goods and energy) and its output is defined as:

$$z_f = \frac{IC_f}{Y_f} = \frac{X_f + pE_f}{Y_f} = x_f + pq_f \tag{6.32}$$

Using the input-output tables again, we find for z_f an estimate of 50% at the global level for 2015. It means that to produce 1 unit of output the FS needs to invest 0.5 units in intermediate consumption.
To perform the calculation, the sectors associated with the ES (see the estimate of α) are removed from the intermediate consumption and output. For the United States, the value obtained is 43% which corresponds to the values of other sources (42.9% in [244]). For China, *the world's factory*, this value increases to 61%.
The estimated value for z_f used in the reference calibration is therefore 50%, with a range of variation equal to $[40, 60]$%.

Calibrated parameters

With the estimates of T_i and μ, the average depreciation rate δ (the weighted average of the sectoral deprecation rates) is calculated. Eq. (6.5) implies:

$$\delta = \frac{\frac{K_e}{T_e} + \frac{K_f}{T_f}}{K} = \frac{\mu}{T_e} + \frac{1-\mu}{T_f} \tag{6.33}$$

With the estimate of η and based on the observations of the energy consumption C_e and total consumption $C = (1-s)GDP$, the energy price p and goods consumption C_f are estimated:

$$p = \frac{\eta C}{C_e}$$

$$C_f = C - pC_e = (1-\eta)C$$

The estimate of α and the observed value of the GDP make it possible to calculate the added values of the two sectors and the NEIC of the ES:

$$AV_e = \alpha GDP$$

$$AV_f = (1-\alpha)GDP$$

$$X_e = p(Y_e - E_e) - AV_e \tag{6.34}$$

The technical coefficient x_e is then directly computed, given Eq. (6.1): $x_e = \frac{X_e}{Y_e}$.

The estimate of the technical coefficient z_f, gives the output Y_f. Indeed we

have:

$$Y_f = AV_f + IC_f = \frac{AV_f}{1 - z_f}$$

E_f being an observed data, the following values can be computed: $q_f = \frac{E_f}{Y_f}$, $x_f = z_f - pq_f$ via Eq. (6.32), and X_f via Eq. (6.1).

Based on the growth rate of the economy, its capital intensity (v, defined by Eq. (6.22)) can be calculated. Indeed, v and g, the GDP growth rate, are linked by the following relationship (see Appendix B.2):

$$g = g_K - g_v = \frac{s}{v} - \delta - g_v \tag{6.35}$$

Where, for any variable x, $g_x = \frac{\Delta x}{x}$. It is empirically verified that v has been approximately constant over the last decades, i.e. $g_v \approx 0$ (see Appendix B.3). Since in this case $g_K = g$, Eq. (6.35) implies:

$$v = \frac{s}{g_K + \delta} \tag{6.36}$$

Knowing v and the GDP, the capital stock K can be calculated via Eq. (6.22). With the estimate of μ, the capital stocks of the two sectors are then determined (K_e and K_f).

Knowing Y_e (observed), Y_f, K_e and K_f (calibrated above), the technological parameters v_f and v_e are directly calculated via Eq. (6.1). With the set of technical parameters (v_i, q_i, x_i, and $\delta_i, i = e, f$), one finally finds the values of the societal EROIs via Eqs. (6.26) and (6.27), and of the different losses described in Section 6.1.1.

Results

Results for the reference calibration ($T_e = 25$ years, $T_f = 20$ years, $\mu = 6.5\%$, $\alpha = 6\%$, $\eta = 4\%$ and $z_f = 50\%$) are included in Table 6.3.

Parameters Table 6.3 provides the following information:

- The ES self-consumption parameter (q_e) indicates that 10% (respectively 8%) of the energy produced is self-consumed by the ES.
- Given the energy intensity of the FS (q_f), it takes 1.7 MJ to produce one US$ 2010 of production goods (i.e. 0.5 kWh/US$ 2010).

	Losses in Y_e	Losses not included
v_f	1.72	
q_f [MJ/US$2010]	1.7	
x_f	0.47	
v	3.45	
v_e [US$2010/GJ]	39.07	39.96
q_e [%]	9.8	7.7
$q_{e,\text{prod}}$ [%]	7.6	7.7
x_e [US$2010/GJ]	3.32	3.39
EROI_{std}	11.9	11.65
EROI_{pou}	8.5	10.75
NER	0.39	0.4

Table 6.3 *– Results for the reference calibration (2018)*

- Regarding the NEIC of the ES, x_e indicates that 3.3 US$ 2010 of production goods are needed per GJ produced.
- Regarding the NEIC of the FS, x_f indicates that 47% of the FS output is self-consumed.
- The capital intensity of the ES (v_e) indicates that around 40 US$ 2010 of installed capital is required to produce a GJ of energy.
- The FS capital intensity (v_f) indicates that it takes 1.72 US$ 2010 of installed capital to produce 1 US$ 2010 of production goods.
- The capital intensity of the economy (v) indicates that it takes about 3.5 US$ 2010 of installed capital to produce 1 US$ 2010 of GDP. This value, consistent with the literature, is directly derived from the observed values of the growth rate, the savings rate and the estimated value of the capital depreciation rate (Eq. (6.35)).

Estimation of the societal EROI Given the reference values of the different parameters, we find a standard EROI of 11.9 and a point-of-use EROI of 8.5 (respectively 11.65 and 10.75 when distribution losses are excluded from both Y_e et E_e). Looking at Eq. (6.26) and Table 6.3, one can see that it is mainly the value of q_e that determines the EROI of the current energy system. Indeed, q_e is around 10% (respectively 8%) while the product $q_f w_e$ equals 0.85%.

The estimate of the standard EROI is close to the EROI of 12 for the current energy system calculated by Capellán-Pérez et al. [62]. But these values are not directly comparable as they considered the total final consumption as the numerator of the EROI while we take the gross energy produced by the ES. And the point-of-use EROI value is higher than the value of 6.1 found by Brockway et al. [40] for the EROI of fossil fuels at final energy stage for the year 2011, the main differences between the two methodologies being the estimation of the indirect energy inputs, and the scope of the calculation (Brockway et al. consider only fossil fuels).

The total energy consumption of the ES (i.e. the denominator of the EROI) is distributed as follows:

- 92.1% (respectively 90%) in the form of direct energy consumption,
- 5.4% (respectively 6.8%) in the form of energy indirectly contained in the NEIC X_e,
- 2.5% (respectively 3.2%) in the form of energy indirectly contained in capital. The energy consumption linked to the infrastructures thus represents only a small fraction of the total.

This distribution corresponds to the estimates found in the literature. Dale postulates in its GEMBA model [64] that final energy production from fossil fuels requires 90% of energy inputs in direct form. It is also consistent with the work of Gagnon et al. [245], which studies the energy return from oil and gas production worldwide. Their results indicate that indirect energy inputs accounted for 11% of total energy inputs in 1992 and 9% in 2006. To obtain these figures, they use production data from oil and gas wells in the United States and the United Kingdom, and oil company expenditures on exploration, development, extraction and production. Brandt [52] also assumes that 10% of the energy produced by fossil fuels is directly self-consumed, and 1% in indirect form. This corresponds to 91% of the inputs in direct form, and 9% in indirect form.

We note that the production of the FS is distributed as follows: 48.4% for the ICCs (47.4% goes to the FS and only 1% to the ES), 38.2% to final consumption and 13.4% to investment.

Estimation of the NER Estimates of the various losses described in Section 6.1.1 are shown in Table 6.4. The variations due to the inclusion of distribution losses are not significant, except regarding the ICC of the ES.

	Losses in Y_e	Losses not included
NER [%]	**38.9**	**39.8**
L_1	**61.1**	**60.2**
=ICC ES	*10.6*	*8.6*
+ICC FS	*50.5*	*51.6*
L_2	**14.1**	**14.5**
=Losses of ug	*15*	*15.4*
-pC_e	*0.9*	*0.9*
$L_1 + L_2$	**75.2**	**74.7**

Table 6.4 *– Losses estimation for the reference calibration [%].*

The losses related to the ICC of the two sectors amount to 60%. These losses are unevenly distributed between the two sectors: around 10% for the ES, and 50% for the FS. Thus, limiting oneself to the concept of EROI (which accounts for the ICC of the ES alone) implies ignoring the significant losses related to the ICC of the FS. The NER ($= 1 - L_1$) equals 40%. Because of the ICC of the two sectors, a little less than 2/5 of the energy produced can potentially be used for the production of goods by the FS (i.e. either for consumption or for economic growth).

The theoretical maximum output measured by NDP_{max} is far from being reached. Table 6.4 shows that a non-negligible poart of Y_e is directly used for private and public consumption (via C_e). Starting from the ratio $\zeta = C_e/Y_e$, equal to around 35% in 2018, and after taking into account the ICC of the FS (measured by $(1 - w_f)\frac{Y_e}{q_f}$), the loss of useful production of goods by the FS reaches 14% of the total. This loss is only very slightly compensated by the value of the private and public energy consumption pC_e (1% of NDP_{max}).

This last observation suggests that the NDP would be higher if (at least part of) the energy consumed by households were instead allocated to the production of goods. At a given net investment, total consumption C would also be higher (since $C = C_f + pC_e = NDP - I_{net}$).

By analogy with the definition of the EROI, which is the ratio between the output and the ICC of the ES, the ratio between NDP and ICC of the two

sectors can be defined here. This gives a ratio of 1.7 (=1/0.6). At the level of the economy, it is thus necessary to invest one unit of production good to produce 1.7 *useful* units.

6.1.3 Sensitivity analysis

As mentioned above, there exists uncertainty regarding the estimated parameters μ, α, η, z_f, T_e and T_f. It is therefore important to know whether or not the calibration of the previous section is sensitive to a variation in these estimated parameters.

	Reference	Min	Max
T_f [years]	20	15	25
T_e [years]	25	20	30
α [/100]	6	4	8
η [/100]	4	3	5
z_f [/100]	50	40	60
μ [/100]	6.5	3	10

Table 6.5 *– Intervals of variation of the estimated parameters.*

The ranges of variation of the estimated parameters with their reference values are given in Table 6.5. All the variations given by this table have been tested, but to ease the presentation of the results only the estimated parameters which have a significant influence on the calibrated parameters are included. Tables 6.6 and 6.7 therefore only includes the variations of η and z_f, and ignores those of T_e, T_f, α and μ.
Remember that all observed quantities remain unchanged through the sensitivity analysis.

Only parameters that differ from Table 6.6 are included in Table 6.7. Then overall trends observed and described hereafter are the same for both tables.

Variations of z_f and η Regarding the various calibrated parameters, the following observations can be made:

- p increases with η because $p = \eta C/C_e$, and C and C_e are observed.
- x_f increases with z_f because $x_f = z_f - pq_f$, p being insensitive to the variations of z_f and q_f being of low weight.

η [/100]		3			**4**			5	
zf [/100]	40	50	60	40	**50**	60	40	50	60
p [\$2010/GJ]	11.38	11.38	11.38	15.18	**15.18**	15.18	18.97	18.97	18.97
q_f [MJ/\$2010]	2.07	1.72	1.38	2.07	**1.72**	1.38	2.07	1.72	1.38
x_f	0.38	0.48	0.58	0.37	**0.47**	0.58	0.36	0.47	0.57
x_e [\$2010/GJ]	0	0	0	3.32	**3.32**	3.32	6.74	6.74	6.74
v	3.45	3.45	3.45	3.45	**3.45**	3.45	3.45	3.45	3.45
v_f	2.06	1.72	1.37	2.06	**1.72**	1.37	2.06	1.72	1.37
v_e [\$2010/GJ]	39.07	39.07	39.07	39.07	**39.07**	39.07	39.07	39.07	39.07
$q_f w_e$ [/100]	0.3	0.25	0.2	1.01	**0.84**	0.67	1.72	1.43	1.15
$EROI_{std}$	12.73	12.81	12.89	11.67	**11.91**	12.15	10.78	11.13	11.49
$EROI_{pou}$	8.97	9.01	9.06	8.38	**8.51**	8.65	7.86	8.06	8.27
NER	46.67	38.9	31.12	46.67	**38.9**	31.12	46.67	38.9	31.12
L_1	53.33	61.1	68.88	53.33	**61.1**	68.88	53.33	61.1	68.88
$=ICC\ ES$	10.06	10.01	9.96	10.77	**10.6**	10.44	11.48	11.19	10.91
$+ICC\ FS$	43.26	51.09	58.92	42.55	**50.5**	58.45	41.85	49.91	57.98
L_2	16.97	14.14	11.31	16.97	**14.14**	11.31	16.97	14.14	11.31
$=Losses\ of\ ug$	17.77	14.81	11.85	18.04	**15.03**	12.03	18.31	15.26	12.21
$-pC_e$	0.8	0.67	0.54	1.07	**0.89**	0.71	1.34	1.12	0.89
$L_1 + L_2$	70.29	75.25	80.2	70.29	**75.25**	80.2	70.29	75.25	80.2

Table 6.6 *– Calibration results for different values of η and z_f (reference and extreme values), with losses in energy distribution, transmission and transport included in Y_e.*

- x_e increases with η because $x_e = X_e/Y_e = p(1 - q_e) - \alpha GDP/Y_e$ varies only through p, the other quantities remaining either observed or fixed.
- q_f decreases if z_f increases because $q_f = \frac{E_f}{Y_f} = \frac{E_f(1-z_f)}{(1-\alpha)GDP}$, where E_f and GDP are observed and α is fixed.
- v_f decreases if z_f increases because $v_f = K_f/Y_f$: (i) $K_f = (1-\mu)vGDP$ where μ is fixed, GDP is observed and v remains unchanged (cfr. infra) and (ii) we saw in the previous point that Y_f increases with z_f.
- v_e remains invariable because $v_e = \frac{K_e}{Y_e} = \frac{\mu v GDP}{Y_e}$ where μ is fixed, GDP and Y_e are observed and v remains unchanged.

η [/100]		3			**4**			5	
zf [/100]	40	50	60	40	**50**	60	40	50	60
x_e [\$2010/GJ]	0	0	0	3.39	**3.39**	3.39	6.89	6.89	6.89
v_e [\$2010/GJ]	39.96	39.96	39.96	39.96	**39.96**	39.96	39.96	39.96	39.96
$q_f w_e$ [/100]	0.31	0.26	0.21	1.03	**0.86**	0.69	1.76	1.46	1.17
$EROI_{std}$	12.45	12.53	12.61	11.42	**11.65**	11.88	10.54	10.88	11.24
$EROI_{pou}$	11.49	11.56	11.63	10.54	**10.75**	10.97	9.73	10.04	10.37
NER	47.73	39.77	31.82	47.73	**39.77**	31.82	47.73	39.77	31.82
L_1	52.27	60.23	68.18	52.27	**60.23**	68.18	52.27	60.23	68.18
$=ICC\ ES$	8.03	7.98	7.93	8.76	**8.59**	8.41	9.48	9.19	8.9
$+ICC\ FS$	44.24	52.24	60.25	43.51	**51.64**	59.77	42.79	51.04	59.28
L_2	17.35	14.46	11.57	17.35	**14.46**	11.57	17.35	14.46	11.57
$=Losses\ of\ ug$	18.17	15.15	12.12	18.45	**15.37**	12.3	18.72	15.6	12.48
$-pC_e$	0.82	0.69	0.55	1.1	**0.91**	0.73	1.37	1.14	0.91
$L_1 + L_2$	69.62	74.69	79.75	69.62	**74.69**	79.75	69.62	74.69	79.75

Table 6.7 *– Calibration results for different values of η and z_f (reference and extreme values), without the inclusion of losses in Y_e.*

Crossing the variations of z_f and η, the societal standard EROI varies between 10.8 and 12.9 (respectively 10.5 and 12.6), with a reference value of 11.9 (respectively 11.65). The point-of-use EROI varies varies between 7.9 and 9.1 (respectively 9.7 and 11.6), with a reference value of 8.5 (respectively 10.75). We observe that the estimated parameter that has the most influence on the EROI is η, but that the EROI is very insensitive to changes in z_f. This is due to the fact that it is mainly determined by q_e, which is observed and therefore does not depend on the estimated parameters (see Section 6.1.2). Now q_e equals 9.8% (respectively 7.7%), while the product $q_f w_e$ is worth at most 1.72% (respectively 1.76%) (for the maximum value of η and minimum value of z_f). This product varies mainly because of the variations in the NEIC intensity of the energy sector x_e. But in any case, it remains low and q_e remains predominant in the determination of EROI. This observation is again inherent to the current structure of the energy sector.

We also notice that the losses L_1 and L_2 change significantly with z_f, but

little with η. Consequently, the only parameter that has a significant influence on the NER is z_f.

Table 6.6 also shows that the capital intensity of the economy v is almost insensitive to the variation of the estimated parameters. This is because v is calculated from Eq. (6.36), where (i) s and $g_K = g$ are observed and do not depend on η and z_f and (ii) δ varies very little with the estimated parameters.

Variations of α and μ The variations of the α parameter have a slight influence on the standard EROI (it goes from 11.1 to 12.8 (respectively from 10.9 to 12.5) when α varies between 4 and 8%), and on the point-of-use EROI (it goes from 8.1 to 9 (respectively from 10.1 to 11.6) when α varies between 4 and 8%), but have much less impact on the NER (which goes from 38.4 to 39.4% (respectively from 39.3 to 40.3%)). The only parameter which varies significantly with α is the technical parameter x_e which goes from 6.8 to 0 US$2010/GJ (corresponding to an extreme case without NEIC in the ES) when α increases from 4 to 8%. Indeed, if α increases, the added value of the ES increases. The price p being fixed by the value of η and the observed parameters, an increase of AV_e leads to a decrease of X_e via Eq. (6.34).

Changes in μ have no influence on the NER (which increases from 38.8 to 39% (respectively from 39.7 to 39.9%) when μ increases from 3 to 10%), and only slightly changes the EROI (the standard EROI decreases from 12.1 o 11.7 (respectively from 11.85 to 11.45) and the point-of-use EROI decreases from 8.6 to 8.4 (respectively from 10.9 to 10.6)). The EROI decreases when μ increases as more of the available capital has to be devoted to the energy sector. At a given energy production Y_e, it follows that the capital intensity of the energy sector v_e increases.

6.2 Articulation with the energy model

As mentioned in the introduction of this chapter, the macroeconomic model will allow to fully exploit the results from the methdology developed in Chapters 3 and 4, referred to as the energy model (EM) in the followings. In order to simulate the energy transition, the ES from the macroeconomic model is decomposed into two subsectors: the renewable and non-renewable subsectors, indexed re and nre, respectively. The total ES production Y_e, EIC E_e, NEIC X_e, and capital stock K_e are the sum of the values of the 2 subsectors (i.e.

$Y_e = Y_{nre} + Y_{re}$, $E_e = E_{nre} + E_{re}$, $X_e = X_{nre} + X_{re}$, $K_e = K_{nre} + K_{re}$). The dynamic model developed in this section aims at simulate the energy transition (ET), from the current, fossil-fuel based, energy system, to an energy system relying only on wind and solar technologies. The methodology developed to assess global wind and solar potentials will be used to estimate the evolution of the technical parameters of the ES with the penetration of renewable energies, as explained in Section 6.2.1.

Then in Section 6.2.2 the dynamic model is presented, based on an innovative principle of exploring all possible trajectories of the economy during the energy transition.

6.2.1 Outputs of the energy model

As explained in Section 5.1.3, only PV technologies are considered in this analysis. Among PV technologies, mono-Si-PV are always preferred as they present higher EROIs than poly-Si-PV. Wind and solar power plants do not compete for land use, as a given area can be occupied simultaneously by both types of installations.

Once the technological choices have been made at the level of each site, the EM calculates, per site and for each of the technologies used on the site, (i) the production potential, (ii) the direct and indirect energy inputs required per unit of energy produced and, by relating the two previous quantities, (iii) the site EROI. On this basis, by ranking all combinations of sites and technologies in descending order of EROI, the EM provides the direct and indirect energy inputs $E_{X_{re}}$ and $E_{K_{re}}$ required to produce a given aggregated amount of renewable energy Y_{re}.[7]

The EM thus provides two curves $E_{X_{re}}(Y_{re})$ and $E_{K_{re}}(Y_{re})$ over the interval $[0, Y_{re}^{max}]$, where Y_{re}^{max} designates the *maximum* production potential of wind and solar energy (potential calculated by the EM, expressed in ue per year). These curves correspond to a discrete set of points, each value corresponding to the potential of a given technology in a given geographical location. These two curves are used by the macroeconomic model (MM) in order to calculate the technical parameters of the ES. The energy flows $E_{X_{re}}$ and $E_{K_{re}}$ are the energy contents (in ue) of X_{re} and K_{re}, which refer respectively to the NEIC and capital consumption of the renewable energy subsector (in ug). These

[7] It is shown in Appendix B.4 that the EROI ranking criterion leads to the same results as a ranking by profitability.

quantities are related by:

$$X_{re} = \frac{E_{X_{re}}}{q_f}$$

$$K_{re} = \frac{E_{K_{re}}}{q_f}$$

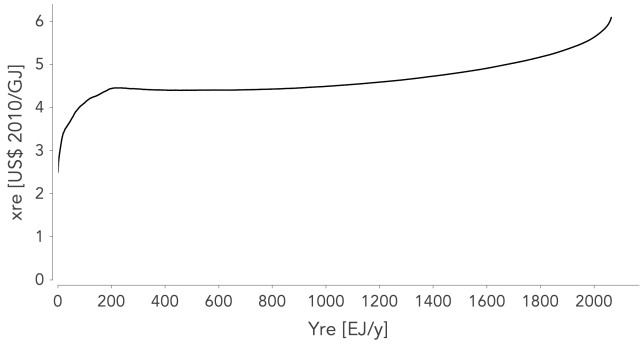
where q_f is the energy intensity (i.e. the energy content) of a unit of good produced by the FS. It is then possible to calculate the technical coefficients of the renewable energy subsector depending on its production :

$$\begin{aligned} q_{re}(Y_{re}) &= \frac{E_{re}(Y_{re})}{Y_{re}} \\ x_{re}(Y_{re}) &= \frac{X_{re}(Y_{re})}{Y_{re}} \\ v_{re}(Y_{re}) &= \frac{K_{re}(Y_{re})}{Y_{re}} \end{aligned}$$

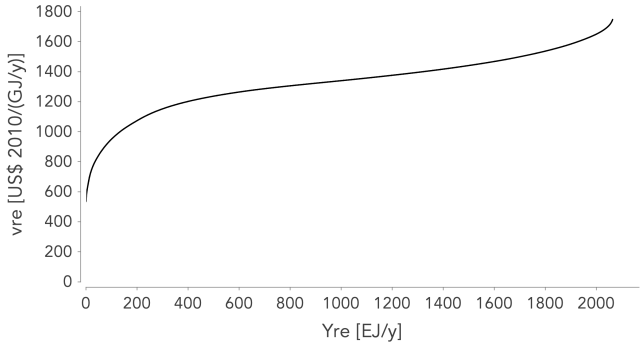
Two assumptions are taken regarding the direct energy inputs E_{re}. First, as explained in Section 6.1.2, internal energy inputs are not accounted for in the MM. As wind and solar facilities only consume operationnal electricity directly produced by the installation, the direct energy inputs related to the production of renewable electricity is assumed to be zero (i.e. $E_{re,prod} = 0$). $E_{re,dist}$ should however account for the losses in electricty associated with transport and distribution. According to the data described in Section 5.1.1, they represent about 9.5% of the electricity consumed worldwide, i.e. 8.7% of the electricity produced. It gives that $q_{re} = (E_{re,prod} + E_{re,dist})/Y_{re} = E_{re,dist}/Y_{re} = 8.7\%$. The increase in distribution losses with renewable penetration (as described in the MEDEAS documentation [229]) is not taken into account in the model, i.e. q_{re} remains constant during the energy transition.

The intensities x_{re} and v_{re} as a function of Y_{re} are shown in Fig. 6.2 (q_{re} being constant). The increasing rate of these intensities highlights the *location effect*. Because of the lower quality of the sites that can receive the additional installations exploiting wind and solar resources, more and more capital and NEIC are needed to produce one unit of energy.

The renewable energy penetration rate is defined by the ratio $\varkappa = \frac{Y_{re}}{Y_e}$. If Y_e is given, the total renewable ($Y_{re} = \varkappa Y_e$) and non-renewable ($Y_{nre} = (1-\varkappa)Y_e$) energy productions can be deduced. The technical parameters q_{re}, x_{re}, v_{re} can



(a) $x_{re}(Y_{re})$



(b) $v_{re}(Y_{re})$

Figure 6.2 *– Evolution of the technical parameters of the renewable energy subsector as a function of Y_{re}, the amount of renewable energy produced. q_{re} is assumed to be constant (=8.7%).*

also be expressed as functions of $\varkappa$.

The parameters of the non-renewable energy subsector are determined by the following ratios:

$$\begin{aligned} q_{nre} &= \frac{E_{nre}}{Y_{nre}} \\ x_{nre} &= \frac{X_{nre}}{Y_{nre}} \\ v_{nre} &= \frac{K_{nre}}{Y_{nre}} \end{aligned}$$

If they are known, the technical parameters of the ES are then determined as

an average, weighted by $\varkappa$, of the technical parameters of the two subsectors:

$$q_e(\varkappa) = \varkappa\, q_{re}(\varkappa) + (1-\varkappa)\, q_{nre} \tag{6.37}$$

$$x_e(\varkappa) = \varkappa\, x_{re}(\varkappa) + (1-\varkappa)\, x_{nre} \tag{6.38}$$

$$v_e(\varkappa) = \varkappa\, v_{re}(\varkappa) + (1-\varkappa)\, v_{nre} \tag{6.39}$$

Knowing the technical parameters of the ES in 2018 (see Section 6.1.2), the corresponding renewable penetration rate, and the evolution of the technical parameters of the renewable subsector thanks to the EM, the technical parameters of the non-renewable subsector (i.e. q_{nre}, x_{nre}, v_{nre}) are found via Eqs. (6.37) to (6.39). According to IEA statistics[8], wind and solar accounted for 2% of the total primary energy supply in 2018, i.e. $\varkappa(2018) = 0.02$. With the calibration of 2018 and the energy model, the technical parameters for both subsectors in 2018 are estimated (see Table 6.8).

	Total energy sector	Non-renewable subsector	Renewable subsector
q_e [%]	9.76	9.78	8.68
x_e [US$2010/GJ]	3.32	3.32	3.01
v_e [US$2010/GJ]	39.07	26.65	647.63

Table 6.8 *– Estimation of the technical parameters of both subsectors of the ES in 2018, corresponding to a penetration rate of 2%.*

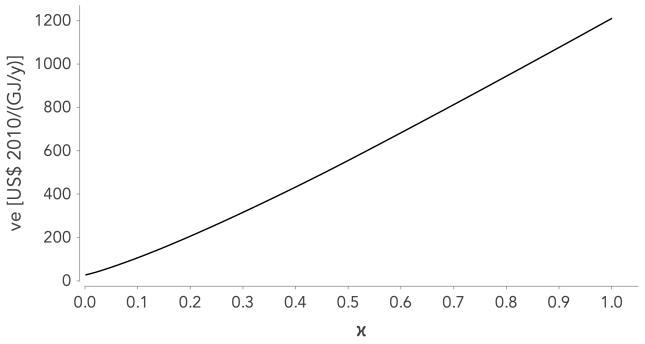
The evolution of the technical parameters of the ES as a function of the penetration rate $\varkappa$ is represented in Fig. 6.3, in the particular case where Y_e is also set at its 2018 value (thus for $\varkappa = 1$, $Y_{re} = Y_e(2018)$). $\varkappa$ evolves between 0 (all energy production is provided by non-renewable energies) and 1 (all energy production is provided by wind and solar technologies).

- Fig. 6.3a shows that the capital intensity v_e increases considerably with the penetration rate $\varkappa$: $v_e(1)/v_e(0) > 45$, which is consistent with the common assumption that renewable energies are much more capital intensive than non-renewable energies.

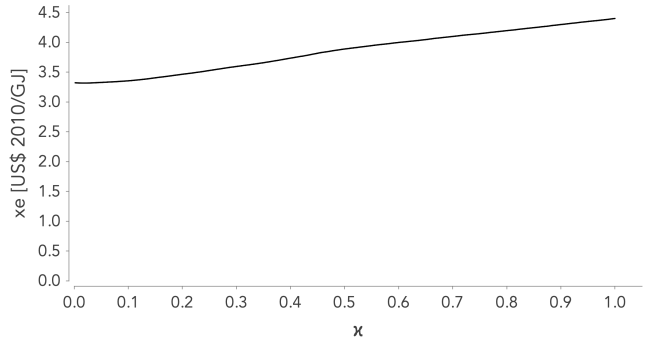
- Fig. 6.3b shows that x_e increases slightly with the ET : $x_e(1)/x_e(0) = 1.3$. NEIC requirements are not much higher for renewable energies than for non-renewable energies.

[8] `https://www.iea.org/data-and-statistics`

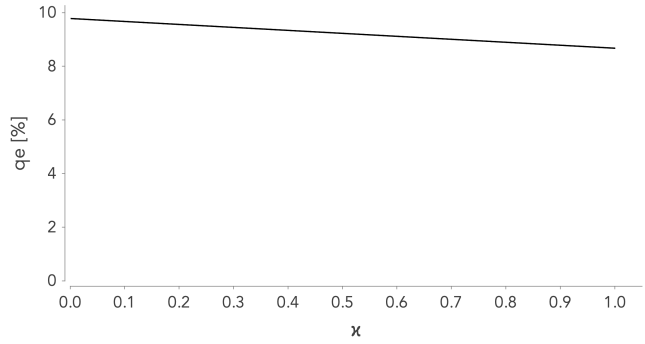
- Since $q_{nre} = 9.8\%$ (see Section 6.1.2 and Table 6.3) and $q_{re} = 8.7\%$, the energy intensity q_e slightly decreases with $\varkappa$ (Fig. 6.3c).



(a) $v_e(\varkappa)$



(b) $x_e(\varkappa)$



(c) $q_e(\varkappa)$

Figure 6.3 *– Evolution of the technical parameters of the ES as a function of the penetration rate $\varkappa$ ($\varkappa = 1$ corresponds in this case to $Y_{re} = Y_e(2018)$).*

6.2.2 Allowable space and transition curve

Allowable space

The concept of allowable space (AS) emerges from the attempt to determine an *exhaustive set of trajectories satisfying a given criterion.* In the present case, the retained criterion is simply that the net sectoral added values are both positive:

$$NV_i \geq 0, i = e, f \tag{6.40}$$

This criterion reflects the fact that both sectors should contribute positively to the useful output of the economy (as measured by the NDP).

From this criterion, an allowable interval for the energy price p can be derived (Appendix B.5):

$$I_p \equiv \underline{p} = \frac{w_e}{1 - q_e} < p < \frac{1 - w_f}{q_f} = \overline{p} \tag{6.41}$$

From Eqs. (6.14) and (6.15) we know that NV_f decreases and NV_e increases with p. Beyond $\overline{p}$, the price of energy is so high that NV_f is negative. Below $\underline{p}$, the price of energy is so low that NV_e is negative.

Under assumptions about the economic choices in terms of consumption and investment, the allowable interval for the energy price I_p (Eq. 6.41) can be transformed into an interval for k, the capital/energy ratio of the economy (Appendix B.6):

$$k = \frac{K}{Y_e} \tag{6.42}$$

$$I_k = \left[\underline{k}(x_f, v_f, q_f, x_e, v_e, q_e, \mathbf{z}), \overline{k}(x_f, v_f, q_f, x_e, v_e, q_e, \mathbf{z})\right] \tag{6.43}$$

where $\mathbf{z}$ is a vector of behavioural parameters.[9] As was the case for the interval bounds for p, beyond $\overline{k}$, NV_f becomes negative (p is too high) and below $\underline{k}$, NV_e becomes negative (p is too low).

Among the technical parameters on which I_k depends, v_e, q_e and x_e are functions of $\varkappa$ according to Eqs. (6.37) to (6.39), while the others do not vary with $\varkappa$. We can therefore write Eq. (6.43) as:

$$I_k = \left[\underline{k}(\varkappa), \overline{k}(\varkappa)\right] \tag{6.44}$$

[9] Here $\mathbf{z}$ contains either s and η or s and g_K, where g_K refers to the capital growth rate.

$\underline{k}(\varkappa)$ and $\overline{k}(\varkappa)$ are the top and bottom envelopes of the *allowable space* (AS), defined as all the $(\varkappa, k)$ couples that satisfy the criterion from Eq. (6.40). The envelopes $\overline{k}(\varkappa)$ and $\underline{k}(\varkappa)$ are both increasing functions of $\varkappa$, partly because renewable energies are more NEIC and capital intensive than non-renewable energies. The equations determining these envelopes are specified in Appendices B.6.1 and B.6.3, depending on the assumed economic choices in terms of consumption and investment.

An example of AS is illustrated by the space between the lower ($\underline{k}(\varkappa)$) and upper ($\overline{k}(\varkappa)$) curves in Fig. 6.4.

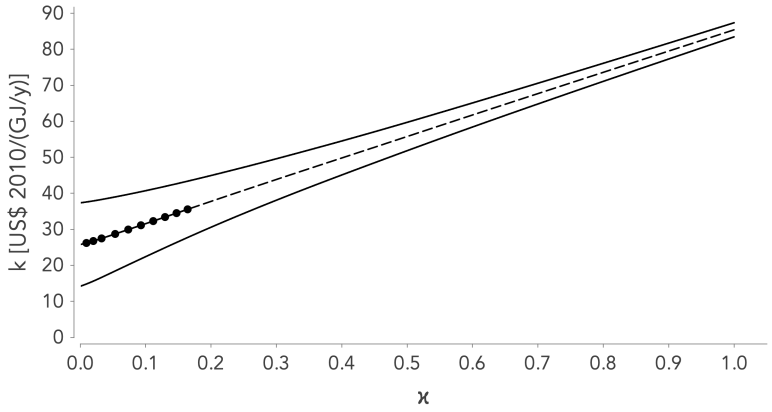


Figure 6.4 *– Representation of the AS and of a TC, for a fictitious scenario with Y_e and q_f fixed. The solid curves represent the bounds of the interval for k (Eq. (6.44)), and the AS is the space between these two curves. The dashed curve shows a particular TC, and the dots show the trajectory of the ET, thus the discrete pairs $(\varkappa(t), k(t))$ for a few successive years.*

Transition curve

A *transition curve (TC)* is a function Φ such that:

$$k = \Phi(\varkappa), \quad \varkappa \in [0, 1] \tag{6.45}$$

derivable, increasing and contained in the AS. Consequently, a TC respects the following inequalities:

$$\underline{k}(\varkappa) \leq \Phi(\varkappa) \leq \overline{k}(\varkappa), \quad \forall \varkappa \in [0, 1]$$

An example of TC is shown by the dotted curve in Fig. 6.4. It is entirely located between the two envelopes and therefore respects the previous inequalities.

The reduced dynamic model

The reduced dynamic model (RDM) is obtained from the MM, while integrating the notion of TC. It makes it possible to fully characterize the trajectory of an economy during its ET and, more precisely, to determine numerically whether (i) the ET is feasible or not in a finite time and (ii) if it is feasible, the time needed to complete it. Thanks to the MM, it is then possible to see the impact of the ET on all economic variables.

Two versions of the RDM are considered, corresponding to Exercises 1 and 2 described below, and which depend on different assumptions in terms of consumption and investment:

- Exercise 1 : s and η fixed.
- Exercise 2 : g_K and η fixed.

Exercise 1 assumes a constant savings rate and a constant share of energy expenditure in total consumption. In this case, the capital growth rate g_K is endogenous. Exercise 2 instead assumes that the economy has a given capital growth rate g_K to achieve at constant η, and results in an endogeneous savings rate.[10]

Exercise 1 - s and η fixed Within the context of Exercise 1, it is possible, thanks to the MM, to express g_K as a function of k, $\varkappa$, s and the other

[10]Exercises 1 and 2 are based on the common assumption that $\eta = pC_e/C$ is constant. As part of this work, in order to test the sensitivity of the results to this hypothesis, a third exercise was analysed where s is constant and final good and energy consumption are assumed to be strictly complementary (in other words, the ratio C_e/C_f is constant). Compared to Exercise 1, in that case the substitution between final good and energy is less easy at the level of consumption choices. Exercise 1 and this third exercise are in fact polar cases in the sense that, for a given budget, they are respectively based on the assumption that the agents maximise either a Cobb-Douglas or a Leontief utility function (whose elasticities of substitution are respectively unitary and zero).

The results from Exercise 3 were most of the time favourable to the ET. For some TCs and in the framework of the *sustainable development* scenario, it can even be completed in a few decades. However, these results are questionable as they imply a sharp rise of the price of energy during the ET, making the constant C_e/C_f hypothesis unlikely.

parameters (Appendix B.6.2):

$$g_K(k,\varkappa) = \frac{s}{1-\eta[1-s]}\left[\frac{1-x_f}{v_f} - \frac{[1-x_f]\,\frac{v_e(\varkappa)}{v_f} + x_e(\varkappa)}{k}\right] - \delta(\varkappa,k) \quad (6.46)$$

where

$$\delta(\varkappa,k) = \delta_f + [\delta_e - \delta_f]\,\frac{v_e(\varkappa)}{k} \quad (6.47)$$

The first term of the right-hand side member of Eq. (6.46) is an increasing function of k, η and s (because $\eta < 1$), and a decreasing one of $\varkappa$. As the second term, $-\delta(\varkappa,k)$, is also an increasing function of k and a decreasing one of $\varkappa$, g_K follows the same trends. It follows that, if g_K is positive, K increases as well and thus, for a given Y_e, k increases also. *Ceteris paribus*, there exists a positive feedback loop between g_K and k. However, this loop does not result in explosive growth, since if k tends to $+infty$, g_K tends to a positive constant. On the other hand, g_K is negatively affected by the ET. As $\varkappa$ increases, so do x_e and v_e, resulting in a lower share of the FS output available for its own investment. This exacerbation of the needs of the ES (mainly in terms of capital) to the detriment of the FS, mathematically translated by the fact that $\frac{\partial g_K}{\partial \varkappa} < 0$, is the manifestation of the *crowding out effect* mentioned in the introduction.

Exercise 2 - g_K and η fixed Within the context of Exercise 2, it is possible, thanks to the MM, to express s as a function of k, $\varkappa$, g_K and the other parameters (Appendix B.6.4):

$$s(k,\varkappa) = \frac{[1-\eta]\,[g_K + \delta(\varkappa,k)]}{\frac{1-x_f}{v_f} - \eta\,[g_K + \delta(\varkappa,k)] - \left[\frac{1-x_f}{v_f}v_e(\varkappa) + x_e(\varkappa)\right]\frac{1}{k}} \quad (6.48)$$

where $\delta(\varkappa,k)$ is defined by Eq. (6.47). s is a decreasing function of k and an increasing function of g_K and $\varkappa$, provided that δ_f is not too much higher than δ_e. For a constant Y_e, an economy with more capital produces more goods, allowing a lower relative savings rate to achieve the investment needed to sustain the desired growth rate g_K. On the contrary, a higher renewable penetration rate diverts capital away from the FS, resulting in less goods being produced and the need of more relative savings to reach g_K.

The RDM for Exercise 1 consists of Eqs. (6.44), (6.45), (6.46), (6.37) to

(6.39), and the identity defining g_K (Eq. (6.6)). The RDM for Exercise 2 consists of the same equations, except that Eq. (6.48) replaces Eq. (6.46).

Although the time dependency has not been explicited in the formulas, the RDM is a (discrete) dynamic model.

Simulation procedure The solution procedure of the RDM works as follows. Given the evolutions over time of the energy demand Y_e, of the technological parameters (in particular q_f), and of the TC, the RDM is used to determine the trajectory of $\varkappa(t)$ and $k(t)$ during the ET and the time needed to complete it (i.e. to reach $\varkappa = 1$). Knowing the capital stock $K(t-1)$, the capital growth rate $g_K(t-1)$ is either calculated via Eq. (6.46) (Exercise 1) or imposed (Exercise 2), and the capital stock $K(t)$ is calculated via (6.6). $Y_e(t)$ being exogenously determined, $k(t)$ can be deduced via Eq. (6.42). The penetration rate of renewable energy $\varkappa(t)$ is then determined by inverting Eq. (6.45). Finally, thanks to Eqs. (6.37) to (6.39), the values of the ES parameters ($v_e(t)$, $q_e(t)$, and $x_e(t)$) are calculated. Once the previous variables have been determined, all the other economic variables (sectoral production, consumption, GDP, etc.) can be calculated via the MM.

The first time periods of an example of ET in the AS are illustrated by the black dots in Fig. 6.4, in the particular case where all exogenous technical parameters are constant (the envelopes of the AS and the TC are therefore not time-dependent). It is important to clearly distinguish the TC (dotted curve) from the trajectory representing the ET (the points). Mathematically, the TC is continuous while the trajectory is a discrete set. If the TC is postulated and therefore exogenous, the pace of the ET along the curve is endogenous and it is this pace that determines the ET actually observed.

Finally, it should be noted that there are two contradictory forces influencing the ET. On the one hand, the positive loop between k and g_K noted above favours the growth of k, and thus the ET. On the other hand, the ET results in an increase of x_e and v_e, which have a negative effect on growth. If an increase of k were to be accompanied by a too strong increase in these parameters, g_K could become negative, leading to further decreases of k and g_K, which would block the transition. Therefore, for the ET to have a chance to continue, it must be done with enough available capital.

6.3 Simulations of the energy transition

All the variables and parameters used for the simulations are listed in Table 6.11.

6.3.1 Exogeneous parameters

Historical values of s and g_K

Within the framework of the simulations, either the value of the savings rate s or the capital growth rate g_K will be set at its *historical level*. To do this, the value averaged over the last 5 years was used. We find, for the period 2014-2018, for s an average value of 25.05% and for g_K an average value of 2.27%.

Future evolution of Y_e and of the technical parameters

Future changes in the technical parameters of the two sectors and in the energy demand Y_e are based on the following assumptions:

- The evolution of the technical parameters of the ES with the ET is described by Eqs. (6.37) to (6.39), where the technical parameters of the non-renewable energy subsector are assumed to be constant and equal to their calibrated value in 2018 (see Table 6.8). Assuming that the parameters of the non-renewable energy subsector will not change in the future can be considered optimistic.[11]

- Based on past values, the parameters x_f and v_f are assumed to be constant. Indeed, the MM calibration performed over the last 30 years shows that these parameters have not changed since 1990 (see Appendix B.3).

- The changes in Y_e and q_f are based on the IEA's "World Energy Outlook" 2020 report [5]. There are 2 scenarios: (i) the *business-as-usual* scenario (BAU), where changes in Y_e and q_f are extrapolated on the basis of the last 30 years (by 2040, Y_e increases by 45% and q_f decreases by 15%), and (ii) the *sustainable development* scenario (SD), which assumes a constant energy demand Y_e and a rapidly decreasing energy intensity q_f in the coming decades (by 2040, q_f would decrease by 40%, which corresponds

[11] Given the maturity of the technologies, technological progress seems limited and not able to counterbalance the depletion of the resources. It is therefore likely that in the future there will be an increase in energy and capital intensities of the non-renewable energy subsector.

to a rate of decline never observed in the past) (see Appendix B.7 for further details). In the long term, both scenarios have the same technical progress potential in the FS (q_f is asymptotically reduced by 50%), the difference between the two scenarios being the pace at which this limit is reached.[12]

Thereafter, we consider TCs in the form of weighted averages of the AS envelopes, i.e. curves of the form :

$$\Phi(\varkappa) = [1-\theta]\,\underline{k}(\varkappa) + \theta\overline{k}(\varkappa) \tag{6.49}$$

where (i) θ is the weighting parameter and (ii) $\underline{k}(\varkappa)$ and $\overline{k}(\varkappa)$ are the envelopes of the AS defined by Eqs. (B.10) (Exercise 1) and (B.15) (Exercise 2). As the energy intensity of the FS q_f decreases over time (see Section 6.3.1), both the envelopes of the AS and the TC are functions of t. θ is exogenous, constant or a function of t, chosen so as to always respect inequalities $0 \leq \theta \leq 1$. The formulation from Eq. (6.49) then ensures that the TC remains within the AS in each time period.

6.3.2 Exercise 1 - s and η given

Impact of θ

The purpose of this subsection is to scan the *entire AS* and measure how the results change when the TC move through this space. A simple way to do this is to consider all the TCs with a constant weighting parameter θ.

The graphs in Figs. 6.5 and 6.6 provide, for the 2 scenarios: (i) $\varkappa(2100)$, the renewable penetration rate in 2100, (ii) $\varkappa_l$, the asymptotical value of $\varkappa$, (iii) if it is completed in a finite time, the year of the end of the ET, T_f[13], and (iv) if any, the residual capital growth rate at the end of the transition, g_{Kl}. When the transition is completed in a finite time $\varkappa_l$=1, if not, $\varkappa_l$ is obtained when $\varkappa$ no longer varies, because g_K tends towards 0. There is a residual capital growth rate when the transition is completed in a finite time. However, this residue is very low and never exceeds 0.06%.

Business-as-usual scenario (plain curves)

[12] A third scenario based on the IEA's *New Policies* scenario was also tested, but did not lead to fundamentally different results from those of the BAU scenario.

[13] Not to be confused with the average lifetime of the FS capital stock which has the same notation.

- Fig. 6.5a gives the value of the penetration rate $\varkappa$ in 2100. The curve is slightly increasing, but $\varkappa(2100)$ is approaching 30% at best.
- Fig. 6.5b shows that the ET is never completed in *a finite time*. Nevertheless we see that $\varkappa_l$ is approaching 1 for $\theta = 1$, and $\varkappa_l$ is above 65% for all values of θ. The non-completion of the ET is due to the fact that the growth rate of the capitak stock g_K decreases down to zero.
- As mentioned above, the residual growth rate of the capitak stock g_{Kl} is 0 for all the simulations. The economy tends towards a stationary state with no growth.

Sustainable development scenario (dotted curves)

- Fig. 6.5a shows that the renewable penetration rate $\varkappa$ in 2100 is significantly higher for SD than for BAU.
- Fig. 6.5b shows that if $\theta < 0.86$, no scenario allows for a complete ET in a finite time.
- Fig. 6.6a shows for $\theta \geq 0.86$ the duration of the ET decreases with θ (from 248 years for $\theta = 0.86$ to 131 years for $\theta = 1$). The minimum value of T_f is reached for $\theta = 1$ (complete transition by 2149).
- Fig. 6.6b shows that the residual capital growth rate g_{kl} is 0 for $\theta < 0.86$ and sightly increasing for $\theta \geq 0.86$. At best it reaches 0.056%.

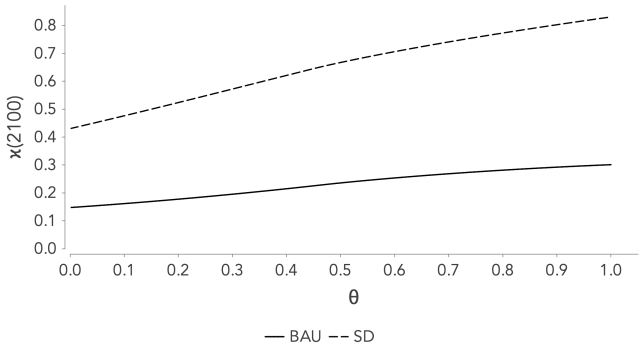
The previous results only concern TCs with a constant weighting rate. Numerically, however, the following conjecture is verified :

Conjecture 1 *Consider a TC Φ^v defined by Eq. (6.49), whose weighting parameter is variable and described by the sequence $\{\theta_t : t \geq 0\}$. Let $\overline{\theta}$ (≤ 1) be the maximum of this sequence. Let $\Phi^{\overline{\theta}}$ be the TC whose weighting parameter is constant and equal to $\overline{\theta}$. Then $T_f(\Phi^{\theta}) > T_f(\Phi^{\overline{\theta}})$.*

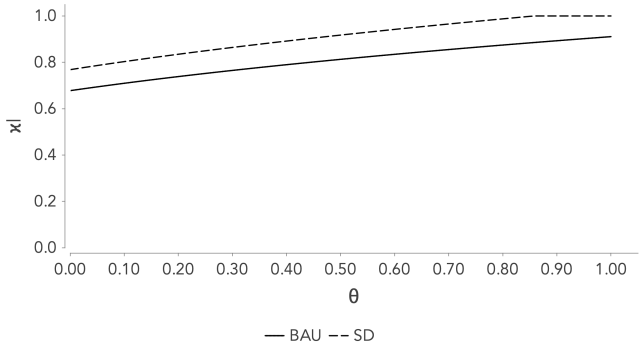
The interest of this result is to provide a *minimum bound* for the duration of an ET based on a TC with variable weighting parameter, from the values of T_f calculated for TCs with constant weighting parameter (values given by Fig. 6.6a).

As a corollary of this conjecture, the *duration of any ET* will be greater than or equal to $T_f(\Phi^1)$, where Φ^1 designates the TC characterised by $\theta = 1$

(i.e. greater than 131 years for SD). Simulations with $\theta = 1$ would correspond to an economy where the net added value of the FS is zero. The price of energy is so high that all the added value of the economy comes from the ES.

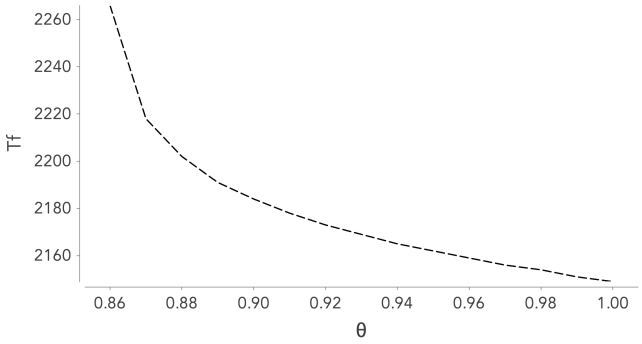


(a) $\varkappa(2100)(\theta)$

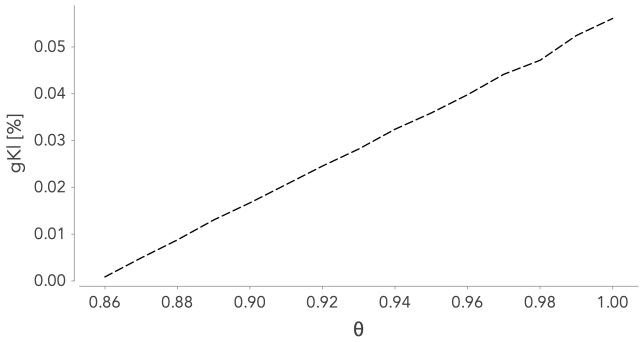


(b) $\varkappa_l(\theta)$

Figure 6.5 *– Exercise 1, evolution as a function of θ for both scenarios of: the renewable penetration rate in 2100 $\varkappa(2100)$, and its asymptotical value $\varkappa_l$.*



(a) $T_f(\theta)$, SD scenario



(b) $g_{Kl}(\theta)$, SD scenario

Figure 6.6 *– Exercise 1, evolution as a function of θ, only for the SD scenario and $\theta \geq 0.86$, of: the year of the end of the transition T_f and the residual capital growth rate g_{Kl}.*

Impact of the technical progress rate

Whether for BAU or SD, the technical progress potential is assumed to be very high, since the energy intensity of the FS is asymptotically divided by 2. The difference between the 2 scenarios lies in the potential already realised in 2040 (30% for BAU, 80% for SD).

Further increasing the potential realised in 2040 under SD does not fundamentally change the results of the previous subsection. For the record, the evolution of q_f is governed by Eq. (B.17). If the rate of change r_{q_f} is increased sharply to the point that the potential of technical progress is realised in a few years, the end of the ET (measured by T_f) is slightly advanced but remains beyond 2100.

Consequently, it appears from the previous simulations that, *unless assuming unreasonable progress in terms of energy efficiency, it is not possible to achieve a complete ET before the end of the century, even assuming energy demand control (as required by the SD scenario).*

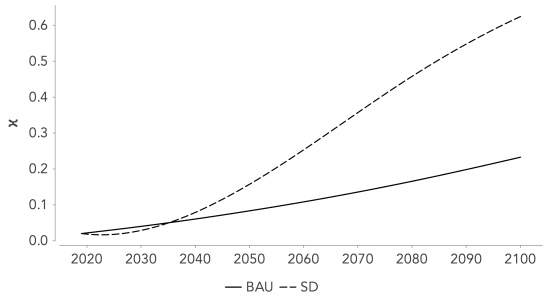
Temporal analysis

In Figs. 6.7 to 6.10 the temporal evolution until 2100 of several parameters of the model is shown. θ (i.e. the TC) is kept constant and chosen so as that the initial value of k corresponds to its calibrated value (i.e. $= K(2018)/Y_e(2018)$). With Eq. 6.49 we find $\theta = 0.42$.

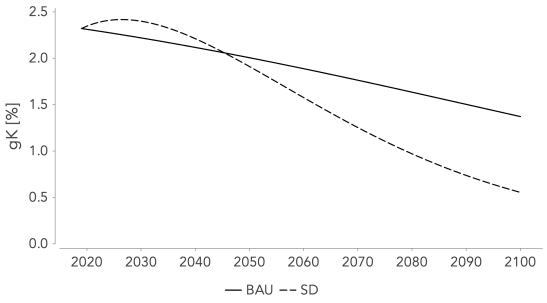
These graphs confirm that, under the asumptions of Exercise 1, the transition is too slow in relation to the necessary CO_2 emission reductions. Figs. 6.7a and 6.7b highlight the negative correlation between the penetration rate and the capital growth rate, and Figs. 6.7a and 6.7c the relationship between $\varkappa$ and k. Under the SD scenario, the transition is more avanced: the capital growth rate is much lower and the capital energy ratio k is significantly higher than for the BAU scenario. According to the results of the previous sections, g_K and g will ultimately go down to 0% in both scenarios, much faster for SD than for BAU. Finally we see in Fig. 6.7d that the EROI only slighty decreaeses in both scenarios, more in the SD scenario as the energy transition is more advanced. By 2100, it reaches 8.1 for the BAU scenario and 7.6 for the SD scenario. The temporal evolution of the NER is not shown as it remains more or less constant (it reaches 38% in 2100 for the BAU scenario and 37% for the SD scenario).

We see in Fig. 6.8a that non-renewable production continue to increase until 2100 with BAU (it actually starts to decrease around 2110). It means that CO_2

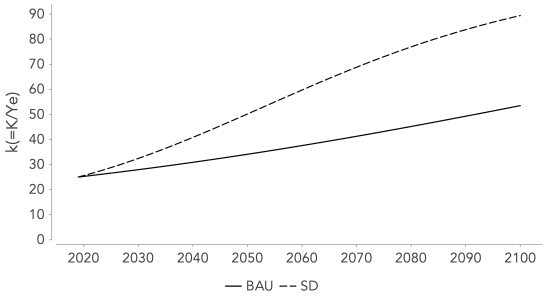
emissions will continue to increase until after 2100. For the SD scenario, given that Y_e is kept constant and that $\varkappa$ is increasing, the non-renewable production decreases from the beginning of the simulation (Fig. 6.8b). According to the faster decrease of g_K observed in Fig. 6.7b, the GDP begins to flatten out by the end of the simulation in the SD scenario (Fig. 6.9b), while this effect is not yet present for the BAU scenario (Fig. 6.9a). Finally, in Figs. 6.10a and 6.10b we observe the significant increase in the capital allocated to the ES, compared to the capital allocated to the FS which begins to stagnate for the SD scenario.



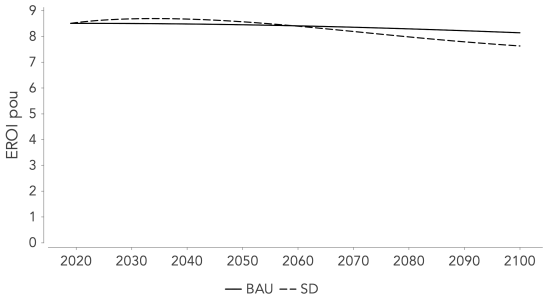
(a) $\varkappa(t)$



(b) $g_K(t)$

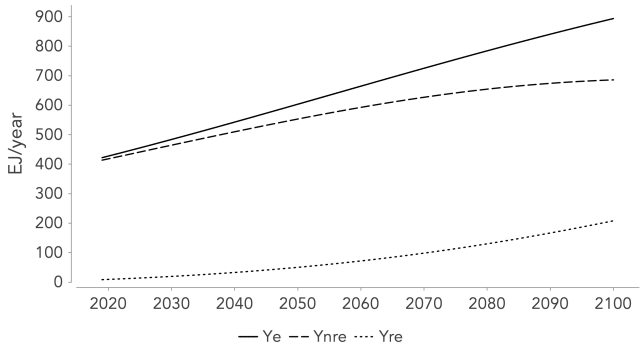


(c) $k(t)$

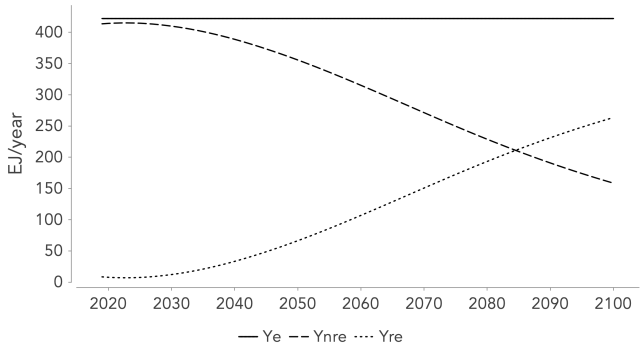


(d) $\text{EROI}_{pou}(t)$

Figure 6.7 *– Exercise 1: temporal evolution until 2100, for both scenarios, of: Fig. 6.7a: the renewable penetration rate $\varkappa(t)$, Fig. 6.7b: the capital growth rate $g_K(t)$, Fig. 6.7c: the capital energy ratio $k(t)$ and Fig. 6.7d: the societal point-of-use EROI.*

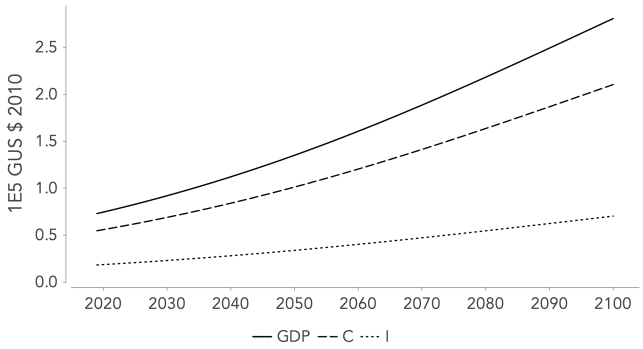


(a) BAU

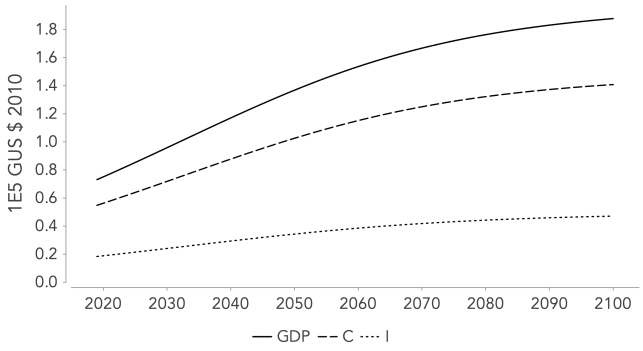


(b) SD

Figure 6.8 *– Exercise 1: temporal evolution until 2100 for both scenarios of the total, non-renewable, and renewable energy production ($Y_e(t)$, $Y_{nre}(t)$ and $Y_{re}(t)$).*

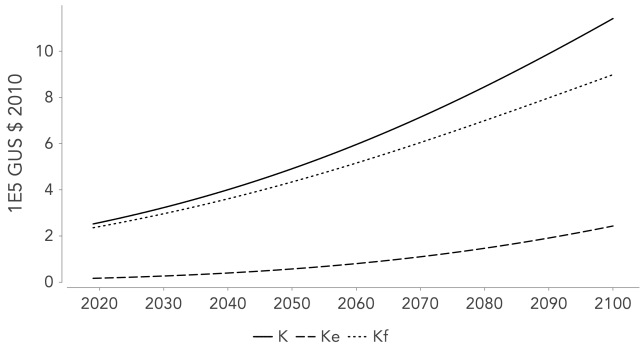


(a) BAU

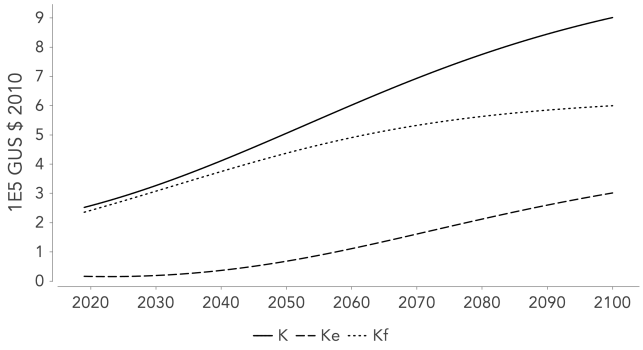


(b) SD

Figure 6.9 *– Exercise 1: temporal evolution until 2100 for both scenarios of the GDP and its repartition between consumption $C(t)$ and investment $I(t)$.*



(a) BAU



(b) SD

Figure 6.10 *– Exercise 1: temporal evolution until 2100 for both scenarios of the total capital stock $K(t)$ and its repartition between the two sectors ($K_e(t)$ and $K_f(t)$).*

6.3.3 Exercise 2 - η and g_K fixed

Previous simulations have shown how difficult it would be to achieve a complete ET before the end of the century if consumption and savings choices remain unchanged. The aim of this section is to study an alternative strategy, aiming at supporting capital growth through an increase in the savings rate.

Impact of θ

As in Section 6.3.2, the following simulations are based on a constant weighting parameter θ. The values of T_f, s and $\varkappa$ (in 2050, 2100 and T_f) obtained for Exercise 2 are shown in Table 6.9 for $\theta = 0$ and $\theta = 1$. The changes in the variables between these extreme values are monotonous. The capital growth rate g_K is fixed at its average value over the last 5 last years: 2.27%.

	BAU						SD			
	$\theta = 0$			$\theta = 1$			$\theta = 0$		$\theta = 1$	
	2050	2100	2129	2050	2100	2133	2050	2085	2050	2090
$\varkappa$ [%]	16.8	46.1	100	0	17	100	31.2	100	0	100
s [%]	29.8	34.8	44	24.4	25.9	41.1	30.7	40.1	23.9	36.8

Table 6.9 *– Exercise 2: values for $\theta = 0$ and $\theta = 1$ of the renewable penetration rate $\varkappa$ and of the savings rate s, in 2050, 2100 and at the end of the transition (i.e. in T_f), for the 2 scenarios.*

Business-as-usual scenario The table shows that :

- The ET is completed in a finite time for $\theta = 0$ and $\theta = 1$, and thus for all values of $\theta \in [0, 1]$. T_f is slightly increasing with θ but varies little (T_f goes from 2129 for $\theta = 0$ to 2133 for $\theta = 1$). In Exercise 1, an increase of θ stimulated capital growth and thereby accelerated the ET. In Exercise 2, this effect is not present since g_K is fixed.
- The ET is far from being completed by the end of the century. $\varkappa(2100)$ varies between 46% for $\theta = 0$ and 17% for $\theta = 1$.
- As for T_f, the observed values of s at the end of the ET evolve little with θ (from 44% for θ=0 to 41% for θ=1).

In summary, this analysis reveals that *all the TCs included in the AS lead to a complete ET in about 115 years, with a significant increase in the savings rate.*

Sustainable development scenario Previous results have shown that under the BAU scenario, maintaining the capital growth rate at its historical level through a gradual increase in the savings rate would allow a complete ET in about 115 years. The end of the transition does not occur until the next century.

However, in the context of Exercise 1, we have seen that the SD scenario made it possible to significantly reduce the duration of the ET compared to BAU (see Section 6.3.2). Intuition then suggests that the combination of the hypotheses of Exercise 2 and the SD scenario should enable a complete ET before the end of the century.

In order to verify this, the previous analysis made for BAU is repeated for SD. Table 6.9 shows the values obtained. We observe that :

- The previous intuition is confirmed since the completion of the ET is obtained after a period of 67 to 72 years, i.e. a value of T_f around 2090.
- Maintaining the capital growth rate g_K during the ET requires a significant increase in the savings rate s. However, this increase is less than for BAU, as s reaches between 37 and 40% at the end of the ET, depending on the value of θ.

From the above, it appears that the SD scenario combined with the support of capital growth allows to complete the ET before 2100. However, its duration would be at least 67 years in the best case.

SD : g_K required for $T_f = 2070$

With the previous simulations, in the best case scenario we are still beyond certain target dates retained in the literature in the fight against climate change. Indeed, according to a recent IPCC report [246], limiting the global temperature increase to 2°C requires the achievement of carbon neutrality by 2070 (and a reduction of 25% in emissions by 2030 compared to their 2010 level). The latter key date (2070) is also chosen by the IEA to achieve global carbon neutrality [32] as part of the *sustainable development* scenario.

The previous point showed that maintaining the capital growth rate at its historical level (i.e. 2.27%, its average value over the last 5 years period) within the framework of SD made it possible to complete the ET in about seventy years. Intuition suggests that increasing the capital growth rate should lead to an even shorter transition.

The following simulation results are based on the objective of an end of the ET in 2070, and aim at determining the growth rate g_K necessary to reach this goal, as a function of θ. Table 6.10 shows that :

- g_K increases slightly with θ, from 2.91% to 3.12%.
- The savings rate observed at the end of the ET decreases slightly with θ, while still remaining above 40%.[14]

θ	g_K [%]	$s(T_f)$ [%]
0	2.91	43.5
0.2	2.96	43.1
0.4	3	42.5
0.6	3.04	42
0.8	3.08	41.5
1.0	3.12	41.1

Table 6.10 *– Minimum capital growth rate for a transition completed by 2070 (Exercise 2, scenario SD), and the corresponding savings rate at the end of the ET.*

Temporal analysis

Previous results show that an ET completed before the end of the century requires a significant increase in the savings rate, highlighting that the transition has a profound effect on the economy. Using the MM, the following analysis aims to shed light on the behaviour of economic variables during the transition of the ES.

The observations below correspond to an ET completed in 2070 with a capital growth rate g_K equal to 3%, under the SD scenario. The TC is chosen to ensure a gradual transition without delay.[15]

Figs. 6.11 to 6.14 show that :

- Maintaining the growth rate g_K during the ET requires a gradual increase in the savings rate s (Fig. 6.11b). *This increase is significant since s*

[14]Note: Similar simulations can be carried out within the framework of BAU. To complete the transition by 2070, a capital growth rate of around 4.1% is required, depending on θ. To maintain this growth rate, a savings rate of more than 55% is then necessary (s at the end of the ET decreases from 58.6% for $\theta = 0$ to 56.2% for $\theta = 1$).

[15]The chosen TC has a constant weighting rate $\theta = .418$. TCs associated with lower θ values lead to a "strong" start of the transition followed by a slowdown. TCs associated with higher θ values lead to a delay before the start of the ET.

increases from 25 to about 40% at the end of the ET. This figure is similar to those of Režný and Bureš [87] and of Fagnart et al. [85].

- As shown in Fig. 6.11c, the transition is characterised by a strong increase in the share of capital devoted to the ES ($\mu = \frac{K_e}{K}$), which exceeds 40% at the end of the trajectory. This result is similar to those of Dale [64] and of Fagnart et al. [85].

- Unsurprisingly, the ET results in a significant increase in the real price of energy p (Fig. 6.12a). Despite the decrease of q_f due to technical progress, the growth of the economy results in an increased demand for energy which pushes up its price. At the end of the ET, the price p reaches 6 times its initial value. This results contradicts the one of Jacobson [18], claiming that the price of energy will not increase with the ET.

- As shown in Fig. 6.12b, the rise in the price of energy translates into a significant increase in the share of the ES gross added value in GDP ($\alpha = \frac{AV_e}{GDP}$). The increase in the share of the ES net added value in NDP (measured by $\alpha_n = \frac{NV_e}{GDP}$) is more moderate.

- Fig. 6.12c illustrates the evolution of the FS production (Y_f), as well as how it is distributed between final consumption C_f, investment I and intermediate consumption deliveries to the two sectors $X(= X_e + X_f)$. While final output remains growing during the transition, there is a decline in the growth of consumption of goods C_f which, like C, is almost constant at the end of the ET. In other words, because of the increase in the savings rate, the allocation of Y_f changes to the detriment of C_f and to the benefit of I (the share of the intermediate consumption deliveries remaining almost constant).

- The increase in s translates into a slowdown in aggregate consumption C with respect to the GDP. C becomes quasi-stationary at the end of the ET, while the economy is still growing (Fig. 6.13a).

- Fig. 6.13b illustrates how the ES production Y_e is split between self-consumption E_e, deliveries to the FS E_f, and final energy consumption C_e. It can be observed that the share of E_f in Y_e increases significantly to the point of taking up most of the energy production at the end of the ET.

- The ET is accompanied by a strong increase in v_e, the ES capital intensity. As the share of capital in the economy devoted to this sector continues to grow, the capital intensity of the economy, defined as $v = \frac{K}{GDP}$, increases (Fig. 6.13c).

- We show in Appendix B.2 that the GDP growth is decomposed into the growth of the capital stock and the decline in the capital intensity of the economy (defined as $g_v = \frac{\Delta v}{v}$): $g \approx g_K - g_v$. Given the previous observation (v is increasing), the GDP growth rate declines despite the constancy of g_K, as confirmed by Fig. 6.14a.

- Fig. 6.14b illustrates the decrease in the ratios GDP/Y_T (where $Y_T = Y_f + pY_e$ denotes the total output of the economy, including all intermediary consumptions) and NDP/GDP during the ET. The decrease in the first ratio indicates that the ET results in a faster growth of the intermediary consumptions compared to GDP (the end-use consumption). The decrease of the second ratio is linked to the increase in the share of capital consumption δK in GDP, induced by the increase in capital intensity v.[16] The share of *useful* production (i.e. for consumption or growth) in total production tends to decrease with the ET.

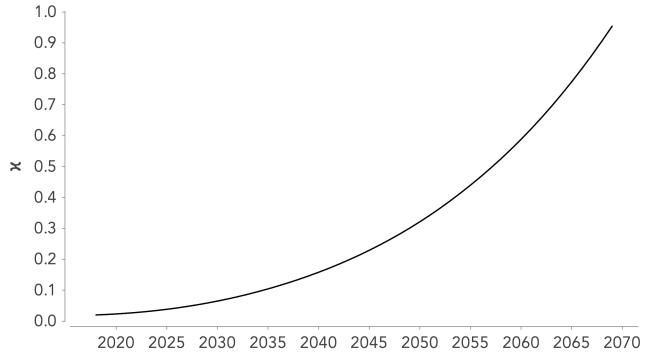
- Fig. 6.14c shows that the societal point-of-use EROI decreases during the ET, from 8.6 to 6.9 (this value corresponding to the estimate found in Fig. 5.5b, for an improvement of 50% and a production around 400 EJ/year). Several opposing forces are at work: (i) the ET results in an increase of v_e and x_e, which lowers the EROI, (ii) the decrease of q_e increases the EROI and, (iii) the technical progress behind the efficiency gains in the FS increases the EROI.
  This decline does not appear to be significant, yet the macroeconomic implications are, as evidenced by the significant rise in the savings rate.

- The NER of the economy decreases from 39 to 35.7%. The amount of energy available for final consumption and net investment does not decrease much, but the allocation of the "net" final energy available between consumption and investment varies significantly.

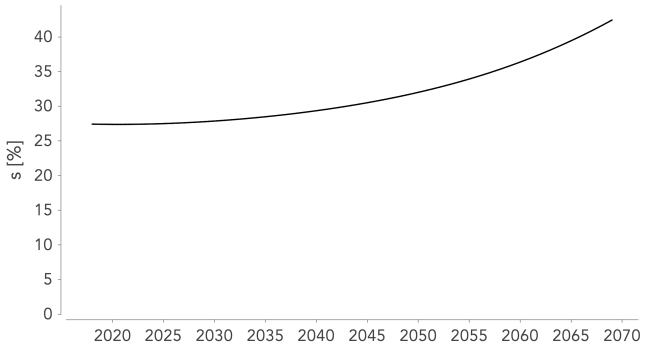
In conclusion, *a strategy aiming at supporting the growth of capital through an increase in the savings rate makes it possible to reach the desired duration*

[16] The increase of v outweighs the decrease of δ, the latter being due to the fact that the life span of capital is higher in the ES than in the FS.

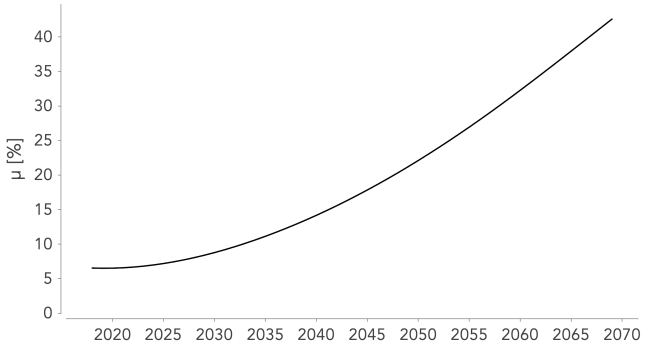
for the ET. The price to pay is a slowdown in the growth of total consumption which ends up stagnating at the end of the transition.



(a)

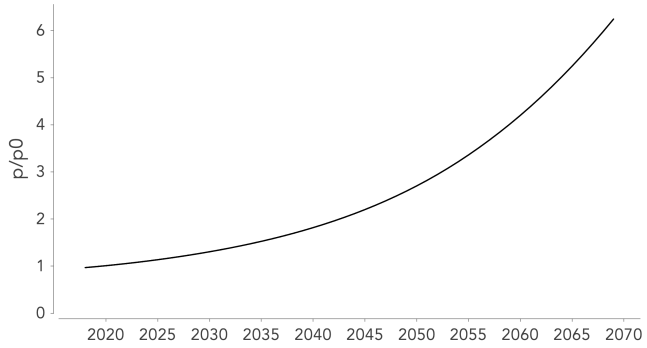


(b)

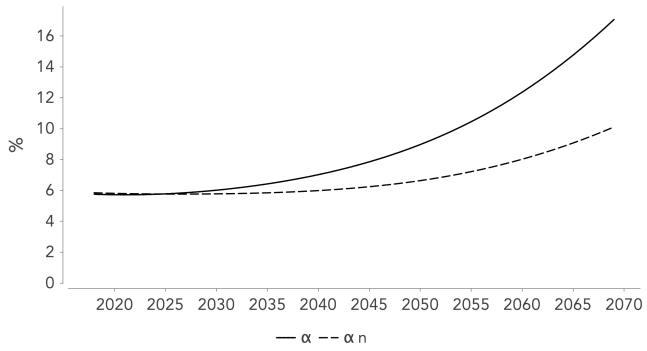


(c)

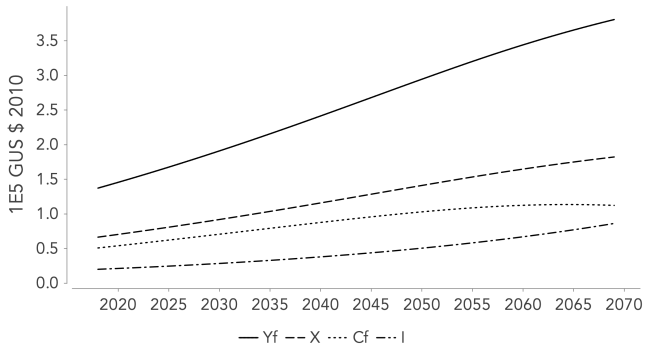
Figure 6.11 *– Exercise 2: Temporal evolution for SD scenario, with g_K=3% and θ=0.418, of: Fig. 6.11a: the renewable penetration rate $\varkappa(t)$, Fig. 6.11b: the savings rate $s(t)$, Fig. 6.11c: the share of capital stock devoted to the ES $\mu(t)$*



(a)

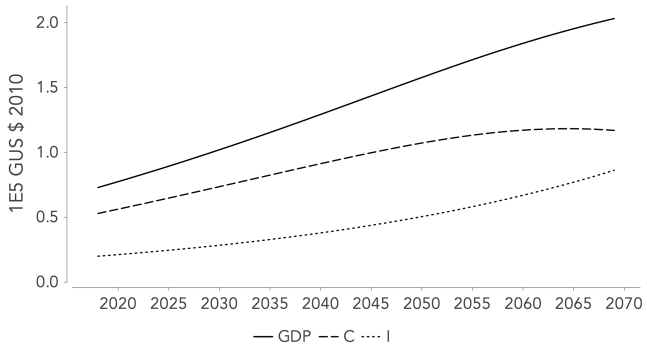


(b)

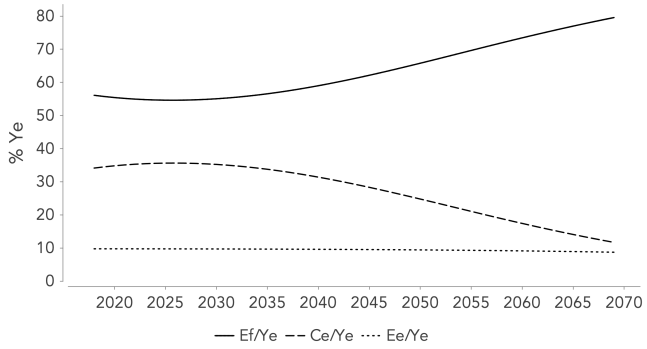


(c)

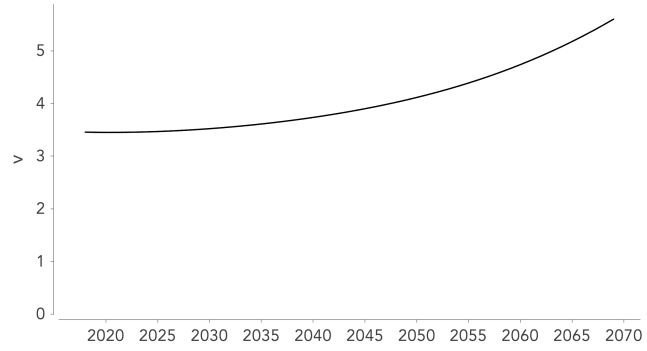
Figure 6.12 *– Exercise 2: Temporal evolution for SD scenario, with g_K=3% and θ=0.418, of: Fig. 6.12a: the energy price compared to its price in 2018 $p(t)/p(2018)$, Fig. 6.12b: the share of the ES gross added value in GDP $\alpha(t)$, and the share of the ES net added value in NDP $\alpha_n(t)$, Fig. 6.12c: the FS output $Y_f(t)$ and its distribution: NEIC $X(t) = X_f(t) + X_e(t)$, final consumption $C_f(t)$ and investment $I(t)$.*



(a)

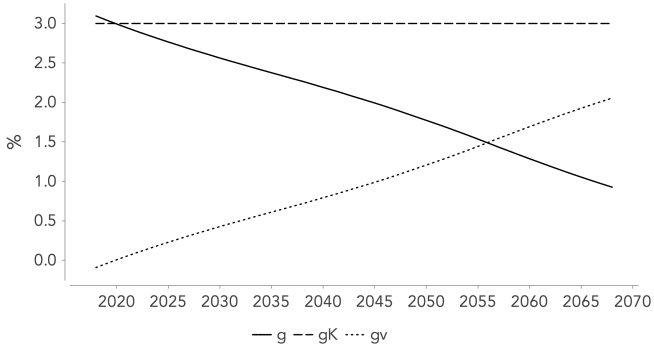


(b)

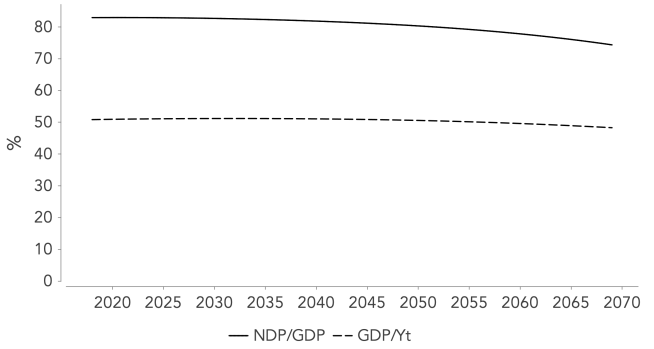


(c)

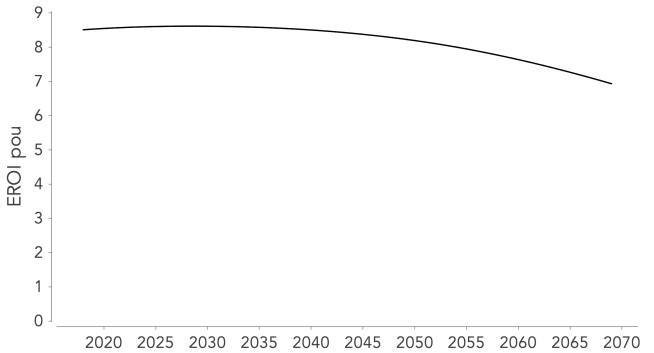
Figure 6.13 *– Exercise 2: Temporal evolution for SD scenario, with g_K=3% and θ=0.418 of: Fig. 6.13a: the gross domestic product GDP(t) and its distribution between consumption $C(t)$ and investment $I(t)$, Fig. 6.13b: the distribution of the ES output $Y_e(t)$, in relative terms, between self-consumption ($E_e(t)/Y_e(t)$), deliveries to the FS ($E_f(t)/Y_e(t)$), and final energy consumption ($C_e(t)/Y_e(t)$), Fig. 6.13c: the capital intensity of the economy (i.e. the capital/GDP ratio) $v(t)$.*



(a)



(b)



(c)

Figure 6.14 *– Exercise 2: Temporal evolution for SD scenario, scenario SD, with g_K=3% and θ=0.418 of: Fig. 6.14a: the capital growth rate $g_K(t)$ (constant) and its distribution between the GDP growth rate $g(t)$ (decreasing) and the growth rate of the capital intensity of the economic $g_v(t)$ (increasing), Fig. 6.14b: the ratios of the GDP to the total output of the economy (defined as $Y_T(t) = Y_f(t) + pY_e(t)$), and the ratio between the NDP and GDP, Fig. 6.14c: the point-of-use societal EROI, $EROI_{pou}(t)$.*

6.3.4 Discussion

Simulation results confirm the main findings of the models of the critical literature cited in the introduction [31, 36, 70, 247], in particular those presenting the evolution of certain macroeconomic variables in the context of the energy transition [85, 87]. It is observed that, if completed in time, the energy transition would be accompanied by a considerable increase in the economy's savings rate, exceeding 40% in all the scenarios simulated, as well as in the share of capital devoted to the energy sector, rising from less than 10% to more than 40%. At unchanged consumption behaviours (i.e. Exercise 1), the energy transition is almost never completed (except for the SD scenario and a few values of θ) because the economy tends towards a stationary state.

In the model of Fagnart et al. [85] the transition is fully completed after a certain period of time, but it is accompanied (with a few exceptions) by a decrease in GDP. This is the case also with the MEDEAS model, where the economy decreases from 2050 onwards in most of the scenarios envisaged [36]. Compared to these general equilibrium models, we are in a partial equilibrium context where energy demand does not depend on the future evolution of the economy, which might explain why we do not observe a decrease in GDP.

It is important to stress that the results obtained can be considered optimistic. Indeed, the underlying assumptions upon which the previous results were obtained can be considered quite "conservative"; in particular:

(a) At the beginning of the simulation, the technical progress potential lowering the FS energy intensity is assumed to be significant, since it is (asymptotically) divided by 2. For the BAU scenario, 55% of the gains are obtained in 50 years, and 80% in 100 years. For the SD scenario, most of the gains (97%) are assumed to be obtained before 50 years.

(b) Production factor intensities (q_{nre}, x_{nre} and v_{nre}) of the non-renewable energy subsector are assumed constant. However, given the maturity of technologies, technological progress does not seem likely to continue to offset the gradual depletion of resources and the fact that their extraction is becoming increasingly costly in terms of energy and capital. A future increase in these intensities therefore seems plausible. The same goes for the energy intensity of the renewable subsector (q_{re}), which is expected to increase with renewable penetration, as modeled in MEDEAS [229].

(c) Capital is assumed to be perfectly malleable, in the sense that it can move between the final and energy sectors on the one hand, and between the two subsectors of the ES on the other.

(d) As indicated in Section 6.2.1, the site selection criterion is a criterion of cost-effectiveness, whether this is measured in energy or economic terms. However, many other factors come into play when setting up a new renewable energy park. This means that, in practice, less profitable sites could be selected before more profitable ones.

Assumptions (a) and (b) explain a large part of the relatively small decrease in EROI during the ET compared to other models, while at the same time the growth rate of the economy declines. Eqs. (6.16) and (6.26) show that the EROI would decrease more if (i) q_f decreased less as a result of lower technical progress potential, (ii) v_e and x_e increased even more as a result of the increase in x_{nre} and v_{nre} and (iii) q_e increased as a results of the increase of q_{re}.

Hypothesis (c) allows to reduce a capital stock faster than what its "natural" depreciation rate would allow. It is not applicable if (i) the stock is increasing or (ii) it decreases less quickly than its depreciation rate. Within the framework of the simulations studied, the cause (i) is verified for the FS and the renewable energy subsector because their respective stocks are always growing. Cause (ii) applies to the non-renewable energy subsector during much of the ET, but no longer when its end is approaching. Hypothesis (c) then becomes operative and everything happens "as if" thermal power plants were transformed into solar panels or wind turbines, which is of course unrealistic.

Removing any of the hypotheses (a) to (d) would complicate the ET and result in its lengthening.

6.4 Conclusion

In order to study the feasibility and pace of the energy transition at the global level, this chapter develops a modeling scheme articulating a macroeconomic input-output model with two sectors (energy and non-energy) and an energy model able to calculate the maximum potentials of solar and wind energy. This methodology allows to take into account two effects: a crowding out effect of the final sector in terms of capital allocation, and a location effect due to the declining quality of the sites that can receive the additional wind and solar installations.

The main findings obtained thanks to the macroeconomic model are as follows:

- *At an unchanged savings rate*, the transition to a 100% renewable energy system seems unachievable before the end of the century. Controlling energy demand at its current level will drastically reduce the duration of the transition, but is not enough. The reason lies under the higher capital needs of the renewable energy technologies, resulting in the crowding out of the FS in terms of capital allocation. This effect weighs ever more negatively on growth, slowing down and then blocking the transition in most of the scenarios considered, as the economy tends towards a stationary state.

- The strategy aiming at *supporting capital growth* through an increase in the savings rate allows to counteract the crowding out effect and to reduce significantly the duration of the ET. If the demand for energy continues to grow significantly (an increase of 150% by 2100 is expected in the BAU scenario), the transition is however completed only after the end of the century.

- In order to allow for a complete transition by 2070, the energy demand should be kept at its current level and the capital growth rate should be maintained at a value above its historical level. However, due to the significant increase in the savings rate, total consumption ends up stagnating at the end of the transition (while the economy is still growing).

- Technical progress affecting the energy intensity of the FS proves to be a fundamental determinant of whether or not the ET is feasible in a finite

time. Within the framework of the strategy of the previous point, this intensity must decrease by at least 50% by the end of the ET in 2070.

- During the ET, the economy is characterised by several important evolutions: (i) following the increase in the real price of energy, the share of the ES in the total added value increases appreciably (whether measured in gross or net terms), (ii) the allocation of sectoral productions is modified, in particular to the detriment of consumption, (iii) despite the maintenance of the capital growth rate, the GDP growth rate decreases as a result of the increase in the capital intensity of the economy (measured by the capital/GDP ratio) and, (iv) because of a faster increase of intermediate and capital consumptions than of GDP, the share of useful production (i.e. intented for final consumption or growth) in overall production tends to decrease.

- The societal EROI decreases during the ET, but not as much as observed in other models (indeed it decreases form 8.6 to 6.9). This relatively small decrease does not explain the significant impacts of the ET on the economy, and suggests and suggests that it is more the increased capital intensity of ET that weighs on economic growth.

The previous results confirm those of the critical literature reviewed in the introduction, in particular concerning the impact of the crowding out effect on growth and the need to control energy demand in order to be able to complete the ET in a sufficiently short period of time.

The above conclusions can be considered optimistic as they are based on several conservative assumptions, as discussed in Section 6.3.4.
In order to increase the relevance of the model and to refine the results, several developments are possible. Modelling the non-renewable energy subsector in the same way as what was done for the renewable energy subsector and removing the hypothesis of perfect malleability of capital would contribute to greater realism. Endogenising (i) consumption and investment behaviours and (ii) energy demand would enrich the interactions between the economy and the energy transition and would enable to capture a potential rebound effect. Taking into account the labour factor next to the capital factor while requiring that their respective remunerations be positive would make it possible to refine the space of allowable trajectories.

Finally it would be interesting to add the cumulative CO_2 emissions to

the simulations. Indeed, although we manage, under certain conditions, to complete the transition by 2070, there is no guarantee that the cumulative quantities of CO_2 emitted do not exceed the critical threshold necessary to limit the increase in global temperature.

Type	Parameter	Value
Exogenous, variable	q_f(t)	Eq. B.17 (IEA scenarios)
	Y_e(t)	Eq. B.18 (IEA scenarios)
Exogenous, constant	x_f, v_f, δ_e, δ_f	Table 6.3 (Calibration 2018)
	η (Eq. 6.21)	4% (OECD Input-output tables)
	g_K	Exercice 1: endogenous, see below
		Exercice 2: 2.27% (mean 2013-2018)
	s	Exercice 1: 25.05% (mean 2013-2018)
		Exercice 2: endogenous, see below
Endogenous, reduced dynamic model (successively)	$K(t)$	$= K(t-1)(1+g_K(t-1))$ (Eq. 6.6)
	$k(t)$	$= \frac{K(t)}{Y_e(t)}$ (Eq. 6.42)
	$\varkappa(t)$	Inverting Eq. 6.45
	$q_e(t)$	$= q_e(\varkappa(t))$, Eq. 6.37 (EM)
	$x_e(t)$	$= x_e(\varkappa(t))$, Eq. 6.38 (EM)
	$v_e(t)$	$= v_e(\varkappa(t))$, Eq. 6.39 (EM)
	$g_K(t)$	Exercice 1: $= g_K(k, \varkappa)$, Eq. 6.46
		Exercice 2: 2.27%
	$s(t)$	Exercice 1: 25.05%
		Exercice 2: $= s(k, \varkappa)$, Eq. 6.48
Endogenous, result variables	T_f	End of the transtion, if applicable (either $\varkappa(T_f) = 1$, or $T_f = \infty$)
	$\varkappa_l$	$=\varkappa(T_f)$
	$g_{K,l}$	$=g_K(T_f)$
	$\mu(t)$	$= \frac{v_e(t)}{k(t)}$
	$K_e(t)$, $K_f(t)$	$= \mu K(t)$, $= (1-\mu)K(t)$
	$Y_f(t)$, $X_f(t)$, $X_e(t)$, $E_f(t)$, $E_e(t)$	Eq. 6.1
	$C_e(t)$	Eq. 6.8
	$GDP(t)$	Eq. 6.12
	$C(t)$, $I(t)$	Eqs. 6.19 and 6.20
	$p(t)$	Eq. 6.21
	$AV_f(t)$,$AV_e(t)$	Eqs. 6.10 and 6.11
	$\text{EROI}_{pou}(t)$	Eq. 6.26

Table 6.11 *– Parameters of the macroeconomic model used for the simulation of the energy transition*

L'utopie a changé de camp : est aujourd'hui utopiste celui qui croit que tout peut continuer comme avant.

Pablo Servigne

7

Conclusion and perspectives

7.1 Conclusion

This thesis contributes to the current debate about whether the transition to a fully renewable energy system is possible or not, without challenging the underlying economic model.

From the energy model ... Starting from the observation that current estimates of the technical potential of the main renewable energy sources suffer from significant disparities, the first contribution of this thesis consists in proposing an innovative methodology to estimate, in the most realistic way possible, an upper limit for the wind and solar potentials that can be achieved globally. This methodology has the advantage of reconciling the *bottom-up* approaches, i.e. summing up local potentials, with the *top-down* approaches, based on studies of the energy continuously generated at the global level.

To achieve better estimates, various constraints are taken into account: geographical constraints on land use, technological constraints on the conversion

efficiency of natural resources into electricity, and physical constraints on the actual availability of the resources. Concerning solar energy, since there is little or no interaction between installations, the top-down approach does not constrain the results obtained with the bottom-up approach. For wind energy however, we show that taking into account the results of top-down studies (like the ones of Miller et al. [109] and de Castro et al. [77]) constrains the amount of energy that can actually be extracted per unit of area. Most of the available bottom-up studies consider power densities that are well above the achievable limit (estimated at a production of 1 W/m^2). Removing this upper limit in the model indeed leads to a wind potential more than 2.5 times greater.

The energy theoretically produced taking into account all these constraints is then compared with the energy that had to be invested over the lifetime of the different facilities, allowing the calculation of the local standard EROIs, i.e. taken at the exit of the production site. This part of the model was carried out in close collaboration with Rembrandt Koppelaar, whose expertise in the field of life cycle analysis (LCA) was very valuable. In particular, he co-authored a study comparing the LCA, material and labour requirements, and CO_2 emission reduction potentials of 19 power generation technologies [48].

Finally, the methodology presented in this thesis is the first to propose an optimisation procedure, making it possible to adapt certain design parameters of wind and solar technologies to local resources, and thus to maximise the energy produced.

- For wind energy, two parameters are optimised : (i) the rated speed, i.e. the wind speed at which the wind turbine begins to produce at its rated power, and (ii) the distance between successive rows of wind turbines within a farm.

    1. The optimisation of the rated speed makes it possible to consider, in areas with less favourable resources, wind turbines with lower rated speeds, and therefore necessarily larger rotor diameters, i.e. a larger swept area.
    2. Optimising the distance between wind turbines makes it possible to maximise the production of a wind farm by minimising wake effects. These wake effects are largely underestimated in "optimistic" esti-

mates of the wind potential, which consider installed capacity densities up to 5 times higher than the optimum found in this study. When the model results are calculated by applying the installed capacity densities of the literature, the standard EROIs fall significantly, since the output of each turbine is strongly impacted when the farms are very dense.

- For solar thermal power plants, the relative size of the heliostat field in relation to the nominal power of the plant is optimised. This procedure is done via the solar multiple, which is the ratio between the actual size of the mirror field and the surface area that would be required to produce the nominal power at a given design point. By increasing the size of the field, the amount of energy captured and concentrated on the receiver is increased, and the production is maximised in areas with less favourable resources. In order to do this, it was necessary to develop, on the basis of simulations with the SAM software, a model characterising the evolution of the load factor with the relative size of the heliostat field, for the different technologies and thermal storage capacities considered in the study.

Comparing our results with the literature, we find that they are in the lower range of the available estimates. The overall wind potential without a minimum EROI constraint is comparable to the world current final energy consumption, and the solar potential is about 2.5 times higher.

The model also shows that the amount of renewable energy theoretically available varies considerably depending on the EROI threshold considered as the limit before the economic system declines. In the literature, estimates for this threshold vary between 5 and 12. The total global potential between these two values is divided by about 20, with wind potential divided by more than 6 and solar energy reaching at best a standard EROI of 10 (see Table 7.1).

Without a better knowledge of the EROI that would be considered desirable, these results only present an upper envelope of the achievable potential. They say nothing about the changes actually needed in order to reach a given penetration rate of renewable energies. To better understand the implication of these curves, it was necessary to introduce them into an economic model, taking into account the interactions between the production of the energy system, and its needs, in direct form and in the form of capital and services.

$\mathbf{EROI}_{std,min}$	**5**	**12**
Total [EJ/year]	1,972	99
Wind [EJ/year]	*630*	*99*
Solar [EJ/year]	*1,342*	*0*
TFC 2018 [EJ/year]	416	

Table 7.1 *– Total gross potential calculated with the energy model, for the extreme values of $EROI_{std,min}$ estimates found in the literature.*

... to the economic model Starting from the need to deepen the economic dimension, and to measure, in terms of economic variables, the impacts of a gradual transition towards a fully renewable energy system, the second part of this thesis consisted in developing an economic model capable of exploiting the results of the energy model. To do this, we worked in collaboration with Marc Germain, who had already developed macroeconomic models of transition [83, 85], but without a detailed representation of the energy sector.

The macroeconomic model developed is a model with two sectors: the energy sector and the rest of the economy. The factors of production are of 3 forms: energy, goods and capital. This relatively simple model has the advantage of being more transparent than the more complex models found in literature. This advantage is also its disadvantage, since the interactions are represented in a very simplified way.

As the societal EROI of the economic model is an endogenous variable, the results of the energy model had to be adjusted. For this purpose, the curves of the evolution of the EROI as a function of the cumulative potential were transformed into marginal cost curves. By further separating the costs in the form of direct energy uses, services, and capital, these curves made it possible to determine how the technical parameters of the energy system, i.e. its energy, capital and intermediate consumption intensities, are likely to evolve with the penetration rate of renewable energies. We see that, while the energy and intermediate consumption intensities only slighty vary, the capital intensity is multiplied by a factor of 45 when a penetration rate of 100% is reached.

The macroeconomic model and the marginal cost curves then make it possible, on the basis of an innovative approach based on the principle of exploring all the future trajectories of the economy leading to positive net added values in

both sectors, to evaluate the feasibility or not of the transition to a energy system based on wind and solar power and, if it is feasible, to estimate its duration.

The results obtained confirm those of the previous models, in particular those presented in the introduction of this thesis. When considering simulations where the behaviour of economic agents in terms of savings and consumption is unchanged, the energy transition is unfeasible by the end of the century, even under very optimistic assumptions in terms of the evolution of the demand for final energy and of the improvement of the energy efficiency. The only scenario allowing a complete transition by 2070 corresponds to a scenario aiming at stimulating the transition by maintaining the capital growth rate at an annual rate of 3%, which corresponds to a growth rate higher than what has been observed in recent years. The savings rate then exceeds 40% at the end of the transition, to the detriment of public and private consumption which end up stagnating while the economy is still growing. The share of capital devoted to the energy sector also increases considerably, from about 6.5% to more than 40%, which confirms the intuition that the energy sector will take more and more place, to the detriment of other parts of the economy.

During the energy transition, the societal EROI only slighty decreases. It would suggest that it is rather the increase in the capital intensity of the energy sector which would be a brake on the transition, by the effect of capital exacerbation to the detriment of other sectors of the economy. Contrary to what is currently done, it would therefore be judicious in the models to study the different components of the denominator of the EROI, and to estimate in particular how the contributions in indirect form evolve, since they have to be provided by the rest of the economy.

Some assumptions of the model are considered as conservative, in the sense that they favor a smooth transition. The declining trend of the EROI of the non renewable subsector has not been taken into account, as well as the increasing needs for storage, grid adaptation and over-capacities to manage the intermittency of the renewable subsector. The energy demand is endogenous, so a possible rebound effect due to energy efficiency improvements has not been taken into account. Finally, the energy efficiency improvements considered for the coming decades correspond to annual gains never observed to date. Lifting

these assumptions leads unsurprisingly to even more unfavourable results for the transition. These favourable assumptions partly explain why the EROI does not decrease much with the transition.

7.2 Perspectives

There are many potential areas for improvement, the most important of which are listed below.

7.2.1 Energy model

Different aspects of the energy model can be further developed to improve the accuracy of the results obtained. Most of them were discussed during the course of this thesis, and were finally put aside, due to lack of time.

The two main aspects related to the general methodology were discussed in Sections 3.4.2 and 4.3.1. They concern the use of a static approach, which neglects the current uncertainty and future evolution of a number of model parameters, and the study of the standard EROI, which biases the profitability of certain sites compared to an approach that would take into account the point-of-use EROI. In addition to working on these aspects in general, the following points can be incorporated into the energy model.

Biomass potential As mentioned in the introduction, biomass is likely to play a role in the energy transition. However its contribution remains subject to many controversies, as shown for example in the literature review made by Hoogwijk et al. [248], and the fact that it is excluded from a lot of 100% renewable scenarios.

In the initial research project, it was planned to develop a model similar to those developed for wind and solar to characterise its global potential and the associated EROIs. However, a preliminary bibliographic search revealed that this task alone would be the subject of a thesis, given the extent of the deposits and the many conversion technologies.

An easy way to include biomass would be to assimilate it to the non-renewable sector in the economic model, as the conversion technologies are similar to those of fossil fuels. The objective of the economic model would therefore not be to achieve 100% wind and solar power, but to leave a part to

biomass (the proportion satisfied by biomass would then have to be estimated based on studies taking biomass into account in their transition scenarios).

Intermittency management Already mentioned several times in this thesis, the management of the intermittency of renewable energies is a crucial issue. It was envisaged to take these effects into account in the energy model, and to evaluate the overproduction and storage capacities that would be necessary in order to match supply with demand. However, the estimation of these needs necessarily requires a temporal model, in order to have a representation of the energy demand profile, like it is done in [35, 249, 250]. Combining a temporal discretisation with the spatial discretisation of the model, which is relatively fine, considerably complicates the modelling work and was therefore too complex in the context of this thesis.

The MEDEAS model takes into account these storage needs in a globally aggregated model, in a simplified way. Based on NREL studies, they establish relationships between the penetration rate of intermittent renewables and (i) the storage capacity required, (ii) the decrease in the load factors due to the oversizing of the installations. As a start, one could therefore imagine implementing a similar methodology as part of the energy transition simulations.

Critical materials Although the energy transition is supposed to increase energy independence through the decentralisation of the production, it will be accompanied by new dependencies, particularly with regard to certain so-called *critical* materials.[1] On the one hand, some of these materials may be in short supply in the future, putting a brake on the development of certain technologies necessary for the transition. On the other hand, because of the decline in the ore content of some deposits, the energy required for the extraction and refining of certain metals will increase with the energy transition. It would therefore be necessary to be able to assess the impact of this increasing energy demand on the results of the model.

The model developed by the Institut Français du Pétrole Energies Nouvelles (IFPEN) makes it possible to assess the evolution of the demand for certain materials until 2050, under different energy transition scenarios (including scenarios on mobility and recycling). They show, for example, that up to 90%

[1] A raw material is said to be critical when it is characterised by both a high supply risk and high economic importance.

of known copper reserves [251], between 65 and 85% of cobalt reserves [252], and about 43% of nickel reserves [253] could be consumed by 2050 in a scenario aimed at reducing the rise in the earth's temperature to 2°. However, the model does not study the evolution of the energy demand associated with these extraction processes.

The MEDEAS model also takes into account the demand for materials necessary for the energy transition, in order to identify possible risks of shortages. However, in the current version of the model these indicators are given for information purposes, the demand being in all cases fully satisfied. They studied the possible impacts of an increase in the extraction costs of certain metals, but finally decided to take a conservative approach and to ignore this possible increase. Indeed, according to their analysis, the impact would be rather limited, as for a large number of materials, these extraction and refining phases would account for less than 10% of the total energy inputs.

Only Fizaine and Court [58] established a relationship between the EROI of different renewable technologies (and nuclear) and the ore grade degradation of different rare metals. Taken individually, the impact of the ore grade degradation of a given metal on the EROIs is relatively small. But if the quality of these different metals decreases at the same time, then the impact on the EROIs could be significant. It would therefore be crucial to be able to assess the possible future increase in the energy requirement associated with metals extraction.

Geographical distribution of the resources The study of the potential of the European countries has shown that these resources at the level of our continent are relatively limited, when compared to our current final energy consumption. In view of these results, the possibility of the energy independence of Europe seems very compromised, at least without a paradigm shift. The energy transition would then only be possible through the import of a part of our energy, with the geopolitical consequences that this may entail.

We should therefore consider taking into account in the model these effects of distance between resources and end users, in order to propose more realistic strategies than what is currently done, where we only look at aggregated world production.

7.2.2 Economic model

Finally, different aspects of the economic model can be further explored, in order to increase the relevance of the model and to refine the allowable space of possible trajectories for the energy transition. These points have been mentioned at the end of Chapter 6, this list being non-exhaustive :

- Modelling the non-renewable subsector in the same way as it was done for the renewable sub-sector, i.e. obtain curves for the evolution of energy, capital and intermediate consumption intensities with future production.
- Removing the hypothesis of perfect malleability of capital between the two sectors, as well as between the subsectors of the energy sector.
- Endogenising of the behaviours in terms of investment and consumption, as well as the evolution of energy demand, in order to capture more precisely the interactions between the two sectors.
- Including labour in addition to capital.

Choosing rather than suffering economic slowdown ?

The transition to a decarbonised energy system is essential for the survival of our societies. Renewable energies are the only possible alternative, and they offer a huge potential for development given their current rate of exploitation. But the answer to the colossal challenges we face cannot be solely technological. It is indeed illusory to believe that we can continue to rely blindly on unlimited economic growth. The signal was already given by the Club of Rome almost 50 years ago, but this time it can no longer be ignored.

Those who dare to say this are often seen as pessimists. On the contrary, most of them enthusiastically campaign for an energy transition associated with social changes. They are trying to imagine a fair and equitable society and to take measures as soon as possible to accompany the changes in our lifestyles required by the climate emergency.
How pleasant it is indeed to listen to those people who have made the choice of change, who have chosen a system more respectful of all their fundamental values.

Les plus intelligents, eux, ont déjà compris qu'il fallait mettre en place quelque chose d'entièrement nouveau. Mais de multiples acteurs agissent déjà, de façon désordonnée et inconsciente, pour faire émerger de nouvelles solutions, sans que l'on sache encore quel système sortira de ces tâtonnements.

Nous sommes dans une période, assez rare, où la crise et l'impuissance des puissants laissent une place au libre arbitre de chacun : il existe aujourd'hui un laps de temps pendant lequel nous avons chacun la possibilité d'influencer l'avenir par notre action individuelle. Mais comme cet avenir sera la somme du nombre incalculable de ces actions, il est absolument impossible de prévoir quel modèle s'imposera finalement. Dans dix ans, on y verra peut-être plus clair ; dans trente ou quarante ans, un nouveau système aura émergé. Je crois qu'il est tout aussi possible de voir s'installer un système d'exploitation hélas encore plus violent que le capitalisme, que de voir au contraire se mettre en place un modèle plus égalitaire et redistributif.

Extrait de l'interview d'Immanuel Wallerstein: "Le capitalisme touche à sa fin", propos recueillis par Antoine Reverchon pour *Le Monde*, publié le 11 octobre 2008 [254].

Nomenclature

EJ	Exajoule
EROI	Energy Return On Investment
ERRs	Energy Return Ratios
GDP	gross domestic product
GEER	gross external energy ratio
GER	gross energy ratio
Mtoe	Million tonnes of oil equivalent
NEER	net external energy ratio
NRE	non-renewable energies
PEF	primary energy conversion factor
PROI	Power Return On Investment
RE	renewable energies
TFC	total final consumption
TPES	total primary energy supply

Economic Model

q_i	sectoral energy intensities
ue	units of energy
ug	units of general-purpose good

v_i sectoral capital intensities

x_i sectoral non-energy intermediate consumption intensities

AS allowable space

AV_i sectoral *gross* added values

BAU *business-as-usual* scenario

CC capital consumption

EIC energy intermediate consumption

EIOU energy industry own use

EM energy model

ES energy sector

ET energy transition

FS non-energy sector

ICC intermediate and capital consumption

MM macroeconomic model

NDP net domestic product

NEIC non-energy intermediate consumption

NER Net Energy Ratio

NV_i sectoral *net* added values

RDM reduced dynamic model

SD *sustainable development* scenario

TC transition curve

Models / Softwares

GEMBA Global Energy Modeling with a Biophysical Approach [63]

IAMs integrated assessment models

MEDEAS Modeling Energy System Development under Environmental and Socioeconomic constraints [229]

SAM the System Advisor Model [204]

Organisations / Agencies

EEA European Environment Agency

EIA U.S. Energy Information Administration

IEA International Energy Agency

IPCC Intergovernmental Panel on Climate Change

IRENA International Renewable Energy Agency

NREL National Renewable Energy Laboratory

OECD Organisation for Economic Cooperation and Development

Solar Energy

CSP concentrated solar power

DNI direct normal irradiation

GCR ground cover ratio

GHI global horizontal irradiation

HTF heat transfer fluid

mono-Si-PV monocrystalline silicon photovoltaic power plant

poly-Si-PV polycrystalline silicon photovoltaic power plant

PR performance ratio

PT-oil parabolic trough power plant with oil as heat transfer fluid

PT-salt-TES parabolic trough power plant with molten salt as heat transfer fluid and 12 hours capacity of thermal energy storage

PV solar photovoltaic

SM solar multiple

ST-salt-TES solar tower power plant with molten salt as heat transfer fluid and 12 hours capacity of thermal energy storage

STC standard test conditions (an irradiation of 1 kW/m^2, a cell temperature of 25°C, and no wind)

STPP solar tower power plant

TES thermal energy storage

Wind Energy

ρ air density (= 1.225 kg/m^3)

C_f capacity factor

C_p performance coefficient

P_r rated power

v_c cut-in wind speed [m/s]

v_f cut-off wind speed [m/s]

v_r rated wind speed [m/s]

A rotor swept area (=π RD^2)

RD rotor diameter

Bibliography

[1] Cutler J Cleveland, Robert Costanza, Charles A S Hall, and Robert K Kaufmann. Energy and the U.S. Economy : A Biophysical Perspective. *Science (80-.).*, 225, 1984.

[2] I. Dincer and S. Dost. Energy and GDP. *Int. J. Energy Res.*, 21:157–167, 1997.

[3] Michael T. Toman and Barbora Jemelkova. Energy and Economic Development: An Assessment of the State of Knowledge. *Energy Journal, Int. Assoc. Energy Econ.*, 0(4):93–112, 2003.

[4] David I Stern. The role of energy in economic growth. *Ann. N.Y. Acad. Sci.*, 1219:26–51, 2011.

[5] IEA. World Energy Outlook 2020. Technical report, 2020.

[6] Kjell Aleklett, Mikael Höök, Kristofer Jakobsson, Michael Lardelli, Simon Snowden, and S Bengt. The Peak of the Oil Age – Analyzing the world oil production Reference Scenario in World Energy Outlook 2008. *Energy Policy*, 38:1398–1414, 2010.

[7] Steve Sorrell, Richard Miller, Roger Bentley, and Jamie Speirs. Oil futures : A comparison of global supply forecasts. *Energy Policy*, 38(9):4990–5003, 2010.

[8] N.L. Madureira. Oil Reserve and Peak Oil, In: Key Concepts in Energy. pages 101–130. 2014.

[9] Patrick Moriarty and Damon Honnery. Can renewable energy power the future? *Energy Policy*, 93:3–7, 2016.

[10] L Miller. Limits and consequences of the large-scale deployment of renewable energy technologies. *Tech. Reports 27, Max-Planck-Institut fÃŒr Biogeochem.*, 2011.

[11] Donella H Meadows, Dennis L Meadows, Jorgen Randers, and Wiliam W. Behrens III. *The limits to growth : A report for the club of Rome's project on the predicament of mankind.* Universe Books New York, 1972.

[12] Graham M. Turner. A comparison of The Limits to Growth with 30 years of reality. *Glob. Environ. Chang.*, 18:397–411, 2008.

[13] United Nations. World Social Report 2020 Inequality in a rapidly changing world. Technical report, 2020.

[14] Oxfam. Combattre les inégalités des émissions de CO2. Technical report, Oxfam, 2020.

[15] Cory Budischak, Deanna Sewell, Heather Thomson, Leon Mach, and Dana E Veron. Cost-minimized combinations of wind power , solar power and electrochemical storage , powering the grid up to 99.9% of the time. *J. Power Sources*, 225:60–74, 2013.

[16] Omar Ellabban, Haitham Abu-rub, and Frede Blaabjerg. Renewable energy resources : Current status , future prospects and their enabling technology. *Renew. Sustain. Energy Rev.*, 39:748–764, 2014.

[17] Mark Z Jacobson, Mark A Delucchi, Guillaume Bazouin, Zack A F Bauer, Christa C Heavey, Emma Fisher, Sean B Morris, Diniana J Y Piekutowski, Taylor A Vencill, and Tim W Yeskoo. Environmental Science the 50 United States †. *Energy Environ. Sci.*, 8:2093–2117, 2015.

[18] Mark Jacobson. 100 % Clean and Renewable Wind , Water , and Sunlight All-Sector Energy Roadmaps for 139 Countries of the World 100 % Clean and Renewable Wind , Water , and Sunlight All-Sector Energy Roadmaps for 139 Countries of the World. *Joule*, 1:108–121, 2017.

[19] Mark Z Jacobson. Roadmaps to Transition Countries to 100 % Clean, Renewable Energy for All Purposes to Curtail Global Warming, Air Pollution, and Energy Risk. *Earth's Futur.*, 5:948–952, 2017.

[20] Steven J Davis, Nathan S Lewis, Matthew Shaner, Sonia Aggarwal, Doug Arent, Inês L Azevedo, Sally M Benson, Thomas Bradley, Jack

Brouwer, Yet-ming Chiang, Christopher T M Clack, Armond Cohen, Stephen Doig, Jae Edmonds, Paul Fennell, Christopher B Field, Bryan Hannegan, Bri-mathias Hodge, Martin I Hoffert, Eric Ingersoll, Paulina Jaramillo, Klaus S Lackner, Katharine J Mach, Michael Mastrandrea, Joan Ogden, Per F Peterson, Daniel L Sanchez, Daniel Sperling, Joseph Stagner, Jessika E Trancik, Chi-jen Yang, and Ken Caldeira. Net-zero emissions energy systems. *Science (80-.).*, 360(eaas9793), 2018.

[21] M Ram, D Bogdanov, A Aghahosseini, A Gulagi, S A Oyewo, M Child, U Caldera, K Sadovskaia, J Farfan, L.S.N.S. Barbosa, M Fasihi, S Khalili, C Breyer, H Fell, T Traber, F de Caluwe, G Gruber, and B Dalheimer. Global Energy System based on 100% renewable energy: Power, Heat, Transport and Desalination Sectors. Technical Report April, Lappeenranta, Berlin, 2019.

[22] Dmitrii Bogdanov, Ashish Gulagi, Mahdi Fasihi, and Christian Breyer. Full energy sector transition towards 100 % renewable energy supply : Integrating power , heat , transport and industry sectors including desalination. *Appl. Energy*, 283:116273, 2021.

[23] T Parrique, J Barth, F Briens, C Kerschner, A Kuokkanen, and J H Spangenberg. Decoupling debunked: Evidence and arguments against green growth as a sole strategy for sustainability. Technical report, (EEB) European Environmental Bureau, 2019.

[24] Steven J Davis and Ken Caldeira. Consumption-based accounting of CO 2 emissions. *PNAS*, 107(12), 2010.

[25] C L Archer and M Z Jacobson. Evaluation of global wind power. *J. Geophys. Res.*, 110, 2005.

[26] Xi et al. Lu. Global Potential for wind-generated electricity. *PNAS*, 106:10933–10938, 2009.

[27] Jonathan Bosch, Iain Staffell, and Adam D Hawkes. Temporally-explicit and spatially-resolved global onshore wind energy potentials. *Energy*, 131:207–217, 2017.

[28] Kelly Eurek, Patrick Sullivan, Michael Gleason, Dylan Hettinger, Donna Heimiller, and Anthony Lopez. An improved global wind resource estimate for integrated assessment models. *Energy Econ.*, 64:552–567, 2017.

[29] Elise Dupont, Rembrandt Koppelaar, and Hervé Jeanmart. Global available wind energy with physical and energy return on investment constraints. *Appl. Energy*, 209:322–338, 2018.

[30] Manish Ram, Arman Aghahosseini, and Christian Breyer. Technological Forecasting & Social Change Job creation during the global energy transition towards 100 % renewable power system by 2050. *Technol. Forecast. Soc. Chang.*, 151(September 2018):119682, 2020.

[31] Patrick Moriarty and Damon Honnery. Feasability of a 100% Global Renewable Energy System. *Energies*, 13(5543):1–16, 2020.

[32] IEA. Key World Energy Statistics 2020. Technical Report August, 2020.

[33] EIA. Annual Energy Outlook 2020. 2020.

[34] Manfred Lenzen. Current state of development of electricity-generating technologies: A literature review. *Energies*, 3(3):462–591, 2010.

[35] Gauthier Limpens and Hervé Jeanmart. Electricity storage needs for the energy transition: An EROI based analysis illustrated by the case of Belgium. *Energy*, 152:960–973, 2018.

[36] Iñigo Capellán-Pérez, Ignacio de Blas, Jaime Nieto, Carlos de Castro, Luis Javier Miguel, Oscar Carpintero, Margarita Mediavilla, Luis Fernando Lobejon, Noelia Ferreras-alonso, Paula Rodrigo, Fernando Frechoso, and David Alvarez-Antelo. MEDEAS : a new modeling framework integrating global biophysical and socioeconomic constraints. *Energy Environ. Sci.*, (February), 2020.

[37] David J. Murphy, Charles A S Hall, Michael Dale, and Cutler Cleveland. Order from chaos: A preliminary protocol for determining the EROI of fuels. *Sustainability*, 2011.

[38] David J Murphy, Michael Dale, and Devin Moeller. Comparing Apples to Apples : Why the Net Energy Analysis Community Needs to Adopt the Life-Cycle Analysis Framework. *Energies*, 9(917), 2016.

[39] Marco Raugei. Net energy analysis must not compare apples and oranges. *Nat. Energy*, 4:86–88, 2019.

[40] Paul E Brockway, Anne Owen, Lina Brand-correa, and Lukas Hardt. Article : Estimation of global final stage energy-return-on-investment for fossil fuels with comparison to renewable energy sources. *Nat. Energy*, 4(7):612–621, 2019.

[41] Marco Raugei. Energy Return on Investment : Setting the Record Straight. *Joule*, 3(8):1810–1811, 2019.

[42] Carlos de Castro and Iñigo Capellán-Pérez. Standard , Point of Use, and Extended Energy Return Return on Energy Invested (EROI) from Comprehensive Material Requirements of Present Global Wind, Solar, and Hydro Power Technol. *Energies*, 13, 2020.

[43] Adam R. Brandt and Michael Dale. A General Mathematical Framework for Calculating Systems-Scale Efficiency of Energy Extraction and Conversion: Energy Return on Investment (EROI) and Other Energy Return Ratios. *Energies*, 4:1211–1245, 2011.

[44] Michael Carbajales Dale. When is EROI Not EROI ? *Biophys. Econ. Resour. Qual.*, 4(16):1–4, 2019.

[45] Kenneth Mulder and Nathan John Hagens. Energy Return on Investment: Toward a Consistent Framework. *Source AMBIO A J. Hum. Environ.*, 37(2):74–79, 2008.

[46] Carey W King, John P Maxwell, and Alyssa Donovan. Comparing World Economic and Net Energy Metrics , Part 1 : Single Technology and Commodity Perspective. *Energies*, 8:12949–12974, 2015.

[47] Marco Raugei, Enrica Leccisi, Brian Azzopardi, Christopher Jones, Paul Gilbert, Lingxi Zhang, Yutian Zhou, Sarah Mander, and Pierluigi Mancarella. A multi-disciplinary analysis of UK grid mix scenarios with large-scale PV deployment. *Energy Policy*, 114(October 2017):51–62, 2018.

[48] Zoltán Kis, Nikul Pandya, and Rembrandt H.E.M. Koppelaar. Electricity generation technologies: Comparison of materials use, energy return on investment, jobs creation and CO2emissions reduction. *Energy Policy*, 120(May):144–157, 2018.

[49] Charles A S Hall, Stephen Balogh, and David J R Murphy. What is the minimum EROI that a sustainable society must have? *Energies*, 2009.

[50] Victor Court and Florian Fizaine. Energy expenditure , economic growth , and the minimum EROI of society. *Energy Policy*, 95(June 2018):172–186, 2016.

[51] Victor Court. An Estimation of Different Minimum Exergy Return Ratios Required for Society. *Biophys. Econ. Resour. Qual.*, 4(3):1–13, 2019.

[52] Adam R Brandt. How Does Energy Resource Depletion Affect Prosperity ? Mathematics of a Minimum Energy Return on Investment (EROI). *Biophys. Econ. Resour. Qual.*, 2(1):1–12, 2017.

[53] Jessica G. Lambert, Charles A S Hall, Stephen Balogh, Ajay Gupta, and Michelle Arnold. Energy, EROI and quality of life. *Energy Policy*, 64:153–167, 2014.

[54] David J. Murphy and Charles A S Hall. Energy return on investment, peak oil, and the end of economic growth. *Ann. N. Y. Acad. Sci.*, 2011.

[55] David J Murphy. The implications of the declining energy return on investment of oil production. *Phil. Trans. R. Soc. A*, 372, 2013.

[56] Iñigo Capellán-Pérez, Margarita Mediavilla, Carlos de Castro, Oscar Carpintero, and Luis Javier Miguel. Fossil fuel depletion and socio-economic scenarios : An integrated approach. *Energy*, 77:641–666, 2014.

[57] Victor Court and Florian Fizaine. Long-Term Estimates of the Energy-Return-on-Investment (EROI) of Coal, Oil, and Gas Global Productions. *Ecol. Econ.*, 2017.

[58] Florian Fizaine and Victor Court. Renewable electricity producing technologies and metal depletion: A sensitivity analysis using the EROI. *Ecol. Econ.*, 110:106–118, 2015.

[59] D. Weißbach, G. Ruprecht, A. Huke, K. Czerski, S. Gottlieb, and A. Hussein. Energy intensities, EROIs (energy returned on invested), and energy payback times of electricity generating power plants. *Energy*, 2013.

[60] Michael Dale, Susan Krumdieck, and Pat Bodger. A dynamic function for energy return on investment. *Sustainability*, 2011.

[61] Michael Dale, Susan Krumdieck, and Pat Bodger. Future Scenarios for the Global Energy Supply System - a Biophysical Perspective. (May 2014), 2013.

[62] Iñigo Capellán-Pérez, Carlos de Castro, Luis Javier, and Miguel González. Dynamic Energy Return on Energy Investment (EROI) and material requirements in scenarios of global transition to renewable energies Energy Return On energy Invested Energy Stored On energy Invested. *Energy Strateg. Rev.*, 26(July):100399, 2019.

[63] M. Dale, S. Krumdieck, and P. Bodger. Global energy modelling - A biophysical approach (GEMBA) Part 1: An overview of biophysical economics. *Ecol. Econ.*, 73:152–157, 2012.

[64] M Dale, S Krumdieck, and P Bodger. Global energy modelling - A biophysical approach (GEMBA) part 2: Methodology. *Ecol. Econ.*, 73:158–167, 2012.

[65] F. G. Tyron. An index of consumption of fuels and water power. *J. Am. Stat. Assoc.*, 22(159), 1927.

[66] N. Georgescu-Roegen. *The entropy law and the economic process.* Harvard University Press, 1971.

[67] N. Georgescu-Roegen. Energy and economic myths. *South. Econ. J.*, 41:347–381, 1975.

[68] Charles A S Hall, Cutler J Cleveland, and Robert K Kaufmann. Energy and Resource Quality : The Ecology of the Economic Process. *Environ. Hist. Rev.*, 225(4665):890–897, 1988.

[69] Robert U. Ayres and Benjamin Warr. *The Economic Growth Engine: How Energy and Work Drive Material Prosperity.* Edward Elgar Publishing, 2009.

[70] Jaime Nieto, Luis J Miguel, and Ignacio De Blas. Macroeconomic modelling under energy constraints: Global low carbon transition scenarios. *Energy Policy*, 137(111090), 2020.

[71] Michael Dale. *Global Energy Modeling: A Biophysical Approach (GEMBA).* PhD thesis, University of Canterbury, 2010.

[72] Monique Maria Hoogwijk. *On the global and regional potential of renewable energy sources.* PhD thesis, Universiteit Utrecht, 2004.

[73] Bert J M de Vries, Detlef P. van Vuuren, and Monique M. Hoogwijk. Renewable energy sources: Their global potential for the first-half of the 21st century at a global level: An integrated approach. *Energy Policy*, 35(4):2590–2610, 2007.

[74] Damon Honnery and Patrick Moriarty. Estimating global hydrogen production from wind. *Int. J. Hydrogen Energy*, 2009.

[75] P Ruiz, W Nijs, D Tarvydas, A Sgobbi, A Zucker, R Pilli, R Jonsson, A Camia, A Brosowski, and D Thrän. ENSPRESO - an open , EU-28 wide , transparent and coherent database of wind , solar and biomass energy potentials. *Energy Strateg. Rev.*, 26(September 2019):100379, 2020.

[76] E. Dietzenbacher, B. Los, R. Stehrer, M. Timmer, and G. de Vries. The construction of world input-output tables in the WIOD project. *Econom*, 25(1):71–98, 2013.

[77] Carlos de Castro, Margarita Mediavilla, Luis Javier Miguel, and Fernando Frechoso. Global wind power potential: Physical and technological limits. *Energy Policy*, 39:6677–6682, 2011.

[78] Margarita Mediavilla, Carlos De Castro, Iñ Igo Capellá N, Luis Javier Miguel, Iñ Aki Arto, and Fernando Frechoso. The transition towards renewable energies: Physical limits and temporal conditions. *Energy Policy*, 52:297–311, 2012.

[79] Carlos De Castro, Margarita Mediavilla, Luis Javier Miguel, and Fernando Frechoso. Global solar electric potential: A review of their technical and sustainable limits. *Renew. Sustain. Energy Rev.*, 28:824–835, 2013.

[80] Iñigo Capellán-pérez, Carlos De Castro, and Iñaki Arto. Assessing vulnerabilities and limits in the transition to renewable energies : Land requirements under 100 % solar energy scenarios. *Renew. Sustain. Energy Rev.*, 77(September 2016):760–782, 2017.

[81] Carlos de Castro and Iñigo Capellán-Pérez. Concentrated Solar Power: Actual Performance and Foreseeable Future in High Penetration Scenarios of Renewable Energies. *Biophys. Econ. Resour. Qual.*, 3(3):14, 2018.

[82] Craig D. Rye and Tim Jackson. A review of EROEI-dynamics energy-transition models. *Energy Policy*, 122(November 2017):260–272, 2018.

[83] Jean-François Fagnart and Marc Germain. Can the energy transition be smooth? *CEREC Work. Pap.*, (March), 2014.

[84] Jean-François Fagnart and Marc Germain. Net energy ratio , EROEI and the macroeconomy. *Struct. Chang. Econ. Dyn.*, 37:121–126, 2016.

[85] Jean-François Fagnart, Marc Germain, and Benjamin Peeters. Can the Energy Transition Be Smooth ? A General Equilibrium Approach to the EROEI. *Sustainability*, 12(1176):1–29, 2020.

[86] Victor Court, Pierre-André Jouvet, and Frédéric Lantz. Long-term endogenous economic growth and energy transitions. *Energy Journal, Int. Assoc. Energy Econ.*, 39(January), 2018.

[87] Lukáš Režný and Vladimír Bureš. Energy Transition Scenarios and Their Economic Impacts in the Extended Neoclassical Model of Economic Growth. *Sustainability*, 11(3644), 2019.

[88] Michael R W Walmsley, Timothy G Walmsley, Martin J Atkins, Peter J J Kamp, and James R Neale. Minimising carbon emissions and energy expended for electricity generation in New Zealand through to 2050. *Appl. Energy*, 135:656–665, 2014.

[89] Benedikt Lunz, Philipp Stöcker, Sascha Eckstein, Arjuna Nebel, Sascha Samadi, Berit Erlach, Manfred Fischedick, Peter Elsner, and Dirk Uwe Sauer. Scenario-based comparative assessment of potential future electricity systems - A new methodological approach using Germany in 2050 as an example. *Appl. Energy*, 171:555–580, 2016.

[90] Peng Zou, Qixin Chen, Yang Yu, Qing Xia, and Chongqing Kang. Electricity markets evolution with the changing generation mix: An empirical analysis based on China 2050 High Renewable Energy Penetration Roadmap. *Appl. Energy*, 185(2011):56–67, 2017.

[91] L. M. Miller, F. Gans, and A. Kleidon. Estimating maximum global land surface wind power extractability and associated climatic consequences. *Earth Syst. Dyn.*, 2(1):1–12, 2011.

[92] GEA. *Global Energy Assessment - Toward a Sustainable Future*. Cambridge University Press, Cambridge, UK and New York, NY, USA and the International Institute for Applied Systems Analysis, Laxenburg, Austria, 2012.

[93] Patrick Moriarty and Damon Honnery. What energy levels can the Earth sustain? *Energy Policy*, 37(7):2469–2474, 2009.

[94] EEA. Europe's onshore and offshore wind energy potential, An assessment of environmental and economic constraints. Technical Report ISSN 1725-2237, European Environment Agency, 2009.

[95] J Meyers and C Meneveau. Optimal turbine spacing in fully developed wind-farm boundary layers. *Wind Energy*, 15:305–317, 2011.

[96] S A Abbasi, Tabassum-Abbasi, and Abbasin T. Impact of wind-energy generation on climate : A rising spectre. *Renew. Sustain. Energy Rev.*, 59:1591–1598, 2016.

[97] E Lorenz. Available potential energy and the maintenance of the general circulation. *Tellus*, 7:271–281, 1955.

[98] E Lorenz. Generation of available potential energy and the intensity of the global circulation. *Dyn. Clim. Pergamon Press. Oxford, UK*, pages 86–92, 1960.

[99] M R Gustavson. Limits to wind power utilization. *Science*, 204(4388):13–17, 1979.

[100] J P Peixoto and A H Oort. Physics of climate. *Am. Inst. Physics, Springer-Verlag, New York, USA*, 1992.

[101] A Kleidon. Life, hierarchy, and the thermodynamic machinery of planet Earth. *Phys. Life Rev.*, 7:424–460, 2010.

[102] Weston A. Hermann. Quantifying global exergy resources. *Energy*, 31(12):1349–1366, 2006.

[103] M Z Jacobson and C L Archer. Saturation wind power potential and its implications for wind energy. *PNAS*, 109(39):15679–15684, 2012.

[104] L M Miller and A Kleidon. Wind speed reductions by large-scale wind turbine deployments lower turbine efficiencies and set low generation limits. *PNAS*, 113(48):13570–13575, 2016.

[105] L M Miller, F Gans, and A Kleidon. The problem of the second wind turbine - a note on a common but flawed wind power estimation method. *Earth Syst. Dyn.*, 3:79–86, 2012.

[106] D W Keith, J F DeCarolis, D C Denkenberger, D H Lenschow, S L Malyshev, S Pacala, and P J Rasch. The influence of large-scale wind power on global climate. *PNAS*, 101(46):16115–16120, 2004.

[107] A S Adams and D Keith. Are global wind power resource estimates overstated? *Environ. Res. Lett.*, 8, 2013.

[108] Enrico G A Antonini and Ken Caldeira. Atmospheric pressure gradients and Coriolis forces provide geophysical limits to power density of large wind farms. *Appl. Energy*, 281(November 2020):116048, 2021.

[109] L M Miller, Brunsell N.A., D B Mechem, F Gans, A J Monaghan, R Vautard, D W Keith, and A Kleidon. Two methods for estimating limits to large-scale wind power generation. *PNAS*, 112:11169–11174, 2015.

[110] R. W B Best. Limits to wind-power. *Energy Convers.*, 19(2):71–72, 1979.

[111] D P Dee and Others. The ERA-Interim reanalysis: configuration and performance of the data assimilation system. *Q. J. R. Meteorol. Soc.*, 137:553–597, 2011.

[112] Patrick Moriarty and Damon Honnery. Is there an optimum level for renewable energy? *Energy Policy*, 39(5):2748–2753, 2011.

[113] ESA and UCL. GlobCover 2009 (Global Land Cover Map). \url{http://due.esrin.esa.int/page_globcover.php}, 2009.

[114] IUCN and UNEP-WCMC. The World Database on Protected Areas (WDPA), 2016.

[115] Flanders Marine Institue. Union of the ESRI Country shapefile and the Exclusive Economic Zones (version 2), 2014.

[116] Aaron Smith, Tyler Stehly, and Walter Musial. 2014–2015 Offshore Wind Technologies Market Report. Technical Report NREL/TP-5000-64283, National Renewable Energy Laboratory, 2015.

[117] Chang Tian-Pau, Liu Feng-Jiao, Ko Hong-Hsi, Cheng Shih-Ping, Sun Li-Chung, and Kuo Shye-Chorng. Comparative analysis on power curve models of wind turbine generator in estimating capacity factor. *Energy*, 73:88–95, 2014.

[118] C G et al. Justus. Methods for Estimating Wind Speed Frequency Distributions. *J. Appl. Meteorol.*, 17:350–353, 1978.

[119] R J Templin. An Estimate of the Interaction of Windmills in Widespread Arrays. Technical report, Rep. N.A.E. LTR-LA-171, National Research Council of Canada, Ottawa, 1974.

[120] C Crafoord. An estimate of the interaction of a limited array of windmills. Technical report, International Meteorological Institute, Stockholm, 1975.

[121] R Stevens, F Dennice, and C Meneveau. Effects of turbine spacing on the power output of extended wind farms. *Wind Energy*, 19(2):359–370, 2016.

[122] R Stevens and C Meneveau. Flow Structure and Turbulence in Wind Farms. *Annu. Rev. Fluid Mech.*, 49:311–339, 2017.

[123] Daniel (Vestas New Zealand) Belton. Technology evolution and new market developments. In *NZWEA Conf. 2016*, 2016.

[124] The Crown Estate. Offshore wind operational report. Technical Report December, 2017.

[125] M Lenzen and J Munksgaard. Energy and CO2 life-cycle analyses of wind turbines—review and applications. *Renew. Energy*, 26:339–362, 2002.

[126] R. H. Crawford. Life cycle energy and greenhouse emissions analysis of wind turbines and the effect of size on energy yield. *Renew. Sustain. Energy Rev.*, 13(9):2653–2660, 2009.

[127] E Martinez, F Sanz, B Pellegrini, E Jimenez, and J Blanco. Life cycle assessment of a multi-megawatt wind turbine. *Renew. Energy*, 34:667–673, 2009.

[128] Brice Tremeac and Francis Meunier. Life cylce analysis of 4.5 MW and 250 W wind turbines. *Renew. Sustain. Energy Rev.*, 13:2104–2110, 2009.

[129] R.H.E.M. Koppelaar. Solar-PV energy payback and net energy: Meta-assessment of study quality, reproducibility, and results harmonization. *Renew. Sustain. Energy Rev.*, 72:1241–1255, 2017.

[130] Marco Raugei. Methodological Guidelines on Net Energy Analysis of Photovoltaic Electricity. Technical Report IEA-PVPS T12-07, International Energy Agency, 2016.

[131] British Petroleum. BP Statistical Review of World Energy. Technical report, BP, 2016.

[132] NASA. Distance to the Nearest Coast, 2009.

[133] Peter Garrett and Klaus Ronde. Life Cycle Assessment of Electricity Production from an onshore V90-2.6 MW Wind Plant. Technical report, Vestas, 2013.

[134] R S K Environmental and E.ON Climate & Renewables UK. Rampion Offshore Wind Farm ES Section 30 – Carbon Balance. Technical Report December, E.ON, 2012.

[135] E.ON Climate & Renewables UK Rampion Offshore Wind Limited and RSK Environmental Limited. Rampion Offshore Wind Farm - Draft Environmental Statement. Technical Report RSK/HE/P41318/03/04/Section 30, E.ON, 2012.

[136] Energinet.dk. Technical Project Description for Offshore Wind Farms (200 MW). Technical Report April, Energinet.dk, 2015.

[137] A Kielkiewicz, A Marino, C Vlachos, F Maldonado, and I Lessis. The Practicality and Challenges of Using XL Monopiles for Offshore Wind Turbine Substructures, 2015.

[138] C Amante and B W Eakins. ETOPO1 1 Arc-Minute Global Relief Model: Procedures, Data Sources and Analysis. *NOAA Tech. Memo. NESDIS NGDC-24*, 2009.

[139] European Wind Energy Association. Deep water: the next step for offshore wind energy. Technical report, European Wind Energy Association, 2013.

[140] D Snieckus. French wind lobbying for 2GW floating tender early next year, mar 2017.

[141] Statoil. Hywind Scotland Pilot Park - Environmental Statement. Technical report, Statoil, 2015.

[142] Jose Ramon Muro Pereg and Javier Fernandez de la Hoz. Life cycle assessment of 1kWh generated by a wind farm Gamesa G90-2.0 MW onshore. Technical report, Gamesa, 2013.

[143] ABB Power Transmission. Environmental Product Declaration - Power transformer TrafoStar 500 MVA. Technical report, ABB, 2000.

[144] GAMESA. Environmental Product Declaration GAMESA G132 - 5.0 MW onshore wind farm. Technical report, Gamesa, 2015.

[145] S Livaniou, S Iordanis, P Anaxagorou, B Mocanu, R Sykes, J Goormachtigh, J M Christensen, J T Kristensen, and M Antrobus. Logistic Efficiencies And Naval architecture for Wind Installations with Novel Developments. Technical Report 614020, Leanwind, 2015.

[146] Anders Arvesen, Christine Birkeland, and Edgar G Hertwich. The importance of ships and spare parts in LCAs of offshore wind power. *Environ. Sci. Technol.*, 47(6):2948–2956, 2013.

[147] Fulvio Ardente, Marco Beccali, Maurizio Cellura, and Valerio Lo Brano. Energy performances and life cycle assessment of an Italian wind farm. *Renew. Sustain. Energy Rev.*, 12(1):200–217, 2008.

[148] GAMESA. Environmental Product Declaration European G114-2.0MW On-shore Wind Farm. Technical report, Gamesa, 2013.

[149] Adem Atmaca and Recep Yumrutaş. Thermodynamic and exergoeconomic analysis of a cement plant: Part I - Methodology. *Energy Convers. Manag.*, 79:790–798, 2014.

[150] Adem Atmaca and Recep Yumrutas. Thermodynamic and exergoeconomic analysis of a cement plant: Part II - Application. *Energy Convers. Manag.*, 79:790–798, 2014.

[151] Eurofer. Welcome to EUROFER, the European Steel Association. \url{http://www.eurofer.org/About us/Eurofer Portrait.fhtml}, 2015.

[152] B De Lamberterie. Steel production - energy efficiency working group. Technical Report January, EUROFER, 2014.

[153] Dorota Burchart-Korol. Life cycle assessment of steel production in Poland: A case study. *J. Clean. Prod.*, 54(August):235–243, 2013.

[154] International Aluminium Institute. Global Life Cycle Inventory Data for the Primary Aluminium Industry - 2010 Data. Technical Report August, International Aluminium Institute, 2013.

[155] Alcoa Fjardaal. Aluminum Plant in Reydarfjordur: Fjardabyggd. Technical Report July, Alcoa Fjardaal, 2006.

[156] R H E M Koppelaar and H Koppelaar. The Ore Grade and Depth Influence on Copper Energy Inputs. *Biophys. Econ. Resour. Qual.*, 1(2):1–16, 2016.

[157] M F Ashby. *Materials and the Environment: eco-informed material choice*. Butterworth-Heinemann, 1st edition, 2009.

[158] AkzoNobel International. Interplus 1118 Polyester Polyurethane. Technical report, AkzoNobel, 2011.

[159] Nils-Olof Nylund and Kimmo Erkkilä. Heavy-duty truck emission and fuel consumption: Simulating real-world driving in laboratory conditions. In *Proceeding 2005 DEER Conf.*, pages 1–23, 2005.

[160] B E N Sharpe and Rachel Muncrief. Literature Review : Real-World Fuel Consumption of Heavy-Duty Vehicles in the United States , China , and the European Union. Technical report, ICCT, 2015.

[161] Oscar Franzese. Effect of Weight and Roadway Grade on the Fuel Economy of Class-8 Freight Trucks. Technical Report October, Oak Ridge National Laboratory, Oak Ridge, Tennessee, 2011.

[162] D J C Mackay. Sustainable Energy Without the Hot Air, 2015.

[163] EIA. U.S. Energy Information Association, International Energy Statistics. \url{http://www.eia.gov/beta/international/data/browser}, 2014.

[164] WEC. World Energy Scenarios. Technical report, World Energy Concil, 2016.

[165] IEA. World Energy Outlook. Technical report, International Energy Agency, 2016.

[166] Andreas Krenn, Pieter Jan Jordaens, Matthew Wadham-Gagnon, Neil Davis, Niels-Erik Clausen, Ville Lehtomäki, Tuomas Jokela, Saara Kaija, Zouhair Khadiri-Yazami, Göran Ronsten, Helena Wickman, Rebecka

Klintström, and René Cattin. IEA Wind Task 19 - Available Technologies report of Wind Energy in Cold Climates. Technical Report July, 2016.

[167] Eurostat. No Title. \url{http://ec.europa.eu/eurostat}, 2014.

[168] A Gulagi, P Choudhary, D Bogdanov, and C Beyer. Electricity system based on 100% renewable energy for India and SAARC. *PLoS One*, 12(7), 2017.

[169] Franz Trieb, Christoph Schillings, Marlene O Sullivan, Thomas Pregger, and Carsten Hoyer-klick. Global Potential of Concentrating Solar Power. In *SolarPaces Conf. Berlin*, pages 1–11, 2009.

[170] Yvonne Y Deng, Martin Haigh, Willemijn Pouwels, Lou Ramaekers, Ruut Brandsma, Sven Schimschar, and Jan Gro. Quantifying a realistic , worldwide wind and solar electricity supply. *Glob. Environ. Chang.*, 31:239–252, 2015.

[171] Manish Kumar and Arun Kumar. Performance assessment and degradation analysis of solar photovoltaic technologies: A review. *Renew. Sustain. Energy Rev.*, 78(April):554–587, 2017.

[172] Turlough F Guerin. Impacts and opportunities from large-scale solar photovoltaic (PV) electricity generation on agricultural production. *Environ. Qual. Manag.*, 28(4):7–14, 2019.

[173] Justin Brewer, Daniel P Ames, David Solan, Randy Lee, and Juliet Carlisle. Using GIS analytics and social preference data to evaluate utility-scale solar power site suitability. *Renew. Energy*, 81:825–836, 2015.

[174] G Fischer, F Nachtergaele, S Prieler, H T van Velthuizen, L Verelst, and D Wiberg. Global Agro-ecological Zones Assessment for Agriculture. Technical report, IIASA, Laxenburg, Austria and FAO, Rome, Italy, 2007.

[175] Enerdata. Entranze Building floor area per capita, 2019.

[176] J Melius, R Margolis, and S Ong. Estimating Rooftop Suitability for PV: A Review of Methods, Patents, and Validation Techniques. *Natl. Renew. Energy Lab.*, (December):35, 2013.

[177] World Bank Group ESMAP. Global Solar Atlas, 2019.

[178] Oliver Knight. Assessing and Mapping Renewable Energy Resources. Technical report, World Bank Group, Washington DC, 2016.

[179] E Skoplaki and J A Palyvos. On the temperature dependence of photovoltaic module electrical performance: A review of efficiency/power correlations. *Sol. Energy*, 83(5):614–624, 2009.

[180] Xiaoting Wang and Allen Barnett. The Evolving Value of Photovoltaic Module Efficiency. *Appl. Sci.*, 9(6):1227, 2019.

[181] J Trube, ITRPV, and VDMA. International Technology Roadmap for Photovoltaic (ITRPV): 2018 Results. Technical report, VDMA, 2016.

[182] Cao Yu, Shengzhi Xu, Jianxi Yao, and Shuwei Han. Recent Advances in and New Perspectives on Crystalline Silicon Solar Cells with Carrier-Selective Passivation Contacts. *Crystals*, 8(11):430, 2018.

[183] V Fthenakis, R Frischknecht, and M Raugei. Methodology guidelines on life cycle assessment of photovoltaic electricity. *IEA PVPS T12-03*, 2011.

[184] Jonathan Leloux, Rodrigo Moreton Villagra, Luis Narvarte Fernandez, Jamie Taylor, David Trebosc, and Adrien Desportes. Monitoring 30,000 PV Systems in Europe: Performance, Faults, and State of the Art. In *31st Eur. Photovolt. Sol. Energy Conf. Exhib.*, number September, pages 1–21, 2015.

[185] Jamie Taylor, J Leloux, L M H Hall, A M Everard, J Briggs, and A Buckley. Performance of Distributed PV in the UK: A Statistical Analysis of Over 7000 Systems. In *31st Eur. Photovolt. Sol. Energy Conf. Exhib.*, number September, pages 2263–2268, 2015.

[186] Nils H Reich, Bjoern Mueller, Alfons Armbruster, Wilfried G.J.H.M. Van Sark, Klaus Kiefer, and Christian Reise. Performance ratio revisited: Is PR >90% realistic? *Prog. Photovoltaics Res. Appl.*, 20(6):717–726, 2012.

[187] Nattakarn Sakarapunthip, Dhirayut Chenvidhya, Surawut Chuangchote, Krissanapong Kirtikara, Tanokkorn Chenvidhya, and Wandee Onreabroy. Effects of dust accumulation and module cleaning on performance ratio of solar rooftop system and solar power plants. *Jpn. J. Appl. Phys.*, 56(8), 2017.

[188] Irene Romero-Fiances, Emilio Muñoz-Cerón, Rafael Espinoza-Paredes, Gustavo Nofuentes, and Juan De La Casa. Analysis of the performance of various pv module technologies in Peru. *Energies*, 12(1), 2019.

[189] Saeed Edalati, Mehran Ameri, and Masoud Iranmanesh. Comparative performance investigation of mono- and poly-crystalline silicon photovoltaic modules for use in grid-connected photovoltaic systems in dry climates. *Appl. Energy*, 160:255–265, 2015.

[190] Chong Li. Comparative performance analysis of grid-connected PV power systems with different PV technologies in the hot summer and cold winter zone. *Int. J. Photoenergy*, 2018, 2018.

[191] N Hemanthbabu, Sujata Shivashimpiger, N Samanvita, and V M Parthasarathy. Performance Ratio and Loss Analysis for 20MW Grid Connected Solar PV System - Case Study. *Int. J. Eng. Adv. Technol.*, 8(2):20–25, 2019.

[192] Vikrant Sharma and S S Chandel. Performance analysis of a 190kWp grid interactive solar photovoltaic power plant in India. *Energy*, 55:476–485, 2013.

[193] Rajesh Arora, Ranjana Arora, and S N Sridhara. Performance assessment of 186 kWp grid interactive solar photovoltaic plant in Northern India. *Int. J. Ambient Energy*, 40:1–14, 2019.

[194] Satish Kumar Yadav and Usha Bajpai. Performance evaluation of a rooftop solar photovoltaic power plant in Northern India. *Energy Sustain. Dev.*, 43(February):130–138, 2018.

[195] Sandeep Singh Bhullar and Mahendra Lalwani. Performance analysis of 25 MW grid connected solar photovoltaic plant in Gujarat, India. In *3rd Int. Conf. Innov. Appl. Comput. Intell. Power, Energy Control. with their Impact Humanit. CIPECH 2018*, pages 20–25. IEEE, 2018.

[196] D Okello, E E Van Dyk, and F J Vorster. Analysis of measured and simulated performance data of a 3.2 kWp grid-connected PV system in Port Elizabeth, South Africa. *Energy Convers. Manag.*, 100:10–15, 2015.

[197] David A Quansah, Muyiwa S Adaramola, George K Appiah, and Isaac A Edwin. Performance analysis of different grid-connected solar photo-

voltaic (PV) system technologies with combined capacity of 20 kW located in humid tropical climate. *Int. J. Hydrogen Energy*, 42(7):4626–4635, 2017.

[198] M Halwachs, L Neumaier, N Vollert, L Maul, S Dimitriadis, Y Voronko, G C Eder, A Omazic, W Mühleisen, Ch Hirschl, M Schwark, K A Berger, and R Ebner. Statistical evaluation of PV system performance and failure data among different climate zones. *Renew. Energy*, 139(March):1040–1060, 2019.

[199] D. C. Jordan and S. R. Kurtz. Photovoltaic degradation rates - An Analytical Review. *Prog. Photovoltaics Res. Appl.*, 21(1):12–29, 2013.

[200] CSP Bankability. Draft for an Appendix C – Solar Field Modeling to the SolarPACES Guideline for Bankable STE Yield Assessment. Technical Report 0325293, 2017.

[201] Md Tasbirul Islam, Nazmul Huda, A B Abdullah, and R Saidur. A comprehensive review of state-of-the-art concentrating solar power (CSP) technologies: Current status and research trends. *Renew. Sustain. Energy Rev.*, 91(November 2017):987–1018, 2018.

[202] IRENA. Estimating the Renewable Energy Potential in Africa A GIS-based approach. Technical report, International Renewable Energy Agency, 2014.

[203] David Kearney. Utility-Scale Parabolic Trough Solar Systems: Performance Acceptance Test Guidelines: April 2009 - December 2010. Technical Report May, NREL, Oak Ridge, 2011.

[204] NREL. System Advisor Model 2014.1.14, 2017.

[205] Nate Blair, Nicholas Diorio, Janine Freeman, Paul Gilman, Steven Janzou, Ty Neises, Michael Wagner, Nate Blair, Nicholas Diorio, Janine Freeman, Paul Gilman, Steven Janzou, Ty Neises, and Michael Wagner. System Advisor Model (SAM) General Description (Version 2017.9.5). Technical Report May, 2018.

[206] S Ong, C Campbell, P Denholm, R Margolis, and G Heath. Land-Use Requirements for Solar Power Plants in the United States. Technical Report June, 2013.

[207] Nuria Martín-Chivelet. Photovoltaic potential and land-use estimation methodology. *Energy*, 94:233–242, 2016.

[208] K P Bhandari, J M Collier, R J Ellingson, and D S Apul. Energy payback time(EPBT) and energy return on energy invested (EROI) of solar photovoltaic systems: A systematic review and meta-analysis. *Renew. Sustain. Energy Rev.*, 47:133–141, 2015.

[209] Graham Palmer and Joshua Floyd. An Exploration of Divergence in EPBT and EROI for Solar Photovoltaics. *Biophys. Econ. Resour. Qual.*, 2(4):1–20, 2017.

[210] John Burkhardt, Garvin Heath, and Elliot Cohen. Life Cycle Greenhouse Gas Emissions of Trough and Tower Concentrating Solar Power Electricity Generation: Systematic Review and Harmonization. *J. Ind. Ecol.*, 16, 2012.

[211] BP. BP Statistical Review of World Energy. Technical report, 2018.

[212] IEA. World Energy Outlook 2017. Technical report, International Energy Agency, 2017.

[213] Y Ohshita, T Kamioka, and K Nakamura. Technology Trends of High Efficiency Crystalline Silicon Solar Cells. *AAPPS Bull.*, page 7, 2017.

[214] Guofu Hou, Honghang Sun, Ziying Jiang, Ziqiang Pan, Yibo Wang, Xiaodan Zhang, Ying Zhao, and Qiang Yao. Life cycle assessment of grid-connected photovoltaic power generation from crystalline silicon solar modules in China. *Appl. Energy*, 164:882–890, 2016.

[215] Zhiqiang Yu, Wenhui Ma, Keqiang Xie, Guoqiang Lv, Zhengjie Chen, Jijun Wu, and Jie Yu. Life cycle assessment of grid-connected power generation from metallurgical route multi-crystalline silicon photovoltaic system in China. *Appl. Energy*, 185:68–81, 2017.

[216] A Louwen, W.G.J.H.M. Sark, R E I Schropp, W C Turkenburg, and A P C Faaij. Life-cycle greenhouse gas emissions and energy payback time of current and prospective silicon heterojunction solar cell designs. *Prog. Photovoltaics*, 23:1406–1428, 2015.

[217] A Louwen. *Assessment of the energy performance , economics and environmental footprint of silicon heterojunction photovoltaic technology.* PhD thesis, University of Utrecht, 2016.

[218] Craig Turchi, Parthiv Kurup, Sertac Akar, Francisco Flores, Craig Turchi, Parthiv Kurup, and Sertac Akar. Domestic Material Content in Molten-Salt Concentrating Solar Power Plants Domestic Material Content in Molten-Salt Concentrating Solar Power Plants. *Nrel/Tp-5500-64429*, (August), 2015.

[219] Jennie Jorgenson, Paul Denholm, Mark Mehos, and Craig Turchi. Estimating the Performance and Economic Value of Multiple Concentrating Solar Power Technologies in a Production Cost Model. (December), 2013.

[220] Justin Raade, Travis Starns, Cam Martin, Ron Hanson, and Jon Lagarenne. Utilizing Molten Salt Energy Storage at Thermal Power Plants Halotechnics , Inc . – Corporate Profile. pages 1–19, 2015.

[221] Nathan Schuknecht, Jennifer Mcdaniel, and Harrison Filas. Achievement of the $ 100 / m 2 Parabolic Trough. In *SolarPaces 2017 , 26-29 Sept. Santiago, Chile*, page 8 pages, 2017.

[222] A Mathur, R Kasetty, J Oxley, J Mendez, and K Nithyanandam. Using encapsulated phase change salts for concentrated solar power plant. *Energy Procedia*, 49:908–915, 2013.

[223] Rhys Jacob, Martin Belusko, Ines A Fernandez, Luisa F Cabeza, Wasim Saman, and Frank Bruno. Embodied energy and cost of high temperature thermal energy storage systems for use with concentrated solar power plants. *Appl. Energy*, 180:586–597, 2016.

[224] E Batuecas, C Mayo, R Díaz, and F J Pérez. Life Cycle Assessment of heat transfer fluids in parabolic trough concentrating solar power technology. *Sol. Energy Mater. Sol. Cells*, 171(June):91–97, 2017.

[225] E Dupont, R Koppelaar, and H Jeanmart. Global available wind energy with physical and energy return on investment constraints. *Appl. Energy*, 209, 2018.

[226] Diane Palmer, Ralph Gottschalg, and Tom Betts. The future scope of large-scale solar in the UK : Site suitability and target analysis. *Renew. Energy*, 133:1136–1146, 2019.

[227] Albert Boretti, Stefania Castelletto, and Sarim Al-Zubaidy. Concentrating solar power tower technology: present status and outlook. *Nonlinear Eng.*, 8(10):10–31, 2019.

[228] Dirk-Jan van de Ven, Iñigo Capellan-Peréz, Iñaki Arto, Ignacio Cazcarro, Carlos de Castro, Pralit Patel, and Mikel Gonzalez-Eguino. The potential land requirements and related land use change emissions of solar energy. *Sci. Rep.*, 11(2907), 2021.

[229] Iñigo Capellán-Pérez, Ignacio de Blas, Jaime Nieto, Carlos de Castro, Luis Javier Miguel, Margarita Mediavilla, Oscar Carpintero, Paula Rodrigo, Fernando Frechoso, and Santiago Cáceres. Guiding European Policy toward a low-carbon economy. Modelling sustainable Energy system Development under Environmental And Socioeconomic constraints. D4.1 (D13) Global Model: MEDEAS-World Model and IOA implementation ot global geographical level. Technical report, 2017.

[230] Marzella Görig and Christian Breyer. Energy learning curves of PV systems. *Environ. Prog. Sustain. Energy*, 35:914–923, 2016.

[231] Atse Louwen, Wilfried G.J.H.M. Van Sark, André P.C. Faaij, and Ruud E.I. Scrhopp. Re-assessment of net energy production and greenhouse gas emissions avoidance after 40 years of photovoltaics development ´. *Nat. Commun.*, 7(13728), 2016.

[232] Juhua Yang, Lixiao Zhang, Yuan Chang, Yan Hao, Gang Liu, Qin Yan, and Yuanhao Zhao. Understanding the material e ffi ciency of the wind power sector in China : A spatial-temporal assessment. *Resour. Conserv. Recycl.*, 155(August 2019), 2020.

[233] Energy datasheets: EU-28 countries. Technical report, European Commission, 2018.

[234] Ric Hoefnagels, Martin Junginger, Christian Panzer, Gustav Resch, and Anne Held. Long Term Potentials and Costs of RES Part I : Potentials , Diffusion and Technological learning. Technical Report May, 2011.

[235] R Mckenna, S Hollnaicher, P Ostman v. d. Leye, and W Fichtner. Cost-potentials for large onshore wind turbines in Europe. *Energy*, 83:217–229, 2015.

[236] D. Connolly, H. Lund, and B. V. Mathiesen. Smart Energy Europe: The technical and economic impact of one potential 100% renewable energy scenario for the European Union. *Renew. Sustain. Energy Rev.*, 60:1634–1653, 2016.

[237] Kahn Ribeiro, S Kobayashi, M Beuthe, J Gasca, D Greene, D S Lee, Y Muromachi, P J Newton, S Plotkin, D Sperling, R Wit, P J Zhou, O R Davidson, P R Bosch, R Dave, and United Kingdom. Transport and its infrastructure. In *Clim. Chang. 2007 Mitigation. Contrib. Work. Gr. III to Fourth Assess. Rep. Intergov. Panel Clim. Chang. [B. Metz, O.R. Davidson, P.R. Bosch, R. Dave, L.A. Meyer (eds)]*. Cambridge University Press, Cambridge, United Kingdom and New York, NY, USA., 2007.

[238] Carey W King, John P Maxwell, and Alyssa Donovan. Comparing World Economic and Net Energy Metrics , Part 2 : Total Economy Expenditure Perspective. *Energies*, 8:12975–12996, 2015.

[239] Lina Brand-Correa, Paul E Brockway, Claire L Copeland, Timothy J Foxon, Anne Owen, and Peter G Taylor. Developing an Input-Output Based Method to Estimate a National-Level Energy Return on. *Energies*, 10(534):1–21, 2017.

[240] European Central Bank. Estimates of the Euro Area capital stock. *ECB Mon. Bull.*, (May):45–47, 2006.

[241] Statistics Canada. Depreciation Rates for the Productivity Accounts. *Can. Product. Rev.*, 2007.

[242] Reiner Kümmel, Dietmar Lindenberger, and Florian Weiser. The economic power of energy and the need to integrate it with energy policy. *Energy Policy*, 86:833–843, 2015.

[243] Robert U. Ayres, Jeroen C J M van den Bergh, Dietmar Lindenberger, and Benjamin Warr. The underestimated contribution of energy to economic growth. *Struct. Chang. Econ. Dyn.*, 27:79–88, 2013.

[244] FRED. Intermediate inputs dynamics, 2018.

[245] Nathan Gagnon, Charles A S Hall, and Lysle Brinker. A Preliminary Investigation of Energy Return on Energy Investment for Global Oil and Gas Production. (September), 2009.

[246] IPCC. Global Warming of 1.5C. Technical report, Intergovernmental Panel on Climate Change, 2018.

[247] Martin R Sers and Peter A Victor. The Energy-emissions Trap. *Ecol. Econ.*, 151(February):10–21, 2018.

[248] Goran Berndes, Monique Hoogwijk, and Richard Van Den Broek. The contribution of biomass in the future global energy supply : a review of 17 studies. *Biomass and Bioenergy*, 25:1–28, 2003.

[249] Seán Collins, John Paul Deane, Kris Poncelet, Evangelos Panos, Robert C. Pietzcker, Erik Delarue, and Brian Pádraig Ó Gallachóir. Integrating short term variations of the power system into integrated energy system models : A methodological review. *Renew. Sustain. Energy Rev.*, 76:839–856, 2017.

[250] Robert C Pietzcker, Falko Ueckerdt, Samuel Carrara, Harmen Sytze de Boer, Jacques Després, Shinichiro Fujimori, Nils Johnson, Alban Kitous, Yvonne Scholz, Patrick Sullivan, and Gunnar Luderer. System integration of wind and solar power in integrated assessment models : A cross-model evaluation of new approaches. *Energy Econ.*, 64:583–599, 2017.

[251] Emmanuel Hache, Charlène Barnet, and Gondia-Sokhna Seck. Le cuivre dans la transition énergétique : un métal essentiel, structurel et géopolitique ! *Les métaux dans la Transit. énergétique*, 2(IFPEN), 2020.

[252] Emmanuel Hache, Charlène Barnet, and Gondia-Sokhna Seck. Le cobalt dans la transition énergétique : quels risques d'approvisionnements ? *Les métaux dans la Transit. énergétique*, 1(IFPEN), 2020.

[253] Emmanuel Hache, Charlène Barnet, and Gondia-Sokhna Seck. Le nickel dans la transition énergétique : pourquoi parle-t-on de métal du diable ? *Les métaux dans la Transit. énergétique*, 5(IFPEN), 2021.

[254] Antoine Reverchon. Interview d'Immanuel Wallerstein, "Le capitalisme touche à sa fin", oct 2008.

[255] Elise Dupont, Marc Germain, and Hervé Jeanmart. Estimate of the Societal Energy Return on Investment (EROI). *Biophys. Econ. Sustain.*, 6(2), 2021.

A

Estimated rooftop area by country

	Residential	**Commercial and industrial**	**Total** [km^2]
World	**110,660**	**46,343**	**157,003**
Albania	25	17	43
Algeria	688	387	1,075
Angola	856	272	1,129
Argentina	593	412	1,005
Armenia	29	16	45
Australia	872	529	1,400
Austria	79	66	145
Azerbaijan	141	85	226
Bahrain	11	4	15
Bangladesh	1,373	193	1,566
Belarus	37	62	99
Belgium	22	19	41
Benin	281	41	321
Bolivia	267	105	372
Bosnia & Herzegovina	43	24	67
Botswana	70	33	103
Brazil	3,729	1,641	5,370
Brunei	19	7	27
Bulgaria	54	53	108
Cambodia	364	56	420
Cameroon	508	114	621
Canada	376	729	1,105
Chile	212	140	352
China	15,170	9,221	24,391
Colombia	1,075	401	1,477
Congo	203	66	268
Congo, DRC	2,173	257	2,430
Costa Rica	63	26	89
Cote d'Ivoire	504	116	620
Croatia	43	35	78
Cuba	139	66	205
Cyprus	31	10	41
Czech Republic	60	60	120

Table A.1 *– Estimated rooftop area by country, retrieved from the study of Jacobson et al. [18] (table 1/4).*

	Residential	**Commercial and industrial**	**Total** [km^2]
Denmark	23	40	63
Dominican Republic	81	38	119
Ecuador	433	140	573
Egypt	1,945	694	2,639
El Salvador	67	22	89
Eritrea	152	15	168
Estonia	6	11	17
Ethiopia	3,856	272	4,128
Finland	30	75	105
France	558	488	1,045
Gabon	95	41	136
Georgia	40	25	65
Germany	452	500	952
Ghana	524	124	648
Greece	85	74	159
Guatemala	292	88	380
Haiti	84	15	100
Honduras	160	46	206
Hungary	69	72	141
India	19,366	5,069	24,435
Indonesia	5,914	1,888	7,801
Iran	1,212	728	1,941
Iraq	661	363	1,024
Ireland	48	55	103
Israel	80	37	117
Italy	737	259	995
Jamaica	42	13	55
Japan	496	274	769
Jordan	90	48	138
Kazakhstan	415	363	778
Kenya	1,240	192	1,432
Kuwait	31	16	46
Kyrgyzstan	78	30	109
Latvia	12	22	34

Table A.2 *– Estimated rooftop area by country, retrieved from the study of Jacobson et al. [18] (table 2/4).*

	Residential	**Commercial and industrial**	**Total** [km^2]
Lebanon	23	12	35
Libya	208	115	322
Lithuania	24	43	67
Luxembourg	2	2	3
Macedonia	23	15	38
Malaysia	846	326	1,172
Malta	2	1	2
Mexico	1,966	983	2,949
Moldova	16	9	25
Mongolia	45	46	90
Montenegro	7	5	12
Morocco	452	193	645
Mozambique	751	92	843
Myanmar	946	235	1,180
Namibia	44	21	65
Nepal	433	54	487
Netherlands	29	46	75
Netherlands Antilles	2	1	3
New Zealand	83	63	145
Nicaragua	107	33	140
Nigeria	5,037	1,326	6,363
North Korea	145	39	184
Norway	45	82	127
Oman	143	79	222
Pakistan	2,566	736	3,301
Panama	111	44	155
Paraguay	139	59	198
Peru	638	255	893
Philippines	2,292	523	2,815
Poland	202	357	559
Portugal	140	71	211
Qatar	17	8	26
Romania	176	89	264
Russia	891	1,633	2,523

Table A.3 *– Estimated rooftop area by country, retrieved from the study of Jacobson et al. [18] (table 3/4).*

	Residential	**Commercial and industrial**	**Total** [km^2]
Saudi Arabia	1,104	614	1,719
Senegal	336	58	394
Serbia	61	61	123
Slovakia	43	39	83
Slovenia	18	19	37
South Africa	672	344	1,017
South Korea	372	210	581
Spain	566	257	823
Sri Lanka	559	111	670
Sudan	1,683	365	2,047
Sweden	53	97	150
Switzerland	79	68	147
Syria	300	140	440
Tajikistan	115	32	147
Tanzania	1,074	176	1,251
Thailand	1,217	486	1,702
Togo	195	20	215
Trinidad & Tobago	38	9	47
Tunisia	132	69	201
Turkey	908	624	1,533
Turkmenistan	125	80	205
Ukraine	218	191	410
United Arab Emirates	125	64	189
United Kingdom	196	334	530
United States	8,424	5,783	14,207
Uruguay	37	22	59
Uzbekistan	353	160	513
Venezuela	641	249	889
Vietnam	1,367	325	1,692
Yemen	666	157	823
Zambia	603	143	745
Zimbabwe	347	46	393

Table A.4 *– Estimated rooftop area by country, retrieved from the study of Jacobson et al. [18] (table 4/4).*

B

Mathematical developments for the macroeconomic model

B.1 Relationship between the NDP and the technical parameters

Unlike in the model developed by Fagnart and Germain [84], there are in the present model deliveries of the ES to private and public consumption ($C_e \neq 0$). In the following, we develop a relationship between the useful ouput of the economy and the energy production Y_e.

Eqs. (6.1), (6.4)-(6.8) lead to the following equations linking sectoral outputs Y_i and final consumptions C_i:

$$\begin{aligned} Y_e &= q_e Y_e + q_f Y_f + C_e \\ Y_f &= (x_e + \delta_e v_e) Y_e + (x_f + \delta_f v_f) Y_f + C_f + \Delta K \\ &= w_e Y_e + w_f Y_f + C_f + \Delta K \end{aligned}$$

We then isolate the two components of the NDP : C_e and $C_f + I_{net} = C_f + \Delta K$ (see Eq. 6.18).

$$C_e = (1 - q_e)Y_e - q_f Y_f \tag{B.1}$$

$$C_f + \Delta K = (1 - w_f)Y_f - w_e Y_e \tag{B.2}$$

The first equation gives an expression for Y_f that we incorporate in the second equation to write the following relationship between Y_e, C_e and $C_f + \Delta K$:

$$C_f + \Delta K = (1 - w_f)\frac{(1 - q_e)Y_e - C_e}{q_f} - w_e Y_e$$

Let $\zeta = C_e/Y_e$ be the fraction of energy production sold for final consumption. Then the previous equation becomes:

$$\begin{aligned} C_f + \Delta K &= \Big((1 - w_f)\,(1 - q_e - \zeta) - q_f w_e \Big) \frac{Y_e}{q_f} \\ &= \Big((1 - q_e - \zeta) - \Big(q_f w_e + (1 - q_e - \zeta) w_f \Big) \Big) \frac{Y_e}{q_f} \end{aligned} \tag{B.3}$$

This equation gives the quantity of goods that can be delivered to final demand (sum of consumption and net investment) from a certain amount of final energy. The theoretical maximal output is given by the ratio $\frac{Y_e}{q_f}$. The fraction that actually reaches the FS is given by $(1 - q_e - \zeta)$, it corresponds to the energy flow E_f. Then the first loss is the fraction of Y_e consumed by the NEIC and capital consumption (CC) of the ES, measured by $q_f w_e$, and the second loss is the fraction of Y_e consumed by the NEIC and CC of the FS, measured by $(1 - q_e - \zeta) w_f$. These losses can be further distributed between C_e and the rest of the ouput Y_e (see Section 6.1.1).

Given the definition of the net domestic product from Eq. (6.18), Eq. (B.3) gives an expression for the NDP as a function of the technical parameters, the fraction ζ, and the production Y_e:

$$\begin{aligned} NDP &= C_f + \Delta K + pC_e \\ &= C_f + \Delta K + pq_f \zeta \frac{Y_e}{q_f} \\ &= \Big((1 - w_f)(1 - q_e) - q_f w_e + \zeta(-1 + w_f + pq_f) \Big) \frac{Y_e}{q_f} \end{aligned}$$

which corresponds to Eq. (6.28).

B.2 Link between v, g and g_K

Using Eq. (6.4), (6.19) and (6.22) we write:

$$\Delta K = sGDP - \delta K = \left(\frac{s}{v} - \delta\right) K$$

Hence the capital growth rate g_K is given by :

$$g_k = \frac{\Delta K}{K} = \frac{s}{v} - \delta$$

Be g the GDP growth rate : $g = \frac{\Delta GDP}{GDP}$. Starting from Eq. (6.22), one can write at first order $g_v = \frac{\Delta v}{v} = \frac{\Delta K}{K} - \frac{\Delta GDP}{GDP}$, which implies Eq. (6.35) :

$$g = g_K - g_v = \frac{s}{v} - \delta - g_v$$

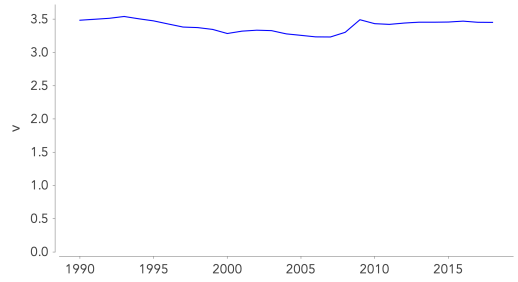
GDP growth is decomposed into the growth of the capital stock and the decline in the capital intensity of the economy.

B.3 Historical evolution of v, x_f and v_f

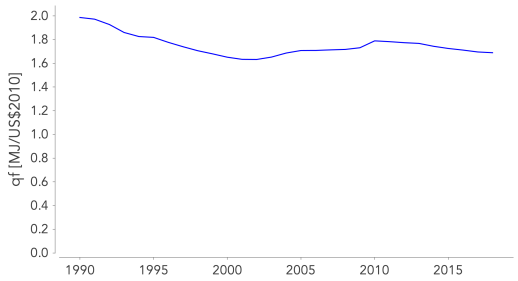
Starting from the estimation of the total capital stock for the reference year ($K(2018)$), and with historical data regarding the total GDP and savings rate s, we find capital stock estimates for the time period 1990-2018.

$$\begin{aligned} K(t+1) &= K(t) - \delta K(t) + I(t)) \\ &= K(t)(1-\delta) + s(t)GDP(t) \\ K(t) &= \frac{K(t+1) - s(t)GDP(t)}{1-\delta} \end{aligned}$$

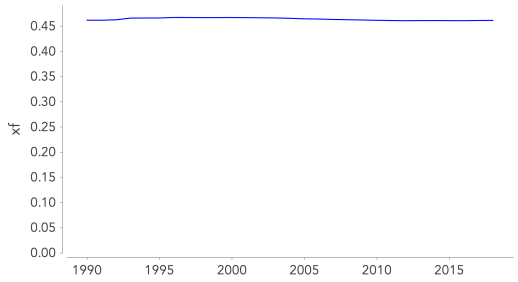
With theses estimates for $K(t)$ and the observed data for the GDP and the savings rate$s$, the historical evolution of v is estimated. Then thanks the calibration procedure developed by Dupont et al. [255] and the yearly estimations of K and v, the historical evolution of the technical parameters of the FS can be retraced. These are shown in Figure B.1. While q_f has decreased by an average of 0.6% per year over the last 30 years, v, v_f and x_f have not seen any significant change.



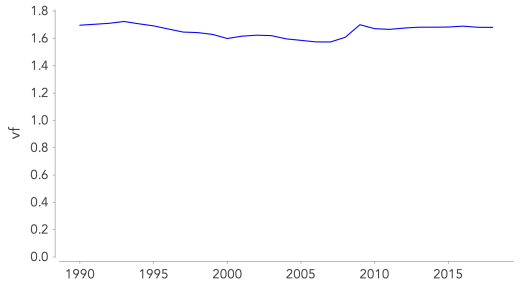
(a) $v(t)$



(b) $q_f(t)$



(c) $x_f(t)$



(d) $v_f(t)$

Figure B.1 *– Historical evolution of :* ***(a)****:* $v(t)$ *the capital intensity of the economy (i.e. the capital/GDP ratio),* ***(b)****:* $q_f(t)$*, the EIC intensity of the FS,* ***(c)****:* $x_f(t)$*, the NEIC intensity of the FS and* ***(d)****:* $v_f(t)$*, the capital intensity of the FS.*

B.4 Site selection criteria

In this section we show that the EROI maximisation criterion from the energy model (EM) corresponds to a profit maximisation criterion in the macroeconomic model (MM).
For the renewable technologies of interest here (wind and solar), (i) the energy intensity of an installation is the same for all sites considered, (ii) the capital required K_e and the maintenance costs included in X_e are fixed costs, which are not site-dependent.

In view of the above, the profits related to sites a and b for a given technology are written:

$$\Pi_a = p(Y_{e,a} - E_{e,a}) - X_{e,a} - \delta_e K_{e,a}$$

$$\Pi_b = p(Y_{e,b} - E_{e,b}) - X_{e,b} - \delta_e K_{e,b}$$

Profits per unit of energy produced are then written :

$$\pi_a = p(1 - q_{e,a}) - \frac{X_e + \delta_e K_e}{Y_{e,a}} = p(1 - q_{e,a}) - w_{e,a}$$

$$\pi_b = p(1 - q_{e,b}) - \frac{X_e + \delta_e K_e}{Y_{e,b}} = p(1 - q_{e,b}) - w_{e,b}$$

If $\Pi_a > \Pi_b$, then necessarily $Y_{e,a} > Y_{e,b}$, which implies $w_{e,a} < w_{e,b}$ (while $q_{e,a} = q_{e,b}$).

Now, the point-of-use EROI of the two sites are written respectively (from Eq. (6.27)):

$$EROI_{pou,a} = \frac{1 - q_{e,a}}{q_{e,a} + q_f w_{e,a}}$$

$$EROI_{pou,a} = \frac{1 - q_{e,b}}{q_{e,b} + q_f w_{e,b}}$$

It follows that $\Pi_a > \Pi_b \Rightarrow EROI_{pou,a} > EROI_{pou,b}$.

B.5 Interval for p

Criterion defined in Eq. (6.40) requires that the net sectoral added values are both positive. With Eqs. (6.10) and (6.14), criterion $NV_f > 0$ translates into the following inequality:

$$1 - pq_f - x_f - \delta_f v_f = 1 - pq_f - w_f > 0$$

With Eqs. (6.11) and (6.15), criterion $NV_e > 0$ translates into the following inequality:

$$p(1-q_e) - x_e - \delta_e v_e = p(1-q_e) - w_e > 0$$

which implies $1 - w_f > pq_f$ and $p(1-q_e) > w_e$, hence the following allowable interval for p :

$$I_p \equiv \frac{w_e}{1-q_e} < p < \frac{1-w_f}{q_f} \tag{B.4}$$

I_p can be transformed into an interval for k, but this will depend on assumptions made about the parameters, in particular the behavioural parameters s (or g_K) and η.

B.6 Calculation of the allowable spaces

Thereafter, the allowable range for the ratio $k = \frac{K}{Y_e}$ is established for the 2 exercises, as well as the equation that links $\varkappa$ and k with g_K (Exercise 1) or s (Exercise 2).
For the developments that will follow, let us define $D_f = C_f + I$, the final demand to the FS.

Eqs. (6.7) and (6.8) give the following relationships for the final demands D_f and C_e:

$$D_f = Y_f - X_e - X_f = (1-x_f)\,Y_f - x_e Y_e \tag{B.5}$$

$$C_e = Y_e - E_e - E_f = (1-q_e)\,Y_e - q_f Y_f \tag{B.6}$$

By the expenditure approach of GDP, we have:

$$\begin{aligned} GDP &= D_f + pC_e = D_f + \eta C \\ &= D_f + \eta(1-s)\,GDP \end{aligned}$$

Hence the following relationship between the GDP, D_f, η and s (useful for Exercise 1):

$$GDP = \frac{D_f}{1-\eta(1-s)} \tag{B.7}$$

And, as $GDP = C + I$, the following relationship between C, D_f, I and η

(useful for Exercise 2):

$$\begin{aligned} C+I &= Df+\eta C \\ C &= \frac{D_f - I}{1-\eta} \end{aligned} \tag{B.8}$$

B.6.1 Exercise 1 - k interval

With Eqs. (6.21), (6.20), (B.5)-(B.7), p is expressed as a function of the technical parameters and the final outputs Y_i:

$$\begin{aligned} p &= \frac{\eta C}{C_e} = \frac{\eta\left(1-s\right) GDP}{C_e} \\ &= \frac{\eta\left(1-s\right)}{1-\eta\left(1-s\right)} \frac{D_f}{C_e} \\ &= \frac{\eta\left(1-s\right)}{1-\eta\left(1-s\right)} \frac{\left(1-x_f\right) Y_f - x_e Y_e}{\left(1-q_e\right) Y_e - q_f Y_f} \end{aligned}$$

Let $y = \frac{Y_f}{Y_e}$, then the last equality becomes:

$$p = \frac{\eta\left(1-s\right)}{1-\eta\left(1-s\right)} \frac{\left(1-x_f\right) y - x_e}{1-q_e-q_f y}$$

As a result, and with $\eta' = \frac{\eta(1-s)}{1-\eta(1-s)}$, $A = \frac{w_e}{1-q_e}$, and $B = \frac{1-w_f}{q_f}$, Eq. (B.4) becomes:

$$A < \eta' \frac{\left(1-x_f\right) y - x_e}{1-q_e-q_f y} < B$$

$\Rightarrow$

$$A\left(1-q_e-q_f y\right) < \eta'\left(\left(1-x_f\right) y - x_e\right) < B\left(1-q_e-q_f y\right)$$

$\Rightarrow$

$$\begin{aligned} A\left(1-q_e\right)+\eta' x_e &< \left(Aq_f+\eta'\left(1-x_f\right)\right) y \\ \left(Bq_f+\eta'\left(1-x_f\right)\right) y &< B\left(1-q_e\right)+\eta' x_e \end{aligned}$$

$\Rightarrow$

$$\frac{A\left(1-q_e\right)+\eta' x_e}{Aq_f+\eta'\left(1-x_f\right)} < y < \frac{B\left(1-q_e\right)+\eta' x_e}{Bq_f+\eta'\left(1-x_f\right)}$$

$\Rightarrow$

$$I_y \equiv \underline{y} = \frac{w_e+\eta' x_e}{\frac{w_e q_f}{1-q_e}+\eta'\left(1-x_f\right)} < y < \frac{\frac{\left(1-w_f\right)\left(1-q_e\right)}{q_f}+\eta' x_e}{1-w_f+\eta'\left(1-x_f\right)} = \overline{y} \tag{B.9}$$

To I_y corresponds an interval for k. Indeed, k and y are linked by:

$$k = \frac{K}{Y_e} = \frac{K_f + K_e}{Y_e} = \frac{v_f Y_f + v_e Y_e}{Y_e} = v_f y + v_e$$

Therefore, we have:

$$\begin{aligned} \underline{k}(\varkappa) &= v_f \frac{w_e(\varkappa) + \eta' x_e(\varkappa)}{\frac{w_e(\varkappa) q_f}{1 - q_e(\varkappa)} + \eta'(1 - x_f)} + v_e(\varkappa) \\ \overline{k}(\varkappa) &= v_f \frac{\frac{(1-w_f)(1-q_e(\varkappa))}{q_f} + \eta' x_e(\varkappa)}{1 - w_f + \eta'(1 - x_f)} + v_e(\varkappa) \end{aligned} \tag{B.10}$$

These bounds are increasing functions of $\varkappa$ (since $x'_e(\varkappa)$, $v'_e(\varkappa)$ and thus $w'_e(\varkappa) > 0$, and $q'_e(\varkappa) < 0$), and decreasing functions of q_f.

Indeed, the EM results show that solar and wind power are more intensive in final goods than the technologies they replace. It should also be noted that the lower the energy intensity of the FS q_f, the higher the envelopes are in the $\{\varkappa, k\}$ space.

B.6.2 Exercise 1 - Capital growth rate

Given Eqs. (6.4) and (6.19), the capital growth rate is calculated as follows :

$$g_K = \frac{\Delta K}{K} = \frac{s\,GDP}{K} - \delta \tag{B.11}$$

Yet Eq. (B.7) gives:

$$\frac{s\,GDP}{K} = \frac{s}{1 - \eta(1 - s)} \frac{D_f}{K}$$

Substituting D_f by Eq. (B.5), one finds:

$$\begin{aligned} \frac{s\,GDP}{K} &= \frac{s}{1 - \eta(1 - s)} \frac{(1 - x_f) Y_f - x_e Y_e}{K} \\ &= \frac{s}{1 - \eta(1 - s)} \frac{(1 - x_f) \frac{K - K_e}{v_f} - x_e Y_e}{K} \\ &= \frac{s}{1 - \eta(1 - s)} \frac{(1 - x_f) \frac{k - v_e}{v_f} - x_e}{k} \\ &= \frac{1}{v_f} \frac{s}{1 - \eta(1 - s)} \left((1 - x_f) \left(1 - \frac{v_e}{k} \right) - \frac{x_e v_f}{k} \right) \end{aligned} \tag{B.12}$$

Given Eq. (B.12), Eq. (B.11) rewrites :

$$g_K = \frac{1}{v_f}\frac{s}{1-\eta(1-s)}\left((1-x_f)\left(1-\frac{v_e}{k}\right)-\frac{x_e v_f}{k}\right)-\delta(k) \tag{B.13}$$

Where $\delta(k)$ writes (starting from Eq. 6.5):

$$\begin{aligned}
\delta(k) &= \frac{\delta_e K_e + \delta_f K_f}{K} \\
&= \frac{\frac{\delta_e K_e}{Y_e} + \frac{\delta_f K_f}{Y_e}}{k} \\
&= \frac{\delta_e v_e + \frac{\delta_f (K-K_e)}{Y_e}}{k} \\
&= \delta_f + (\delta_e - \delta_f)\frac{v_e}{k}
\end{aligned} \tag{B.14}$$

The first term of Eq. (B.13) is an increasing function of k, and $\delta(k)$ is an increasing function of k if $\delta_f \leq \delta_e$, and negative otherwise. It follows that g_K is an increasing function of k if $\delta_f - \delta_e$ is not too high (which is confirmed by the estimations of T_e and T_f).

B.6.3 Exercise 2 - k interval

Given Eqs. (B.8) and (6.21) (which gives $p = \eta C/C_e$):

$$p = \frac{\eta}{1-\eta}\frac{D_f - I}{C_e}$$

Eq. (B.11) gives an expression for I (i.e. $I = (g_K + \delta(k))K$). Combined with Eqs. (B.6), (B.8) and (B.14) the previous equation becomes:

$$\begin{aligned}
p &= \frac{\eta}{1-\eta}\frac{(1-x_f)\,Y_f - x_e Y_e - (g_K + \delta(k))\,K}{(1-q_e)\,Y_e - q_f Y_f} \\
&= \frac{\eta}{1-\eta}\frac{(1-x_f)\,\frac{K - v_e Y_e}{v_f} - x_e Y_e - (g_K + \delta(k))\,K}{(1-q_e)\,Y_e - q_f \frac{K - v_e Y_e}{v_f}} \\
&= \frac{\eta}{1-\eta}\frac{(1-x_f)\,\frac{k - v_e}{v_f} - x_e - \left(g_K + \delta_f - (\delta_f - \delta_e)\,\frac{v_e}{k}\right)k}{1 - q_e - q_f \frac{k - v_e}{v_f}} \\
&= \frac{\eta}{1-\eta}\frac{\left(\frac{1-x_f}{v_f} - (g_K + \delta_f)\right)k + (\delta_f - \delta_e)\,v_e - (1-x_f)\,\frac{v_e}{v_f} - x_e}{1 - q_e + q_f \frac{v_e}{v_f} - \frac{q_f}{v_f}k}
\end{aligned}$$

With notations $\eta' = \frac{\eta}{1-\eta}$, $A = \frac{1}{\eta'}\frac{w_e}{1-q_e}$, $B = \frac{1}{\eta'}\frac{1-w_f}{q_f}$, and the expression found for p, Eq. (B.4) becomes:

$$A < \frac{\left(\frac{1-x_f}{v_f} - (g_K + \delta_f)\right) k + (\delta_f - \delta_e)\, v_e - (1 - x_f)\, \frac{v_e}{v_f} - x_e}{1 - q_e + q_f \frac{v_e}{v_f} - \frac{q_f}{v_f} k} < B$$

Both the numerators and the denominator are positive, so the inequality rewrites as follows:

$$A\left(1 - q_e + q_f \frac{v_e}{v_f} - \frac{q_f}{v_f} k\right) < \left(\frac{1 - x_f}{v_f} - (g_K + \delta_f)\right) k + (\delta_f - \delta_e)\, v_e - (1 - x_f)\, \frac{v_e}{v_f} - x_e$$
$$< B\left(1 - q_e + q_f \frac{v_e}{v_f} - \frac{q_f}{v_f} k\right)$$

Which gives two inequalities:

$$A\left(1 - q_e + q_f \frac{v_e}{v_f}\right) - (\delta_f - \delta_e)\, v_e + (1 - x_f)\, \frac{v_e}{v_f} + x_e < \left(A\frac{q_f}{v_f} + \frac{1 - x_f}{v_f} - (g_K + \delta_f)\right) k$$

$$\left(B\frac{q_f}{v_f} + \frac{1 - x_f}{v_f} - (g_K + \delta_f)\right) k < B\left(1 - q_e + q_f \frac{v_e}{v_f}\right) - (\delta_f - \delta_e)\, v_e + (1 - x_f)\, \frac{v_e}{v_f} + x_e$$

If $\delta_f < \delta_e$, or if $\delta_f - \delta_e > 0$ is not too high, the left-hand side of the first inequality is positive, which implies that the other members of the 2 inequalities are also positive (because $A < B$). Hence the following interval is found for k :

$$\frac{A\left(1 - q_e + q_f \frac{v_e}{v_f}\right) - (\delta_f - \delta_e)\, v_e + (1 - x_f)\, \frac{v_e}{v_f} + x_e}{\frac{q_f}{v_f} + \frac{1-x_f}{v_f} - (g_K + \delta_f)} < k$$
$$< \frac{B\left(1 - q_e + q_f \frac{v_e}{v_f}\right) - (\delta_f - \delta_e) v_e + (1 - x_f)\frac{v_e}{v_f} + x_e}{B\frac{q_f}{v_f} + \frac{1-x_f}{v_f} - (g_K + \delta_f)}$$

Or equivalently :

$$\begin{aligned}
\underline{k}(\varkappa) &= \frac{\frac{1}{\eta'}\frac{w_e(\varkappa)}{1-q_e(\varkappa)}\left(1 - q_e(\varkappa) + q_f \frac{v_e(\varkappa)}{v_f}\right) + \left(\frac{1-x_f}{v_f} - (\delta_f - \delta_e)\right) v_e(\varkappa) + x_e(\varkappa)}{\frac{1}{\eta'}\frac{w_e(\varkappa)}{1-q_e(\varkappa)}\frac{q_f}{v_f} + \frac{1-x_f}{v_f} - (g_K + \delta_f)} \\
\overline{k}(\varkappa) &= \frac{\frac{1}{\eta'}\frac{1-w_f}{q_f}\left(1 - q_e(\varkappa) + q_f \frac{v_e(\varkappa)}{v_f}\right) + \left(\frac{1-x_f}{v_f} - (\delta_f - \delta_e)\right) v_e(\varkappa) + x_e(\varkappa)}{\frac{1}{\eta'}\frac{1-w_f}{v_f} + \frac{1-x_f}{v_f} - (g_K + \delta_f)}
\end{aligned} \tag{B.15}$$

B.6.4 Exercise 2 - Savings rate

With Eq. (B.8) we write:

$$GDP = C + I = \frac{D_f - I}{1-\eta} + I = \frac{D_f - \eta I}{1-\eta}$$

With the definition of s and the previous equation we have:

$$s = \frac{I}{GDP} = \frac{(1-\eta)I}{D_f - \eta I}$$

Yet $I = (g_K + \delta(k))\, K$, so :

$$s = \frac{(1-\eta)\,(g_K + \delta(k))}{\frac{D_f}{K} - \eta\,(g_K + \delta(k))}$$

In addition, with Eq. (B.5) we have:

$$\begin{aligned}
\frac{D_f}{K} &= \frac{(1-x_f)\,Y_f - x_e Y_e}{K} \\
&= \frac{(1-x_f)\,\frac{K - v_e Y_e}{v_f} - x_e Y_e}{K} \\
&= \frac{(1-x_f)\,\frac{k - v_e}{v_f} - x_e}{k} \\
&= \frac{1-x_f}{v_f}\left(1 - \frac{v_e}{k}\right) - \frac{x_e}{k} \\
&= \frac{1-x_f}{v_f} - \left(\frac{1-x_f}{v_f} v_e + x_e\right)\frac{1}{k}
\end{aligned}$$

As a result we find an expression for s as a function of the technical parameters, g_K, η, k (and $\varkappa$).

$$s = \frac{(1-\eta)\left(g_K + \delta_f - (\delta_f - \delta_e)\,\frac{v_e}{k}\right)}{\frac{1-x_f}{v_f} - \eta\left(g_K + \delta_f - (\delta_f - \delta_e)\,\frac{v_e}{k}\right) - \left(\frac{1-x_f}{v_f} v_e + x_e\right)\frac{1}{k}} \tag{B.16}$$

B.7 Future evolution of Y_e and q_f

We consider 2 scenarios for the future evolution of the final energy demand and the energy intensity of the FS. The first scenario is the *business as usual* scenario (BAU), which is an extrapolation of past trends of Y_e and q_f (see Table B.1). The second scenario is based on the *sustainable development* (SD) scenario of the IEA "World Energy Outlook" report ([5]). It represents an accelerated energy transition in order to achieve sustainable development goals in terms of energy access (universal access to modern energy by 2030), climate change (limiting the average temperature increase to below 2°C) and air quality (significant reduction in air pollution-related deaths).

For BAU, extrapolating the annual growth rates observed over the period 1990-2018 (see Table B.1), we obtain for 2040: $Y_e(2040) = 1.45Y_e(2017)$, and $q_f(2040) = 0.85q_f(2017)$.

	1990-2018	1990-1999	2000-2009	2010-2018
Y_e [%]	1.63	1.02	2.05	1.16
q_f [%]	-0.58	-1.85	0.56	-0.72

Table B.1 *– Historical annual growth rates of Y_e and q_f.*

The IEA SD scenario assumes a final energy consumption for 2040 similar to today, and a higher annual rate of decline in the energy intensity of the economy than has been observed in the past. The IEA considers an annual decline rate for the primary energy intensity of GDP of 3.5%. Since only final energy is considered here, the rate of decrease of q_f will be lower. If we consider an annual decrease rate of 2.25 % (a rate never observed over the 1990-2018 period), we find $q_f(2040) = 0.6q_f(2017)$.

In the long term, asymptotic values are given for Y_e and q_f, which are Y_{el} and q_{fl}. For BAU, $Y_{el} = 3Y_e(0)$, while for SD, $Y_{el} = Y_e(0)$. For both scenarios, $q_{fl} = 0.5q_f(0)$.

The evolution of q_f is estimated as follows:

$$q_f(t) = q_{fl} + (q_f(0) - q_{fl})(1 - r_{q_f})^t \tag{B.17}$$

which assumes that the difference between the initial value of q_f and its limit value (q_{fl}) decreases exponentially. Knowing q_f in 2040, we can estimate r_{q_f}, the rate of change of the gap from $q_f(t)$ to its stationary value q_{fl}. In the BAU

framework, the evolution of Y_e is modelled according to a logistic curve :

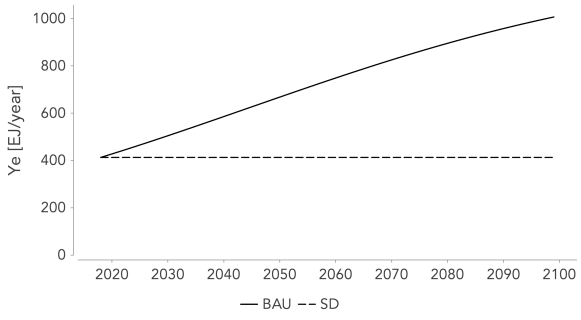
$$Y_e(t) = Y_e(t-1)\left(1 + r_{Y_e}\left(1 - \frac{Y_e(t-1)}{Y_{el}}\right)\right) \tag{B.18}$$

The rate r_{Y_e} is calibrated iteratively, starting from the value of Y_e in 2040.

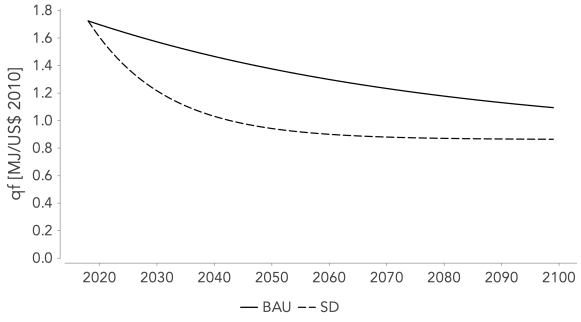
The values of r_{q_f} and r_{Y_e} for the two scenarios are shown in Table B.2. The corresponding temporal evolutions of Y_e and q_f are shown in Fig. B.2.

	r_{Y_e} [%]	r_{q_f} [%]
BAU	2.72	1.6
SD	0	7

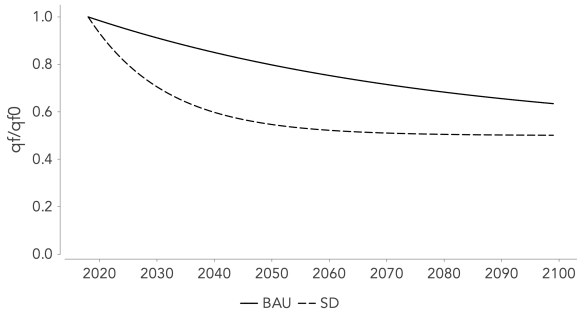
Table B.2 *– Calculated values of r_{q_f} and r_{Y_e} for both scenarios.*



(a) $Y_e(t)$



(b) $q_f(t)$



(c) $q_f(t)/q_{f0}$

Figure B.2 *– Future evolution of Y_e and q_f for the 2 scenarios*

.